Royal Holloway University of London
School of Biological Science
Biomedical Science Research Centre

Modelling SMA using induced pluripotent stem cells from a discordant affected family

PhD student: María Gabriela Boza
Supervisor: Dr Rafael Yáñez

Thesis presented for the degree of Doctor of Philosophy at the University of London
December 2012

DECLARATION OF AUTHORSHIP

I, María Gabriela Boza, hereby declare that this thesis and the work presented in it is entirely my own. Where I have consulted the work of others, this is always clearly stated.

Signed:

Date:

SUMMARY

Spinal muscular atrophy (SMA) is an autosomal recessive neuromuscular disease in which low levels of survival of motor neuron (SMN) protein lead to the degeneration of alpha motor neurons (MNs) in the spinal cord. The pathological mechanism of SMA is highly controversial and until recently it was not possible to obtain human MNs to study the disease. The development of induced pluripotent stem cell (iPSC) technology has made it possible to bypass this obstacle and iPSC-based models of SMA type I have already been validated by two separate groups. Encouraged by these pioneering findings I have produced and characterized iPSCs from several members of a discordant consanguineous family in which four haploidentical siblings share the same homozygous *SMN1* mutation, but nonetheless show different phenotypes of the disease. I have differentiated iPSC clones from three of the siblings and the carrier unaffected mother, as well as a control unaffected clone and a clone derived from a patient with SMA type I, into ISL1+/ChAT+ MNs. No obvious phenotypic difference was observed between the MN cultures of the siblings during the period of study, but cells from the SMA type I patient did show an impaired ability to form rosettes. The study of SMN and PLS3 levels during the differentiation from iPSCs to ChAT+ MNs showed a gradual decay of these proteins during MN development in all clones. Furthermore, SMN protein levels did not correlate with the pattern of mRNA expression, suggesting the existence of post-transcriptional and/or post-translational regulation of full-length *SMN* (*FL-SMN)* transcripts and protein. The *FL/Δ7-SMN* mRNA ratio and total *SMN* (*tSMN)* mRNA levels were found to be possible biomarkers to distinguish unaffected individuals from SMA patients and the severity of SMA pathology, respectively. PLS3 protein level was higher in the SMA type IV/asymptomatic sibling than in two of the type III SMA siblings, but it could not be confirmed as a modifier factor in the family. These results suggest that SMN levels are regulated during MN development, and that low levels may impair the generation of rosettes but not necessarily of MNs. SMN levels in MNs only show minor differences between patients, suggesting that there may be a threshold after which reduced levels of SMN within a narrow range become suddenly and increasingly detrimental unless modifier factors can compensate for the cellular function(s) lost.

To my family,
for giving me this opportunity.

ACKNOWLEDGEMENTS

I know I have a lot of people to thank in here, not just for quick and simple advice, but for real contributions to this project and my career.

Nonetheless, I have decided to dedicate my entire thesis to the people that made it possible for me to have the chance to do the kind of research I love, which could not have been done where I come from. My Dad recently told me that he did not know when I started to build up this dream in my head, but that it has been one of the strongest motivations he has ever seen in me. I think he is right because I gave up many things (and people) to do this and I can sincerely say that I did the best I could.

I know that this is a feeling that not many people can understand, not everybody has the need to fight so hard for this chance, and most importantly not everybody has the kind of family I have. I could not have accomplished this without them. I always lacked the faith they had in me, the kind of faith that is so honest and strong that somehow makes everything possible.

When after two years of applying for funded PhD positions I got nothing but rejections, I began giving up my dream. There was one person who offered me an opportunity, something that I really wanted, but he could not fund me. There I was with a dream half fulfilled and half broken, like many of the people who graduated with me in college. I still remember when my family told me: “You are going to the UK, you are going to do the PhD you want, we will get the money”. I still do not really know how, but they did. It is been more than 3 years now that I have been here fully supported by them.

I am thankful more than anything that I have been so lucky in life as to have people that really valued me, supported my dreams and loved me all the way along. Not everybody can say that.

To my family, this has been all because of you, because you never gave up on me.

GENERAL INDEX

INDEX OF FIGURES

INDEX OF TABLES

LIST OF ABBREVIATIONS

- 18S: Ribosomal protein S18
- A1AT: Alpha 1 antitrypsin
- AAV: Adeno-associated virus
- ACh: Acetylcholine
- AChR: ACh receptor
- ACTB: beta actin
- Ad: Adenovirus
- AFM: Association Française contre les Myopathies/ French Muscular Disease Association
- AFP: alpha fetoprotein
- ALD: Adrenoleukodystrophy
- ALS: Amyotrophic lateral sclerosis
- AP: Alkaline phosphatase
- APC: allophycocyanin
- ASO: Antisense oligonucleotide
- BBB: Blood brain barrier
- BDNF: Brain-derived neurotrophic factor
- BMP_2: Bone morphogenetic protein 2
- BSA: Bovine serum albumin
- CA: Capsid
- cAMP: Cyclic adenosine monophosphate
- cDNA: Complementary DNA
- CECS: Centre d'Etude des Cellules Souches/ Centre for the Study of Stem Cells (Evry, France)
- ChAT: Choline Acetyletransferase
- CMV: Cytomegalovirus
- cMYC: v-myc myelocytomatosis viral oncogene homolog
- CNS: Central nervous system
- CO_2: Carbon dioxide
- CT: Cycle threshold
- CX3CL1: Fractalkine chemokine binding domain
- DC: Dyskeratosis congenita
- ddCT: Delta-delta CT
- DMEM: Dulbecco's modified Eagle's medium
- DMSO: Dimethyl sulfoxide
- DNA: Deoxyribonucleic acid
- dsDNA: double-stranded DNA
- DT: Doubling time
- EB: Embryoid body
- EGC: Embryonic germ cell
- EGF: Epidermal growth factor
- eGFP: Enhanced GFP
- EGFR: Epidermal growth factor receptor
- ELISA: Enzyme-linked immunosorbent assay
- ESC: Embryonic stem cell
- EtBr: Ethidium bromide
- FACS: Fluorescence-activated cell sorting
- FBS: Fetal bovine serum
- FD: Familial dysautonomia
- FGF: Fibroblast growth factor

- FITC: Fluorescein isothiocyanate
- FL-SMN: Full length survival motor neuron
- FMO: fluorescence minus one
- FSC-A: Forward scattered light area
- GADPH: Glyceraldehyde-3-phosphate dehydrogenase
- GALV: Gibbon ape leukemia virus.
- GDF3: Growth and differentiation factor 3
- GDNF: Glial cell-derived neurotrophic factor
- GFAP: Glial fibrillary acidic protein
- GFP: Green fluorescent protein
- GPI1: Glucose phosphate isomerase
- GSC: Germline stem cell
- HBSS: Hank's Balanced Salt Solution
- HCM: Hepatocyte culture medium
- HDAC: Histone deacetylase
- HEK: Human embryonic kidney
- HGFR: Hepatocyte growth factor receptor
- HGPS: Hutchinson-Gilford progeria syndrome
- HHL: Human hormone leptin
- TAT: Transactivator of transcription
- HIV: Human immunodeficiency virus
- HN: Hemagglutinin-neuraminidase
- hn: Heterogeneous nuclear
- HSPG: Heparan sulfate proteoglycan
- hTERT: Human telomerase reverse transcriptase
- I-STEM: Institute for Stem cell Therapy and Exploration of Monogenic diseases (Evry, France)
- i.v.: Intravenous injection
- ICM: Inner cell mass of the blastocyst
- IF: Immunofluorescence
- IGF-1: Insulin-like growth factor 1
- IN: Integrase
- IPLV: Integration proficient lentiviral vectors
- iPSC: Induced pluripotent stem cells
- ISL-1: Insulin gene enhancer protein Islet-1
- ITR: Inverted terminal repeat
- JSRV: Jaagsiekte sheep retrovirus
- kDa: Kilo Dalton
- KFL4: Kruppel-like factor 4
- KGF: Keratinocyte growth factor
- LB: Luria Broth
- LCMV: Lymphocytic choriomeningitis virus
- LHX3: LIM/homeobox protein 3
- LIF: Leukemia inhibitory factor
- LQTS: Long QT syndrome
- LTR: Long terminal repeat
- LV: Lentiviral vector
- MA: Matrix
- mCAT-1: Murine cationic amino acid transporter-1
- MEF: Mouse embryonic fibroblast
- MEM: Minimum Essential Media
- mFISH: Multicolor fluorescent *in situ*

hybridization

- mGSC: Multipotent germline stem cell
- Min: Minutes
- MMLV: Moloney Murine Leukemia virus
- MN: Motor neuron
- MOI: Multiplicity of Infection
- mRNA: Messenger RNA
- MSC: Mesenchymal stem cell
- NC: nucleocapsid (RV)
- NE: Neuroepithelial
- NF: Neurofilament
- NGN2: Neurogenin 2
- NMJ: Neuromuscular junction
- NT: Nuclear transfer
- OCT3/4: POU class 5 homeobox 1
- OLIG2: Oligodendrocyte 2
- ORF: Open reading frame
- p: passage number
- P*:* p value
- P75-NGFR: p75 nerve growth factor receptor
- PAS: Periodic Acid-Schiff
- PAX6: Paired box gene 6
- PB: Phenylbutyrate
- PBS: Phosphate buffered saline
- pbs: primer binding site
- PCR: Polymerase chain reaction
- PD: Parkinson's disease
- PDGFR: Platelet-derived growth factor receptor
- PE: Phycoerythrin
- PEG: Polyethylene glycol
- PEI: Polyethylenimine
- Pen&Strep: Penicillin and Streptomycin
- PFA: Paraformaldehyde
- PGC: Primordial germ cell
- PI: Propidium iodide
- PlatE: Platinum retroviral packaging cell line E
- PLS3: Plastin 3
- PNS: Peripheral nervous system
- PO: Poly-L-Ornithine
- PPIA: Peptidylprolyl isomerase A
- PR: Protease
- ppt: Polypurine track
- qPCR: Quantitative PCR
- qRT-PCR: quantitative RT-PCR
- r: recombinant
- RA: Retinoic acid
- RFP: Red fluorescent protein
- H1LVs: HIV-1 Lentivirus
- RHUL: Royal Holloway-University of London (Egham, UK)
- RNA: Ribonucleic acid
- RNP: Ribonuclear protein
- RPL13: Ribosomal protein L13a
- RPM: Revolutions per minute
- RRE: Rev response element
- RRV: Ross River virus
- RS: Rett's syndrome

- RT-PCR: Reverse transcription PCR
- RT: room temperature
- RTF: Reprogramming transcription factor
- RV: Retrovirus
- s: Seconds
- SAHA: Suberoylanilide hydroxamic acid
- SB: Sodium butyrate
- sc: Self complementary
- SCH: Schizophrenia
- SCID X1: X linked severe combined inmunodeficiency
- SDS-PAGE: Sodium docecyl sulfate polyacrylamide gel electrophoresis
- SEM: Standard error of the mean
- SeV: Sendai virus
- SHH: Sonic hedgehog
- SM: Skeletal muscle
- SMA: Spinal muscular Atrophy/ Smooth muscle actin
- SMC: Smooth muscle cell
- SMN: Survival motor neuron
- SMNt: SMN total
- sn: Small nuclear
- SOX1: Sex determining region Y-box1
- SOX2: (sex determining region Y)-box 2
- SSC-A: Scattered light area
- SSC: Saline-sodium citrate
- ssDNA: Single-stranded DNA
- SSEA: stage specific embryonic gene/antigen
- STR: Short tandem repeats
- SU: Surface protein (RV)
- SV40: Simian virus 40
- TAE: Tris-acetate-EDTA
- TAR: tat response element
- TBS: Tris Buffered Saline
- TE: Tris-EDTA
- TM: Transmembrane protein
- TRA: Tumour related gene/antigen
- trs: Terminal resolution site
- TS: Timothy syndrome
- TSA: Trichostatin A
- TU: transducing units
- TUBA: Alpha tubulin
- TUJ1: Neuronal class III beta tubulin
- UTR: Untranslated region
- VGCC: Voltage-gated calcium channels
- VPA: Valproic acid
- VSMC: Vascular smooth muscle cell
- VSV-G: Vesicular stomatitis virus glycoprotein
- wt: Wild type
- WB: Western blot
- WPRE: Woodchuck hepatitis virus post transcriptional regulatory element
- Ψ: Packaging signal
- Δ7-SMN: Delta seven survival motor neuron (lacks exon 7)

CHAPTER 1: INTRODUCTION AND BACKGROUND OF THE RESEARCH

SPINAL MUSCULAR ATROPHY

1.1.1 SMA PATHOLOGY AND MOLECULAR BASIS

Spinal muscular atrophy (SMA) is an autosomal, recessive, neurodegenerative disease that affects the functionality and survival of lower alpha motor neurons (MNs), resulting in atrophy of skeletal muscles and generalized weakness (**Figure 1.1**). MN cell loss leads to weakness of proximal muscles responsible for crawling, walking, head/neck control, swallowing as well as the involuntary muscles that control breathing and coughing (Buchthal & Olsen 1970; Emery *et al.* 1976; Passini *et al.* 2010). MNs are borne in specific areas of the central nervous system (CNS): in the brain cortex (upper MNs), the brain stem, and in the spinal cord (lower MNs) (Nizzardo *et al.* 2010). Only the functionality and survival of lower alpha MNs is affected in the SMA pathology. SMA is one of the most common genetic cause of infant mortality, affecting approximately 1/10,000 births, with a carrier frequency of approximately 1/50 (Pearn 1980).

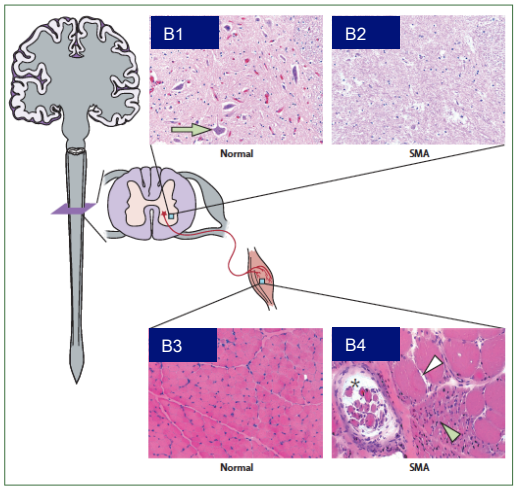

Figure 1.1: Histopathology of SMA.
SMA patients show absence of motor neurons in the spinal cord (B2) and hypertrophic and atrophic fibres in the skeletal muscle (B4). Sections from healthy unaffected patients are shown for comparison (B1 and B3). Taken and modified from (Lunn & Wang 2008).

SMA was first mapped to chromosome 5 (specifically 5q13) in 1990 (Brzustowicz *et al.* 1990). Nevertheless, given that the SMA locus is located in a very unstable region susceptible to intra-chromosomal rearrangements, it was not until 1995 that the exact disease causing-gene was identified: *Survival motor neuron 1* (*SMN1*) (Lefebvre *et al.* 1995). *SMN* is present in multiple copies in the human genome: one *SMN1* (telomeric copy) and several *SMN2* (centromeric copies). The genes differ only by five nucleotides and only one of them is in a coding region, on exon 7. Even though the later nucleotide change does not alter the amino acid sequence, the transition (C to T) is responsible for the alternatively spliced isoform with no exon seven in *SMN2*. Indeed, the transition is localized in an exonic splicing enhancer and the substitution blocks the binding of the U2 class of small nuclear ribonuclear protein (U2 snRNP) (Cartegni & Krainer 2002). This short version of the protein (Δ7-SMN) is thought to be non functional and rapidly degraded (Lorson & Androphy 2000). However, about 10% of the *SMN2* pre-

mRNA is properly spliced and produces functional SMN, which is indiscernible from the one produced from the *SMN1* gene (Lefebvre *et al.* 1995) (**Figure 1.2**).

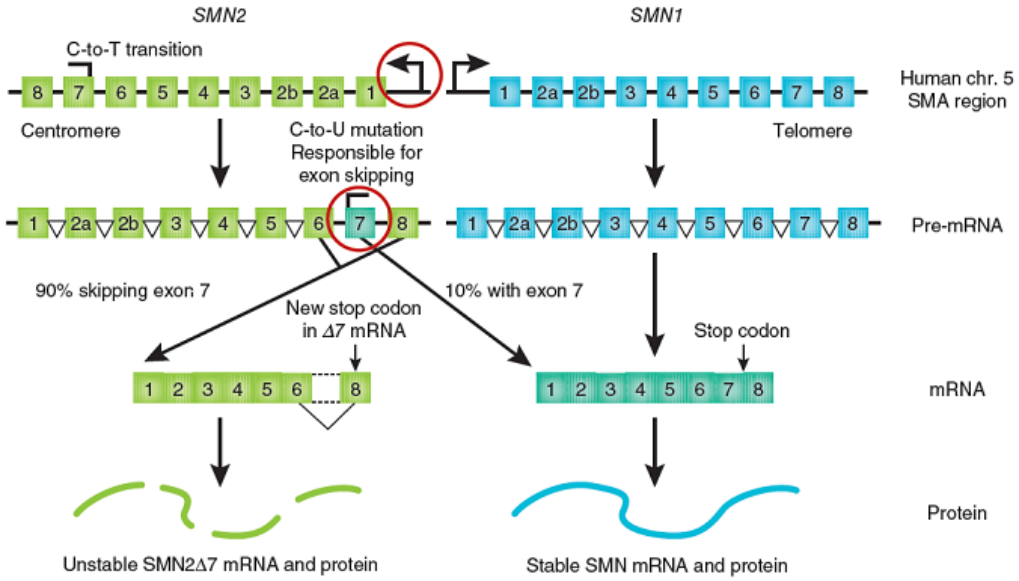

Figure 1.2: *SMN* genes in human chromosome 5.
There are two *SMN* genes in the human genome. *SMN1* produces mainly *FL-SMN*, but *SMN2* only produces 10% of the full length protein due to the presence of a C-to T mutation that causes exon 7 skipping. Taken from *(Sendtner 2010)*.

The molecular cause of SMA is the homozygous disruption of the SMN1 gene by several possible mechanisms (Lefebvre *et al.* 1995; Lunn & Wang 2008). Over 95% of 5q-linked SMA patients have homozygous deletions for the whole SMN1 gene or have gene conversion at exons 7 or 8, whereas the remaining subjects have missense, nonsense or splice site mutations (Alias *et al.* 2009). The severity of the disease is associated with the amount of total SMN protein available and is clinically divided in 4 types mainly grouped by the age of onset and highest motor function achieved (Munsat 1992; Russman 2007). In SMA type I (Werdnig-Hoffman disease), the onset of the disease occurs before the 6 months of age and patients usually die within the first two years of life. SMA type I children present profound and severe hypotonia which prevents them from controlling the movements of the head and generates problems for breathing, swallowing and sucking, as well as a impaired airway protection (which makes them more prompt to infections). In SMA type II patients the onset of the disease is between 6-18 months of age and patients usually die within 10-40 years. SMA2 patients can sit but not stand or walk independently. They also present respiratory insufficiency and weak swallowing. In SMA type III the onset of the disease is after the 18 months of life, but the phenotype is very heterogeneous: some patients walk, some are in wheelchairs and some develop an abnormal shape of the column

(scoliosis). The respiratory function in these patients is not compromised. Finally in SMA type IV, the onset of SMA is during the second or third decade of life and patients only present mild motor impairment (Munsat 1992; Russman 2007).

1.1.2 SMA PROTEIN AND INTERACTIONS WITHIN THE CELLULAR CONTEXT

The full length *SMN (FL-SMN)* has nine exons (eight of which are coding exons), and it encodes a protein of 38 KDa with 294 aminoacids. The protein is present in the cytoplasm and nucleus of all somatic tissues with particular high amount in the MNs of the spinal cord (Lefebvre *et al.* 1997). In the nucleus of the cell, SMN associates with gemins proteins (through direct interaction with gemin2, gemin3, gemin5, gemin7 and gemin8, and indirectly with gemin4 and gemin6) and forms nuclear bodies termed gems which are very similar and often found associated with Cajal bodies, another nuclear structure (Liu & Dreyfuss 1996; Carissimi *et al.* 2006a; Carissimi *et al.* 2006b). Gemin-SMA associations are also found in granules located in growth cones and neural processes of MNs (Fallini *et al.* 2010; Fallini *et al.* 2011).

SMA is a multifunctional protein that has been implicated in a variety of cellular processes, mostly involved in RNA metabolism. The first and most described function of SMN is its ubiquitous role in the splisosome machinery of cells (Meister *et al.* 2002). SMN together with gemins2-8 and unrip proteins forms a macromolecular complex (SMN complex) that functions in the assembly of small nuclear ribonucleoproteins (snRNPs) of both the major and the minor splicing pathways through their interaction with Sm proteins (Pellizzoni 2007). snRNPs are the principal components of spliceosomes, the system in charge of the proper splicing of the pre-mRNAs (Otter *et al.* 2007). There are two splicesomes in the eukaryotic cells, a major one that processes most of the introns in pre-mRNAs and a minor one that processes a small fraction (Brow 2002). SMN complex seems to be particularly necessary for a subset of snRNPs and the lack of SMN preferentially affects the accumulation of U11 snRNP—a component of the minor spliceosome—in tissues of severe SMA mice (Gabanella *et al.* 2007).

The assembly of the snRNPs takes place in the cytoplasm, where Sm proteins (which interact with the SMN complex) combine with snRNAs that are exported from the nucleus. The assembled snRNPs are further modified and then translocated back to the nucleus where they function in pre mRNA splicing (**Figure 1.3**) (Chari *et al.* 2009) . The specific role of SMN, along with gemin 2-6 and unrip (SMN complex) is to recruit Sm proteins and small nuclear ribonucleic acids (snRNAs) and mediate the formation of the Sm core

domain. All this process occurs in the cytoplasm, before the import of the assembled snRNPs into the nucleus (**Figure 1.4**) (Chari *et al.* 2009).

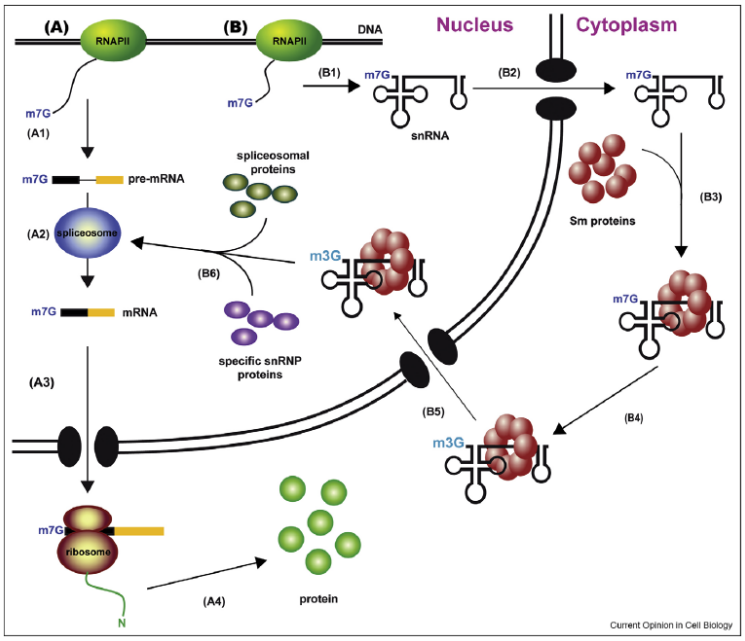

Figure 1.3: snRNPs Biogenesis and pre-mRNA splicing.
Within the nucleus, mRNA is transcribed (**A1**) and spliced (**A2**) before it is further exported into the cytoplasm (**A3**) where it is translated into protein (**A4**). Meanwhile, snRNA is also transcribed (**B1**) and exported to the cytoplasm (**B2**) where it assembles with the Sm proteins to form the snRNP (**B3**). The complex is then hypermethylated (**B4**) and imported back into the nucleus (**B5**) where other proteins are added to the snRNP before its incorporation in the spliceosome (**B6**). SMN complex specifically modulates the step B3. Taken from *(Chari et al. 2009)*.

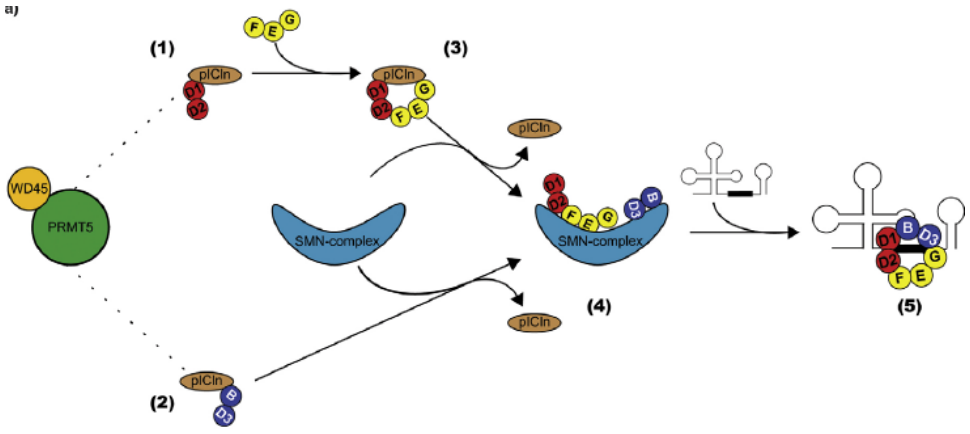

Figure 1.4: **SMN role in the snRNPs assembly.**
The assembly chaperone pICln binds the Sm proteins D1-D2 (**1**), D3-B (**2**), and E-F-G (**3**). These proteins are further transferred to the SMN-complex (**4**) which then recruits snRNA, catalyses Sm ring closure, and releases the assembled RNP (**5**). Taken from: *(Chari et al. 2009)*.

The influence of the lack of SMN in the mRNA processing has been studied *in vitro* and in tissues of mouse models of SMA. The *in vitro* study of Dreyfuss's group (University of Pennsylvania, USA) showed that a dominant-negative mutant SMN inhibited pre mRNA

splicing (and thus mRNA biogenesis), as opposed to wild type SMN (Pellizzoni *et al.* 1998). Furthermore, Pellizoni's group (Dulbecco Telethon Institute, Italy) found that a subset of gemin proteins, as well as the snRNP assembly activity were dramatically reduced in the spinal cord of severe SMA mice and that these reductions were proportional to the severity of the disease (Gabanella *et al.* 2007). Interestingly, this impairment was also found in brain and kidney tissues, although the defects were less pronounced in non-neural tissue.

Even though the results seems to point out that the SMA phenotype is strongly correlated with the snRNP assembly efficacy, it is not really known if the same is true *in vivo* and if so, if there is indeed a defective processing of specific mRNAs that contributes to the preferential vulnerability of MNs to reduced levels of SMN (Rossoll *et al.* 2003; Gabanella *et al.* 2007).

It has been hypothesised than SMN might serve additional functions in the axons of MNs by forming different complexes as the ones traditionally and consistently studied in the cytoplasm for the snRNP assembly (Rossoll *et al.* 2003). Sendtner's group (University of Wuerzburg, Germany) has shown in MNs of SMA mouse models and in differentiated PC12 cells, that SMN associates with heterogeneous nuclear ribonucleoprotein (hnRNP) R and promotes the binding of the later to the 3' untranslated region (UTR) of the β-actin mRNA, influencing by an unknown mechanism the localisation of beta-actin in the growth cones. β-actin plays a major role in growth cone movement and neurite growth. Furthermore, lack of SMN protein or hnRNP causes a significant decrease in neurite length of mouse MNs, which is reversed by their exogenous restoration (Rossoll *et al.* 2003). SMN-hnRNP complex might be involved in the axonal transport of the mRNA, its stability or its translation. Given the length MNs develop in order to accomplish their function in the organism, SMN's influence in β-actin metabolism could explain the cell specificity of this disease.

Apart from SMN localisation in the nucleus, the cytoplasm and the neural processes, SMN has also been localized in the leading edge of neurite outgrowths (growth cones) and in the neuromuscular junctions (NMJs) (Broccolini *et al.* 1999; Fan & Simard 2002). SMN active transport through the axon has also been reported (Fallini *et al.* 2010).

Supporting the idea that SMN forms other complexes that are not related to the splicing machinery, but to the transport of mRNAs along the axon, Bassell's group (Emory University School of Medicine) has demonstrated that SMN interacts with the neuronal-

specific mRNA-binding protein HuD, a protein that binds to AU-rich elements in the 3' UTR of target mRNAs and controls their stability and translation (Tiruchinapalli *et al.* 2008; Fallini *et al.* 2011). Furthermore, SMN and HuD co-localized in actively transported axonal granules and low SMN levels impaired the localisation of HuD and of poly(A)-positive mRNAs specifically in the axons of primary motor neurons, supporting a role for SMN in mRNA trafficking.

It seems logical to think that impaired mRNA trafficking will affect the more distal parts of the cells. In this regard Monani's group (Columbia University) has demonstrated in mouse models of SMA and in human tissues of SMA patients that MNs nerve terminals have pre-synaptic defects (they appeared thick and swollen with abnormal neurofilament (NF) aggregates, poor terminal arborisation, dispersed synaptic vesicles and smaller mitochondria) and that these are correlated with post-synaptic defects in the motor end plate as well (persistence of immature plaque-like acetylcholine receptor [AChR] clusters and presence of its embryonic γ subunit, which is supposed to switch to the ε subunit in the adult) (usaKariya *et al.* 2008). Indeed, electrophysiological recordings showed synapse defects. Surprisingly, there was not an increase of unoccupied endplates as compared to wild type mice. Furthermore, all the defects were found only in α-MNs (which terminate in NMJs) and not in γ-MNs (which terminate in muscle spindles). NF accumulation in the terminal axons of NMJs seems to be a key characteristic of SMA phenotype, but the molecular mechanism has not been properly studied yet. It is important to consider that this feature could very well be a symptom rather than a cause for MN dysfunction, which could also be the case for the absence of β-actin in the growth cones (Cifuentes-Diaz *et al.* 2002).

Another observation that have been highlighted in mouse SMA MNs is that there are defects in the clustering of Cav2.2 channels in axonal growth cones, which are directly associated with a reduced frequency of local Ca^{2+} transients. Furthermore, stimulation of mSmn production from the transgenic *SMN2* gene by cyclic adenosine monophosphate (cAMP) restores Cav2.2 accumulation and excitability (Jablonka *et al.* 2007). It is reasonable to think that these defects could lead to disturbances of active zones in the presynapse, causing reduced transmitter release at the motor endplate. Monani's group has also proposed that reduced levels of calcium in SMA terminals fails to activate calcium proteases at the synapse, eventually causing a build-up of NF protein, which would consequently aggravate the presynaptic function (usaKariya *et al.* 2008).

If we set the facts in order, we could think that by a splicing/stability/transport defect of the β-actin mRNA, as well as other cytoskeletal proteins, the lack of β-actin protein in SMN-deficient MNs interferes with axonal elongation and voltage-gated calcium channels (VGCC) translocalisation to membrane clusters. The alteration in the VGCC could in turn cause NF accumulation by improper activation of proteases and impair transmitter release from the axon terminals finally affecting the global functionally of NMJs and causing the death of MNs.

Taken together, these results suggest that SMN may indeed fulfil neuronal- and muscle-specific functions, providing a more plausible mechanism explaining MN degeneration and associated denervation atrophy of skeletal muscles in SMA (Fan & Simard 2002).

1.1.3 KNOWN MODIFIERS OF SMA PHENOTYPE

As previously mentioned (**Section 1.1.1**), *SMN2* produces ~10% of FL-SMN protein and consequently the *SMN2* gene copy number determines the final amount of this protein when *SMN1* is absent or not functional, constituting the most important clinical prognostic indicator in SMA patients (Wirth *et al.* 2006). In accordance to this, Wirth's group (University of Bonn, Germany) quantified the copy number of *SMN2* in 375 patients with type I, type II, and type III SMA showing a significant correlation between *SMN2* copy number and type of SMA, as well as duration of survival (Feldkotter *et al.* 2002). Their results show that 80% of patients with SMA type I carry one or two *SMN2* copies, 82% of patients with type II SMA carry three *SMN2* copies and 96% of patients with type III SMA carry three or four *SMN2* copies.

The number of *SMN2* copies is indeed variable within the population, which is thought to be derived from the fact that the gene is part of a 500 kb inverted duplication on chromosome 5q13 (involving also *SMN1*), which is susceptible to rearrangements (Lefebvre *et al.* 1995). *SMN* gene duplication is thought to have occurred more than 5 million years ago, but the appearance of *SMN2*, which so far is unique to *Homo sapiens,* seems to have occurred later during evolution (Rochette *et al.* 2001).

Interestingly, the *SMN2* copy number-SMA phenotype correlation has been found not to be as strong as initially thought, suggesting that there must be other proteins apart from SMN involved in the pathology. Several cases have been published supporting this idea. Asymptomatic carriers with bi-allelic deletions of the *SMN1* gene have been found within families where the rest of the siblings are indeed affected, in many cases with different degrees of severity. All the members within each family posses the same copy number of

SMN2 and the same haplotype (Cobben *et al.* 1995; Hahnen *et al.* 1995; Capon *et al.* 1996; Wang *et al.* 1996; Bussaglia *et al.* 1997; Cusco *et al.* 2003; Cusco *et al.* 2006; Jedrzejowska *et al.* 2008). It is important to mention however, that a variant of the *SMN2* gene has been found to produce higher amount of *FL-SMN* transcripts than the amount expressed by the wild type *SMN2* gene, showing that not all *SMN2* genes are the same (Prior *et al.* 2009). Indeed, it has also been shown that *SMN2* alleles are functionally not equivalent due to differences in DNA methylation and that the latter correlates with SMA severity, but a functional basis has not been found (Hauke *et al.* 2009).

Another factor that has been reported as a modifier of the SMA phenotype severity is the levels of plastin 3 (PLS3). Wirth's group (University of Bonn, Germany) found in several discordant families of SMA, that the unaffected siblings showed high levels of *PLS3* in immortalized lymphoblasts, whereas only a small percentage of the affected members and healthy individuals expressed it in these particular cells (**Figure 1.5**). This co-relation was only found in females, and not in males (Oprea *et al.* 2008). It is important to mention nevertheless that *PLS3* is highly expressed in the human foetal and adult spinal cord, even though it is rare in blood cells. Further studies trying to identify the function of PLS3 showed that it promoted axonogenesis by increasing F-actin levels. Actin cytoskeleton dynamics (G-actin/F-actin(G/F-actin) ratio] is know to play a major role in axon growth, path finding, and branching, three vital processes MN function and survival (Dent & Gertler 2003). Indeed, overexpression of *PLS3* rescued the axon length and outgrowth defects associated with *Smn* down-regulation in MNs of SMA mouse and zebrafish embryos. Even though PLS3 and Smn co-localized in axons and growth cones, they did not interact directly, and *PLS3* overexpression alone overcame the SMA phenotype induced by the lack of Smn (**Figure 1.6**) (Oprea *et al.* 2008).

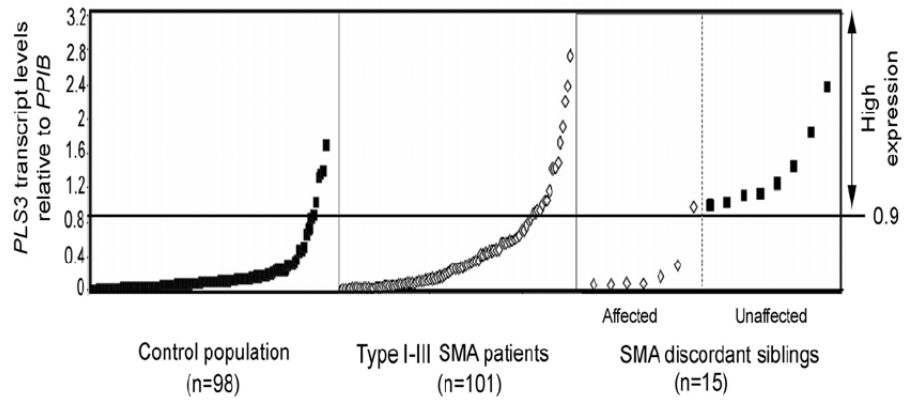

Figure 1.5: *PLS3* expression in blood samples and lymphoblats.
PLS3 expression was measured by qRT-PCR and compared between healthy control individuals, type I-III SMA patients and six SMA discordant families. *PLS3* expression values were empirically defined as high (more than 0.9), low (0.5-0.9) and no expression (less than 0.5). Taken from *(Oprea et al. 2008)*.

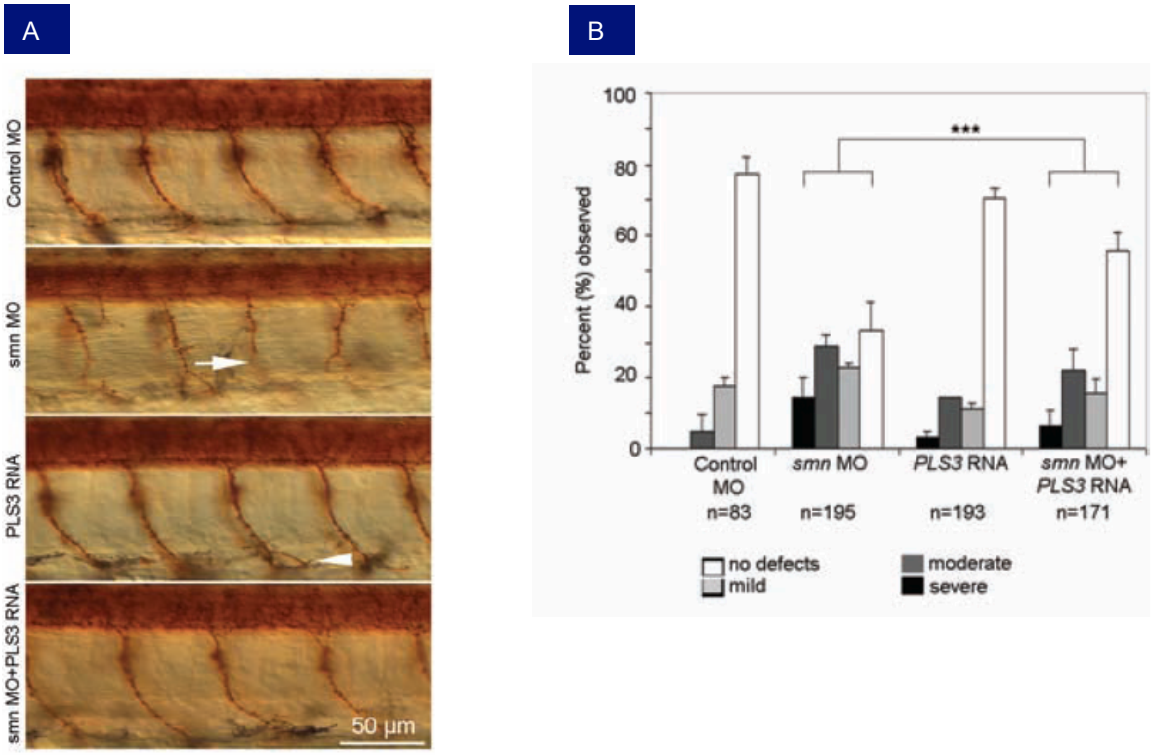

Figure 1.6: Overexpression of *PLS3* rescues SMA phenotype.
(**A**) Zebrafish embryos were treated with control morpholinos (MO), *smn* MO, PLS3 RNA, and smn MO + PLS3 RNA. Pictures taken 36 hours post fertilisation show a severely truncated motor axon in an smn morphant (arrow), and a mild ventral branch in a PLS3 injected embryo (arrowhead). (**B**) Classification of the defects found in embryos. Taken from *(Oprea et al. 2008)*.

1.1.4 CURRENT TREATMENT IN SMA

There is no current curative therapy for SMA, nevertheless current treatment is focused in increasing by several methods the amount of functional SMN in the MNs of the affected patients. The main limitations of these approaches are the heterogeneous responses between

patients in drug-derived therapies and the specific targeting and long lasting SMN expression in MNs for viral-based gene therapies.

Several drugs have been found to increase the expression of the *SMN2* gene and/or to promote the inclusion of exon 7 during *SMN2* pre-mRNA splicing with the subsequent increased translation of the *FL-SMN* transcript into a functional protein (Van Meerbeke & Sumner 2011). The most popular group of drugs are the histone deacetylase (HDAC) inhibitors sodium butyrate (SB) (Chang *et al.* 2001), phenylbutyrate (PB) (Andreassi *et al.* 2004), valproic acid (VPA) (Brichta *et al.* 2003; Sumner *et al.* 2003), suberoylanilide hydroxamic acid (SAHA) (Hahnen *et al.* 2006) and trichostatin A (TSA) (Avila *et al.* 2007) all which have shown to increase FL-SMN protein *in vitro* and in animal models of SMA. VPA and PB were taken to clinical trials without much success (Mercuri *et al.* 2004; Swoboda *et al.* 2010; Kissel *et al.* 2011), but other clinical trials with related drugs are currently in progress.

It is worth mentioning within this category (drug therapy) the use of antisense oligonucleotides (ASOs), modified oligonucleotides that target specific sequences in the *SMN2* pre-mRNA in order to promote the inclusion of exon 7 by blocking the binding of splicing repressors. This potential therapy has shown promising results in SMA mouse models, although repetitive administrations are required (Passini *et al.* 2011). A different drug-derived mechanism to the ones described previously is the one employed by aminoglycosides. These molecules have been shown to induce translational read-through of stop codons in the *SMN2* transcripts giving a longer C terminal to the truncated SMN protein, which is more stable and functional than the shorter Δ7 counterpart (Mattis *et al.* 2009).

The second approach that has been showing very positive results in the past few years is the adeno-associated viral vector (rAAV)-mediated introduction of the complementary DNA (cDNA) of the *SMN1* gene directly into the affected MNs in order to promote the continuous expression of the functional protein. rAAV-mediated *SMN* gene augmentation studies have been performed in SMA mouse models through intravascular injections (Foust *et al.* 2010; Valori *et al.* 2010; Dominguez *et al.* 2011) and intracerebroventricular/intraparenchymal injections (Passini *et al.* 2010). The most successful results have been obtained thought the systemic injection of self complementary AAV serotype 9 (scAAV9s) encoding the therapeutic gene, where complete rescue was achieved (Foust et al. 2010). It is important to mention nonetheless that there seems to be a

unique time frame in which viral gene delivery of this vector through this route is effective, which is associated with the maturation state of the blood brain barrier (BBB) (Foust *et al.* 2009). Moreover, it seems that there is a different transduction pattern in the intravascular delivery method in non-human primates, as well as pre-exiting neutralizing antibodies (Gray *et al.* 2011). New routes of delivery are currently being tested and compared (Glascock *et al.* 2012; Barkats Unpublished data), including the use of new SMA animal models (Duque Unpublished data) .

A third approach for SMA therapy has been proposed by Comi's group (University of Milan, Italy) within a different category: cellular therapy. Comi's group have shown that transplantation of neural stem cells can ameliorate SMA phenotype in mouse models (Corti *et al.* 2008; Corti *et al.* 2010). The mechanism behind the recovery of the animal is not understood, but it seems to come from the support (neuroprotection) of the grafted cells more than from their differentiation into new MNs.

Even though we have gained important insights into the pathology and into the potential reach of various therapies for SMA through the use of animal models, we require alternative systems in which we could systematically study the initiation and progress of the disease in the human context, something that until recently could only be achieved with limited post mortem samples. Several studies have now shown than human MNs can be efficiently obtained from stem cells. Furthermore, the use of a new type of stem cells called "induced pluripotent stem cells or iPSCs" has shown that aspects of several human pathologies can be modelled *in vitro*. As such, iPSCs provide a new and promising platform for the modelling, drug screening and therapeutic designs for SMA.

1.2 INDUCED PLURIPOTENT STEM CELLS (iPSC)

1.2.1 INDUCTION OF PLURIPOTENT STATE

The study of human disease mechanisms, the determination of suitable targets for reversing disease phenotypes and the approaches to effectively reconstitute a cellular function, a defective tissue or even an organ are all issues encountering new possibilities in the last decade. For many years, the most accessible way to study diseases and general mechanisms in the human being was through the use animal models, preferentially mice and rats. During the course of the experiments, scientists have found critical differences between these models and the real situation in the human; either because the cause of the disease is not clearly known and single transgenic modifications do not recreate the pathology, because

the genetic background differs or simply because even by introducing the same genetic defect, the development of the disease is not comparable, frequently presenting a very different physiopathology (Miranda *et al.* 2004; Nelson & Gibbs 2004; Olson *et al.* 2004; Coppola *et al.* 2006; Roep 2007; Dambrot *et al.* 2011; Yazawa *et al.* 2011) *In vitro* models, where the target human cells affected by a disease are cultured in the laboratory, have then come into play to bypass these limitations. Unfortunately cells do not grow in culture as they do inside the organism and many of the primary cells affected by human diseases have a very restricted access due to their nature and localisation, in particular in the case of neurodegenerative diseases (Dimos *et al.* 2008; Ebert *et al.* 2009; Soldner *et al.* 2009). Furthermore, most of cells that can be easily and ethically obtained from a human patient are somatic cells and these are known by their incapability to renew themselves (and thus to be cultured *in vitro*) and for their compromised developmental potential (lineage restriction). Even after immortalisation with genetic/epigenetic modification (which introduces questionable additional variables), many human cell types have never properly been adapted for growth in vitro. Over the past few years it has been discovered that somatic cells can be converted into a pluripotent state, very similar to the one observed in embryonic stem cells (ESCs) derived from the blastocyst, using several mechanisms (**Figure 1.7**) (Amabile & Meissner 2009):

- ✓ Exposure to factors in the enucleated oocyte through somatic nuclear transfer (NT) in order to generate NT-ESCs. This technique besides being highly inefficient also requires the donation of a very large number of oocytes and it has not been achievable in human cells so far (Wilmut *et al.* 1997; Byrne *et al.* 2007; Amabile & Meissner 2009).
- ✓ Exposure to factors expressed in an ESC (or any other pluripotent cell) through fusion and generation of a tetraploid cell. This technique usually requires the use of ESCs obtained from human embryos (with the concomitant ethical and moral issues) and gives rise to a pluripotent hybrid cells with an abnormal karyotype (Tada *et al.* 2001; Cowan *et al.* 2005).
- ✓ Direct reprogramming through over-expression of defined reprogramming transcription factors (RTFs). This recent technique allows the generation of the so-called "induced pluripotent stem cells" (iPSCs), which will be the focus in this project *(Takahashi et al. 2007; Yu et al. 2007).*

✓ Culture induced reprogramming using specific culture conditions for isolated cells from the germ line. This technique has been performed with some success through the use of primordial germ cells (PGC) from human embryos in order to generate embryonic germline cells (EGCs). Unfortunately, the maintained culture has been shown to be prone to spontaneous differentiation (Turnpenny *et al.* 2003). It was later also shown that adult germline stem cells (GSCs) can also be obtained from culture induced reprogramming of spermatogonial cells from adult human testis, bypassing the need to manipulate human embryos (Conrad *et al.* 2008). Recent reports suggest nonetheless, that the later cells are not pluripotent, but only multipotent and very similar to mesenchymal stem cells (MSC) (Chikhovskaya *et al.* 2012).

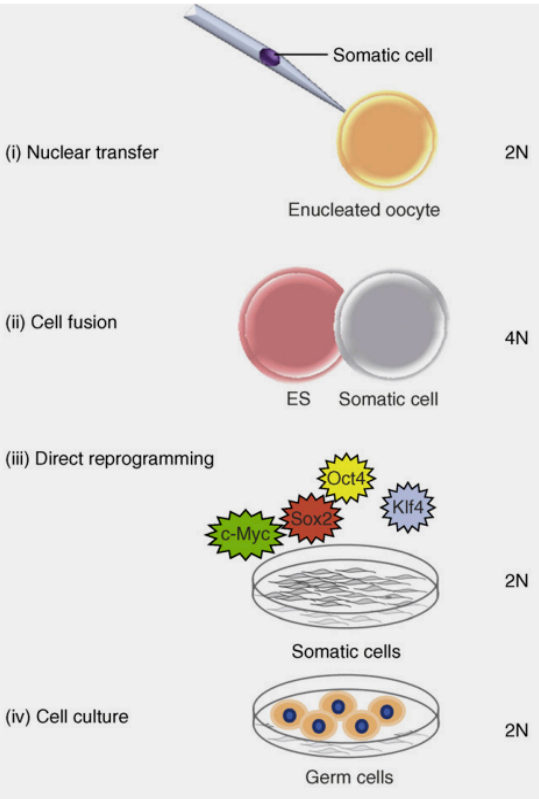

Figure 1.7: Strategies to induce a pluripotent state. Pluripotent cells can be obtained by nuclear transfer from a somatic cell into an enucleated oocyte (**i**); somatic cell fusion with a pluripotent stem cell, such as an ESC (**ii**); ectopic expression of RTFs associated with pluripotency (**iii**) and culture induced reprogramming of cells of the germline. Taken from: (Amabile & Meissner 2009).

1.2.1.1 DISCOVERY OF iPSCS

Of the four previously described techniques, the generation of iPSCs is the most recent and outstanding technology developed in the molecular and cell biology field and its potential has drawn an immense attention from the scientific and medical worlds. In 2006, Kazutoshi Takahashi and Shinya Yamanaka (Kyoto University, Japan) demonstrated that mouse embryonic and adult fibroblast could be reprogrammed into a pluripotent state, very similar to that of the embryonic stem cell (ESC) through the ectopic expression of four RTFs: *OCT4, SOX2, C-MYC* and *KFL4 (Takahashi & Yamanaka 2006)*. A year later these authors published similar results, but this time using the four factors to reprogram adult human fibroblast (Takahashi *et al.* 2007). Each factor was expressed from a different retroviral vector and even though there was a different pattern of integration in each cell, in

all the cases the four retroviruses were strongly down-regulated once the human iPSCs were established. These authors stated in consequence, that ectopic expression was only necessary at the beginning and that once the reprogramming occurred there was an activation and further maintenance of the endogenous expression. The process of reprogramming nevertheless was not understood (Takahashi et al., 2007).

In the same year Thomson's group (University of Wisconsin-Madison, USA) also demonstrated the capacity to reprogram human somatic cells, (IMR90 primary foetal fibroblasts and human newborn foreskin fibroblasts), but using a different combination of lentiviral-delivered factors. While *OCT4* and *SOX2* were still included, *c-MYC* and *KFL4* were replaced by *NANOG* and *LIN28* (Yu et al., 2007). Even though both groups (Yamanaka's and Thompson's) acknowledge the critical role of *OCT4* and *SOX2* on the reprogramming of the cells, the rest of the cocktail seemed to be potentially dispensable. Indeed, it has now been shown that somatic cells can be reprogrammed with as little as one RTF, namely *OCT4*, and that reprogramming efficiency and timing can be modulated by other parameters such as the type of somatic cell to be reprogrammed, the delivery method of the RTFs and the use of small molecules (Kim *et al.* 2009b; Kim *et al.* 2009c).

Initially the selection of factors from both research groups came from the screening of optimal combinations of genes with known enriched expression in human ES cells. *OCT4* also known as *POU class 5 homeobox 1* (*Entrez gene ID 5460*) and *SOX2* also known as *SRY (sex determining region Y)-box 2* (*Entrez gene ID 6657*) are key RTFs that up-regulate genes involved in pluripotency while suppressing differentiation associated genes. It seems that these RTFs are unable to bind to their target genes in differentiated cells because of other inhibitory mechanisms, including DNA methylation and histone modification and here is where the other factors play their role (Takahashi *et al.* 2007). c-*MYC* also known as *v-myc myelocytomatosis viral oncogene homolog* (*Entrez ID 4609*) is an RTF with many downstream targets (more than 25000 potential binding sites) that enhance proliferation and transformation and it also associates with acetyltransferase complexes which could help *OCT4* and *SOX2* to bind to their specific target loci (Takahashi & Yamanaka 2006). Nevertheless, *c-MYC* is extremely oncogenic and mutations, overexpression, rearrangement and translocation of this gene have been associated with a variety of hematopoietic tumours, leukemias and lymphomas (*NCBI, Entrez ID 4609*). *KFL4* also known as *Kruppel-like factor 4* (*Entrez ID 9314*) is a RTF that seems to contribute to the activation of *NANOG* and other ESC specific genes through the repression of the *tumour protein p53*, a

growth inhibitor (*Entrez ID 7157*). NANOG (*Entrez ID 79923*) is one the highest expressed genes in ESCs, since its activity is directly involve in embryonic development, a feature that makes it the preferable marker for the assessment of pluripotency. Finally *LIN28* (*Entrez ID* 79727) is a RTF involved in developmental timing more than in self-renewal. Indeed, it has been found that even though *LIN28* is highly expressed in undifferentiated cells, its overexpression increases differentiation and a slow cell cycle (Darr & Benvenisty 2009). The role of most these RTFs is still poorly understood, a situation that explains why there has been more than one combination of factors able to reprogram somatic cells.

1.2.1.2 METHODS OF REPROGRAMMING

Several methods have been employed for the generation of iPSCs since the first retroviral-based reprogramming; including other integrative approaches with the same retroviral/lentiviral vectors (polycistronic constructs, inducible promoters) (Brambrink *et al.* 2008; Somers *et al.* 2010) and many other non-integrative/excisable methods. The latter category includes: transient plasmid transfection (Okita *et al.* 2008; Yu *et al.* 2009), adenoviruses (Stadtfeld *et al.* 2008), Sendai viruses (Seki *et al.* 2010), and episomal vectors with excisable cassettes containing *loxP* sites (Kaji *et al.* 2009) or the piggyBac transposon (Woltjen *et al.* 2009). iPSC reprogramming using only proteins and a combination of subsets of RTFs and small molecules has also been achieved, although with less success (Huangfu *et al.* 2008a; Kim *et al.* 2009a; Zhou *et al.* 2009). The most successful method developed so far to reprogram iPSCs free of genetic integrations (which was quickly commercialized by Stemgent) is the mRNA transfection method designed by Rossi's group (Children's Hospital Boston, USA) (Warren *et al.* 2010). This method is as efficient as the retroviral reprogramming and is also 100% free of transgenes and vectors, bypassing the need to screen colonies as in the case of excisable methods (Gonzalez *et al.* 2011). Recently, a very different approach has been reported: mouse and human cells were reprogrammed to a pluripotent state by using microRNAs (post-transcriptional regulators) delivered either with lentiviral vectors or by direct transfection, and without the addition of any of the previously described RTFs (Anokye-Danso *et al.* 2011; Miyoshi *et al.* 2011). Each reprogramming method has its advantages and its disadvantages, but the common perspective in the field is the improvement of these methods should aim to fulfil three main criteria: high reprogramming efficiency, absence of integration or genetic modification and simplicity in the methodology. As it can be anticipated some criteria are more or less

important than others, depending on the downstream application: study of reprogramming or differentiation mechanisms, disease modelling or cell therapy *(Gonzalez et al. 2011)*. A diagram of the different reprogramming methods is shown in **Figure 1.8.**

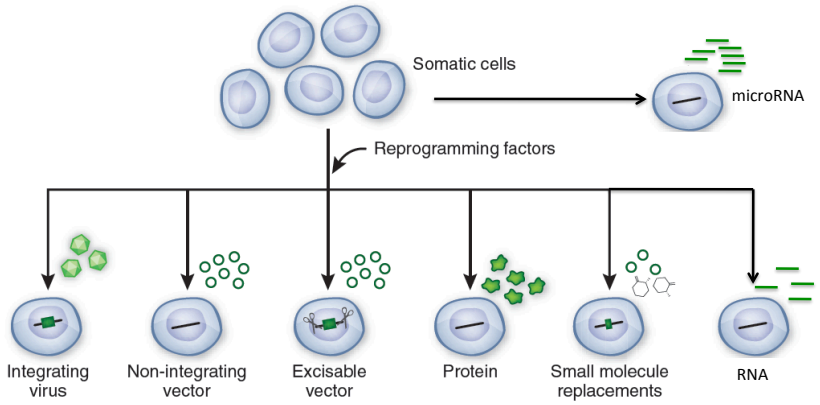

Figure 1.8*:* Methods for the delivery of reprogramming factors.
Diagram showing current integrating, excisable and non-integrating methods for the delivery of reprogramming factors/microRNAs during the generation of iPSCs. Taken and modified from (De Souza 2010)

Independently of the method used for reprogramming, established iPSCs clones should behave like ESCs including aspects such as: morphology, proliferation, surface antigen and RTF expression, methylation status of the promoters of pluripotency genes, telomerase activity and ability to differentiate into representative cells/tissues of the three embryonic layers *in vitro* (through embryoid body) and *in vivo* (through teratoma formation) (Takahashi et al., 2007; De Sousa, 2009*)*. Mouse iPSCs, should also be able to form chimaeric mice with subsequent germline transmission and to produce adult mice by tetraploid complementation assays (Maherali *et al.* 2007; Boland *et al.* 2009; Kang *et al.* 2009).

1.2.2 STEM CELL DIFFERENTIATION

During *in vitro* differentiation of pluripotent stem cells as well as during mammalian development, cells go through a process of differentiation, in which pluripotency pathways are repressed and lineage specific pathways are activated (Boyer *et al.* 2005). The early studies in embryology provide the first knowledge on cell developmental potential and differentiation, and in this regard Waddington´s epigenetic landscape idea, published in his book ¨The Strategy of the Genes¨ in 1957 set the stage for the subsequent studies. The epigenetic landscape is a visual depiction of a set of developmental choices that is faced by a cell in the embryo and according to it, the cells are under the influence of inducing signals that will ultimately lead them to different pathways down the "valley¨, pathways that are

associated with different states of terminal differentiation (Waddington 1957; Slack 2002). A modern version of this idea is depicted in **Figure 9**, where it is also shown how the process of differentiation is accompanied by changes in the epigenetic status of the cell. In a totipotent cell, which is able to give rise to all the cells of an organism, including embryonic and extra-embryonic tissues, there is a global DNA demethylation which is similar to the one observed in pluripotent cells (ESCs from the inner cell mass of the blastocist, EGCs derived from explanted PGCs and iPSC), nevertheless, pluripotent cells are not able to give rise to extra embryonic tissues and can only form a whole organism by tetraploid complementation (Howlett & Reik 1991; Boland *et al.* 2009; Hochedlinger & Plath 2009; Zhao *et al.* 2009). Further along the process of differentiation cells become multipotent, pluripotency genes become methylated and the X chromosome inactivation takes place (Gardner & Lyon 1971; Santos *et al.* 2002). These multipotent or somatic stem cells reside in various organs such as bone narrow, brain, liver, skeletal muscle and dermal tissue (Yoshida & Yamanaka 2010). When the repression of lineage-specific genes starts to get lost, cells acquire a unipotent state in which their developmental potential is compromised to a specific lineage (cell determination and subsequent commitment), such as muscle cells, B cells, macrophages and fibroblast (Hochedlinger & Plath 2009) (**Figure 1.9**).

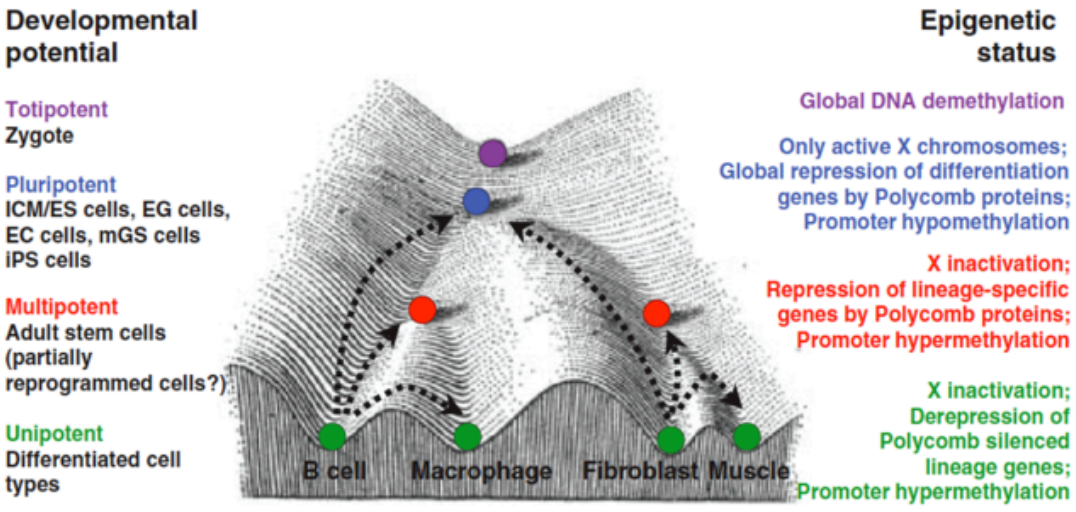

Figure 1.9: Developmental potential and epigenetic states of cells at different stages of development. According to Waddington's model cell differentiation occurs as a ball going down a valley subjected to different forces that influence its course. ICM: inner cell mass. ES cells: embryonic stem cells. EG cells: Embryonic germline cells. EC cells: embryonic carcinoma cells. mGS cells: multipotent germline cells. iPSC cells: induced pluripotent stem cells. Take from: (Hochedlinger & Plath 2009)who took and modified a previous version from (Waddington 1957).
* human mGS cells are not considered pluripotent

Cell differentiation is governed by co expression of cross-antagonist regulatory factors that drive alternative lineage specific programs of gene expression leading to lineage priming (a promiscuous expression in progenitors of transcriptional programs associated with an specific lineage) (Graf & Enver 2009). As cells continue to specialize, there is a different set of cross-antagonist regulatory factors coming into action and the temporal expression of each set has been shown to be important (Iwasaki & Akashi 2007). **Figure 1.10** shows the main differentiation pathways that a pluripotent cell can follow, describing the main cell types derived from the three germ layers: ectoderm, mesoderm and endoderm. As we know by the process of embryogenesis, cells derived from the ectoderm form the outer layer of the skin and the nervous system; cells derived form the mesoderm form the muscles, bones, some organs, the hematopoietic system and the endothelium lining the blood vessels; and cells derived from the endoderm form the lining of the digestive, respiratory and urinary tracts and a number of other organs and glands.

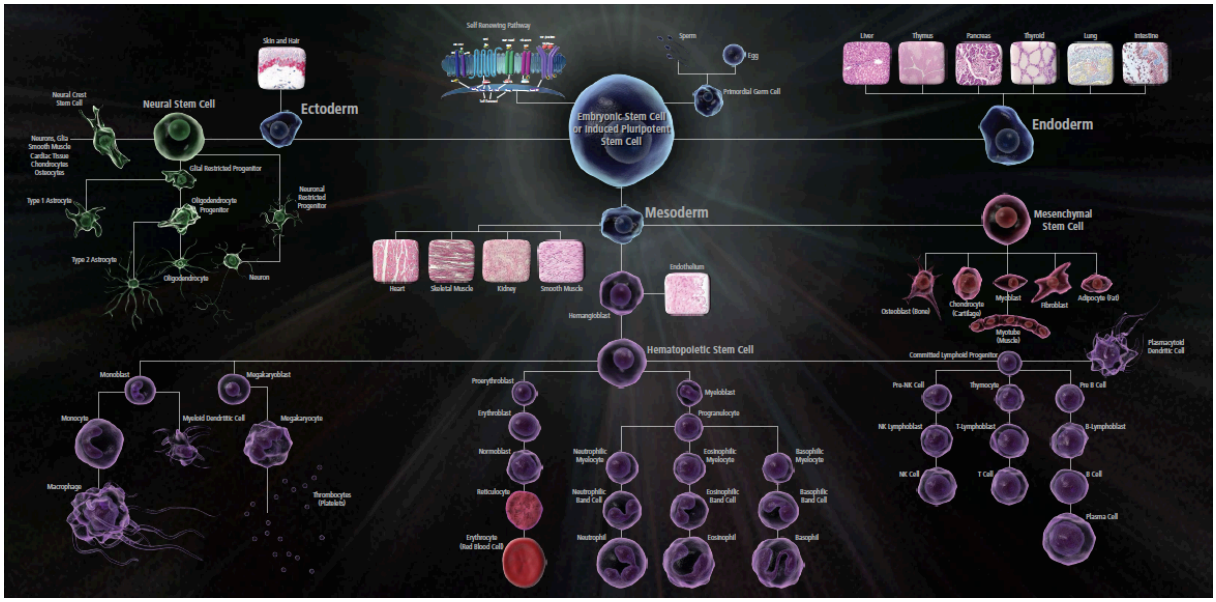

Figure 1.10: Differentiation pathways of a pluripotent cell.
Pluripotent cells differentiate into multiple cellular lineages (and their associated mature cells) of the three germ layers: ectoderm, mesoderm and endoderm. Taken from: BD Stem Cell Resource. Markers of Self-Renewal and differentiation. bdbiosciences.com/stemcell.

A distinct type of situation of that previously described, is the so called "trans-differentiation process", in which there is a conversion of one differentiated cell type into another without any gain in differentiation potential. Such is the case of differentiated B cells reprogrammed to macrophages and embryonic fibroblasts reprogrammed to myoblasts

in the mouse context (Davis *et al.* 1987; Xie *et al.* 2004; Hochedlinger & Plath 2009). These first studies provided the insights that gave birth to a limited list of publications with human cells were lineage-specific RTFs introduced into fibroblasts created cardiomyocyte-like cells (Ieda *et al.* 2010) neurons (Pang *et al.* 2011), and dopaminergic neurons (Caiazzo *et al.* 2011; Pfisterer *et al.* 2011). Other types of "lineage switches" have also been reported.

1.2.2.1 iPSC DIFFERENTIATION AND THEIR USE IN DISEASE MODELLING

In the previously described context, iPSCs have defied all the rules, since they have, taking the previously described Waddington's model as reference, found a way to roll up the valley to then be coaxed to roll down in many different pathways (as opposed to the trans-differentiation process). Many cells have already been repeatedly differentiated from human iPSCs, including, but not limited to: motor neurons (Dimos *et al.* 2008), dopaminergic neurons (Soldner *et al.* 2009; Cooper *et al.* 2010), retinal pigment epithelium cells (Carr *et al.* 2009), astrocytes and oligodendrocytes (Krencik & Zhang 2011; Song *et al.* 2012), mature pancreatic insulin-producing cells (Zhang *et al.* 2009a), hematopoietic progenitors of the myeloid and erythroid lineages (Raya *et al.* 2009), functional osteoclasts (Raya *et al.* 2009), smooth muscle cells (Lee *et al.* 2010), functional cardiomyocytes (Zhang *et al.* 2009b), neuroepithelial, neural crest, endothelial and endodermal cells (Lee *et al.* 2009) and hepatocytes (Song *et al.* 2009).

Furthermore, several diseases have now been modelled through the differentiation of iPSCs generated directly from cells of the patients suffering the pathology. In these studies, iPSCs were differentiated to the cell type affected in the disease, which then showed an expected cellular phenotype or molecular mechanism already seen *in vivo* and not present in a control unafected iPSC line. These studies include: Familial dysautonomia (Lee *et al.* 2009), Parkinson's disease (Soldner *et al.* 2009; Devine *et al.* 2011; Nguyen *et al.* 2011; Seibler *et al.* 2011), Type 1 diabetes (Maehr *et al.* 2009), LEOPARD syndrome (Carvajal-Vergara *et al.* 2010), Friedreich Ataxia (Liu *et al.* 2010), Dyskeratosis congenital (Agarwal *et al.* 2010), Rett's syndrome (Marchetto *et al.* 2010; Cheung *et al.* 2011), Long QT syndrome (Moretti *et al.* 2010; Itzhaki *et al.* 2011; Matsa *et al.* 2011), Schizophrenia (Brennand *et al.* 2011), Hutchinson-Gilford progeria syndrome (Liu *et al.* 2011; Zhang *et al.* 2011), Timothy syndrome (Yazawa *et al.* 2011), Multiple sclerosis (Song *et al.* 2012), Alzheimer's disease (Yahata *et al.* 2011; Israel *et al.* 2012) and of course Spinal muscular

atrophy (Ebert *et al.* 2009; Chang *et al.* 2011; Sareen *et al.* 2012). **Table 1.1** summarizes the methods and findings of several of these disease-modelling studies, as example of what can be achieved with iPSC models.

Table 1.1: iPSC-based human disease modelling and drug screening studies.
Taken from(Tiscornia *et al.* 2011).

Disease	Gene	Cell type	Molecular mechanism	Cellular phenotype	New findings	Drugs tested
ALS	*SOD1*	Neurons; glia	Not well characterized	Neuronal death	–	–
FD	*IKBKAP*	Neurons	Not well characterized	Degeneration; migration defects	Tissue-specific mis-splicing; differentiation defects	Kinetin; tocotrienol
SMA	*SMN1*; *SMN2*	Neurons	*SMN1* downregulation	Motor neuron death	–	Valproic acid; tobramycin
DC	*TERC*	Multiple	Telomerase deficiency	Degeneration	*TERC* locus silenced and has a deletion	–
LQTS	*KCNQ1*	Cardiomyocytes	K^+ pump defect	Long QT interval	Altered cellular localization of KCNQ1	Isoproterenol
RS	*MECP2*	Neurons	Altered Ca^{2+} signaling	Conduction defects	Reduced synaptic connectivity	IGF1; gentamicin
SCH	Polygenic	Neurons	Deficient synaptic activity	Reduced cell size	cAMP and Wnt signaling defects	Loxapine
LQTS	*KCNH2*	Cardiomyocytes	Long QT interval	Conduction defects	–	Cisapride; nifedipine
PD	*LRRK2*	Neurons	α-synuclein aggregates in substantia nigra	Degeneration	Increased oxidative-stress response	ROCK inhibitor
HGPS	*LMNA*	VSMCs	Nuclear envelope defects	Abnormal nuclear lamina	DNAPKc target of progerin	–
TS	*CACNA1C*	Cardiomyocytes	Inactivation of Ca^{2+} pump	Long QT interval	–	Roscovitine
HGPS	*LMNA*	MSCs; VSMCs	Nuclear envelope defects	Differentiation defects; stem cell pool exhaustion	Increased DNA damage calponon; inclusions sensitivity to hypoxia	–

ALS, amyotrophic lateral sclerosis; FD, familial dysautonomia; SMA, spinal muscular atrophy; DC, dyskeratosis congenita; LQTS, long QT syndrome; RS, Rett's syndrome; SCH, schizophrenia; PD, Parkinson's disease; HGPS, Hutchinson-Gilford progeria syndrome; TS, Timothy syndrome; VSMC, vascular smooth muscle cell; MSC, smooth muscle cell.

As described previously, in SMA, the main cell type affected is the MN, more specifically the lower alpha MNs. The differentiation of iPSCs to MNs, which is an extrapolation of the differentiation protocols from hESC to MNs, is based in the same developmental process that these cells go through *in vivo* during embryogenesis and which will be summarized in the following section,

1.2.2.2 MN DIFFERENTIATION

MNs are the postmitotic neurons borne in the CNS and projecting out to the peripheral nervous system (PNS) to control the movement of all the muscles in the body (Ericson *et al.* 1997). They are divided in somatic and visceral MNs (depending on the type of tissue they innervate, skeletal or visceral respectively). Within the somatic MN classification, they are further divided into upper and lower MNs (depending on whether they are located in the brain stem or the spinal cord) as well as in alpha, beta and gamma MNs (depending of the type of fibre they innervate). Alpha MNs are somatic MNs that specifically project their axons toward the skeletal muscle forming a synapse, which is always cholinergic in nature,

called neuro-muscular junction (NMJ) (Bear *et al.* 2007). The study of the generation and degeneration of this cell type in humans has always been hampered by its inaccessibility from human tissues. As a result, most of what is known about MNs in humans is based on studies performed in other organisms, particularly in chicken, and in some limited studies in human embryos (Jessell 2000; Muhr *et al.* 2001; Jakovcevski & Zecevic 2005). After the formation of the three germ layers in the developing embryo, the neuroectoderm gives rise to the neural tube, which makes up the CNS. In general, the specification of different cell types in the neural tube is regulated by the precise spatiotemporal expression of particular genes, which results in a sequential generation of neurons, oligodendrocytes, and astrocytes. Thus, regionalisation along the rostro-caudal and dorso-ventral axes through gradients of signalling molecules (morphogens) is key for defining the identity of the cells in the nervous system (Jessell 2000; Lee & Pfaff 2001). In the rostro-caudal axis, retinoid acid (RA) switches the default anterior state of the cells in the neural tube to a caudal fate, whereas in the dorso-ventral axe sonic hedgehog (SHH) determinates the fate of different domains (Durston *et al.* 1998; Briscoe *et al.* 2000). Indeed, a gradient of SHH generates the organisation of five different progenitor cell domains in the ventral neural tube through the repression and induction of a set of homedomain proteins (class I and II respectively). MNs are generated in the pMN domain (Briscoe *et al.* 2000). The subtype specification of MNs progenitors within the pMN domain, as well as the generic neural differentiation and cell cycle exit is given by the co-expression of the *helix–loop–helix transcription factors oligodendrocyte 2* (*OLIG2*) and *neurogenin 2* (*NGN2*) (Mizuguchi *et al.* 2001; Novitch *et al.* 2001). Once MN progenitors exit the cell cycle, post mitotic MNs are established. Post-mitotic MNs express specific transcription factors such as *homeobox gene HB9* and the LIM homeodomain transcription factor *insulin gene enhancer protein Islet-1* (*ISL-1*) (Pfaff *et al.* 1996; Arber *et al.* 1999). As they mature, post-mitotic MNs also express choline acetyltransferase (ChAT), an enzyme catalysing the synthesis acetylcholine (identifying cholinergic neurons, which in the ventral spinal cord are exclusively MNs) for signal conduction through the NMJs (Wichterle *et al.* 2002; Hu & Zhang 2009).

In vitro, functional maturity of MNs can be evaluated though the assessment of electrophysiological properties, specifically through the presence of fast inactivating sodium currents and the ability to fire action potentials. Functional maturity can also be assessed through MN co-culture with muscle in order to evaluate the formation of NMJs

with features such as the presence of synaptic markers and the induction of the clustering of acetylcholine receptors in the myotubes (Li *et al.* 2005; Li *et al.* 2008; Hester *et al.* 2011). Since there is a temporal pattern in the expression of the transcription factors, gene transfer techniques have provided a very useful approach for the study and follow up of MN differentiation. Furthermore, in the context of disease modelling, many diseases, including SMA are of monogenic, and as such, gene therapy strategies directed towards the affected gene have proven to be successful in the restoration of the normal phenotype in cells differentiated from iPSCs derived from patients (Chang *et al.* 2011). Given the extensive use of gene transfer techniques in the iPSC field, the next section will summarize the current methods for gene transfer, emphasizing the viral systems.

1.3 GENE TRANSFER AND GENE THERAPY

Gene transfer is the exogenous delivery of genetic material (DNA, RNA or a molecule containing both or parts of them) to a cell. This technique has been widely used as a reporter tool by the transference of fluorescent proteins whose transgenic expression is controlled by a cell-type specific promoter (Marchetto *et al.* 2008). When effective reporter expression is the only parameter considered, the selection of the most adequate delivery system will depend mainly in its transfection/transduction efficiency and its sustained expression within the target cell. Likewise, gene transfer is the basis for iPSC reprogramming and coaxed differentiation, but as described previously the method of choice is highly dependable in these cases in the absence of integration or genetic modification if therapeutic approaches are desired (Gonzalez *et al.* 2011; Hester *et al.* 2011).

Gene transfer also constitutes the basis of gene therapy. In gene therapy, the transfer of genetic material aims at the correction of a cellular dysfunction, which has a proven genetic cause or at the provision of a novel cellular function, which can ameliorate or counteract the existing dysfunction (Friedmann & Roblin 1972; Nonnenmacher & Weber 2012). Different gene transfer/ gene therapy delivery systems have been developed so far, including viral vectors (Nanou & Azzouz 2009), naked DNA (Herweijer & Wolff 2003), cationic lipid/DNA complexes (Abe *et al.* 1998) and cell encapsulation (Orive *et al.* 2003). Particularly, viral vectors have received a lot of attention because of their natural ability to infect human cells. Up to date, there are 1843 clinical trials using gene therapy, 1218 of

which are based on viral vectors, particularly on adenovirus and retrovirus (Wiley Last updated June 2012).

For clarity, all the names of wild type viruses and recombinant viral vectors will be preceded by a "wt" and a "r" respectively. When referring to both types, no letter will be used.

Several viral vectors have been studied for the treatment of numerous diseases, especially cancer, but viral-based gene therapy studies for neurological diseases evolving to clinical trials, currently account for a much smaller percentage, with Parkinson's being the most studied so far (Feigin *et al.* 2007; Kaplitt *et al.* 2007; Eberling *et al.* 2008; Marks *et al.* 2008; Herzog *et al.* 2009; Marks *et al.* 2010). Unfortunately, viral vectors have encountered important obstacles that have raised doubts about the safety of their use over the past few years (Deakin *et al.* 2009). One of the most well known cases was the human gene transfer study conducted by Alain Fischer in France to correct X linked severe combined inmunodeficiency (SCID X1) (Hacein-Bey-Abina *et al.* 2003). In this study, autologous CD34+ cells were transduced with a replication-incompetent Moloney murine leukemia viral vector (rMMLV) carrying the common gamma chain transmembrane protein subunit gene shared by the receptors of six different interleukins. Even though this has been until recently one the most successful trials in gene therapy, showing an impressive improvement in most of the children treated, there were four unfortunate cases in which insertional mutagenesis at or near oncogenes occurred, causing T cell leukemia 31–68 months after gene therapy (Hacein-Bey-Abina *et al.* 2003; Hacein-Bey-Abina *et al.* 2008). rAAV, nonetheless, has recently shown very positive results in several clinical trial for the treatment of Leber congenital amaurosis, an inherited eye disease leading to retinal degeneration. So far no significant secondary effects have been found (Jacobson *et al.* 2012; NIH).

Ever since the observation of the first adverse events, much of the gene therapy research in viral vectors has been focused in finding a way to bypass the safety issues, related mainly to integration of the viral DNA in the host genome and the immunotoxicity, without compromising the activity and efficiency of the encoded transcript/protein. One of the major discussions about the safety of viral vectors is strongly related to the features and properties of each of them and their original source. Each viral vector studied so far, has shown relevant advantages and disadvantages, and the selection depends mainly on the

target cell, whether or not integration occurs, the cloning capacity, the elicited immunogenicity and the transduction efficiency (**Table 1.2**) (Nanou & Azzouz 2009).

Table 1.2: Characteristics of the most common vectors used in gene therapy.
Taken and modified from: *(Nanou & Azzouz 2009)*.

Vector	Insert size (kb)	Expression	Advantages	Disadvantages
Adeno-associated virus	4.5 (not all serotypes)	Stable	Little immunogenicity; *integrates; transduces nondividing cells	Small cloning capacity
Adenovirus	36	Transient	High viral titer; wide host-cell range; transduces nondividing cells	Immunogenicity; does not integrate; short-term expression
Retrovirus	8	Stable	No immune response against the vector; integrates	Low viral titers; transduces only dividing cells; variable expression
Lentivirus	8	Stable	Transduces nondividing cells; high transduction efficiency	Potential safety risk
Herpes simplex virus	>30	Stable	Large cloning capacity; transduces nondividing cells; wide host-cell range	Safety concerns; short-term expression; possibly immunogenic
Vaccinia virus	186	Transient	High expression, best for immunization strategies	Transient expression; transduces only dividing cells; safety concerns

*** Wild type AAV integrates, but recombinant AAV rarely does**

Adenoviral vectors (rAd) and retroviral vectors (rRVs) have been the most commonly used vectors so far in gene therapy, but their high immunogenicity and high integration frequency respectively, have motivated the research and development of other type of viral vectors. In this regard, and specifically considering the context of neurodegenerative diseases, even though adeno-associated viral vectors (rAAV) have only been used in 4.9% of the clinical trials in gene therapy (*Gene Therapy Clinical Trials Wordwide, updated in June 2012*), the findings from Kaspar´s group where an rAAV9 is able to bypass the BBB after intravenous injection in a mouse model, has drawn an increased attention to these viral vectors, particularly to serotype 9 *(Foust et al. 2009)*. In fact, as described before, *in vivo* rAAV9 transfer of h*SMN1* has already been shown to rescue SMA in mouse models (Foust *et al.* 2010; Valori *et al.* 2010; Dominguez *et al.* 2011). In the current study I employed three different viral vectors for gene transfer including rAAV9. The other vectors used belong to the *Retroviridae* family and they were used for iPSC reprogramming and iPSC-derived MN identification respectively: rMMLVs and HIV-1 based lentiviral vectors (rH1LVs). Their structure, cell cycle, recombinant production and transduction pattern are described in the following sections.

1.3.1 VIRAL VEHICLES FOR GENE TRANSFER

1.3.1.1 AAVs

1.3.1.1.1 wtAAV structure

wtAAV is a small non-enveloped virus that belongs to the Dependovirus genus of the Parvovirus family. The single stranded DNA viral genome is approximately 4.7 Kb in length, and it is composed of two open reading frames (ORF) flanked by two inverted terminal repeats (ITR) (Ding *et al.* 2005) (**Figure 1.11 A**). The 5' ORF (*rep*) encodes 4 replication proteins generated from two different promoters: Rep 78 and Rep 68 which are translated from the p5 promoter and Rep52 and Rep40 which are translated from the p19 promoter; each pair or proteins differ by alternative splicing (Virag *et al.* 2009). The 3' ORF (*cap*) encodes 3 capsid proteins VP1, VP2, and VP3, generated through alternative mRNA splicing and alternative start codon usage (Ding *et al.* 2005). VP1 is translated from an ATG codon on the 2.4 Kb mRNA, while VP2 and VP3 are translated from the 2.3 Kb mRNA, using a weaker ACG start codon for VP2 (amino acid T138) and a read through translation to the next ATG codon for VP3 (amino acid M203), the most abundant capsid protein (Warrington *et al.* 2004) (**Figure 1.11B**).

The ITR 's at both ends of the genome contains 145 nucleotides organized in a T shape hairpin structure, a feature that allows the genome to replicate itself without the need to synthesize a primer (**Figure 1.11C**). ITRs are required in *cis* for gene expression, DNA synthesis, rescue from integrating genomes and packaging of the DNA into preformed capsids (Hermonat & Muzyczka 1984; Berns 2007). ITRs contain a terminal resolution site (trs), which is cleaved by rep proteins in order to replicate monomeric copies of the wtAAV genome (McCarty 2008). ITRs seem to be the only necessary viral component in recombinant vector genomes since they are the only requirement for packaging DNA into capsids (Ding *et al.* 2005; Schultz & Chamberlain 2008).

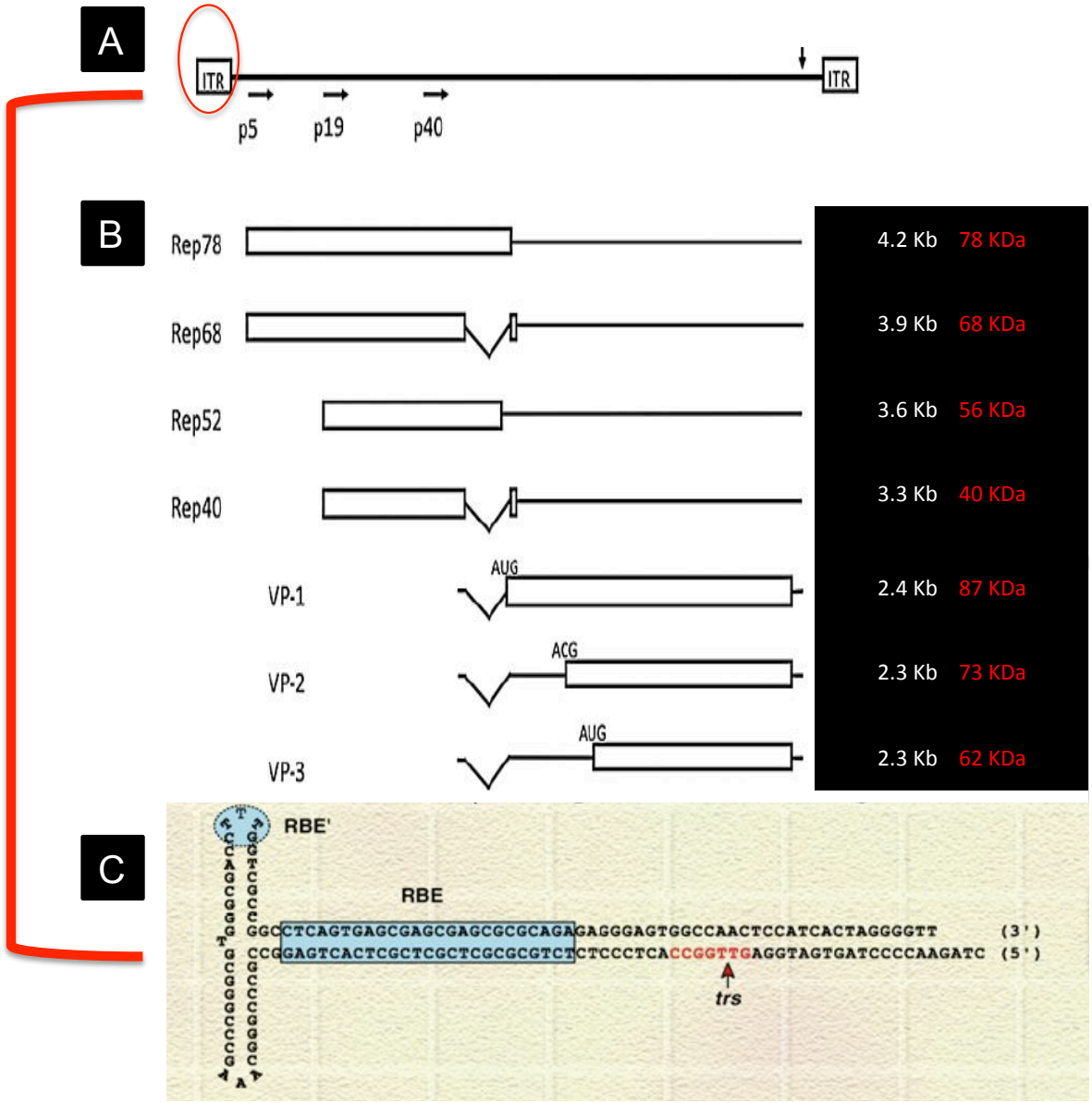

Figure 1.11: wtAAV structure.
(**A**) Complete wtAAV genome. (**B**) Proteins translated from the two open reading frames, REP and CAP: Rep78, Rep68, Rep52, Rep40, VP-1, VP-2 and VP-3. (**C**) Detailed map of the structure of the ITRs. RRE/RRE': Rep binding element. Trs: terminal resolution site. Taken and modified from (Berns 2007; Virag *et al.* 2009).

1.3.1.1.2 wtAAV cell cycle

Most of the studies in wtAAV and have been performed in the serotype 2 (wtAAV2), comprising the understanding of events ranging from virus-cell attachment through vector genome conformation in the target cell and expression patterns (Schultz & Chamberlain 2008). wtAAV enters the cell through attachment or binding to specific receptors and co-receptors, and each serotype has its own, although some are shared between two or more serotypes **(Table 1.3)** (Schultz & Chamberlain 2008; Nonnenmacher & Weber 2012). Interestingly, the specific transduction behaviour of the serotype 9 after systemic

administration has shown that by some unknown mechanism, these viral vectors (like no other wtAAV serotype described so far) are able to enter the cells that form the BBB without un-coating, being then released on the other side of this barrier where they are able to infect the adjacent cells (Foust *et al.* 2009). Nevertheless, not obvious mechanism can be explained by the currently known wtAAV9 receptors/co-receptor: the 37/67-kDa laminin receptor and N-linked glycans with terminal galactosyl residues (Akache *et al.* 2006; Shen *et al.* 2011)**.** After binding to the cell receptor, the most common entry mechanism for wtAAV is through receptor mediated endocytosis in clathrin coated vesicles, which is followed by intracellular trafficking of the virus through the endosomal compartment, endosomal escape, nuclear import, virion un-coating and viral genome conversion into double stranded DNA (dsDNA) (Ding *et al.* 2005). The process of wtAAV trafficking before nuclear import is still controversial and it seems that the mechanism differs between and within serotypes (Ding *et al.* 2005; Schultz & Chamberlain 2008; Nonnenmacher & Weber 2012). After the conversion of the wtAAV genome into dsDNA, and in the absence adenoviruses or herpes viruses (helper viruses), wtAAV integrates into a specific site in chromosome 19 called AAVS1 through the interaction of the wtAAV ITR´s and the rep protein (lysogenic pathway) *(Howarth et al. 2009).* In the presence of helper viruses, the wtAAV genome is excised from the host cell chromosome for replication and packaging. The further generation of new particles of wtAAVs, requires the assembly of 60 units of the three structural proteins (VP1 87 kDa, VP2 73 KDa and VP3 62 kDa) of the capsid in an approximate ratio of 1:1:18 (Warrington *et al.* 2004). Nevertheless, It has been shown that AAV-like particles can also be formed with VP3 alone (Rabinowitz *et al.* 1999; Warrington *et al.* 2004). Since Rep proteins and wtAAV DNA co-localized with the capsids in intra-nuclear area outside the nucleoli, it is now commonly accepted that wtAAV packaging and assembly occurs in the nucleus instead of the cytoplasm (Wistuba *et al.* 1997; Warrington *et al.* 2004). After packaging, the newly assembled particles are released through helper virus-induced cell lysis (Goncalves 2005).

1.3.1.1.3 rAAV production

Based on the knowledge of wtAAV, rAAV has been designed using a two or a three plasmids transfection method in HEK293T cells, which enhances the safety of the viral vectors produced through this technology (Xiao *et al.* 1998). Since the ITRs are the only structures necessary in *cis* for wtAAV rescue, replication and packaging, the wtAAV genome is split in two plasmids for recombinant production: one plasmid contains the

transfer/therapeutic gene (between 4.1 and 4.9 kb) flanked by the two ITRs, and the second plasmid contains the CAP and REP genes (Dong *et al.* 1996; Goncalves 2005).

Given that wtAAV is a replication defective virus, a third element is required. In order to avoid the use of wild type adenovirus/herpes virus, current rAAV production requires co-transfection with a helper plasmid (derived from the sequences of the wildtype helper virus) to supply the necessary genes to produce viable particles (Xiao *et al.* 1998). Between the helper plasmid and the producer cell, the following molecules should be provided: (i) early genes E1A, E1B, E2 and E4 for trans-activation of viral regions, modification of host cellular and immunological environment, enhancement of viral gene expression over host protein synthesis and initiation of viral replication, and (ii) untranslated RNAs (VA RNA´s) for combatting the cellular defence mechanisms by blocking activation of the interpheron response (Howarth *et al.* 2009) (**Figure 1.12**).

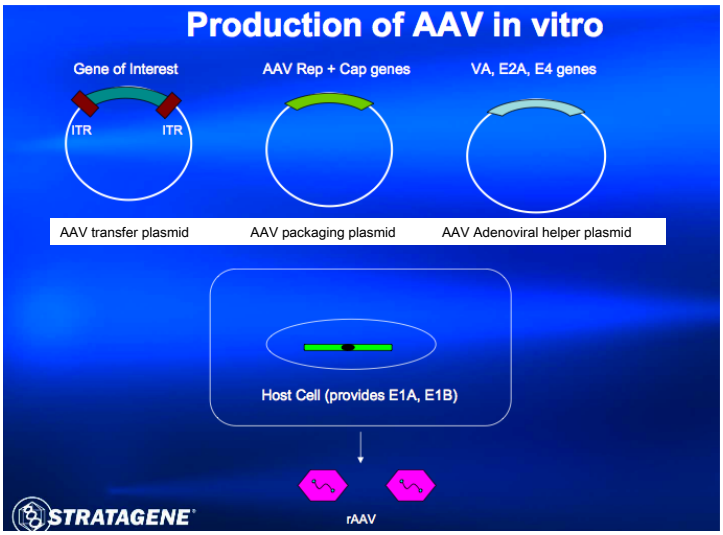

Figure 1.12: General outline of rAAV production *in vitro*.
For rAAV production, a transfer plasmid containing the gene of interest flanked by the wtAAV ITRs is co-transfected with a packaging plasmid containing the open reading frames of REP and CAP and a helper plasmid containing the adenoviral genes into HEK293T cells. Taken and modified from: (White).

In the absence of a helper virus/plasmid during transduction, AAV establishes a long lasting infection within the cell, which is predominantly characterised by persistent episomal forms in circular concatamers, and in rare cases by integration events (Wu *et al.* 2006; Schultz & Chamberlain 2008).

1.3.1.1.3.1 Self-complementary adeno-associated viral vectors (scAAV)

Once inside the nucleus, one of the limiting steps regarding effective transduction with rAAV is the conversion of single stranded DNA (ssDNA) into double stranded DNA (dsDNA). Recently, this step has been bypassed by the development of scAAV (Wu *et al.* 2006). In scAAV, the terminal resolution site of one of the ITR **(Figure 1.13**) is deleted so the resolution is inhibited and dimeric genomes are formed and packed into virions in the producer cell (**Step 5d, Figure 1.13**). One important disadvantage of this technique however is that the coding capacity of the vector is reduced to 50% in order to accommodate the duplicated genome (McCarty 2008). The increase in efficiency gained by the scAAV varies from moderate to impressive depending on the tissue, cell type and route of administration. It is also important to consider that in the case of the CNS, higher transduction efficiency does not have an important impact if the virus does not reach widespread distribution, as it usually occurs due to the presence of the BBB. This means that even if the viral vectors have a very high probability of getting into target cells in a free environment (like an *in vitro* culture), the overall efficiency of the gene delivery will be mostly determined by the ability of the virus to reach all the cells in the target region (and not just a very restricted zone) from the site of injection, as it is the case in an *in vivo* scenario.

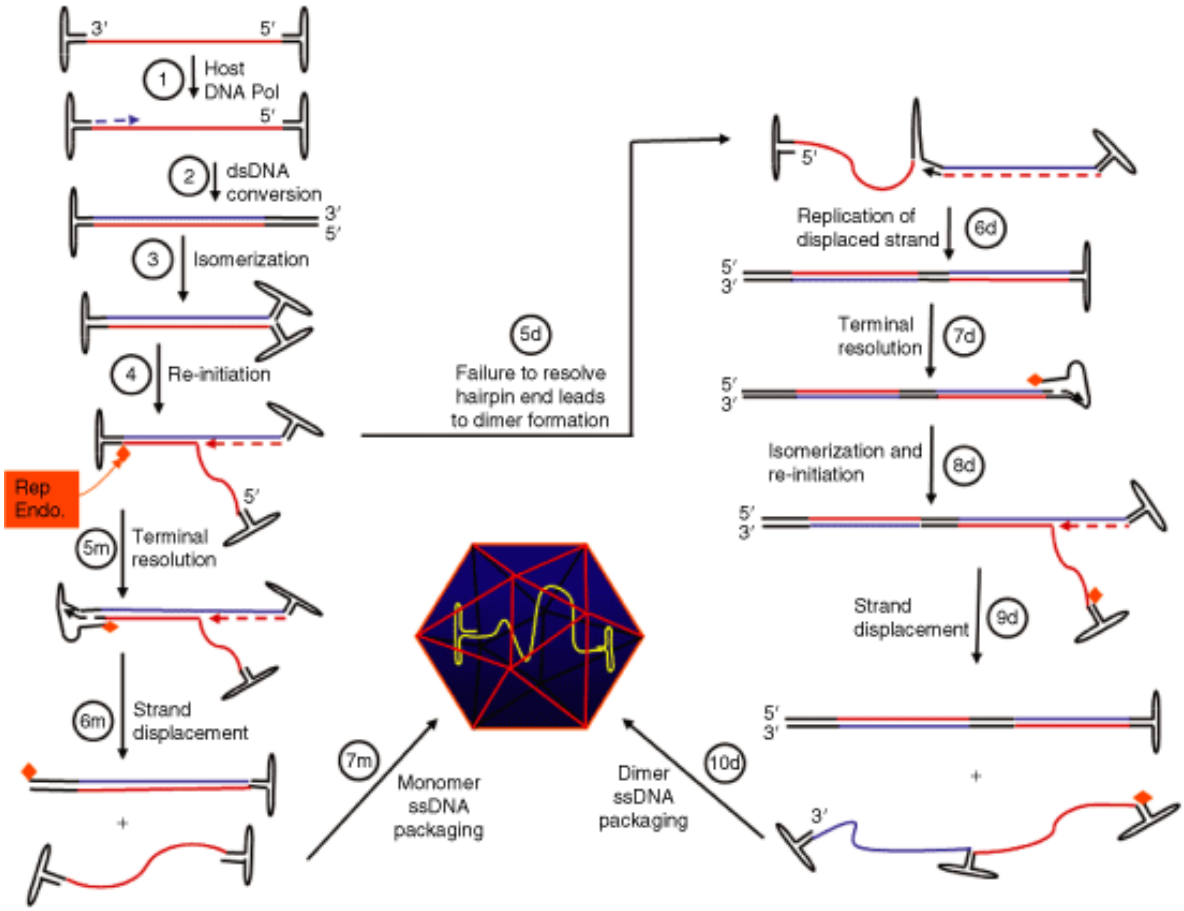

Figure 1.13: Formation of dimeric inverted repeats genomes during scAAV replication.
ssDNA virion enters the host-cell nucleus and the 3´ ITR acts as a primer for host DNA polymerase. The 3´-ITR primer is elongated, displacing and replicating the ITR at the 5´ end (**1**). The duplex ITR is re-folded into a double-hairpin configuration by host or viral DNA helicase, forming a new primer for DNA synthesis (**2**). While the 3´-ITR is elongated and the complementary strand displaced, AAV Rep protein recognizes and binds to the ITR at the downstream end (**3**). To generate complete monomeric genomes, Rep endonuclease nicks the trs of the downstream ITR, initiating a second DNA replication complex, to copy the ITR before being reached by the complex initiated at the other end (**4**). The original replication complex displaces the daughter strand, including the newly synthesized ITR, and completes replication to the end of the genome, recreating the template for isomerisation in step 3 (**5m**). The displaced single-stranded genome is packaged into the AAV capsid (**6m**). Dimeric genomes are generated when Rep fails to nick the trs before being reached by the replication complex from the other end (**7m**). Replication continues through the ITR (**5d**), and the displaced strand, to generate a dimeric dsDNA template (**6d**) which can initiate a new round of DNA synthesis either by isomerizing the open end (as in step 4) or by terminal resolution of the hairpin end (**7d**). Further isomerisation after terminal resolution allows priming of DNA synthesis from the resolved end (**8d**), and replication of the dimeric template displaces a single-strand dimeric inverted repeat genome (**9d**), which can then be packaged into the AAV virion (**10d**). Taken from (McCarty 2008).

1.3.1.1.4 AAV transduction patterns

There are 12 known human serotypes of AAV, which are grouped according to their functional and immunological characteristics. The only exception to this rule are serotypes 1 and 6, whose capsids differ only in six aminoacids and which have been found to be immunologically indistinguishable from each other (Gao *et al.* 2004; Schultz & Chamberlain 2008). AAV9 is the one of most recent serotypes discovered. This serotype

was found in isolates from 3 humans in 2004 by James Wilson's research group through the recovery and sequencing of full-length capsid genes by PCR in tissue samples (*GenBank: AY530579.1*). In this same study the transduction efficiency *in vitro* and *in vivo* of AAV2 pseudotyped with different capsids were compared and it was found that even though AAV9 had the highest transduction efficiency *in vivo* in liver, lung and muscle tissues, its *in vitro* efficiency was low (less than 40%), contrary to what was seen for AAV2 (Gao *et al.* 2004) (**Figure 1.14**).

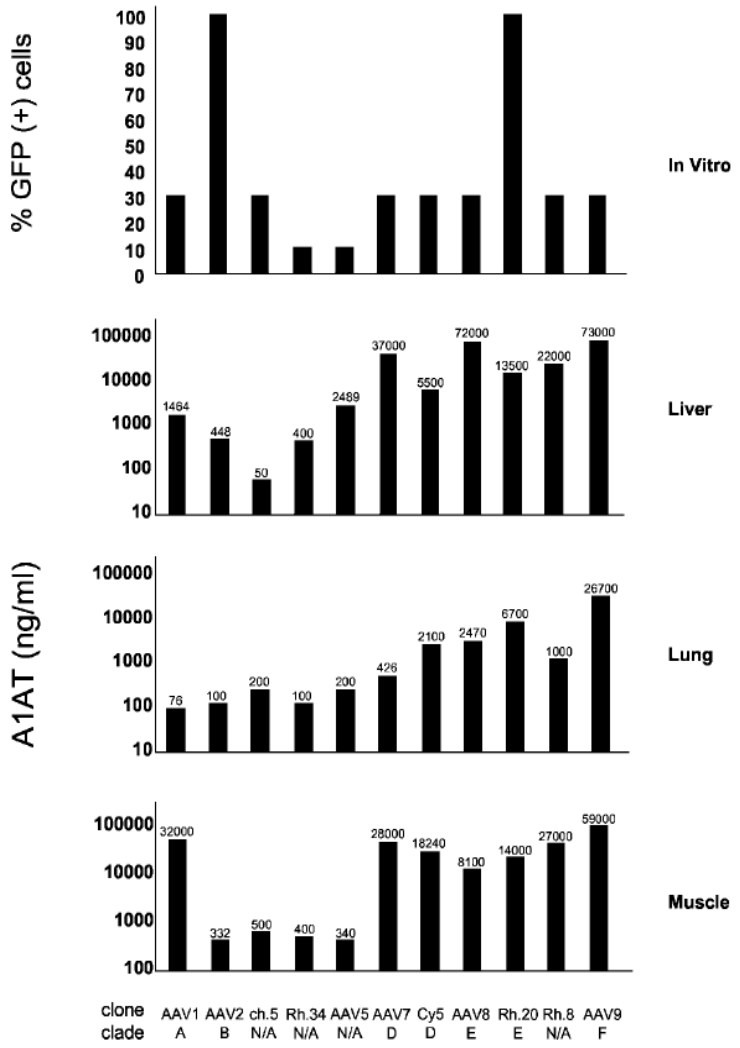

Figure 1.14: Transduction efficiency of novel primate rAAV-based infections *in vitro* and *in vivo*.
For *in vitro* transductions, a construct encoding the green fluorescent protein (GFP) was used and the efficiency is expressed as percentage of GFP+ cells. For *in vivo* transductions a construct encoding Human α- antitrypsin (A1AT) was used and the efficiency is expressed as the concentration of this protein in serum samples. Taken from *(Gao et al. 2004)*.

The evaluation and comparison of transduction efficiencies have been looked at in several studies. In general AAV2 is known to transduce a wide range of tissues with moderate efficiency while the other serotypes have less tropism but higher efficiency of transduction (Wu *et al.* 2006; Schultz & Chamberlain 2008). For AAV9 a high transduction have been reported in striated muscle (heart), liver, pulmonary system, retinal pigmented ephitelium,

pancreas CNS and skeletal muscle (Inagaki *et al.* 2006; Allocca *et al.* 2007; Vandendriessche *et al.* 2007; Foust *et al.* 2009; Yu *et al.* 2011). **Table 1.3** presents an updated list of the preferential (not unique) tissue tropism of different serotypes along with their know receptors/co-receptors.

Table 1.3: AAV receptors and preferential tissue tropism**.**
Taken from *(Nonnenmacher & Weber 2012).*

Virus	*Glycan receptor*	*Co-receptor/other*	*Tissue tropism*[a]
AAV1	N-linked sialic acid[122,123]	Unknown	SM,[124] CNS,[125] retina,[126] pancreas[127]
AAV2	HSPG[25]	FGFR1,[26] HGFR,[30] LamR,[29] CD9 tetraspanin[128]	VSMC,[129] SM,[130] CNS,[131] liver,[132] kidney[133]
AAV3	HSPG[18]	FGFR1,[134] HGFR,[135] LamR[29]	Hepatocarcinoma,[136] SM[124]
AAV4	O-linked sialic acid[137]	Unknown	CNS,[138] retina[139]
AAV5	N-linked sialic acid[137,140]	PDGFR[141]	SM,[124] CNS,[138] lung,[142] retina[126]
AAV6	N-linked sialic acid,[123] HSPG[122]	EGFR[143]	SM,[144] SM (i.v.),[145] heart,[24] lung[146]
AAV7	Unknown	Unknown	SM,[23] retina,[147] CNS[148]
AAV8	Unknown	LamR[29]	Liver,[23] SM,[23,149] CNS,[148] retina,[147] pancreas,[150] heart[149]
AAV9	N-linked galactose[151]	LamR[29]	Liver,[152] heart (i.v.),[152,153] brain (i.v.),[154] SM (i.v.),[155] lungs,[156] pancreas,[153] kidney (i.v.)[156]

Abbreviations: AAV, adeno-associated virus; CNS, central nervous system; EGFR, epidermal growth factor receptor; FGFR1, fibroblast growth factor receptor 1; HGFR, hepatocyte growth factor receptor; HSPG, heparan sulfate proteoglycan; i.v., intravenous injection; PDGFR, platelet-derived growth factor receptor; SM, skeletal muscle; VSMC, vascular smooth muscle cell.
[a]Preferential tissue tropism following local delivery, unless otherwise indicated.

It seems that the difference in the transduction efficiency of different serotypes is associated with differences in cellular uptake and intracellular trafficking and that this difference is associated with the structural architecture of the capsid (Wu *et al.* 2006).

1.3.1.2 RETROVIRAL VECTORS (RVs)

1.3.1.2.1 wtRVs structure

wtRVs are enveloped ssRNA viruses belonging to the *Retroviridae* family. Within this family, several genus and species have been vectorised and converted into efficient gene transfer tools. wMMLVs are part of the *Gammaretrovirus* genus and are considered simple wtRVs, whereas wtH1LVs belong to the *Lentivirus* family and are considered complex retroviruses (Vogt 1997). Structurally, lentiviruses (wtLVs) contain the same genes as simple wtRVs do, but six more genes are also present. The ssRNA of all wtRVs is approximately 7-13 Kb in length and it is composed of three genes, *gag, pol, env*, flanked by two long terminal repeats (LTRs) (Goff 2006) (**Figure 1.15**). The mRNA of wtRVs is translated in different ways for different species, but in general long polyproteins have to be cleaved by viral-encoded proteases to produce individual proteins (Kay *et al.* 2001). The *gag* gene encodes the matrix (MA), the capsid (CA) and the nucleocapsid (NC); the *pol* gene encodes the protease (PR), the retro-transcriptase (RT) and the integrase (IN); and the

env gene encodes the surface protein (SU) and the transmembrane protein (TM). wtH1LVs also encode the genes *Vif, Vpr, Tat, Rev, Vpu* and *Nef,* but only *Tat,* and *Rev* are essential for effective viral replication. (Goff 2006).

The LTRs at both ends of the RNA genome are formed by the two unique sequences "U5" at the 5' end and "U3" at the 3' end. Both of these sequences are followed by a repeat sequence "R". LTRs are necessary in *cis* during viral gene expression, packaging, retro-transcription and integration of the genome (Kay *et al.* 2001). Other important retroviral elements are the primer binding site (pbs), the polypurine track (PPT), the rev response element (RRE) and the packaging signal (ψ) which are involved in viral replication, nuclear export and packaging (Goff 2006).

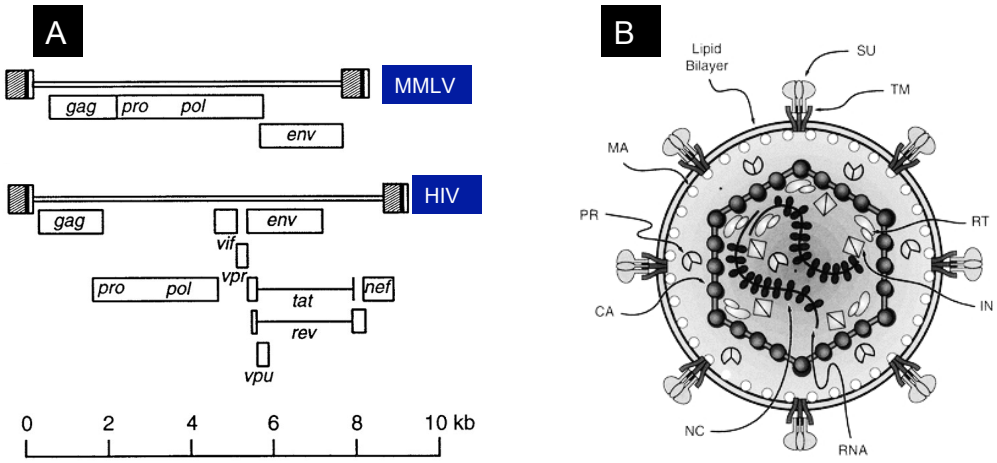

Figure 1.15: Structure of RVs.
(**A**) Genetic organisation of wMMLVs and wHILVs. The fragments of the genome corresponding to different open reading frames are shown for each protein. A scale for genome sizes is shown at the bottom of the panel. Long terminal repeats (LTRs) are located at each end (gray boxes) (**B**) General schematic diagram of retroviruses. The viral envelope is formed by a cell-derived lipid bilayer in which the transmembrane (TM) and the surface (SU) components of the envelope are inserted. They matrix (MA) capsid (CA) and nucleocapsid (NC) proteins form the structural proteins of the virion. The particles are packaged along with their reverse transcriptase (RT), integrase (IN) and protease (PR). Taken and modified from (Vogt 1997).

1.3.1.2.2 wtRV cell cycle

wtRVs have a complex life cycle, which includes ssRNA-dsDNA conversion where many elements are involved. The general steps can be described as follow: (1) wtRVs enter the cell via receptor-mediated fusion with the cellular membrane. (2) Once inside the cytoplasm, the virus un-coats and reverse transcription occurs. (3) The dsDNA is trans-located to the nucleus where it integrates into the host genome as a provirus. (4) Once integrated, the viral genome is transcribed and full length as well as spliced RNAs are produced and exported out of the nucleus. (5) Viral component are translated and (6) full-length genomes are package, budding out the cellular membrane where the envelope

proteins are anchored. (7) Proteolytic process occurs within the assembled particle to give rise to the viral core proteins (Cepko & Pear 2001; Dornburg 2003).

1.3.1.2.3 rRV production

As in the case of rAAVs, rRVs require the splitting of the viral genome in several plasmids. Several strategies have been developed so far for this purpose, but in general, one plasmid contains the LTRs and other necessary sequences in *cis* (PBS, PPT, ψ, and RRE in the case of LVs) along with the gene of interest, whose expression is driven by its own promoter in modern vectors. The rest of the genes are usually split in two or more plasmids. In the case of simple RVs such as MMLVs for example, cell lines stably expressing the *gag, pol* and *env* genes can be used to produce rRVs by the unique transfection of the transfer plasmid (Cell Biolabs 2008). The most recent and safest system developed so far for a rRVs is the non integrating, self inactivating, third generation rLV production, which is a variant of standard LVs **(Figure 1.16)** (Dull *et al.* 1998; Zufferey *et al.* 1998; Philippe *et al.* 2006; Yanez-Munoz *et al.* 2006). For this:

- ✓ The viral genome is split in four plasmids: a packaging plasmid encoding the *gag* and *pol* genes under a CMV promoter, a rev plasmid encoding the rev protein for nuclear export; an envelope plasmid encoding the desired envelope protein; and a transfer plasmid with the gene of interest.
- ✓ The active site of the *integrase* gene has been mutated
- ✓ Wild-type copies of the HIV LTR are replaced: (i) the U3 in the 5' LTR was replaced by an alternative enhancer/promoter, thus rendering the virus replication tat independent (ii) the U3 in the 3' LTR has been partially deleted, which results in inactivation of both viral LTRs after transduction and reverse transcription.
- ✓ A splice donor site is added between the 5' LTR and the internal promoter in order to splice out the ψ and RRE elements.

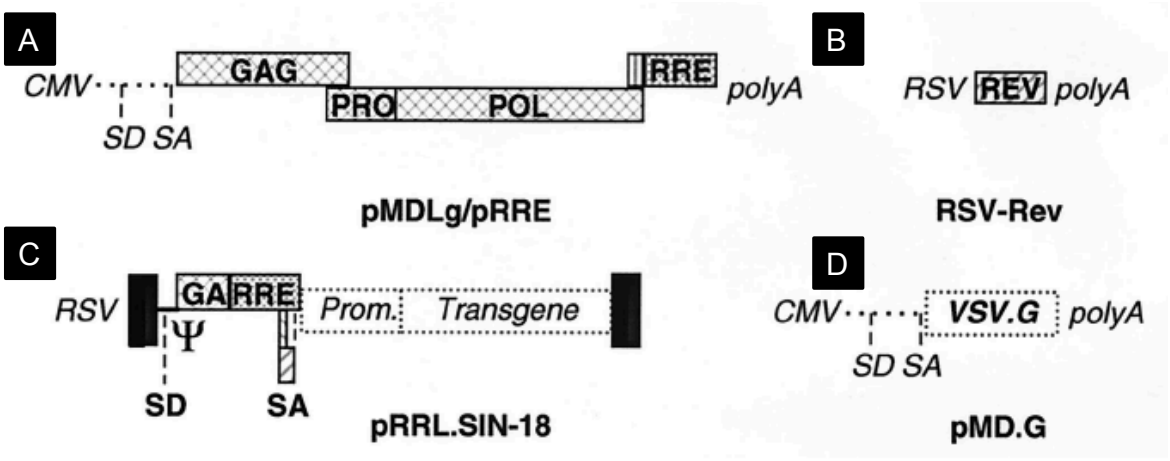

Figure 1.16: Third generation rLVs production.
Four plasmids are necessary for rLV production. The pMDLg/pRRE plasmid (**A**) encodes the viral core proteins gag and pol. The RSV-Rev (**B**) and the pMD.G (**D**) plasmids encode the Rev protein and the envelope protein respectively. The pRRL.SIN-18 (**C**) constitutes the transfer plasmid with a chimeric 5 prime LTR containing the Rous Sacoma Virus (RSV) enhancer/promoter. SD: splice donor site; SA: splice acceptor site. In non-integrating rLVs, the integrase is mutated (*pol* gene) Taken from *(Dull et al. 1998)*.

1.3.1.2.4 RV transduction patterns

The main functional difference between LVs and simple RVs is that the former can efficiently infect dividing and not diving cells, whereas the latter can only infect dividing cells (Goff 2006). The molecular basis for this difference is a subject of controversy, but it is clear that in simple RVs the pre-integration complex (PIC), which mediates the nuclear import of the viral dsDNA, requires the disruption of the nuclear membrane during mitosis (Miller *et al.* 1990).

The envelope of all rRVs can be substituted by another from a different virus in a process called pseudotyping *(Kay et al. 2001)*. The most frequently used pseudotype is with the G glycoprotein of the vesicular stomatitis virus (VSV-G)**,** which can infect most cells through an interaction with what it seems to be an ubiquitous cellular "receptor", the identity of which is still a matter of debate (Akkina *et al.* 1996; Naldini *et al.* 1996; Reiser *et al.* 1996; Coil & Miller 2004). In fact, VSV-G pseudotyping has become the standard to which other pseudotypes are compared to (Cronin *et al.* 2005).

Since LV can transduce non-dividing cells, many of the transduction efficiency studies using rRVs have been performed with them. rLVs pseudotyped with VSV-G are particularly good in transducing hematopoietics stem cells *ex vivo* (Guenechea *et al.* 2000; May *et al.* 2000)and CNS *in vivo* (Yanez-Munoz *et al.* 2006). **Table 1.4** summarizes the preferences of the most common rLVs pseudotypes.

Table 1.4: Tropism of rLV pseudotypes.
Taken from (Cronin *et al.* 2005)

Target cell/organ	Glycoprotein	Remarks
Liver	VSV-G	Toxicity issues
	LCMV	Non-toxic, less inflammatory
	RRV	Tropism for nonhepatocytes (Kupffer cells)
	SeV F	
Lung	Ebola	Transduction of apical surface airway epithelium
	Marburg	
	SeV F and HN	
	JSRV	
Pancreatic islet cells	LCMV	Non-toxic
CNS	VSV-G	Targets primarily neurons
	LCMV	Targets astrocytes
	Rabies	Targets neural progenitor/stem cells
	Mokola	Retrograde transport from periphery to CNS
		Retrograde and anterograde transport within CNS
		Conflicting evidence regarding retrograde and anterograde transport
Retina	VSV-G	Transduces photoreceptors and retinal pigment epithelium
	Mokola	Restricted to retinal pigment epithelium
Myocytes/muscle	Mokola	Transduces cardiomyocytes in utero
	Ebola	Transduces cardiomyocytes in utero
Hematopoietic system	RD114	More efficient and less toxic than VSV-G
	GALV	Increased serum stability
Cancer cells	GALV	Fusogenic glycoprotein
	LCMV	Preference for malignant glioma cells

VSV-G: G glycoprotein of the vesicular stomatitis virus; LCMV: lymphocytic choriomeningitis virus; RRV: Ross River virus; SeV: Sendai virus; F: fusion protein; HN: hemagglutinin-neuramonidase; JSRV: Jaagsiekte sheep retrovirus; GALV: gibbon ape leukemia virus.

1.4 AIMS OF THIS STUDY

1.4.1 GENERAL AIM

To establish human iPSC-derived models that allow the developmental and functional study of SMA, particularly in MNs from a discordant SMA family.

1.4.2 SPECIFIC AIMS

- ✓ To generate iPSCs from human fibroblasts of five members of a discordant SMA family using rMMLVs as vehicles to deliver Yamanaka´s set of reprogramming factors.
- ✓ To assess the efficient reprogramming of selected iPSC clones from each family member through quality control tests and features such as hESC morphology, expression of hESC surface and nuclear markers, down-regulation of transgenic expression, *in vitro* differentiation potential, karyotype stability and genotype analysis.
- ✓ To differentiate selected iPSC clones from each family member, as well as one iPSC clone from a SMA type I patient and one iPSC clone from an unaffected control individual into MNs.
- ✓ To generate rH1LVs carrying a reporter gene under the control of the MN specific HB9 promoter in order to follow and quantify the generation of MNs during iPSC-MN differentiation.
- ✓ To evaluate potential SMA phenotypes during iPSC-MN differentiation, as well as in the derived MNs through the assessment of the MN proportion within the culture, neurite length, and formation of the NMJ.
- ✓ To follow the expression of SMN isoforms and PLS3 at the transcriptional and translational levels during the iPSC-MN differentiation process in clones from unaffected individuals and SMA patients.
- ✓ To compare PLS3 mRNA and protein levels between iPSC-derived MNs in order to determine if PLS3 could be a modifier factor in the discordant SMA family.
- ✓ To generate scAAV9s carrying a human *SMN1* transgene in order to study the SMN expression profile after the restoration of the gene in iPSC-derived MNs from the SMA type I patient.

CHAPTER 2: MATERIALS AND METHODS

2.1 MATERIALS

All reagents, chemicals, buffers, plasticware, cells, culture media, enzymes, DNA and protein size makers, kits, unmodified plasmids, primers, antibodies, instruments and software are listed in this section along with more detailed descriptions in the appendix section.

2.1.1 REAGENTS AND MOLECULES

All reagents whose characteristics are similar between manufacturers and formats are listed in "General reagents" Appendix 1. All reagents whose specific composition, activity and/or functionality are variable between manufacturers and/or between formats from the same manufacturer are shown in "Special reagents and media components" Appendix 1. The latter list includes all components and small molecules used for making up media (section 2.1.9). All tissue culture related molecules were sterilized by filtration with a 0.22 μM pore filter in a class II biosafety cabinet class.

2.1.2 BUFFERS AND SOLUTIONS

2.1.2.1 BUFFERS FOR WESTERN BLOT (WB)

- ✓ 10X WB Migration buffer: 0.25 M Tris-HCl, 1% SDS, 1.92 M glycine, pH 8.3. Prior to use, the buffer was diluted 10 times in ddH20.
- ✓ 10X TBS buffer: 0.5 M Tris-HCl, 1.5 M NaCl, pH 7.5. Prior to use, the buffer was diluted 10 times in ddH20. For washing membranes, Tween-20 was added at a final concentration of 0.1% (TBS-T).
- ✓ 10X WB Transfer buffer: 0.48 M Tris-HCl, 0.37% SDS, 0.39 M glycine, pH 8.3. Prior to use, the buffer was diluted 10 times in ddH20 and methanol (the final concentration of methanol was 20%).
- ✓ WB Blocking buffer: 5% dry milk in TBS.
- ✓ WB 5X Loading buffer: 250 mM Tris-HCl, 50mM DTT, 10% SDS, 0.5% bromophenol blue, 50% Glycerol, pH 6.8.
- ✓ Lower buffer for sodium dodecyl sulfate polyacrylamide gel electrophoresis (SDS-PAGE): 1.5 M Tris-HCL, 0.4% SDS, pH 8.8. To prepare two 12% resolving gels the following solutions were mixed: 4 ml 30% Acrylamide/Bis-acrylamide, 2.5 ml lower buffer, 3.5 ml ddH20, 100 μl 10% APS, 10 μl TEMED.
- ✓ Red Ponceau solution: 0.1% Ponceau S, 1% acetic acid.
- ✓ RIPA buffer: 50 mM Tris-HCl, 1% NP-40, 0.25% Na-deoxycholate, 150 mM NaCl, 1

mM EDTA, pH 7.4. RIPA buffer was supplemented just before use with fresh protease inhibitor cocktail (cOmplete ULTRA Tablets, Mini, EDTA-free, Roche, Cat No. 05892791001).

- ✓ Upper buffer for SDS-PAGE: 1.0 M Tris-HCl, 0.8% SDS, pH 6.8.To prepare two 5% resolving gels the following solutions were mixed: 0.83 ml 30% Acrylamide/Bis-acrylamide, 0.63 ml upper buffer, 3.6 ml ddH20, 50 µl 10% APS, 5 µl TEMED.

2.1.2.2 BUFFERS FOR BACTERIAL WORK

- ✓ Competent cells-Buffer 1: 30 mM KOAc, 100 mM $RbC1_2$, 10 mM $CaCl_2$, 50 mM $MnC1_2$, 15% glycerol, pH 5.8.
- ✓ Competent cells-Buffer 2: 10 mM MOPS/KOH, 75 M $CaC1_2$, 10 mM $RbC1_2$, 15% glycerol, pH 6.5.

2.1.2.3 BUFFERS AND SOLUTIONS FOR IMMUNOFLUORESCENCE/ FLOW CYTOMETRY

- ✓ 10X Tris Buffered Saline (TBS) buffer: 0.5 M Tris-HCl, 1.5 M NaCl, pH 7.5. Prior to use, buffer was diluted 10 times in ddH20. For washing IF stainings in coverslips, Tween-20 was added at a final concentration of 0.1 % (TBS-T).
- ✓ 10X Phosphate buffered saline (PBS) buffer: 1.47 M NaCl, 26.8 mM KCl, 75.2 mM Na_2HPO_4, 17.64 mM KH_2PO_4, pH 7.4. Prior to use, buffer was diluted 10 times in ddH20.
- ✓ IF Blocking buffer: 0.5% BSA in 1X PBS for cells culture in tissue culture plates and 10% BSA, 0.1% Tween-20 and 0.4% Triton X-100 in 1X TBS for cells cultured in coverslips.
- ✓ 4% Paraformaldehyde (PFA) fixative: 4% PFA in 1X TBS, pH 7.3.

2.1.2.4 BUFFERS AND SOLUTIONS FOR rAAV PRODUCTION

(All these solutions were sterilized either by filtration through a 0.22 µM pore filter or by autoclave at 15psi, 121◦C for 20 minutes [min])

- ✓ AAV cell lysis buffer: 0.15M NaCl, 1M Tris-HCl, pH8.5.
- ✓ 2xHBS: 100 mM HEPES, 281 mM NaCl, 1.5 mM Na_2HPO_4, pH 7.12.
- ✓ AAV Precipitation buffer: 40% PEG8000, 2.5 M NaCl.
- ✓ 5X PBS-MK buffer: 5 mM $MgCl_2$ and 12.5 mM KCl in 1XPBS.
- ✓ Iodixanol gradient 15%: 25% Optiprep density gradient medium and 1M NaCl in 1X PBS-MK buffer.

- ✓ Iodixanol gradient 25%: 41.6% Optiprep density gradient medium and 0.2% phenol red in 1X PBS-MK buffer.
- ✓ Iodixanol gradient 40%: 66.6% Optiprep density gradient medium in 1X PBS-MK buffer.
- ✓ Iodixanol gradient 60%: Optiprep density gradient medium (neat), 0.2% phenol red.
- ✓ Proteinase K buffer 2X: 20 mM Tris pH8, 20 mM EDTA, 1% SDS.
- ✓ Tris-EDTA (TE): 10 mM Tris-Cl, pH 7.5, 1 mM EDTA, pH 8.0.
- ✓ Dot blot re-suspension buffer: 0.4M NaOH,10 mM EDTA, pH 8.0.
- ✓ 20x saline-sodium citrate (SSC) buffer: 1.5 M NaCl, 0.3 M Na3 citrate. Prior to use, the buffer was diluted ten times in ddH20.
- ✓ Dot blot primary wash buffer: 6M urea, 0.4% SDS, 0.5x SSC.

2.1.2.5 BUFFERS FOR iPSC-RELATED PROCEDURES

- ✓ Carnoy fixative: 3:1 methanol/acetic acid
- ✓ Hypotonic solution: 5.6 mg/ml KCl
- ✓ Sudan solution: 0.5% sudan III and 0.5% sudan IV in a solution of 35% ethanol/50% acetone. The solution was filtered and protected from light.

2.1.2.6 BUFFERS FOR DNA AND RNA-RELATED PROCEDURES

- ✓ 10X Tris-acetate-EDTA (TAE) buffer (DNA): 0.4 M Tris-HCl; 10 mM EDTA, pH 8.5. Prior to use, buffer was diluted 10 times in ddH20.
- ✓ 10X Formaldehyde (FA) buffer (RNA): 200 mM 3-[N-morpholino]propanesulfonic acid (MOPS), 50 mM sodium acetate, 10 mM EDTA, pH to 7.0. Prior to use as running buffer, it was diluted 10 times in 0.5 M formaldehyde RNAse free H20.

2.1.3 PLASMIDS

All plasmids used, including the ones modified and generated during this project, are described in this section:

- ✓ **pMIG-h*OCT4*:** retroviral transfer plasmid encoding the human *OCT4* cDNA linked to an internal ribosome entry site (IRES) *green fluorescent protein (GFP)*. This plasmid was originally produced in Dr. George Q Daley's laboratory (Harvard Stem Cell Institute, USA) and it was used in *Park et al., 2008* for the generation iPSCs. It is now available through Addgene (Cat. No. 17225).
- ✓ **pMIG-h*SOX2*:** retroviral transfer plasmid encoding the human *Sox2* cDNA linked to an IRES *GFP*. This plasmid was originally produced in Dr. George Q Daley's

laboratory (Harvard Stem Cell Institute, USA) and it was used in *Park et al., 2008* for the generation of iPSCs. It is now available through Addgene (Cat. No. 17226).

- ✓ **pMIG-h*KLF4*:** retroviral transfer plasmid encoding the human *Kfl4* cDNA linked to an IRES *GFP*. This plasmid was originally produced in Dr. George Q Daley's laboratory (Harvard Stem Cell Institute, USA) and it was used in *Park et al., 2008* for the generation of iPSCs. It is now available through Addgene (Cat. No. 17227).
- ✓ **pMSCVh*cMYC*IRES*GFP*:** retroviral transfer plasmid encoding the human *cMyc* cDNA linked to an IRES *GFP*. This plasmid was originally produced in Dr. John Cleveland's laboratory (St. Jude Children's Research Hospital, USA) and it was used in *Park et al., 2008* for the generation of iPSCs.
- ✓ **p5E18-VD2/9:** rAAV9 packaging plasmid encoding the AAV2 rep gene and the AAV9 capsid gene. This plasmid was initially obtained from Dr. Jim Wilson (University of Pennsylvania, USA) and provided by Prof. George Dickson (Royal Holloway, University of London, UK).
- ✓ **pAdDeltaF6:** adenoviral helper plasmid for rAAV production encoding the adenoviral genes required for the generation of rAAV particles. This plasmid was initially obtained from Dr. Jim Wilson (University of Pennsylvania, USA) and provided by Prof. George Dickson (Royal Holloway, University of London, UK).
- ✓ **pscAAVCage*GFP*:** self complementary AAV (scAAV) transfer plasmid with the expression cassette contained between two AAV2 inverted terminal repeats. The original pscAAVCag backbone (Yue & Dongsheng 2002) was used to generate the pscAAVCage*GFP* encoding the green fluorescent protein (eGFP) kindly provided by Dr George Dickson (Royal Holloway, University of London, UK). The e*GFP* in this plasmid is driven by a short version of ubiquitous cytomegalovirus enhancer/ chicken beta actin promoter (CAG promoter).
- ✓ **pscAAVCagh*SMN1*F:** scAAV plasmid generated through the insertion of a flag-tagged version of the human *Survival Motor Neuron 1* (h*SMN1*) cDNA in the pscAAVCage*GFP* backbone, replacing *eGFP*.
- ✓ **pscAAVCagh*SMN1*NoF:** scAAV plasmid generated through the insertion of the h*SMN1* cDNA in the pscAAVCage*GFP* backbone, replacing *eGFP*.
- ✓ **pCCLsc_HB9_e*GFP*_W:** third generation recombinant lentiviral (rLV) transfer plasmid encoding the green fluorescent protein (eGFP) under the control of a short version of the motor neuron-specific HB9 promoter. This plasmid is a kind gift from

Fred Gage's laboratory (Salk Institute, USA).

- ✓ **pCCLsc_HB9_*RFP*_W:** third generation rLV transfer plasmid encoding the red fluorescent protein (RFP) under the control of a short version of the motor neuron-specific HB9 promoter. This plasmid is a kind gift from Fred Gage's laboratory (Salk Institute, USA).
- ✓ **pRRLsc_C_m*Smn*_eIeGFP_W:** third generation rLV transfer plasmid encoding the mouse *Smn* cDNA linked to an IRES *eGFP* under the control of the cytomegalovirus promoter (CMV). The plasmid was made by Dr. Sherif Ahmed in Dr Yáñez's laboratory.
- ✓ **pMDLg/pRREintD64V:** Packaging plasmid for rLV production encoding the *group specific antigen (GAG), polymerase (POL) and integrase (IN)* genes. This plasmid was a kind gift from Luigi Naldini's laboratory (San Raffaele Telethon Institute for Gene Therapy, Italy).
- ✓ **pRSV-REV:** Rev plasmid for rLV production encoding the Rev protein which is necessary for the nucleic acid transfer from the nucleus to the cytosol. This plasmid was a kind gift from Luigi Naldini's laboratory
- ✓ **pMD2.VSV-G:** Envelope plasmid for rLV production encoding the glycoprotein from the vesicular stomatitis virus (VSV-G). Virus pseudo-typed with this envelope can infect both mammalian and non-mammalian cells. This plasmid was a kind gift from Luigi Naldini's laboratory.

2.1.4 DNA/RNA/PROTEIN SIZE MARKERS AND MODIFYING AND RESTRICTIONS ENZYMES

All restriction enzymes were used following manufacturer's recommendations. The type of DNA molecular weight marker used depended on the percentage of the gel and the size of the fragments to be analysed

- ✓ Antarctic Phosphatase (NEB, Cat. No. M0289S)
- ✓ *Asc*I (NEB, Cat. No. R0558S)
- ✓ *Cla*I (NEB, Cat. No. R0197S)
- ✓ *Dde*I (NEB, Cat No. R0175L)
- ✓ FastDigest® *Age*I (*Bsh*TI) (Fermentas, Cat. No FD1464)
- ✓ FastDigest® *BglI*I (Fermentas, Cat. No FD0083)
- ✓ FastDigest® *Sbf*I (SdaI) (Fermentas, Cat. No FD1194)
- ✓ FastDigest® *Sma*I (Fermentas, Cat. No FD0663)

- ✓ GeneRuler™ 100bp Plus DNA Ladder (Fermentas, Cat. No SM0321)
- ✓ GeneRuler™ 1kb DNA Ladder (Fermentas, Cat. No SM0311)
- ✓ GeneRuler™ 1kb Plus DNA Ladder (Fermentas, Cat. No SM1331)
- ✓ GoTaq® Flexi DNA Polymerase (Promega, Cat. No. M8305)
- ✓ Moloney Murine Leukemia Virus Reverse Transcriptase (M-MLV, Promega, cat M1701)
- ✓ Oligo(dT) 15 primer (Promega, Cat No. C1101)
- ✓ Prestained Protein Molecular Weight Marker (Fermentas, Cat. No SM0441)
- ✓ *Pvu*I (NEB Cat. No. R0151T)
- ✓ Recombinant RNasin Ribonuclease inhibitor (Promega, Cat. No. N2611)
- ✓ RiboRuler™ High Range RNA Ladder (Fermentas, Cat. No #SM1823)
- ✓ RQ1 RNase-Free DNase (Promega, Cat No. M6101)
- ✓ T4 ligase (NEB, Cat. No. M0202S)
- ✓ *Xba*I (Promega, Cat. No. R6181)

2.1.5 BIOLOGICAL KITS AND SYSTEMS

- ✓ Amersham ECL Direct Nucleic Acid Labelling And Detection Systems kit (GE Healthcare, Cat No. RPN3000).
- ✓ DC protein Assay (Biorad, Cat No 500-0116)
- ✓ DNeasy Blood & Tissue Kit (Qiagen, Cat. No. 69506)
- ✓ EndoFree Plasmid Giga Kit (Qiagen, Cat. No. 12391).
- ✓ EndoFree Plasmid Maxi Kit (Qiagen, Cat. No. 12362).
- ✓ EndoFree Plasmid Mega Kit (Qiagen, Cat. No. 12381).
- ✓ MycoAlert Mycoplasma Detection Kit (Lonza, Cat. No. LT07-218)
- ✓ Periodic Acid-Schiff (PAS) staining system (Sigma-Aldrich, Cat. No. 395B).
- ✓ Powerplex 1.2 system (Promega, Cat, No DC6101)
- ✓ QIAprep Spin Miniprep Kit (Qiagen, Cat. No. 27104).
- ✓ QIAquick Gel Extraction Kit (Qiagen, Cat. No. 28704).
- ✓ QIAquick Nucleotide Removal Kit instead (Qiagen Cat. No. 28304).
- ✓ QIAquick PCR purification Kit (Qiagen, Cat. No. 28104)
- ✓ Wizard SV genomic DNA purification system (Promega, Cat No. A2361).

2.1.6 PRIMERS

A list of all primers used in this study is shown in **Appendix 2.** The list includes size of the amplicons, sequences of the primers (where available), specific use (cloning, sequencing,

viral titre determination, iPSCs' quality control, follow up of transcripts in cells during MN differentiation and detection of SMN isoforms) and original reference. **Appendix 3** presents the quality control of the primers used for quantitative polymerase chain reaction (qPCR) and quantitative reverse transcription PCR (qRT-PCR).

2.1.7 ANTIBODIES

Antibodies used for immunoblotting, flow cytometry assays/analyses and immunofluorescence are shown in tables 2.1, 2.2 and 2.3 respectively.

Table 2. 1: Antibodies for immunoblotting assays.

Antibody (primaries)	Company	Catalogue number	Dilution
Mouse anti-survival motor neuron (SMN)	BD Biosciences	610646	1 in 5000
Mouse anti FLAG M2	Stratagene	299472	1 in 1000
Rabbit Anti-T Plastin antibody	ABCAM	AB128690	1 in 1000
Rabbit anti-Alpha tubulin	ABCAM	AB4074	1 in 2000
Mouse anti-Actin	DSHB	JLA20. Supernatant	1 in 100
Mouse anti- Glucose phosphate isomerase (GPI1)	DSHB	CPTC-GPI-1. Supernatant	1 in 100
Antibody (secondaries)	**Company**	**Catalogue number**	**Dilution**
IRDye 800CW goat anti-mouse	LI-COR	92632210	1 in 2000
Goat anti-Rabbit alexa flour 680	Molecular Probes	A21076	1 in 5000

Table 2. 2: Antibodies for flow cytometry analysis.

Antibody	Company	Catalogue number	Dilution	Target Cell
Alexa Fluor® 647 anti-human SSEA-3	BioLegend	330308	0.125 µg	iPSCs and EP212
Alexa Fluor® 647 Rat IgM, κ Isotype Ctrl	BioLegend	400813	0.125 µg	iPSCs and EP212
PE anti-human TRA-1-81	BioLegend	330708	0.125 µg	iPSCs and EP212
PE Mouse IgM, κ Isotype Ctrl	BioLegend	401609	0.125 µg	iPSCs and EP212

*Dilutions shown correspond to the labelling of $5x10^5$ cells. All flow cytometry antibodies are already conjugated to a reporter fluorescent dye.

Table 2. 3: Antibodies for immunofluorescence assays

Antibody (primaries)	Company	Catalogue number	Dilution	Target Cell
Mouse anti-OCT4	Chemicon	MAB4401	1 in 500	iPSCs
Mouse anti-TRA-1-60	Chemicon	MAB4360	1 in 500	iPSCs
Rabbit anti-SOX2	Chemicon	AB5603	1 in 500	iPSCs
Mouse anti NANOG	Abcam	AB62734	1 in 100	iPSCs
Mouse anti-Neuronal class III beta tubulin (TUJ1)	Eurogentec	mms-435p	1 in 200	EBs
Rabbit anti-PAX6	Eurogentec	prb-278p	1 in 500	EBs
Mouse anti-Smooth muscle actin (SMA)	DAKO	M0851	1 in 100	EBs
Rabbit anti-Desmin	Abcam	AB15200	1 in 200	EBs
Rabbit anti-Brachyury	Santa Cruz	sc-20109	1 in 100	EBs
Rabbit anti-Alpha Fetoprotein	Molecular Probes	18-0055	1 in 100	EBs
Goat anti-SOX17	R&D systems	AF1924	1 in 100	EBs
Goat anti-SOX1	R&D systems	AF3369	1 in 500	Neural Rosettes
Mouse anti-PAX6	DSHB	Supernatant	1 in 500	Neural Rosettes
Goat anti-OLIG2	Santa Cruz	sc-19969	1 in 50	MN progenitors
Goat anti- ISL1	R&D systems	AF1837	1 in 50	MNs
Goat anti-Choline acetyltransferase (ChAT)	Chemicon	AB144P	1 in 50	MNs
Mouse anti-Nerve-growth factor receptor p75 (P75-NGFR)	Michael Sentners' lab	-	1 in 100	MNs
Rabbit Anti-Neuronal class III beta tubulin (TUJ1)	Sigma	T 2200	1 in 3000	Neurons
α-Bungarotoxin, Alexa Fluor® 555 Conjugate	Molecular Probes	B35451	1 in 500	Muscle
Rabbit anti-Glial Fibrillary Acidic Protein (GFAP)	DAKO	Z0334	1 in 3000	Astrocytes
Mouse Anti-alpha 1 Fetoprotein	Abcam	AB3969	1 in 200	Hepatocytes

Antibody (secondaries)	Company	Catalogue number	Dilution
Alexa Fluor 568 donkey anti - mouse IgG	Molecular probes	A10037	1 in 1000
Alexa Fluor® 488 donkey anti-mouse IgG (H+L)	Molecular probes	A21202	1 in 1000
Alexa Fluor® 488 donkey anti-goat IgG (H+L)	Molecular probes	A-11055	1 in 1000
Alexa Fluor® 546 donkey anti-goat IgG (H+L)	Molecular probes	A11056	1 in 1000
Alexa Fluor® 555 goat anti-rabbit IgG (H+L)	Molecular probes	A21428	1 in 1000
Alexa Fluor® 488 goat anti-rabbit IgG (H+L)	Molecular probes	A-11034	1 in 1000

2.1.8 CELLS

Information about the initial provider (manufacturer's company and catalogue number) is not available for all cells. Continuous cell lines have been stored and maintained in my laboratory for several years in a common stock in liquid nitrogen identified with their passage number. When more information is available, this is stated next to the particular cell type.

2.1.8.1 BACTERIA

- ✓ TOP 10 *E. coli*: *E. coli* strain genetically modified for high-efficiency cloning and plasmid propagation (Invitrogen).

Genotype: F– *mcr*A Δ(*mrr-hsd*RMS-*mcr*BC) Φ80*lac*ZΔM15 Δ*lac*X74 *rec*A1 *ara*D139 Δ(*ara leu*) 7697 *gal*U *gal*K *rps*L (StrR) *end*A1 *nup*G

2.1.8.2 CELL LINES

- ✓ HEK293T: variant of the human embryonic kidney 293 cell line containing a temperature-sensitive SV40 Large T-antigen.
- ✓ HeLa: human cell line derived from cervical cancer.
- ✓ HT1080: human cell line derived from a fibrosarcoma.
- ✓ C2C12: mouse myoblast cell line derived from C3H mice (ATCC, CRL-1772).
- ✓ Platinum retroviral packaging cell line E (PlatE): human cell line based on the HEK293Ts which also containing *GAG, POL* and *ENV* genes for easier retroviral production (Cell Biolabs).
- ✓ BJ1: telomerase-immortalised human BJ1 cell line derived from a skin biopsy (Clontech, Cat. No. C4001-1) and genetically modified in the Institute for Stem cell Therapy and Exploration of Monogenic diseases (I-STEM. Evry, France) for stable production of Fibroblast growth factor (FGF) 2 (Clone HF8).
- ✓ EP2102: human embryonic carcinoma cell line derived from a primary testicular teratocarcinoma. This cell line is used as a reference standard of pluripotency (*Andrews et al., 1982*).

2.1.8.3 PRIMARY CELLS

- ✓ IMR90: human fibroblasts harvested from the lung of a healthy human female at 16 weeks of gestation (ATCC, Cat No. CCL-186).
- ✓ 4603 fibroblasts: human fibroblast harvested from the skin of a healthy adult human

male (Coriell, Cat. No. GM04603).

- ✓ SMA1 and SMA2 fibroblasts: human fibroblast harvested in Santa Creu i Sant Pau Hospital (Barcelona) from skin biopsies of patients with SMA type 1 and type 2 respectively. Cells were obtained with informed consent by our collaborator Dr Eduardo Tizzano.
- ✓ AC, TC, CC, RC and NC fibroblasts: human fibroblasts harvested in Santa Creu i Sant Pau Hospital (Barcelona) from skin biopsies of members of the SMA family of study. Cells were obtained with informed consent by our collaborator Dr Eduardo Tizzano. Samples are coded as follows:

  *RC: healthy mother of the family carrying a mutation in exon 3 (c.399_402delAGAG) of the *SMN*1 gene in heterozygosis.

  *AC: SMA IV/asymptomatic sibling carrying a mutation in exon 3 (c.399_402delAGAG) of the *SMN*1 gene in homozygosis.

  *CC, TC and NC: siblings with SMA type III, all carrying a mutation in exon 3 (c.399_402delAGAG) of the *SMN*1 gene in homozygosis.

A more detailed description of the family members can be found in **Chapter 4**.

2.1.8.4 PLURIPOTENT CELLS

- ✓ iPSC clones derived from the family of study: derived by myself in I-STEM from fibroblasts RC, AC, TC, and NC of the family of study. Several clones were derived from each family member, except for RC. Please refer to **Appendix 4**.
- ✓ 4603: iPSC clone derived in I-STEM from 4603 fibroblasts in the same way as the clones derived in this study.
- ✓ SMA-19: iPSC clone SMA-19 derived in Beckman Research Institute (California, USA) from human primary fibroblasts from a type I SMA patient (Coriell, Cat. No. GM09677) and published in *Chang et al., 2011.*
- ✓ hESC H9: embryo-derived pluripotent cells generated from embryos discarded from an *in vitro* fertilization donation in the University of Wisconsin (USA) and published in *Thomson et al., 1998*.

2.1.9 MEDIA

All media were prepared under sterile conditions in a class II biosafety cabinet. Solutions containing supplements that had to be weighted or that came in non-sterile conditions were filtered with a 0.22 μm pore filter prior to use. All mammalian media were pre-warmed in a

37 °C water bath prior to use. All basal media, supplements and pre-made media are listed in **Appendix 1** under "Special reagents and media components".

2.1.9.1 BACTERIAL MEDIA

All bacterial media were prepared in ddH20 and sterilized by autoclaving at 120 °C for 20 min. After sterilization part of the medium was supplemented with 100 μg/ml of ampicillin and kept at 4°C for up to 1 month.

- ✓ Luria Broth (LB) liquid medium: 2% Luria broth.
- ✓ LB agar medium: 2% Luria broth, 1.5% bacteriological agar. To prepare LB agar plates, the medium was heated until it became liquid and approximately 20 ml were poured onto 100 mm bacterial Petri dishes in a bacterial safety cabinet. If needed, antibiotics were added before pouring the plates, when the medium was approximately at 55 °C.

2.1.9.2 MEDIA FOR EUKARYOTIC CELL LINES

- ✓ Standard growth medium: Dulbecco's modified Eagle's medium (DMEM) high glucose (4.5 g/L) with stable glutamine supplemented with 10% Foetal bovine serum (FBS), 100 U/ml Penicillin and 100 μg/ml Streptomycin (Pen&Strep).
- ✓ Standard freezing medium: 40% DMEM high glucose (4.5 g/L) with stable glutamine, 50% FBS and 10% DMSO.
- ✓ Standard growth medium high serum: DMEM high glucose (4.5 g/L) with stable glutamine supplemented with 20% FBS and Pen&Strep.
- ✓ Plat medium: DMEM high glucose (4.5 g/L) with glutamax supplemented with 10% FBS, 1 mM sodium pyruvate, 50 μM β- mercaptoethanol and 1 μg/ml gentamicine.
- ✓ C2C12 differentiation medium: DMEM high glucose with stable glutamine supplemented with 2% horse serum, and 1 μg/ml gentamicine.

2.1.9.3 MEDIA FOR PRIMARY CELLS

- ✓ Primary human fibroblast medium: 64.8% DMEM high glucose with stable glutamine, 21% M-199, 10% FBS, 10 ng/ml FGF_2, 25 ng/ml Epidermal growth factor (EGF), 1 μg/ml gentamicine.

2.1.9.4 MEDIA FOR iPSCS AND iPSC-DERIVED CELLS

All iPSC-related media were aliquoted into volumes used for one day of work and only this aliquot was pre-warmed.

- ✓ Reprogramming Fibroblast medium: DMEM high glucose (4.5 g/L) with glutamax supplemented with 10% FBS, 1 mM sodium pyruvate, 1X Minimum Essential Media (MEM) non essential amino acids, 1mM L-Ascorbic acid 2-phosphate, 10 ng/ml Recombinant Human FGF_2 and 1 µg/ml gentamicine.
- ✓ hESC medium: Knockout DMEM supplemented with 20% Knockout serum replacement, 1X MEM non essential amino acids, 2mM Glutamax, 10 ng/ml recombinant Human FGF_2, 50 µM β- mercaptoethanol and 1 µg/ml gentamicine.
- ✓ Stemedia™ NutriStem™ XF/FF Culture Medium (premade), supplemented with 1 µg/ml gentamicine.
- ✓ Feeder medium: MEM Alpha Modification Liquid with Ribonucleosides L-glutamine supplemented with 10% FBS, 1X MEM non-essential amino acids and 1 µg/ml gentamicine.
- ✓ Feeder freezing medium: 90% FBS, 10% Dimethyl sulfoxide.
- ✓ Vitrolife freezing medium A: Vitro PBS supplemented with 10% DMSO and 10% Ethylene Glycol.
- ✓ Vitrolife freezing medium B: Vitro PBS supplemented with 20% DMSO, 20% Ethylene Glycol, 0.3 M trehalosa and 10 µM of Rock inhibitor.
- ✓ CryoStem™ Freezing Medium (pre-made)
- ✓ Vitrolife thawing medium A: 0.1 M trehalosa in Vitro PBS.
- ✓ Vitrolife thawing medium B: 0.2 M trehalosa in Vitro PBS.
- ✓ Neural differentiation medium: DMEM Nutrient mix F12 supplemented with 1X N2, 1X MEM non essential amino acids, 2 µg/ml heparin and 1 µg/ml gentamicine.
- ✓ MN differentiation medium 1528: DMEM Nutrient mix F12 supplemented with 1X N2, 1X B27, 1X MEM non essential amino acids, 2 µg/ml heparin, 0.1 µM retinoic acid, 1 µM pumorphamine and 1 µg/ml gentamicine.
- ✓ Complete MN differentiation medium: DMEM Nutrient mix F12 supplemented with 1X N2, 1X B27, 1X MEM non essential amino acids, 2 µg/ml heparin, 50 nM retinoic acid, 0.5 µM pumorphamine, 0.1 µM cyclic adenosine monophosphate (cAMP), 200 ng/ml ascorbic acid, 10 ng/ml Brain-derived neurotrophic factor (BDNF), 10 ng/ml Glial cell-derived neurotrophic factor (GDNF) and 10 ng/ml Insulin-like growth factor 1 (IGF-1) and 1 µg/ml gentamicine.
- ✓ Hepatocyte differentiation medium 1-3: RPMI 1640 medium supplemented with 0.5 mg/ml BSA, 100 ng/ml Activin A and 1 µg/ml gentamicine.

- ✓ Hepatocyte differentiation medium 4-7: complete Hepatocyte Culture Medium (HCM) further supplemented with 30 ng/ml FGF_4, 20 ng/ml Bone morphogenetic protein 2 (BMP_2) and 1 μg/ml gentamicine.
- ✓ Hepatocyte differentiation medium 8-13: complete HCM further supplemented with 20 ng/ml HGF, 20 ng/ml Keratinocyte growth factor (KGF) and 1 μg/ml gentamicine.
- ✓ Hepatocyte differentiation medium 14-18: complete HCM further supplemented with 10 ng/ml oncostatin-M, 0.1 μM dexamethasone and 1 μg/ml gentamicine.
- ✓ Hepatocyte differentiation medium 19-21: DMEM high glucose with stable glutamine supplemented with 1X N2, 1X B27, 1 mM glutamax, 1X MEM non essential amino acids, 0.1 mM β-mercaptoethanol and 1 μg/ml gentamicine.

2.1.10 PLASTICWARE AND CULTURE SURFACES

All plasticware used in this work, including standard and special tissue culture tubes, dishes, flasks, plates, coverslips, centrifuge tubes, filter devices and other general plasticware, are listed in **Appendix 5**.

2.1.11 INSTRUMENTS AND SOFTWARE

All the instruments and software used for the methods employed in this work are shown in the list "Instruments and Software" in **Appendix 6**. Instruments and software used in methods performed by our collaborators are not included on this list.

2.2 MOLECULAR METHODS

2.2.1 CLONING

2.2.1.1 DETERMINATION OF NUCLEIC ACID CONCENTRATION

All quantifications were performed at 260 nm with 1 μl of undiluted nucleic acid in a NanoDrop™ 1000 Spectrophotometer using settings DNA-50 for DNA and settings RNA-40 for RNA. The purity of the sample was also assessed with the ratio of the readings at 260/280 nm.

2.2.1.2 RESTRICTION ANALYSIS

All enzyme digestions in this study were performed at 37 °C for 30 min (for fast Digest Fermentas enzymes) or 1-3 hours (for New England Biolabs enzymes) using 0.4-10 μg of plasmid DNA, 2.5-5 U of the restriction enzyme/s and 1X of the corresponding buffer in a final volume of 20 μl. All enzymes were used with their respective most efficient buffer.

The units of enzyme used in each reaction were adjusted according to the number of target sites within the plasmids. A list of the restriction enzymes used is shown in **section 2.1.4**

2.2.1.3 GEL ELECTROPHORESIS

Plasmid DNA and PCR products were visualized in 0.8-3% agarose gels using 1X TAE buffer and ethidium bromide at a final concentration of 0.5 µg/ul, both in the gel and in the running buffer. 300 ng of 100 bp and 1kb molecular weight ladders were used as reference and each sample was loaded in 1X loading buffer. All the runs were performed in a Flowgen Bioscience chamber and an Electrophoresis Power Pac Basic power source at 50 V. The visualization and recording of the images of the gels were done in an InGenius gel documentation and analysis system, using GeneFlash syngene Bio Imaging software.

2.2.1.4 CLONING IN PLASMID VECTORS

Cloning methods are broad, but they all include (i) generation of a fragment containing the desired sequence (insert), (ii) treatment of both, the plasmid containing the backbone of interest and the insert with suitable restriction enzymes that allow their union, (iii) ligation of backbone and insert, (iv) transformation (v), screening of transformants, (vi) sequencing, (vii) amplification and storage of the new construct.

All inserts generated in this study were produced by PCR amplification

2.2.1.4.1 PCR amplification

Specific fragments of ~70-1000 bp, such as the ones of interest in the current work, can be amplified from a DNA source by the use of primers located at the beginning and the end of the target sequence. A list of the primers used in this study can be found in **Appendix 2**.

PCRs were performed in a PCR gradient Thermal cycler TC-512 under the following general conditions: 0.3-0.6 µM of each primer, 1-3 mM $MgCl_2$, 200 µM deoxynucleotide triphosphates (dNTPs), 0.25U GoTaq® Flexi DNA Polymerase in its 1X Green GoTaq Flexibuffer and 1-100 ng of template in a final volume of 25-50 µl. The cycling conditions were variable, but they all included an initial denaturation cycle at 95 °C for 5 min, and at least 30 cycles of denaturation/anneling/extension with a final extension at 72 °C for 5 min. PCR amplification was assessed by running 5-10 µl of the product in an agarose gel. All PCR products were kept at -20 °C

2.2.1.4.2 Digestion, isolation of bands and ligation

As summarized before, both, the insert (all the volume of the PCR product left after assessing the amplification) and 10 μg of the plasmid, were digested with suitable restriction enzymes as described previously, but scaling up the amount of enzyme (usually 4 times) and performing the digestion in the smallest volume possible. The resulting products were run in agarose gels and the bands with the expected molecular weight were excised with a scalpel in a UV transiluminator Gel doc 2000. The bands were then purified with the QIAquick Gel Extraction Kit following manufacturer's instructions. The purified digested plasmid vector was incubated with 5 U of Antarctic Phosphatase for 30 min at 37 °C/5 min 65 °C to prevent re-ligation.

Both purified fragments were then ligated in a 3:1 insert/backbone ratio using 100 ng of the vector, the respective amount of purified fragment and 400 U of T4 DNA ligase in its 1X ligase buffer in a final volume of 10 μl. The reaction was incubated overnight at approximately 18 °C, time after which the DNA was transformed into *E. coli* TOP10 cells.

2.2.1.4.3 Transformation in E. Coli TOP 10

In order to finalize the ligation process and to amplify the new molecules, the ligation product was transformed into an *E. coli* strain genetically modified for high-efficiency cloning and plasmid propagation. The transformation process includes the conditioning of *E. Coli* TOP 10 for DNA uptake (preparation of competent cells) and the DNA transfer. The calcium chloride method was the chosen transformation strategy. Bacteria and their media were always handled and kept under sterile conditions.

2.2.1.4.4.1 Preparation of competent cells

E. coli TOP 10 was grown in a fresh LB plate and a single colony was inoculated in 5 ml of LB medium and grown overnight at 37 °C, 180 revolutions per minute (RPM) in a bacterial incubator/shaker. This preparation is referred as mini-culture. The next day the 5 ml mini-culture was added to 100 ml of LB medium and grown at 37 °C, 180 RPM for 1.5-2 hours until cells reached an OD550 of 0.5. The optical density measurements were performed in a Biophotometer 613101139. Cells were then chilled on ice-water for 5 min, centrifuged, re-suspended in 40 ml of competent cells-Buffer 1, incubated on ice-water for 10 min, centrifuged, re-suspended in 4 ml of competent cells-Buffer 2, incubated on ice-water for 15 min, aliquoted in 100 ul aliquots, flash-frozen in liquid nitrogen and stored at -80 °C.

2.2.1.4.4.2 DNA transfer

The calcium chloride method for DNA transfer has been modified since it was first discovered in the 1970s. The exact protocol used in this study is briefly described as follows: the entire ligation product (or 100 ng of plasmid DNA) was added to a 100 µl aliquot of competent cells, the solution was gently mixed, kept on ice for 30 min, placed in a 42 °C water bath for 45 seconds (s) (heat shock step) and then placed back in ice again for 10 more min. The transformed cells were then maintained in 1 ml of LB medium at 37 °C 180 RPM for 1 hour, and were finally seeded in LB/ampicilin plates for an overnight incubation at 37 °C. A standard plasmid and pure LB medium were also transformed in separate aliquots of the same competent cells as positive and negative controls of the transformation respectively.

2.2.1.3.4 Screening of transformants

The day after transformation, several colonies were selected from the plates and each one was used to set up a 4 ml mini-culture in LB/ampicillin medium. After an overnight incubation of no more than 16 hours at 37 °C 180 RPM, 1 ml of the mini-culture was used to extract the plasmid DNA using the QIAprep Spin Miniprep kit following manufacturer's instructions. Plasmids were subjected to diagnostic restriction analysis to confirm the correct insertion of the new sequence. Three to five clones with the right restriction pattern were sent for sequencing and the results were analysed using the software Vector NTI.

2.2.1.3.5 Storage of bacteria

Once the sequence of the plasmid in the selected clone was validated, a glycerol stock was made from its mini-cultures. For this, 500 µl of the miniculture was mixed with sterile glycerol at a final concentration of 15% in a cryovial and stored at -80 °C. The map of the plasmid with its key features and available sequences was constructed and analysed with the software Vector NTI. The files were incorporated in the Laboratory database.

2.2.1.5 AMPLIFICATION OF ENDOTOXIN FREE PLASMID DNA

For high, endotoxin free yields of plasmid DNA (up to 2.5 mg), a bacterial streak was prepared in a fresh LB/ampicilin agar plate from the glycerol stock. A mini-culture was set up the next day from a selected colony, and 16 hours later 1 ml of the mini-culture was added to 500 ml of LB/ampicilin in a 1l flask in order to set up a so called "mega-culture". After an overnight incubation of no more than 16 hours at 37 °C 180 RPM, the whole

mega-culture was used to extract the plasmid DNA with the Qiagen EndoFree Plasmid Mega Kit following manufacturer's instructions.

2.2.2 RT-PCR

2.2.2.1 RNA ISOLATION, QUANTIFICATION AND QUALITY CONTROL

RNA was extracted with TRIZOL® Reagent from freshly harvested cells or from cells stored frozen at -80 °C immediately after the harvest, following manufacturer's instructions. RNA yield and purity were measured in a NanoDrop 1000 Spectrophotometer and in some cases also by running 0.5 µg in an agarose gel under denaturing conditions. For this, samples were run using the same procedures used for DNA, but (i) formaldehyde was added to the gel and the running buffer at a final concentration of 0.25 M (ii) a RNA ladder was used and (iii) samples were mixed with RNA loading buffer, incubated 5 min at 65 C and chilled on ice before loading them in the gels. (Please refer to the list of buffers and markers in **sections 2.1.2.6** and **2.1.4** for more details). RNA samples were stored at -80 °C.

2.2.2.2 REVERSE TRANSCRIPTION

Before cDNA synthesis, 1 µg of RNA was subjected to DNase treatment with 1U of RQ1 RNase-free DNase for 30 min at 37 °C. The reaction was stopped by adding 1 µl of RQ1 DNase stop solution and incubating at 65°C for 10 min. 0.5 µg of Oligo(dT) 15 primer was added to the RNA and the mix was incubated at 70°C for 5 min, time after which it was immediately cooled on ice to prevent secondary structures. The RNA was then retro-transcribed to cDNA using 200 U of Moloney Murine Leukemia Virus Reverse Transcriptase (M-MLV), 0.5 mM dNTPs, 20 U of recombinant RNasin ribonuclease inhibitor, and 1X of M-MLV Reaction buffer. The reaction was performed at 37°C for 60 min and the enzyme was inactivated by incubation at 95°C for 5 min. cDNAs were kept at -20 °C.

2.2.2.3 RT-PCR

RT-PCR was performed similarly to PCR, but using RNA as template instead of DNA. For transgene amplification during iPSC quality control, the following specific conditions were used 0.4 µM of each primer, 1.5 mM $MgCl_2$, 200 µM dNTPs, 0.25U GoTaq Flexi DNA Polymerase in its 1X Green GoTaq Flexibuffer and 2 µl of a 1 in 10 dilution of the cDNA (200 ng) in a final volume of 25 µl. The cycling conditions were 95 °C for 5 min, 35 cycles of 95 °C for 60 s/ 60 °C for 30 s/ 72 °C for 30 s and a final extension at 72 °C for 5 min.

RT-PCR amplification was assessed by running 5 µl of the product in an agarose gel. All RT-PCR products were kept at -20 °C.

2.2.2.3.1 Determination of the origin of FL-SMN

An RT-PCR amplifying the junction between exons 6 and 8 followed by a restriction analysis with *Dde*I was performed in order to determine the allelic origin of the FL-SMN mRNAs. During the RT-PCR amplification, internal control primers for the beta actin gene were included in the cocktail as followes: 0.4 µM of each of the exons 6-8 primers, 0.08 µM of each of the beta actin primers, 1 mM $MgCl_2$, 200 µM dNTPs, 0.25U GoTaq Flexi DNA Polymerase in its 1X Green GoTaq Flexibuffer and 2 µl of a 1 in 5 dilution of the cDNA (200 ng) in a final volume of 25 µl. The cycling conditions were 95 °C for 10 min, 30 cycles of 94 °C for 30 s/ 60 °C for 30 s/ 72 °C for 45 s and a final extension at 72 °C for 5 min. RT-PCR amplification was assessed by running 5 µl of the product in an agarose gel. For the *DdeI* restriction analysis, RT-PCR products were digested for at least 4 hours before loading them in an agarose gel.

2.2.3 q RT-PCR and qPCR

2.2.3.1 VALIDATION OF PRIMERS

All primers used for qRT-PCR and qPCR were validated (i) *in silico* for specificity, (ii) in agarose gels by the amplification of a single band of the expected size and (iii) by a qRT-PCR/qPCR run of serial dilutions of a control sample, for assessment of the amplification efficiency and the minimum linear dilution. A summary table of the quality control of the primers used is shown in **Appendix 3**.

Two methods of qRT-PCR were used: the delta-delta cycle threshold (ddCt) method and the semi-quantitative method. Each of them required a specific validation procedure.

2.2.3.1.1 ddCT method

For the ddCT method, the target gene was validated with each of the reference genes used for the normalization step in order to confirm that they behaved in the same way and thus, a standard curve was not required. For the validation, serial dilutions of the cDNA of a control sample were amplified by qRT-PCR with the primers for each combination of target-reference genes. All individual genes had an amplification efficiency of 100% ± 10%, their slope was 3.3 ± 10% and the slope of the difference between the CTs of the target and the reference gene was less than 0.1.

2.2.3.1.2 Semi-quantitative method

For the semi-quantitative method, ten-fold serial dilutions of a plasmid containing the target sequence or a solution containing a known number of target sequences were amplified by qPCR with the corresponding primers. All dilutions (standards) out of the linear range of amplification were discarded and the ones within it were used for the construction of a standard curve in the corresponding reactions. The number of copies of the target sequence in the plasmids was determined based on their molecular weight. **Table 2.4** contains an example of the calculations of the first standard (10^{10} molecules) for the target sequence of the Poly A primers used to assess the rAAV titre by qPCR:

Table 2. 4: **Calculations of the standards for the relative quantification of srAAVs through qRT-PCR**. Calculations are based on the molecular weight of the plasmid pscAAVCagh*SMN1*F

Parameter	pscAAVCAGh*SMN1F*
Base pairs	4868
Molecular weight in Daltons (1 bp=650 Da)	3.16×10^{6}
Moles for 10^{10} molecules (1 mol=6.023×10^{23})	1.66×10^{-14}
Weight for 10^{10} molecules (g)	5.25×10^{-8}
Weight for 10^{10} molecules (ng)	52.54

2.2.3.2 ENDOGENOUS STABILITY TEST

In order to determine the most appropriate reference genes for each particular study, a stability test was performed using the freely available geNorm VBA applet for Microsoft Excel. For this, a sample from all cell types included in the qRT-PCR analysis was amplified in triplicate with the primers of all proposed reference genes. The reference genes with lower variability of expression between cell types were chosen and used for normalization during the corresponding experiments.

2.2.3.3 mRNA LEVEL AND COPY NUMBER ESTIMATIONS

2.2.3.3.1 mRNA levels (ddCt method)

The ddCt method was used for the study of the down-regulation of transgenes in iPSCs and for the follow up of SMN and plastin 3 levels during iPSC-MN differentiation. In all cases, samples were run in triplicate for all target genes and the validated reference genes (as well as negative controls for each reaction). The geometric mean of the most stable reference genes chosen was used for normalization. One sample was chosen as the calibrator, setting its value arbitrarily to one and comparing all other samples to it.

All mRNA levels were calculated with the following formula:

Gene expression= [2^-(sample x target gene CT- normalizing sample target gene CT)]/[2^-(sample x geometric mean of reference genes CT- normalizing sample geometric mean of reference genes CT)]

* CT= cycle threshold

2.2.3.3.1.1 Transgene down-regulation in iPSCs

qRT-PCR was performed in order to measure and compare the endogenous expression and total expression (which includes exogenous and endogenous expression) of *OCT4, SOX2, KLF4* and *c-MYC*. RNA extraction and cDNA synthesis were performed as previously described on colonies carefully selected from each iPSC clone, avoiding the inclusion of feeder cells. mRNA was amplified with primers binding to two internal sequences of the cDNA (for total expression) and a 3' UTR sequence and an internal sequence of the cDNA (for endogenous expression) for all transcription factors. All reactions were run in a Rotor-Gene ™ 6000 real-time rotary analyser using the following conditions: 0.4 µM of each primer, 1X SensiMixPlus SYBR and 2 µl of a ten-fold dilution of cDNA in a final volume of 20 µl. The cycling conditions were: 1 cycle at 95˚C for 10 min and 40 cycles of 95˚C for 15 s/ 60˚C for 30 s. A melting curve calculation was performed at the end with a continuous reading between 50 and 100 ˚C.

mRNA levels of target genes were normalized to the geometric mean of the mRNA levels of Ribosomal protein L13a (RPL13) and ribosomal protein S18 (18S) and calibrated to the value of EP2102, a carcinoma cell line with embryonic stem cell-line expression profile (section 2.1.8.2) . BJ1, IMR90 human fibroblasts undergoing reprogramming (harvested 4 days post transduction) and hESC H9, were included in the analysis as references. EP2102 carcinoma cells were used as the calibrator instead of hESCs H9 because the RNA extraction and cDNA synthesis of the later were performed in I-STEM by different methods as the ones described here (specifically, the endogenous expression might be underestimated compared to the other samples).

2.2.3.3.1.2 mRNA levels during MN differentiation

All qRT-PCR reactions for the follow up of mRNA levels of *full length survival motor neuron (FL-SMN), SMN Delta 7 isoform (D7-SMN), total SMN (FL-SMN + D7-SMN),* and *plastin3 (PLS3)*, along with their respective reference genes, were performed by Dr Sara Bernal in Santa Creu i Sant Pau Hospital (Barcelona, Spain). RNA extraction was performed as previously described, but cDNA synthesis was done in Barcelona from 0.5 ug

of RNA per sample. All reactions were run in an ABI PRISM® 7900HT Sequence Detection System using the following conditions: 0.45 µM of each primer, 0.25 µM of the probe, 1X TaqMan® Universal PCR Master Mix and 2.5 µl of a five-fold dilution of cDNA in a final volume of 12.5 µl. The cycling conditions were: 1 cycle at 50˚C for 2 min, 1 cycle at 95˚C for 10 min and 40 cycles of 95˚C for 15 s/ 60˚C for 1 minute. mRNA levels of target genes were normalized to the geometric mean of the mRNA levels of beta actin, peptidylprolyl isomerase A (PPIA) and glyceraldehyde-3-phosphate dehydrogenase (GAPDH), and calibrated to various samples depending of the analysis.

2.2.3.3.2 Copy number (semi-quantitative method)

The semi-quantitative method was used to determine the titre of rAAVs and rH1LVs produced in this project. The specific determination of the titre is described in the section on viral vectors (**2.3.5**). All reactions were performed in a Rotor-Gene ™ 6000 real-time rotary analyser using the Rotor Gene Software 1.7.

2.2.4 WESTERN BLOTTING

For the isolation of proteins, cells were harvested (using a cell scraper if necessary) and washed carefully with PBS before adding 100-1500 µl of ice-cold RIPA buffer containing a cocktail of protein inhibitors and transferring them to a microfuge tube. The cells were centrifuged at 13,000 rpm 4 °C for 10 min, after which the supernatant was transferred to a new microfuge tube and kept at -80 °C until further use. The total protein concentration was measured following the instructions of the DC protein Assay. From each sample 7-25 µg of protein was loaded onto a discontinous (4% stacking, 12% separation) gel in order to perform a sodium dodecyl sulfate polyacrylamide gel electrophoresis (SDS-PAGE). The samples were loaded with 1X WB loading buffer (after a 10 min incubation at 95 °C) and the run was perform at 150 V in cold 1X WB migration buffer in a Mini-PROTEAN Tetra Electrophoresis System until the bromophenol blue front came out of the gel. Proteins were then transferred to an Amersham Hybond™ ECL™ membrane in a Mini Trans-Blot Cell at 150 mA for 2 hours using fresh cold 1X WB transfer buffer, a cooling unit and a magnetic stirrer. The efficiency of transference was assessed with a fast incubation with Ponceau red solution. After the transfer, the membrane was incubated for 2 hours at room temperature (RT) with WB blocking buffer, and then overnight at 4°C with the primary antibody diluted in 5 ml of WB blocking buffer. The next day, the membrane was washed with TBS-T in a shaker four times (incubating 5 min per wash) at RT before incubating it for 2 hours at RT

with the secondary antibody diluted in 5 ml of WB blocking buffer. The membrane was then washed again four times as described previously before performing the detection and quantification with an Odyssey Infrared Imaging System and the corresponding application software V1. If further proteins were to be detected on the membrane, the same steps were repeated by adding a new primary antibody without stripping.

2.2.5 GENOTYPE ANALYSIS

Two of our collaborators performed the genotype analysis. The analysis for clones AC28, RC26, TC64 and NC21 was performed by Dr. Julien Come in I-STEM and the analysis for clones NC32, NC42 and TC63 was performed by Dr Sara Bernal in Santa Creu i Sant Pau Hospital (Barcelona, Spain).

Cell identity was verified by comparing the short tandem repeat (STR) profile at several loci. The profile was compared between each iPSC clone and the original fibroblast cells that were used for reprogramming. In France, cell identity was verified with STRs included in the Powerplex 1.2 system (D16S539, D7S820, D13S317, D5S818, CSF1PO, TPOX, TH01, vWA and Amelogenin). In Barcelona, cell identity was verified with STRs D1S305, D2S443, D2S291, D19S420, D19S112, D19S562 and INT25-2.0.

DNA was prepared as follows: Cells from each clone were grown in a 30 mm Petri dish for 4 days and colonies were carefully and manually picked (avoiding the inclusion of feeders) for DNA extraction using the Wizard SV genomic DNA purification system.

2.3 CELLULAR METHODS

2.3.1 FLOW CYTOMETRY

All flow cytometry measurements were performed in a BD FACSCanto II and data was collected and analysed using the BD FACSDiva™ Software. The flow rate was set to "low", and the recorded count within the gated population to 10.000 events. For all experiments, a plot showing forward scattered light area (FSC-A) *vs* side scattered light area (SSC-A) (setup in linear scale) was used to define the target population of single, live cells.

2.3.1.1 QUANTIFICATION OF CELLS EXPRESSING eGPF

Cells endogenously expressing GFP were gently harvested by tryptinization and their viability was measured by trypan blue exclusion. Cell were further re-suspended in 4% PFA and immediately quantified in the FITC channel. A mock sample from the same cell type (which did not express GFP) was used as to establish the threshold.

2.3.1.2 QUANTIFICACION OF CELLS EXPRESSING SPECIFIC MARKERS

In order to quantify the number of cells expressing one or more specific surface markers, cells were cultured, harvested gently in a small volume and labelled with primary antibodies already coupled with fluorescent dyes. The flow cytometer settings, including the calibration and thresholds were established before quantification. The experiment was performed in order to assess the pluripotency of the iPSC culture during iPSC quality control.

2.3.1.2.1 Assessment of pluripotency in the iPSC culture

In order to quantitatively assess pluripotency in the iPSC cultures, the number of cells co-expressing surface markers SSEA3 and TRA 1-81 were quantified. For this purpose, cells from each clone were grown in 60 mm Petri dishes for 4 days, washed with PBS and gently detached by a 5 min incubation with Tryple at 37 ºC. Cells were harvested in 1 ml of hESC medium and gently pipetted up and down before passing them through a 40 uM pore size nylon sieve in order to get a single cell suspension. After counting the cells and assessing their viability by trypan blue exclusion, cells from each clone were individually centrifuged at 250 x g for 5 min in order to discard the supernatant and re-suspend them in cold 0.1% BSA in PBS at a final concentration of $1x10^7$ cells/ml. The number of feeders was subtracted from the initial count ($1x10^6$) in order to have a better estimation of the number of iPSCs present in each plate. $5x10^5$ cells (50 µl) were added to each flow cytometry (fc) tube and primary antibodies were added for a one-hour incubation. From this step on, the cells were kept on ice and protected from light. All the antibodies used were directly coupled with a fluorochrome and the specificity was assessed with isotype controls conjugated with the same fluorochrome. For a detailed description of antibodies and their dilutions, please refer to **section 2.1.7**. After the incubation with the antibodies, cells were washed with 0.1% BSA in PBS and re-suspended in 300 µl of this same buffer before analysis. Flow cytometry was performed on the same day. Propidium iodide (PI, 2.5 µg) was added just before analysing the mock tube in order to exclude the dead cells from the analysis. Compensation between the Fluorescein isothiocyanate (FITC), phycoerythrin (PE) and allophycocyanin (APC) channels was performed using EP2102 cells, stained individually with the previously described antibodies. Feeders were included in the compensation (given their stable production of GFP) so they could be excluded from the analysis using a gate in the FITC channel. Fluorescence minus one test tubes (where all

fluorescent markers where present except one) were used to establish the threshold for each fluorochrome after compensation.

2.3.2 STAININGS

2.3.2.1 IMMUNOFLUORESCENCE (IF)

Two different microscopes were used for immunofluorescence imaging, an inverted and a confocal microscope. Most images were taken in the former. The inverted Axio observer.D1 had filters for the red, green and blue channels, and pictures were taken with Axio Vision 4.8.1 software. The Olympus LX81, confocal Fluoview FV1000 (confocal microscope) had four lasers for the cyan, green, red and far-red channels. Pictures were taken with Olympus FV10 –ASW Vs 3 software. Adobe Photoshop CS4 and image J 1.45S were also used for the analysis and improvement of the pictures. More detailed information about the microscopes can be found on the instruments list in the appendix section.

In all IF stainings, secondary antibody negative controls were included. A cell type known to constitutively express the marker recognised by the primary antibody as well as a cell line known not to express it, were included as positive and negative controls respectively when available.

2.3.2.1.1 IF of cells in tissue culture plates

Once cells were cultured to the desired confluence, they were washed once with PBS before a 15 min fixation at RT with 4% PFA. Cells were then washed three times with PBS, permeabilised with 0.2% triton X-100 in PBS for 10 min at RT, washed again two times with PBS, blocked with IF blocking buffer for 1 hour at RT and incubated with the desired primary antibodies in IF blocking buffer overnight at 4 °C. Next day, cells were washed three times with PBS, incubated with the corresponding secondary antibodies in IF blocking buffer for one hour at RT, washed three times with PBS for 5 min, incubated with 100 ng/ µl DAPI in PBS for 5 min and finally washed with PBS one last time. Plates were kept in PBS at 4°C protected from light for up to 2 weeks.

2.3.2.2.2 IF of cells cultured on coverslips

Once cells were cultured to the desired confluence, they were washed once with HBSS before a 15 min fixation at RT with 4% PFA and two washes with TBS-T. After fixation, coverslips were carefully taken out of the tissue culture plate with tweezers and placed on top of labelled parafilm in a sealed container. Cells were then blocked with IF blocking buffer for 1 hour at RT and incubated with the desired primary antibodies in IF blocking

buffer overnight at 4 °C. Next day, cells were washed three times with TBS-T, incubated with the corresponding secondary antibodies in IF blocking buffer for one hour at RT, washed three times with TBS-T for 5 min, incubated with 100 ng/ μl DAPI in TBS for 5 min and finally washed with TBS-T one last time. Coverlips were then mounted on slides using AquaPolymount, left at RT overnight protected from light and then kept in a dark box at 4 °C for long term storage.

2.3.2.2 NON FLUORESCENT STAININGS

For visualisation of all non-fluorescent staining, a Leica DM IRB microscope was used along with the Leica application suite software.

2.3.2.2.1 Alkaline phosphatase (AP) staining

For the AP staining, cells were fixed with 95% ethanol for 10 min at RT and incubated in the dark at 37 °C for 5 min with the substrate SIGMAFAST™ BCIP®/NBT (5-bromo-4-chloro-3-indolylphosphate/nitro blue tetrazolium). After a wash with PBS, cells were left to dry completely and were kept at RT.

2.3.2.2.2 Periodic Acid-Schiff (PAS) staining

PAS staining was performed with the PAS staining system from Sigma-Aldrich following manufacturer's instruction with some modifications. Briefly, Cells were fixed with 4% PFA for 15 min at RT, washed two times with PBS and permeabilized with 0.5% Triton X-100 in PBS. Control cells were incubated with 1mg/ml α-Amylase for 30s-1 min at 37°C. Cells were then incubated with periodic acid for 5 min, washed with water 6 times, incubated with Schiff's solution for 15 min, wash with water 6-10 times, incubated with hematoxylin for 3 min and wash with water another 6 times. Cells were kept in ddH20 at 4°C.

2.3.2.2.3 Sudan staining

Cells were fixed with 4% PFA for 15 min at RT, washed two times with PBS, six times with water, incubated with 50% ethanol for 2 min, 70% ethanol for 1 minute and Sudan solution for 5 min. Cells were washed twice with 70% ethanol, once with 50% ethanol and six times with water. Cells were kept in ddH20 at 4 °C.

2.3.3 KARYOTYPE ANALYSIS

Two of our collaborators performed the karyotype analysis. Multicolor fluorescent *in situ* hybridization (mFISH) and G-Banding analysis for clones AC28, RC26, TC64 and NC21 were performed by Christine Varela in I-STEM and G-banding for clones NC32, NC42 and TC63 were performed in the Karyotyping service in Santa Creu i Sant Pau Hospital

(Barcelona, Spain). Fixed nuclei in metaphase were prepared and shipped as follows: cells from each clone were grown in 60 mm petri dishes for four days and incubated for 90 min at 37 ºC, 5% CO_2 in hESC medium containing 0.9 mg/ml colchicine. Cells were then rinsed with PBS, tryptinised, harvested in PBS 2% FBS and centrifuged at 250 x g for 10 min. After centrifugation, most of the supernatant was removed leaving 0.5 ml of liquid to re-suspend the cells before carefully adding 5 ml of warm hypotonic solution. After incubating for 14 min at 37 ºC, cells were centrifuged as previously described and the supernatant was removed leaving 0.5 ml of liquid to re-suspend the cells for the further addition of 5 ml of CARNOY fixative. Cells were immediately centrifuged and the fixation process was repeated 2 more times. After the final removal of the liquid (leaving 0.5 ml), cells were stored at -20 ºC, and one aliquot was kept overnight at 4 ºC for observation under the microscope.

The next day, the quality and quantity of the fixed nuclei were assessed by direct visualisation under the microscope after spreading them onto glass slides. For this, a 10 µl drop of the suspension containing the cells was spread from a distance of approximately 40 cm on top of a glass slide held over a water bath at 80-90 ºC. The slide was held for 40 s more over the water bath before checking it under the microscope. The procedure for spreading the fixed nuclei in shown in **Figure 2.1**

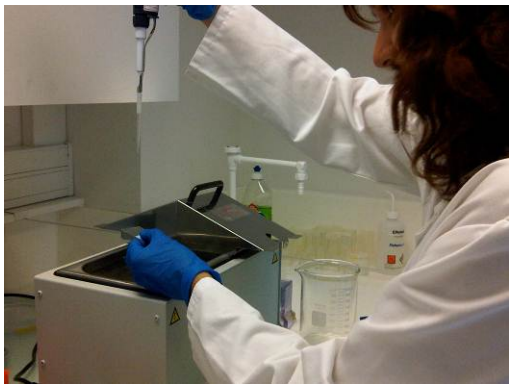

Figure 2. 1: Spreading of fixed nucleus for quality control.
A drop of fixed nuclei is being spread on a glass slide held over a water bath. The impact, humidity and heat break the cell membrane of the cells that were on metaphase at the moment of harvest.

2.3.4 TISSUE CULTURE

All cells were handled and maintained in sterile conditions. All tissue culture-related work was performed in a class II biosafety cabinet, unless otherwise stated. Cells were

maintained in a tissue culture incubator at 37 °C, 5% CO_2 or frozen in aliquots stored in liquid nitrogen.

2.3.4.1 METHODS AND CONDITIONS FOR CONTINOUS MAMALIAN CELL LINES AND PRIMARY CELLS

Cell lines and primary cells were cultured following similar procedures. The main differences between cell types are their growth rate (and senescence), their susceptibility to sub-confluence or over-confluence (and thus their split ratio) and the culture medium required. A brief description of all cells used in this project can be found in **section 2.1.8**

2.3.4.1.1 Culture and maintenance

HEK293T, HeLa, HT1080, EP2102 and C2C12 cells were cultured in standard growth medium and split every 2-4 days. EP2102 sub-confluence leads to lost of pluripotency and C2C12 over-confluence leads to myotube formation and thus under general maintenance conditions this was avoid. In order to intentionally induce the latter, C2C12 differentiation medium was used and cells were no longer split. PlatE were cultured in Plat medium, BJ1 in feeder medium and human fibroblasts in primary human fibroblast medium, except when they were cultured for iPSC reprograming, in which case they were cultured in reprogramming fibroblast medium.

All cells were split using the following protocol: cells were washed with PBS, incubated with trypsin-EDTA or TrpLE Express at 37 °C for 3-5 min, re-suspended with mechanical support in the appropriate culture medium and transferred to a conical tube for a 5 min centrifugation at 200 x g. After centrifugation, the medium was removed, the cells were re-suspended in the appropriate culture medium and a fraction of the total volume was transferred to a new tissue culture plate/flask/dish, already containing a suitable volume of the appropriate culture medium. For counting, 10 µl of the re-suspended cells were mixed with 10µl of 0.4% trypan blue, placed in a haemocytometer and counted under the microscope.

2.3.4.1.2 Freezing

For freezing, cells were harvested by tryptinisation (or TrpLE Express treatment) and re-suspended in standard freezing medium in aliquots of 0.5-1.5 ml. BJ1 cells were re-suspended in feeder freezing medium instead. The aliquots were immediately transferred into an isopropanol freezing container and stored and -80°C overnight. The next day, the cryovials were transferred to a liquid nitrogen storage tank for long-term storage.

2.3.4.1.3 Thawing

For thawing, the cryovial was retrieved from the liquid nitrogen storage tank and immediately placed into a 37° C water bath for 2-3 min. The content of the vial was transferred to the bottom of a 15 ml conical tube and 9 ml of pre-warmed cell culture medium was added to the cells, followed by centrifugation the at 200 X g for 5 min. After centrifugation, the supernatant was removed, the cells were re-suspended in cell culture medium and transferred to a tissue culture plate/flask/dish.

2.3.4.1.4 Transfection

The most frequently used method for transfection of mammalian cell lines in this project was the calcium phosphate method. For this, cells were plated 24 h before, to reach 50-60% confluence on the day of transfection. The medium was changed 1-2 hours before starting the procedure in order to boost cell metabolism. $CaCl_2$ was added to the plasmid DNA (2-10 μg) at a final concentration of 0.25 M. Five min later, an equal volume of 2X HBS buffer was added drop-wise to the DNA/$CaCl_2$ mixture while vortexing the mix at full speed. The mixture was then added to the cells and dispersed homogeneously. The cells were grown at 37 °C and 5% CO_2 for 24 hours, when the medium was changed.

For transfection of PlatE cells during retroviral production (which was performed in I-STEM) Fugene HG Transfection Reagent was used according to manufacturer's instructions.

In order to estimate transfection efficiency with plasmids containing a fluorescent reporter, bright-field and fluorescence images of the same field were compared. For quantitative measurements flow cytometry was employed (**section 2.3.1.1**).

2.3.4.1.5 Transduction

The method of transduction was dependant on the viral vector used and the cells to be transduced. Please refer to the viral vector section for details of the transduction strategies (**section 2.3.5**).

2.3.4.2 METHODS AND CONDITIONS FOR iPSCs

Almost all iPSCs culture techniques were performed with the use of a Lynx Stereo Dynascopic microscope (which will be further referred as to as "stereomicroscope"), which was located inside the safety cabinet. Images of the technical procedures for culturing iPSC are shown in **Figure 2.2.**

2.3.4.2.1 Culture and maintenance

Established iPSCs were grown on mytomycin-C growth-arrested human fibroblasts (BJs) in Stemedia™ NutriStem™ XF/FF Culture Medium. Medium was changed daily and colonies were passage either mechanically or enzymatically every 5-7 days. Mechanical passage was performed when the morphology of the colonies was heterogeneous and there were few cells, while enzymatic passage was performed when the morphology of the colonies was homogeneous and there was a high density of cells. A 1 in 4 to 1 in 5 split was the general rule to passage the cells. Cleaning of the colonies (see below) was optional and could be performed one to three times a week.

2.3.4.2.1.1 Growth arrest and seeding of feeder cells

BJ1s cells were cultivated to confluence in feeder medium in T175 flasks. Once the flasks were 90% confluent, mytomicin C was added to the medium at a final concentration of 10 µg/ml. Cells were incubated at 37 °C, 5% CO_2 for 2.5 hours, time after which the medium was removed, cells were washed once with PBS and then harvested with TrpLE Express. After performing a viability count, cells were either frozen at a concentration of $1x10^6$ cells/ml in MEF freezing medium for later use or plated with feeder medium at a density of $5x10^4$ cell/cm^2 in organ cells (OC), 30 mm petri dishes (B3) or 60 mm petri dishes (B6), previously coated for 20 min with 0.1% gelatine.

The day after seeding the BJ1 cells, the feeder medium was removed and after a wash with PBS, Stemedia™ NutriStem™ XF/FF Culture Medium supplemented with 2 µM thiazovivin was added to the plates. iPSC clumps were then seeded on top of these cells.

2.3.4.2.1.2 Monitoring and cleaning

The morphology of iPSC colonies was monitored in an inverted microscope with a 10 X magnification lens every two-three days, and removal of differentiated cells (cleaning) was performed one to three times a week depending on the quality of the culture. For cleaning, the differentiated parts were carefully scratched and then aspirated with a 200 µl tip under the stereomicroscope inside the safety cabinet.

2.3.4.2.1.3 Manual passage

For manual passage, each colony was cut around the edges and divided into squares of approximately 200 µm with a needle mounted on a 1 ml syringe. The colony was then carefully scratched and aspirated with a p200 micropipette and a tip and finally transferred to dish with feeders in Stemedia™ NutriStem™ XF/FF Culture Medium supplemented

with 2 μM thiazovivin. Approximately 10, 50 and 100 clumps were seeded in OCs, B3s and B6s respectively.

2.3.4.2.1.4 Enzymatic passage

For enzymatic passage, cells were washed with PBS and incubated at 37 °C for 3-8 min with 1 mg/ml of dispase until the edges of the colonies began to curl. At this point, dispase was removed, cells were washed once with PBS and then scratched in Stemedia™ NutriStem™ XF/FF Culture Medium with a 5ml pipette. Clumps were collected in a falcon, centrifuged for 2 min at 50 x g, re-suspended in Stemedia™ NutriStem™ XF/FF Culture Medium supplemented with 2 μM thiazovivin and transferred to a dish with feeders.

2.3.4.2.2 Freezing

For the first freezing and thawing of all the clones, the Vitrolife system was use. For all the subsequent freezing and thawing procedures the Stemgent method was used since it was found to be more efficient.

2.3.4.2.2.1 Vitrolife system

Three different drops were added on the lid of a B6: one drop of 200 μl of Vitrolife freezing medium A and two drops of Vitrolife freezing medium B. The lid was closed and the inverted dish was transferred to the incubator for 15 min. Meanwhile, iPSC colonies were cut as previously described for manual passage. After cutting, 15-20 clumps were carefully scratched and aspirated in a volume not exceeding 50 μl and transferred to the drop of Vitrolife freezing medium A. In less than one minute, the clumps were aspirated back in a volume not exceeding 50 ul and transferred into the first drop of Vitrolife freezing medium B. In less than 30 s the clumps were aspirated back in a volume not exceeding 50 μl and transferred into the second drop of Vitrolife freezing medium B. The clumps were then taken back, transferred to a cryovial, plunged immediately in liquid nitrogen and kept in a liquid nitrogen storage tank.

2.3.4.2.2 2 Stemgent system

iPSCs were harvested enzymatically as described previously and after centrifugation and removal of the medium, cells were re-suspended in CryoStem™ Freezing Medium supplemented with 2 μM of thiazovivin. The content of one B6 was re-suspended in 1 ml of supplemented medium and dispensed into 4 cryovials which were immediately transferred

into an isopropanol freezing container and stored at -80°C overnight, as it was described for mammalian cell line and primary cells.

2.3.4.2.3 Thawing

2.3.4.2.3.1 Vitrolife system

Three different B6 lids were used: one drop of 500 µl Vitrolife freezing medium D was added to one B6 lid, 500 µl of hESC medium was added to the second B6 lid and the third B6 lid remained empty. The cryovial was removed from liquid nitrogen and submerged in a water bath at 40°C for 30 s. In less than one minute 500 µl of Vitrolife freezing medium C was added into the cryovial, mixed and placed into the empty B6 lid. Under the stereomicroscope, clumps were aspirated back in a volume not exceeding 50 µl and transferred onto the lid containing Vitrolife freezing medium D. In less than 1 minute the clumps were aspirated and transferred into the drop of solution with hESC medium. In less than 5 min the clumps were further diluted by aspirating them in 50 µl, dispensing on the lid as a separate drop and adding 500 µl hESC medium. The clumps were then transferred with a tip in a volume not exceeding 50 µl into a B3 plated with feeders in Stemedia™ NutriStem™ XF/FF Culture Medium supplemented with 2 µM thiazovivin.

2.3.4.2.3.2 Stemgent system

This method is very similar to the thawing of mammalian cell lines. Briefly, the cells were thawed and transferred to a conical tube where 9 ml of Stemedia™ NutriStem™ XF/FF Culture Medium was added, followed by centrifugation at 200 X g for 5 min. After centrifugation, the supernatant was removed and the cells were re-suspended in Stemedia™ NutriStem™ XF/FF Culture Medium supplemented with 2 µM thiazovivin and transferred to a B3 plated with feeders.

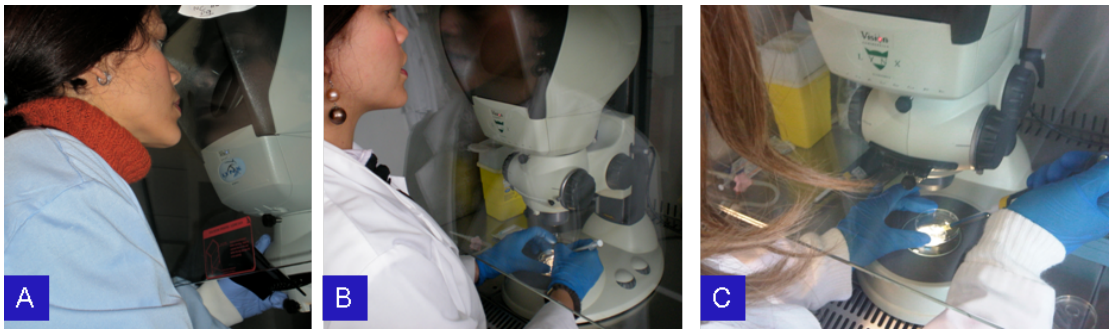

Figure 2. 2: Technical procedure for handling, cutting and picking iPSCs.
The operators are: identifying the colonies through a stereomicroscope located inside a class II BioSafety cabinet (**A**), cutting iPSC colonies with a needle (**B**) and aspirating the colony clumps with a 200 µl tip (**C**).

2.3.5 VIRAL VECTORS

Three types of recombinant viral vectors were used in this study: two derived from members of the *Retroviridae* family: rMMLVs and rH1LVs; and one derived from a member of the *Parvoviridae* family: scAAVs. The self- complementary term is not related to a different species of AVV, but rather to a genetic manipulation of the rAAV genome (Please refer to **section 1.3.1.1.3** in the introduction). The latter two vectors where produced in Royal Holloway-University of London (RHUL. Egham, UK), whereas the former was produced in I-STEM.

2.3.5.1 rMMLVs

2.3.5.1.1 Production

For rMMLV production, PlatE cells were grown to confluence in Plat medium in 10 cm dishes coated with 0.1% gelatine. Cells were transfected separately with 26 μg of each of the four plasmids containing the reprograming factors (pMIG-h*OCT4,* pMIG-h*SOX2*, pMIG-h*KLF4* and pMSCVh*cMYC*IRES*GFP*. Please refer to section 2.1.3) with Fugene HG Transfection Reagent following manufacturer's instructions. The medium was changed 24 hours later and the 8 ml supernatants were harvested the following day (48 hours after transfection). The four supernatants were filtered through a 0.45 μM-pore filter and polybrene and HEPES buffer were added at a final concentration of 4 μg/ml and 1 mM respectively.

MMLVs were produced by Cécile Denis and Mathilde Girard.

2.3.5.2 rH1LVs

2.3.5.2.1 Production

For rH1LV production, a 150 mm culture dish with 50-60% confluent HEK293T cells maintained in standard growth medium, was used for transfection using the calcium phosphate method previously described (**section 2.3.4.1.4**). For each plate, 58 μg of total plasmid DNA in a 1:1:1:5 molar ratio was used [packaging plasmid (pMDLg/pRREintD64V), rev plasmid (pRSV-REV), envelope plasmid (pMD2.VSV-G), and transfer plasmid]. Please refer to **section 2.1.3** for more detailed information about the plasmids. The medium was changed the next day in order to remove the $CaCl_2$. Forty-eight and seventy-two hours after the transfection, the medium was harvested and centrifuged at 215 x g for 10 min. The supernatant was filtered through a 0.22 μM-pore filter and further concentrated by ultracentrifugation on the day of harvest.

2.3.5.2.2 Concentration

The filtered supernatant containing the lentiviral vector was transferred to a Thinwall, Polyallomer, 17 mL, 16 x 102 mm tube and spun at 50,000 x g for 2 h at 4 °C in a Beckman Optima L7 ultracentrifuge using a SW32.1Ti rotor. After centrifugation, the supernatant was discarded, the pellet was re-suspended in 50 µl of DMEM without supplements, transferred to a microfuge tube, centrifuged at 200 x g for 10 min and transferred again to a new microfuge tube. $MgCl_2$ was added to the vector at a final concentration of 10 mM followed by the addition of DNase I (final concentration 5 U/ml) for a 30 min incubation at 37 °C. The vectors were further aliquotated in 5-10 µl aliquots.

2.3.5.2.3 qPCR titration

To assess the titre of rH1LVs (genome copy transducing units; qPCR TU), HeLa cells were transduced with dilutions of the concentrated vectors and qPCR was performed on total DNA extracted from these cells. For this, $1x10^5$ cells were seeded in 6 well plates with standard growth medium the day before transduction. Cells were transduced in parallel with a 1 in 4,000 and 1 in 40,000 dilution of the virus preparation (Each rLV had two preparations, harvest d1 and harvest d2) in 2 ml of standard growth medium containing 8 mg/ml of polybrene. A mock sample incubated only with standard growth medium and polybrene was also included. 24 hours post transduction, cells were harvested by tryptinization and their DNA was extracted using the QIAGEN DNeasy tissue kit. DNA was harvested in a final volume of 400 µl through two sequential column elutions as per manufacturer recommendation.

Once extracted, vector genomic DNA in transduced cells was quantified by qPCR by amplification of the late reverse transcript (LRT) region, common to all lentiviral vectors. The reaction was performed under the following conditions: 0.3 µM of each primer, 1X SensiMixPlus SYBR and 5 µl of the template in a final volume of 20 µl. $1x10^{-2}$-$1x10^{-7}$ copies of the DNA of pCCLsc_HB9_RFP_W were used as standards. Samples were done in duplicate and standards were done in triplicate (including the negative control). The cycling conditions were: 1 cycle at 50˚C for 2 min, 1 cycle at 95˚C for 10 min and 50 cycles at 95˚C for 15 s/ 60˚C for 1 min. A melting curve calculation was performed at the end with a continuous reading between 50 and 100 ˚C. The LRT copy number titre was normalised to the number of cells transduced, which was determined though a parallel qPCR reaction. The number of cells was quantified using primers located in the beta actin gene following the same cycling conditions as the LRT reaction. DNA extracted from

$1x10^6$ HeLa cells with the QIAGEN DNeasy tissue kit was used to prepare the standard curve (10^0-10^5 cells) for this reaction. The final titre was expressed as qPCR transducing units/ml vector stock.

2.3.5.2.4 Transduction of MNs

Four neurospheres were incubated in a microfuge tube for 2 hours (37°C) with 200 µl of MN differentiation medium 1528 containing rLVs for a qPCR MOI of 200. Neurospheres were then seeded on PO-laminin coated coverslips as will be described in the protocol for iPSC differentiation into MNs (**section 2.3.7.2**).

2.3.5.3 rAAVs

2.3.5.3.1 Production

For rAAV production, ten 150 mm culture dishes with 50-60% confluent HEK293T cells maintained in standard growth medium, were transfected using the calcium phosphate method previously described (section 2.3.4.1.4). For each plate, 50 µg of total plasmid DNA in a 1:1:1 molar ratio was used [adenoviral helper plasmid (pAdDeltaF6), packaging plasmid (p5E18-VD2/9) and transfer plasmid]. Please refer to **section 2.1.3** for more detailed information about the plasmids. The medium was changed the next day. Seventy-two hours after the transfection, the cells were detached mechanically from the dishes and centrifuged at 215 x g for 10 min. Cell pellet and supernatant were processed separately. The pellet was re-suspended in 15 ml of AAV cell lysis buffer and stored at -80°C. 50 ml of AAV precipitation buffer was added to the collected supernatant (200 ml), the solution was mixed by inversion and incubated overnight at 4°C. The next day the mix was centrifuged at 2500 x g for 30 min at 4 °C, the supernatant was discarded and the pellet was mixed with the 15 ml lysis buffer containing the cell pellet from the day before.

2.3.5.3.2 Purification

The lysate of the vector producing cells was subjected to three freeze/thaw cycles, by repeatedly placing it in a water bath for 10 min at 37 °C and then in the freezer for 30 min at -80 °C. After the third cycle, benzonase was added at a final concentration of 50 U/ml, incubating for 30 min at 37 °C. The lysate was clarified by a 25 min centrifugation at 3360 x g at RT and further filtration through a 0.45 µm porous size filter.

A discontinuous iodixanol gradient was prepared by layering the iodixanol solutions very carefully into a QuickSeal®, Polyallomer, 39 mL, 25 x 89 mm tube. The layers were added as follows (a representative image of the gradient is shown in **Figure 2.3**):

- ✓ 9 ml of Iodixanol gradient 15% (transparent appearance)
- ✓ 6 ml of Iodixanol gradient 25% (reddish appearance)
- ✓ 5 ml of Iodixanol gradient 40% (transparent appearance)
- ✓ 5 ml of Iodixanol gradient 60% (yellowish appearance)

The clarified and filtered lysate was then layered over the top of the gradient and the tube was filled to the rum with AAV cell lysis buffer and heat-sealed with with a Beckman centrifuge sealer, Tube Topper, 60 Hz. The gradient with the lysate was subjected to ultracentrifugation at 255,000 x g (av.) (60 000 RPM) for 85 min at 18 °C in a Beckman Optima L-100XP ultracentrifuge using a Type 70Ti rotor. After centrifugation, the 40% layer was recovered by perforation of the side of the tube with a needle attached to a syringe and dispensed into a new tube. The vectors were stored at -80 °C in 50-100 µl aliquots.

Figure 2. 3: Ioxidianol gradient ready for rAAV purification.
The lower layer at the bottom of the tube is the 60% fraction, which is characterized by a yellowish colour. The following layer is the 40% fraction, which will contain the virus after the ultracentrifugation, and it is characterized by a transparent colour. Above the latter layer is the reddish 25% fraction followed by the transparent 15% fraction. The top of the tube contains the filtered lysate immediately before centrifugation. Phenol red was used for visualization purposes.

For desalting and concentration of the collected iodixanol fraction, Amicon Ultra -15 PL100 devices were used. The 40% iodixanol fraction was added to the device and washed 3 times with PBS-MK buffer centrifuging at 3360 x g for 17 min at RT. On the final spin, the volume was reduced to 500-1000 µl and dispensed in 50-100 µl aliquots for long-term storage at -80 °C.

2.3.5.3.3 Titration

Two methods were used to assess rAAV titre, both of which estimate genome copy number of viral particles (infectious and not infectious particles). The first step for both methods was the extraction of the vector DNA with phenol/chloroform. For this, 5 µl of the purified vector stock were incubated for 1 hour at 37 °C with 5 U of Dnase I in a final volume of

200 µl pure DMEM. 100 µg of proteinase K in 200 µl 1X proteinase K buffer was mixed with the DNase-treated vectors for a 1 hour incubation at 37 °C. An equal volume of 25:24:1 phenol/chloroform/isoamyl alcohol was then added, the solution was mixed thoroughly and centrifuged at 14,000 rpm for 10 min at 4 °C. The supernatant was transferred to a new microfuge tube and the DNA was precipitated with 1/10 volume of 3M sodium acetate, 40 µg of glycogen and 2.5 volumes of 100% ethanol. The solution was incubated at -80°C for 30 min, centrifuged at 13,000 rpm for 20 min at 4°C and the supernatant was discarded. The pellet was washed with 1 ml of 70% ethanol, spun again and after the centrifugation it was re-suspended either in 400 µl of TE (for qPCR titration) or 400 µl of dot blot re-suspension buffer (for dot blot titration).

2.3.5.3.3.1 Titration by qPCR

The DNA in TE from the previous section was used for qPCR with primers located in the poly A region (present in all rAAV). The reaction was performed under the following conditions: 0.3 µM of each primer, 1X SensiMixPlus SYBR and 5 µl of undiluted, $1x10^{-2}$ and $1x10^{-4}$ dilutions of the template in a final volume of 20 µl. $1x10^{-1}$-$1x10^{-8}$ copies of the DNA of pscAAVh*SMN1*F were used as standards. Samples were done in duplicate and standards were done in triplicate (including the negative control). The cycling conditions were: 1 cycle at 95˚C for 10 min and 45 cycles at 95˚C for 15 s/ 60˚C for 1 min. A melting curve calculation was performed at the end with a continuous reading between 50 and 100 ˚C. The titre was expressed as genome copies per ml of vector stock.

2.3.5.3.3.2 Titration by dot-blot

The dot-blot titration method relied on the hybridization of a PCR amplification product corresponding to the CMV promoter of the pscAAVCAG backbone with the viral DNA. The probe was amplified using the following conditions: 0.6 µM of each primer, 1.5 mM $MgCl_2$, 200 µM dNTPs, 0.25 U GoTaq® Flexi DNA Polymerase in its 1X Green GoTaq Flexibuffer and 5 ng of template (pscAAVh*SMN*1F) in a final volume of 25 µl. The cycling conditions were: 1 cycle at 95 °C for 5 min, 35 cycles at 95 °C for 1 min /56 °C for 1 min/ 72 °C for 45 s and with a final extension at 72 °C for 5 min. 100 ng of the CMV amplification product was labelled on the first day of the dot blot procedure following the instructions of the Amersham ECL Direct Nucleic Acid Labelling And Detection Systems kit.

As standards, a 2-fold serial dilution of pscAAVCAGh*SMN1*F was prepared in a volume of 20 µl (containing 80 ng-0.3125 ng; 9 different standards). All standards were further diluted in 400 µl of dot blot re-suspension buffer. Vector samples and standards were heated at 100°C for 5 min and immediately cooled on ice for 2 min. To blot, denatured viral vector samples and standards were added onto the Hybond N+ hybridization membrane using a minifold (96 well dot blotter) SRC-96/1 with a capex L2C vacuum source. The blotter was dismounted and the membrane was then exposed to UV light for 30 s in a UV trans-illuminator and rinsed with 2x SSC before placing it in a hybridization tube with 15 ml of hybridization buffer. The tube was placed in a hybridization oven for a one-hour incubation at RT with rotation. The labelled probe was then added to the hybridization buffer in the tube and the membrane was incubated overnight at 42°C. The next day the membrane was washed twice with 100 ml of dot blot primary wash buffer for 20 min at 42°C and then twice with 100 ml of 2X SSC. The development of the blot was performed with the Amersham ECL Direct Nucleic Acid Labelling And Detection Systems kit, following manufacturer's instructions. In order to estimate the concentration of the viral samples, their intensity was visually compared to the intensities of the standards. **Figure 2.4** shows the results of the dot blot measurement of several rAAV preparations, where the DNA contained in 2 and 5µl of purified viral stock were probed.

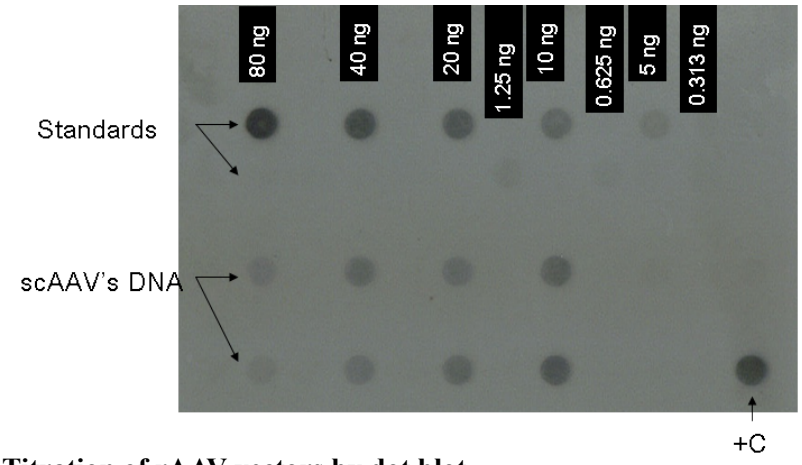

Figure 2. 4: **Titration of rAAV vectors by dot blot.**
2 and 5µl of the purified viral stock were hybridized with a probe against the CMV enhancer. The estimation of the titre was done by visually comparing the intensity of each pair of samples with the ones in the standards.

2.3.5.3.4 Transduction

2.3.5.3.4.1 Mammalian cell lines

Transduction of rAAV in mammalian cell lines was performed to assess transduction efficiency *in vitro*. For this, $1x10^5$ HEK293T or HeLa cells were seeded in wells of a six-well plate with standard growth medium. 24 hours later, the medium was removed and 1 ml of fresh standard growth medium containing 10^9 copies of scAAV9Cage*GFP* (genomes copies as measured by qPCR) was added per well, for a MOI of 10,000. 1 ml of standard growth medium without vector was used as negative control. Cells were incubate at 37°C, 5% CO_2 for 2 hours, shaking the plates at 30-minute intervals during the incubation. After 2 hours, 1 ml of standard growth medium high serum (20% FBS) was added to each well. After 72 hours the cells were harvested by tryptinization and analysed by flow cytometry.

2.3.5.3.4.2 MNs

The transduction of MNs was done in two different ways. For MOI purposes, it was assumed that one neurosphere had approximately $1x10^4$ cells. In the first method, four neurospheres were incubated in a microfuge tube for 2 hours (37°C) with 200 µl of MN differentiation medium 1528 containing rAAVs for a qPCR MOI of 50,000. Neurospheres were then seeded on PO-laminin coated coverslips, as will be described in **section 2.3.7.2.** The second method differs in that the neurospheres were transduced and seeded at the same time. This last method was employed for the transduction of cells later harvested for western blot and qRT-PCR (40 neurospheres and 20 neurospheres respectively).

2.3.6 iPSC GENERATION

All iPSC generation-related procedures, as well as some quality control tests were performed in the Centre for the Study of Stem Cells (CECS, Centre d'Étude des Cellules Souches), a laboratory funded by the French Muscular Disease Association (AFM, Association Française contre les Myopathies), which is integrated in I-STEM at Genopole campus (Evry), France. Most of the protocols presented here are used or modified from those used in I-STEM, where I took part in a three-months workshop (April-July, 2010) and a two-months laboratory visit (February-March, 2011) under the supervision of Cécile Denis and Mathilde Girard.

iPSCs were generated from skin fibroblasts of three siblings of a consanguineous family harbouring the same homozygous deletion (c.399_402delAGAG in exon 3) of the *SMN1*

gene. iPSCs were also obtained from the carrier mother. The coding of the family members, and their pedigree can be found in **Chapter 4 (Figure 4.1).**

2.3.6.1 SKIN BIOPSY AND FIBROBLAST CULTURE

The skin biopsy was performed in Santa Creu i Sant Pau Hospital (Barcelona). A 5 mm punch biopsy was extracted from the forearm after informed consent. The biopsy was placed under sterile conditions on a dish containing HBSS supplemented with 1% Penicillin-Streptomycin-Fungizone (PSF) in order to separate the adipose tissue, connective tissue and blood vessels. The biopsy was then cut with a scalpel into fragments of approximately 4x4 mm, moved to a new 60 mm dish and incubated overnight at 37 °C, 5% $C0_2$ in conditioning media (M-199, 15% FBS, 1% PSF). The next day the fragments were cut in half and seeded over plasma-gelatine coated dishes in biopsy culture medium (65% D-MEM, 22% M-199, 10% FBS, 2 mM glutamine, 10 ng/ml FGF_2, 25 ng/ml EGF and 1% PSF). The medium was changed every three days and a second explant was performed once the cells growing from the fragments got confluent. The fibroblasts that grew out from the first explant were trypsinised as previously described (**Section 2.3.4.1.1**) and expanded twice (to passage 3) before shipping them to I-STEM in 25 cm^2 tissue culture flasks completely filled with biopsy culture medium. The biopsy and culture from CC was performed using a similar procedure, but a 5-years old biopsy (with two previous explants) was used instead of a fresh one given that the patient died before the new biopsies were taken.

2.3.6.2 CELL TRANSDUCTION AND iPSC EMERGENCE

A diagram of the entire procedure for iPSC reprogramming is depicted in **Figure 2.5.** The protocol used for fibroblast transduction and iPSC generation has been recently published (*Mangeot et al., 2011*). It involves the use of the so-called "gesicles", which carry the receptor for the MMLV envelope protein [murine cationic amino acid transporter-1 (mCAT-1)] and allow the infection of ecotropic vectors in human cells. For this study, mCAT-1 gesicles were supplied by I-STEM and details of their production were not provided.

The first step for the reprogramming process was the generation of four rMMLVs, each carrying one of the four transcriptions factors of Yamanaka's cocktail: *OCT4, SOX2, KFL4* and *c-MYC* (*Takahashi et al., 2007*). The transfer plasmids used were the same as the ones published by *Park et al., 2008*. Refer to **section 2.1.3** for more information.

For transduction, 100,000 fibroblasts from each patient were seeded in a well of a 6-well plate in reprogramming fibroblast medium. The next day, most of the medium was removed from, leaving only 0.5 ml per well, and 15 µl of mCAT-1 gesicles were added. Cells were returned to the incubator for one hour, after which 1 ml of a premix containing equal proportions of all four vector supernatants was added to each well. The next day, the medium was changed. Four days port-transduction, cells were harvested by triptinisation and 43,000-100,000 cells from each patient were seeded per well in 6-well plates coated with 0.1% gelatin (a whole plate for each patient) in reprogramming fibroblast medium. Given the different growth rates of cells from different subjects, 0.1% gelatine-coated 100 mm dishes were also seeded with approximately 300,000 cells in some cases. 24 hours after re-plating, the reprogramming fibroblast medium was changed to hESC medium supplemented with 10 ng/ml FGF_2 and 0.5 mM VPA. Cells were incubated without splitting until iPSC colonies emerged. The hESC medium was changed daily for ten days maintaining the FGF_2 and VPA supplementation, time after which VPA supplementation was discontinued.

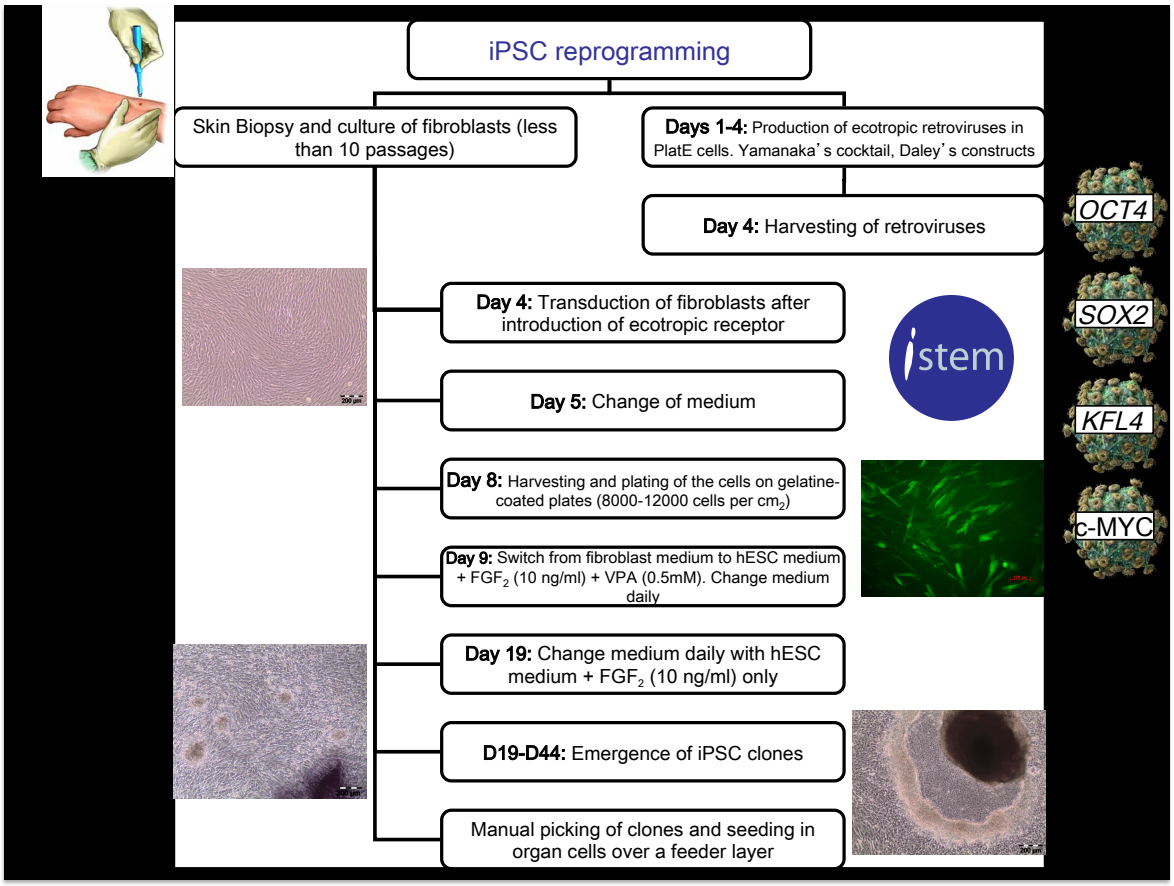

Figure 2. 5: Diagram of the procedure followed for the generation of iPSCs from human fibroblasts.

2.3.6.3 SELECTION AND ESTABLISHMENT OF CLONES

iPSC colonies emerged between 2 to 5 weeks post-transduction. The identification of iPSC colonies was first done under an inverted microscope with 4X magnification lens. The selection was performed based on morphology: round-shaped colonies of tightly packaged cells with scant cytoplasm and bright-defined borders around them, although the morphologies were very heterogeneous at this point. Once the emerging iPSC colonies were identified they were manually passage to an OC with feeder cells in hESC medium supplemented with 2μM thiazovivin as previously described. hESC medium was switched after several passages to Stemedia™ NutriStem™ XF/FF Culture Medium as described in the section for culture of iPSCs.

2.3.7 iPSC DIFFERENTIATION

iPSCs were differentiated into several immature cell types through the platting of embryoid bodies and into more mature cell types such as MNs and hepatocytes through the use of selective cultures. In all cases the differentiation yield very heterogeneous populations, and cell identity was performed by immunofluorescence.

2.3.7.1 *IN VITRO* DIFFERENTIATION ASSESSMENT

When iPSCs are grown in suspension without FGF_2, they form floating, spherical aggregates called EBs. These structures contain cells going though differentiation, and if no coaxing is performed, they give rise to cell types representative of the three germ layers, a major characteristic of *bona fide* iPSCs.

In order to form EBs, iPSCs were grown for 5 days and disaggregated in clumps as described previously for the enzymatic passaging (**section 2.3.4.2.1.4**); the optimal size of the clumps in this procedure was between 50-200 μM. After centrifugation and removal of the medium, clumps were re-suspended in hESC medium and transferred to low-binding 6-well plates. The next day, the remaining feeders in the incipient EBs were removed by filtration through a 20 μm pore cell strainer and transferred to new low-binding 6-well plates. EBs were cultured in suspension in hESC medium for 7 days and then equally distributed in 0.1% gelatine-coated wells of 24 well plates using the same medium. Attached EBs were cultured further for 7 days, fixed and stained with antibodies recognizing epitopes characteristic of the three germ layers: Neuronal Class III β-Tubulin (TUJ1) for the ectoderm; Actin Smooth Muscle Actin (SMA) and desmin for mesoderm;

alpha fetoprotein (AFP) for endoderm. For a detailed description of the antibodies and their dilutions, please refer to the **section 2.1.7.2**.

2.3.7.2 DIFFERENTIATION TO MNS

MN differentiation was performed following Hu and Zhang's protocol, originally designed for hESCs (*Hu and Zhang, 2009*). Briefly, for the first two weeks iPSCs were induced to neuroepithelial (NE) cells that formed neural tube-like rosettes in the absence of morphogens, by generating EBs in the first week and plating them out with neural differentiation medium in laminin-coated 6-well plates during the second week. Between days 10-17 neural tube like-rosettes became apparent within the plated clusters, and the percentage of the area covered by the rosettes within the cluster was used as an indicator of neural induction efficiency, together with the co-expression of the NE markers PAX6 and SOX1. NE cells were then lifted by manual selection under the stereomicroscope and grown in suspension as neurospheres in MN differentiation medium 1528 (containing 0.1 μM retinoic acid [RA], a caudalising agent and 1 μM purmorphamine, a ventralising agent) for two weeks. The aggregates were split by a 5 min incubation at 37 °C with 1ml of accutase when they became too big (more than 300 μm). Neurospheres were then plated on Poly-L-Ornithine-Laminin (PO-laminin)-coated 10 mm coverslips, dishes or plates at day 28 and cultured in a medium supplemented with 10 ng/ml FGF_2, BDNF, GDNF and IGF, 200 ng/ml ascorbic acid, 1 μM cAMP, b27 and N2 as well as 50 nM RA and 0.5 μM purmorphamine (complete MN differentiation medium) to generate post-mitotic MNs. The medium was changed every other day (*Hu and Zhang, 2009*).

All procedures were performed as described in *Hu and Zhang* (2009), except the coating and seeding of neurospheres, which was done as follows: PO (100 μg/ml) was added to the culture surface and incubated at RT for two hours, washed three times with HBSS without drying and incubated overnight at 4°C with 20 μg/ml of murine laminin diluted in neural differentiation medium. The next day, laminin was removed and a minimum amount of complete MN differentiation medium was added just before seeding the selected neurospheres (3-5 neurospheres per coverlip for staining, 10 neurospheres per 30-mm dish for axon growth, 20 neurospheres per well of 12-well plates for qRT-PCR and 40 neurospheres per well of 6-well plate for WB). Two hours later, when the cells were attached, the rest of the MN differentiation medium was added.

2.3.7.2.1 Co-culture of iPSC-derived MNs and mouse myotubes

iPSC-derived MNs were grown on mouse myotubes in order to observe the formation of NMJs. For this, permanox TC chamber slides were coated with 20 μg/ml of murine laminin and incubated at 37 °C for one hour. Laminin was removed and C2C12 cells were then seeded in standard growth medium at two different confluences: 2.3 x 10^5 cells/cm_2 (for 70% confluence at 24 h) and 1.7 x 10^5 cells/cm_2 (for 50% confluence at 24 h). The next day the medium was switched to C2C12 differentiation medium and cells were grown for four more days, at which time 4-6 D39 Neurospheres were seeded on these cells with in 1:1 mix of C2C12 differentiation medium and complete MN differentiation medium. Cells were then cultured for 3 days and fixed at D42 of MN differentiation for staining. In order to accomplish the timings, C2C12 cells were initially seeded at D34 of MN differentiation.

2.3.7.2.2 Axon length measurement

In order to measure axon length growth, ten neurospheres were seeded on PO-laminin coated 30-mm petri dishes on D26. Images of 5 neurospheres were taken on D27, D29, D32 and D34 with an inverted microscope and a 2X lens. For each day, the length of the five longest neurites was measured using Image J and the values were averaged.

2.3.7.3 DIFFERENTIATION TO HEPATOCYTES

Hepatocyte differentiation was performed following Song's protocol (Song *et al.* 2009). A diagram summarizing the complete protocol is shown in **Figure 2.6.** The protocol did not include lifting or manual selection of the cells, but only the addition of coaxing molecules in a stepwise manner. Briefly, iPSCs growing on feeders were maintained in hepatocyte differentiation medium 1-3 (containing 100 ng/ml Activin A) for three days, further supplementing the medium with 0.1 and 1% insulin-transferrin-selenium on days 2 and 3 respectively. After ectodermal induction, cells were cultured for four days in hepatocyte differentiation medium 4-7 (containing 30 ng/ml FGF_4 and 20 ng/ml BMP_2) in order to induce hepatic differentiation. Cells were then maintained for six days in hepatic differentiation medium 8-13 (containing 20 ng/ml HGF and 20 ng/ml KGF), five days in hepatic differentiation medium 14-18 (containing 10 ng/ml oncostatin-M, 0.1 μM dexamethasone) and three days in hepatic differentiation medium 19-21 (containing N2, B27). The protocol was followed exactly as described by the author. For a detail description of the component of the media please refer to section **2.1.9.4**.

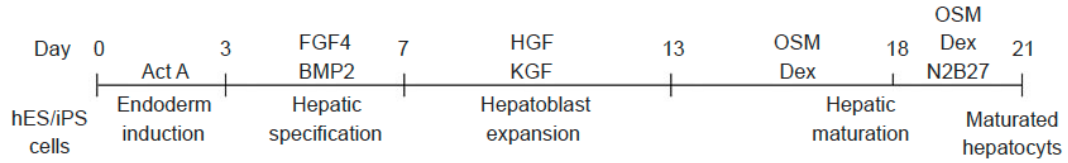

Figure 2. 6: Stepwise differentiation protocol from iPSC to hepatocytes.
Taken from (Song *et al.* 2009).

2.4 STATISTICAL ANALYSES

Statistical Package for the Social Sciences (SPSS) and GraphPad Prism software were used for all statistical analyses. All data are presented as mean ± standard error of the mean (SEM) and groups are compared either by one-way or two-way ANOVA. For the neurite growth analysis one-way ANOVA with repeated measures was used. For the molecular analyses (qPCR and western blot) between patients and unaffected individuals and between cellular types, two-way ANOVA with the Bonferoni *post hoc* was employed to compare control and SMA individuals across each cellular type, and the Scheffe *post hoc* to compare all individuals across each cellular type. One-way ANOVA and the *post hoc* for linear trend were used to assess the decay in the molecular analyses (qPCR and western blot) of all individuals. Differences were considered statistically significant if $P<0.05$ (*), $P<0.01$ (**) and $P<0.001$ (***).

CHAPTER 3: RESULTS- VIRAL VECTOR GENERATION AND CHARACTERISATION

This chapter describes all the work related with the production of viral vectors and their characterisation *in vitro*, including the plasmids used to generate the vectors, the cloning of new transfer plasmids and the transduction efficiency, when feasible and available. For rH1LVs, and rMMLVs no new transfer plasmids were created and particularly for the latter, no accessory plasmids were necessary for production, since they were transfected in the PlatE cells which already contained the necessary genes for rMMLV production. For rH1LVs, only the identity of the transfer plasmid was assessed, given that members of my laboratory have extensively characterised all other plasmids for LV production and they were all produced in large quantities by Plasmid Factory. LV transduction efficiency could not be assessed in continuous mammalian cell lines because a MN specific promoter (HB9) was driving the expression of the reporter gene. LV and AAV transduction efficiency in iPSC-derived MNs is presented in chapter 5. rMMLV transduction efficiency was not assessed in RHUL and final results were not provided by I-STEM.

3.1 rAAVs

3.1.1 CHARACTERISATION OF PLASMIDS FOR rAAV9 PRODUCTION

Restriction analysis was performed on each of the three plasmids used in rAAV production in order to characterise them. The original rAAV transfer plasmid obtained was provided with an enhanced version of the reporter *eGFP*. For the transfer plasmid, pscAAVCage*GFP,* the enzymatic digestion with *Age*I + *Sbf*I produced a 761 bp and a 3945 bp fragment from the original 4706 bp plasmid **(Figure 3.1A).** For the packaging plasmid p5E18-VD2/9, the digestion with *Pvu*II yielded a 2513 bp and a 4816 bp fragment from the original 7329 bp plasmid **(Figure 3.1B).** Finally the helper plasmid pAdDeltaF6 was digested with *Bgl*II yielding several fragments of different sizes from the original 15414 bp plasmid: 1625 bp, 1698 bp, 2151 bp, 4647 bp and 5031 bp (**Figure 3.1C**). The band with the smallest size from pAdDeltaF6 was not visualised in the gel (272 bp).

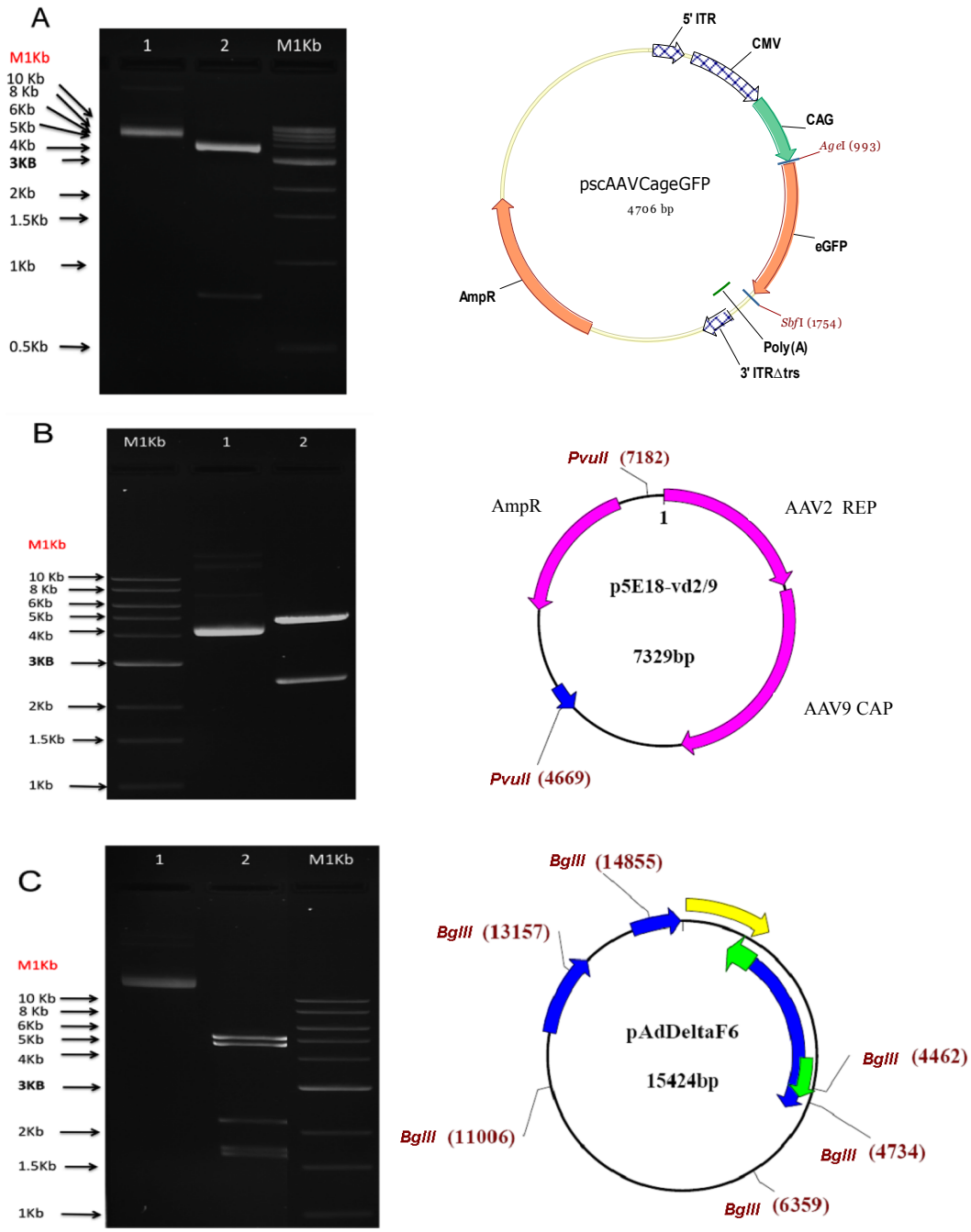

Figure 3. 1: Characterisation of the three basic plasmids for the production of rAAV9 through their restriction pattern.

All plasmids are presented along with their map and the relevant restriction sites. Lane 1 in all images shows the corresponding undigested plasmid and lane 2 the digestion products. (**A**): pscAAVCage*GFP* was digested with *Sbf*I and *Age*I yielding 761 bp and 3945 bp fragments. (**B**): p5E18-VD2/9 was digested with *Pvu*II generating 2513 bp and 4816 bp fragments. (**C**): pAdDelta6 was digested with *BglII* yielding the fragments: 1625 bp, 1698 bp, 2151 bp, 4647 bp and 5031 bp. M1Kb: 1 Kb molecular size marker. 200 ng of DNA were loaded in all lanes except for the marker that contained 500 ng. The main identified elements of the plasmids are as follows: ITR: inverted terminal repeat; CMV: cytomegalovirus promoter; CAG: short version of ubiquitous cytomegalovirus enhancer/ chicken beta actin promoter; eGFP: enhanced green fluorescent protein; Poly(A): poly(A) tail; trs: terminal resolution site; AmpR: ampicillin resistance gene; AAV2 REP: AAV2 replication proteins AAV9 CAP: AAV9 capsid proteins. Depicted sequences in pAdDeltaF6 correspond to adenoviral genes, but details were not made available.

3.1.2 CLONING OF hSMN1 INTO THE rAAV TRANSFER PLASMID

The eGFP cDNA in pscAAVCage*GFP* was replaced by the h*SMN1* cDNA in two versions: a flag-tagged version at the N terminus and a simple version without flag tag, generating pscAAVCagh*SMN1*F and pscAAVCagh*SMN1*NoF respectively. The h*SMN1* cDNA was amplified by PCR from a Genecopoeia clone (product ID: K2843, Cat. No. FL15214), using primers that added the *Age*I restriction site at the 5´end and the *SbfI* restriction site at the 3´end. In the case of the pscAAV9Cagh*SMN1*F, the 5´ primer also included the sequence of the flag tag (24 nucleotides). In order to incorporate the new restriction sites and the flag tag in the amplification product, the melting temperature of the first seven cycles of the PCR reaction was lowered beyond the theoretical one, increasing then 2 °C per cycle (from 59°C to 70 °C).

The 937 bp flag-tagged *hSMN1*amplification product and the 910 bp *hSMN1* amplification products were digested with *Age*I and *Sbf*I and gel-purified. Smaller non-specific bands were distant enough to avoid their presence in the excised fragments when the cutting was performed **(Lanes 1, 2, 4 and 5, Figure 3.2).** pscAAVCage*GFP* was also digested and gel-purified in the same way, releasing a 761 bp fragment containing the *eGFP* cDNA, leaving a 3945 bp backbone fragment to be excised and purified **(Lanes 6 and 7, Figure 3.2).**

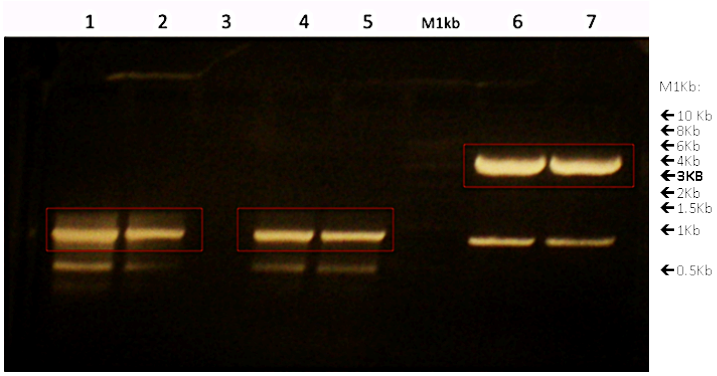

Figure 3. 2: Purification of fragments for the production of the new rAAV transfer plasmids.
A flag-tagged h*SMN1* cDNA (**lanes 1** and **2**) and a h*SMN1* cDNA without any tag (**lanes 4** and **5**) were amplified by PCR generating fragments of 937 bp and 910 bp respectively. The specific products are shown inside red boxes. The pscAAV9Cage*GFP* was digested with *Age*I and *Sbf*I to release the *eGFP* fragment of 761 bp that was further replaced by the new amplified products. The fragment corresponding to the backbone of the rAAV transfer plasmid is also shown inside a red box (**lanes 6** and **7**).

After ligation and bacterial transformation, 5 clones of each construct were screened, performing a double restriction with *Age*I and *Sbf*I. All clones showed the correct restriction pattern: 923 bp and 3945 bp fragments for pscAAVCag*hSMN1*F clones and 896 bp 3945 bp fragments for pscAAV9Cag*hSMN1*NoF clones. The map of the starting plasmid

pscAAVCage*GFP*, the new constructs pscAAVCaghSMN1F and pscAAV9Cagh*SMN1*NoF along with their respective restriction digestion with *Age*I and *Sbf*I are illustrated in **Figure 3.3.**

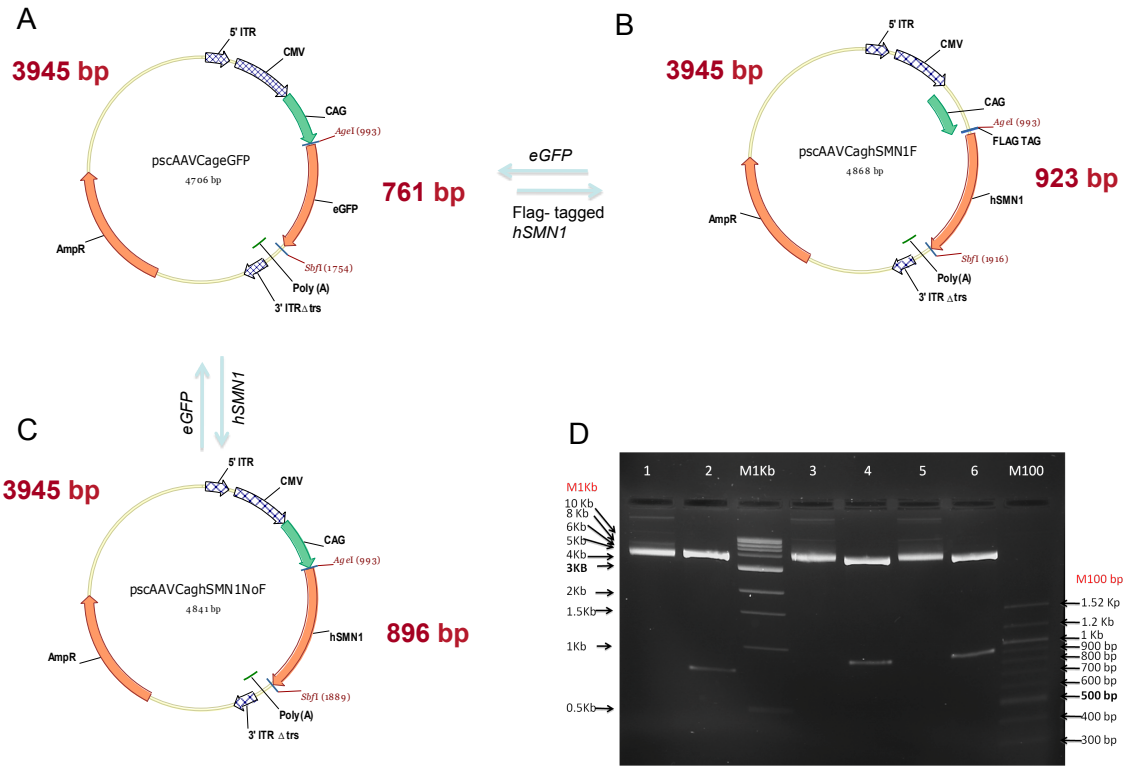

Figure 3. 3: Cloning of h*SMN1* and flag-tagged h*SMN1* in the pscAAV9 backbone.
A, **B**, and **C**: Maps of the starting plasmid pscAAV9Cage*GFP* and the resulting plasmids pscAAV9Cagh*SMN1*F and pscAAV9Cagh*SMN1*NoF, respectively, describing their common elements and the two restriction sites used for cloning the new genes, *Age*I and *Sbf*I. (**D**) Restriction pattern of each of the plasmids with the cloning enzymes *Age*I and *Sbf*I. Undigested (1) and digested pscAAVCage*GFP* (2), with the expected 761 pb band; undigested (3) and digested pscAAVCagh*SMN1*NoF (4), with the expected 896 pb band; undigested (5) and digested pscAAVCagh*SMN1*F (6), with the expected 923 pb band. M1Kb, M100 bp: 1 Kb and 100 bp molecular size markers. 200 ng of DNA were loaded in all lanes except for the marker that contained 500 ng. The main elements of the plasmids are as follows: ITR: inverted terminal repeat; CMV: cytomegalovirus promoter; CAG: short version of ubiquitous cytomegalovirus enhancer/ chicken beta actin promoter; eGFP: enhanced green fluorescent protein; Poly(A): poly(A) tail; trs: terminal resolution site; AmpR: ampicillin resistance gene

Clone 2 of the pscAAVCagh*SMN1*NoF and clone 3 of the pscAAV9Cagh*SMN1*F (the same clones whose restriction analyses are shown in **Figure 3.3**) were sequenced from the 5' end and the 3' end with primers annealing at least 70 bp from the junction sites used for ligation. Both plasmid clones were found to contain the corresponding inserts correctly cloned into the rAAV transfer plasmid backbone, confirming the results from the restriction analysis (**Figure 3.4**). It was also confirmed that the whole inserts, including the *hSMN1* open reading frame, had the expected sequence.

Figure 3. 4: Sequencing and alignment of the new *SMN1* clones.
(**A**) pscAAVCagh*SMN1*NoF clone 2 and (**B**) pscAAVCagh*SMN1*F clone 3 were sequenced from the 5' end, shown in the upper section of each panel, with a primer localized at the Cag promoter, and from the 3' end, showed in the lower section of each panel, with a primer localized around the poly A sequence. Each sequencing product was aligned with the expected PCR product after digestion with *Age*I and *Sbf*I and the complete sequence of the expected plasmid.

3.1.3 ASSESSMENT OF hSMN1 EXPRESSION FROM THE NEW CONSTRUCTS

In order to assess the correct expression of the *hSMN1* genes inserted into the rAAV transfer plasmid backbone, hSMN protein production was assessed by western blot in HEK293T cells transfected with pscAAVCagh*SMN1*F or pscAAVCagh*SMN1*NoF. **Figure 3.5** shows a qualitative control of the transfection efficiency with the original rAAV transfer plasmid pscAAVCage*GFP*. The transfection efficiency of the plasmid used as a positive control of flag expression (a lentiviral backbone with a flag-tagged m*Smn,* pRRLsc_C_m*Smn*_eIeGFP_W) is also shown. eGFP protein production from both plasmids seems to be high and similar.

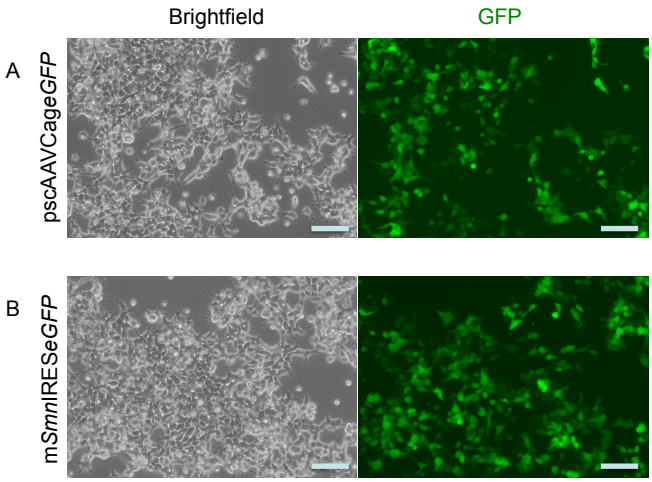

Figure 3. 5: Transfection efficiency in HEK293T cells before harvesting for protein extraction 72h later.
(**A**) pscAAVCage*GFP* transfected into cells as a control for the efficiency of the transfection method using an rAAV transfer plasmid. (**B**) LV plasmid encoding the flag-tagged m*Smn* with an IRES *eGFP* transfected into the cells as a positive control of flag expression. Images are shown as bright field and the corresponding fluorescence field for *eGFP*. Scale bar= 100 µm.

A 40 KDa protein corresponding to the expected size of the flag-tagged hSMN1 was detected in cells transfected with pscAAVCagh*SMN1F* as well as in cells transfected with a similar plasmid containing the flag tag in the C terminus of h*SMN1* (a plasmid produced by Pavlina Petrova, an undergraduate student under my supervision), but not in the cells transfected with pscAAVCagh*SMN1*NoF or in the mock, as expected (**Figure 3.6**). The level of flag-tagged protein was apparently higher from the LV plasmid encoding flag tagged *mSmn*, although similar amount of proteins were loaded onto all the wells.

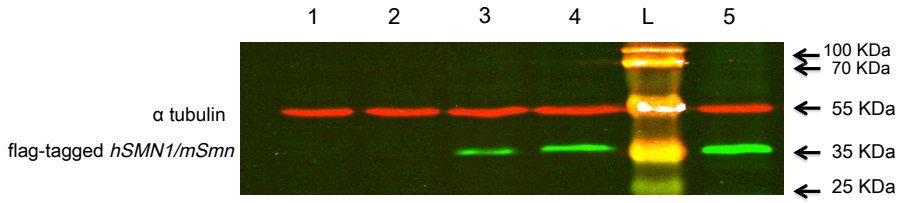

Figure 3. 6: Assessment of the expression of flag-tagged h*SMN1* from the rAAV transfer plasmid.
10 µg of pscAAVCagh*SMN1*NoF (**2**), pscAAVCagh*SMN1*F (**4**), a similar plasmid to pscAAVCagh*SMN1*F, but with a flag tag in the C terminus (**3**) and a positive control LV plasmid expressing flag-tagged *mSmn* downstream of the CMV promoter, pRRLsc_C_m*Smn*_eIeGFP_W (**5**) were transfected into HEK293T cells. Cells were harvested 72 h later. Non-transfected cells were also harvested (**1**). 25 µg of total protein extract were loaded onto a 12% SDS-PAGE gel for western blot analysis with an antibody against the flag tag (for detection of the flag-tagged *hSMN/mSmn*). An anti-α tubulin antibody was used as a loading control. L: protein Ladder

3.1.4. IMPROVEMENTS IN THE PRODUCTION OF rAAVs

For the production of rAAVs, two main parameters have been changed over the time in order to improve the titre. The first parameter considered was the confluence of the HEK293T cells at the time of transfection. For quantification purposes, the reporter plasmid pscAAV9Cage*GFP* was used. As shown in **Figure 3.7**, the transfection efficiency, as assessed by the number of eGFP+ cells by flow cytometry, was higher when the confluence

of the cells was lower, producing 84% eGFP+ cells at 48 h post-transfection when the transfection was performed at confluence of approximately 50%.

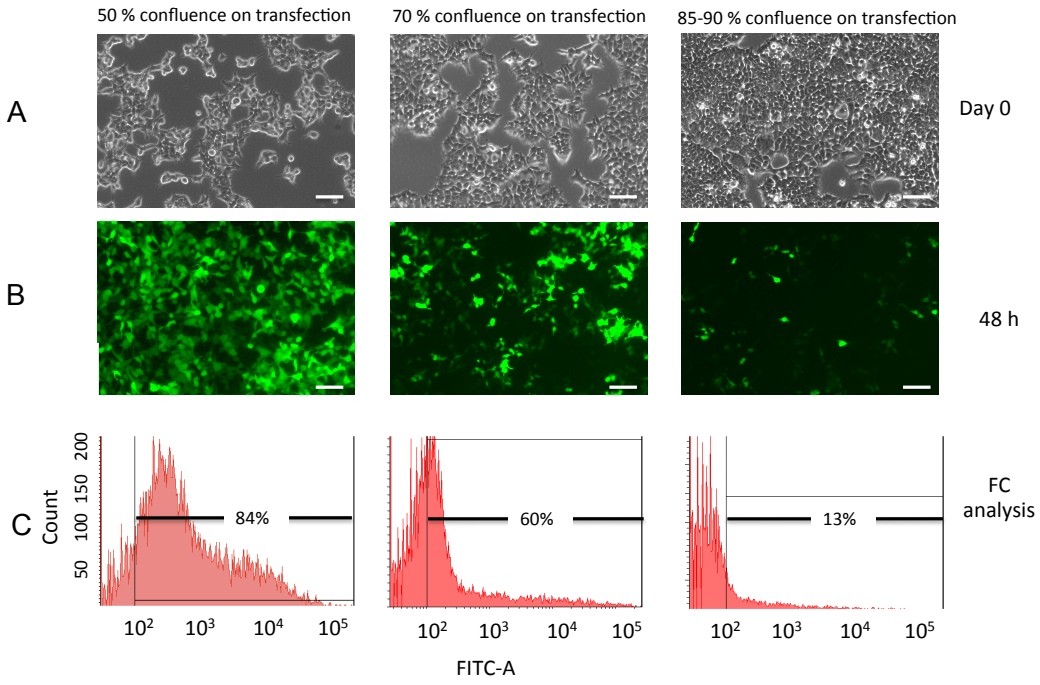

Figure 3. 7: Optimization of HEK293T transfection.
(**A**) Bright field image of the confluence of the cells on the day of transfection. (**B**) Fluorescence (green channel) image of the cells 48 hours after transfection with 3 µg of pscAAV9Cage*GFP*. (**C**) Flow cytometry analysis for the quantification of the percentage of eGPF+ cells. Scale bar= 100 µm.

The second parameter, which was shown to improve the viral titre, was the precipitation of the viral particles in the supernatant of the producer cells with Polyethylene glycol (PEG). Initially, only the viral particles contained within the cells were harvested and purified. **Figure 3.8** shows the titres for several batches of rAAVs**.** The last two batches presented (19mar2010) correspond to productions where the transfection of the plasmids was performed with less confluent cells (~50% as opposed to 85%) and where viral particles in the supernatant were precipitated with PEG (as described in Materials and Methods, Chapter 2). These last two rAAV batches show a higher titre than the previous batches (approximately a total of $7x10^{10}$ qPCR genome copies or $1.7x10^{12}$ dot blot genome copies). It is important to mention that as it can be appreciated from the figure, the titres measured by dot blot were always higher than the ones measured by qPCR, even though both methods assessed genome copy number. The difference between both methods nonetheless is consistent: dot blot titre is always one log unit higher that the qPCR titre.

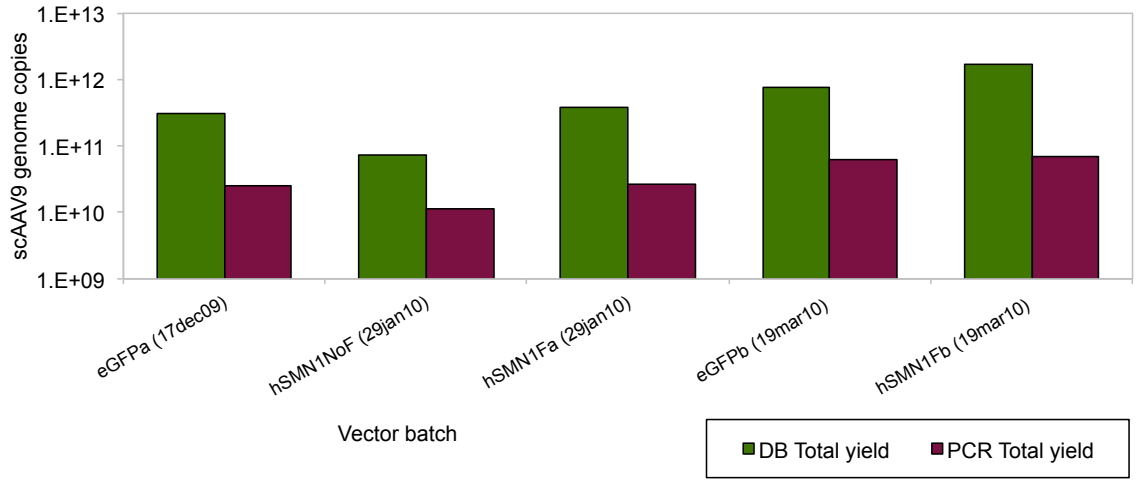

Figure 3. 8: qPCR and dot blot titres of four rAAV batches.
The last two batches, as opposed to the first three, were produced performing the plasmid transfection when cells were 50% confluent and included the harvest of viral particles in the supernatant besides the ones contained within the producer cells. All batches were prepared by the transfection of cells in ten 150 mm plates. Data are presented as total yields instead of concentration, given the fact that batches were not re-suspended in the same volume during the desalting procedure. eGFP: scAAV9Cage*GFP,* hSMNNoF: scAAVCagh*SMN6,* hSMNF: scAAVCagh*SMN1F,* DB: dot blot.

3.2.5 TRANSDUCTION EFFICIENCY IN MAMMALIAN CELL LINES

AAV9 is well known to have very low transduction efficiency *in vitro*, so high multiplicity of infections (MOIs) were used in order to confirm the ability of the rAAV9s produced to transduce cells and to express the target gene. scAAV9Cage*GFP* was used for this purpose given that upon effective transduction it drives the exogenous expression of the eGFP reporter protein, which can be easily quantified by flow cytometry.

As shown in **Figure 3.9** HeLas and HEK293T cells transduced with a qPCR MOI of 10,000 show very low transduction efficiency at 72h, as expected. The higher transduction efficiency obtained was in HEK293T (7.5%).

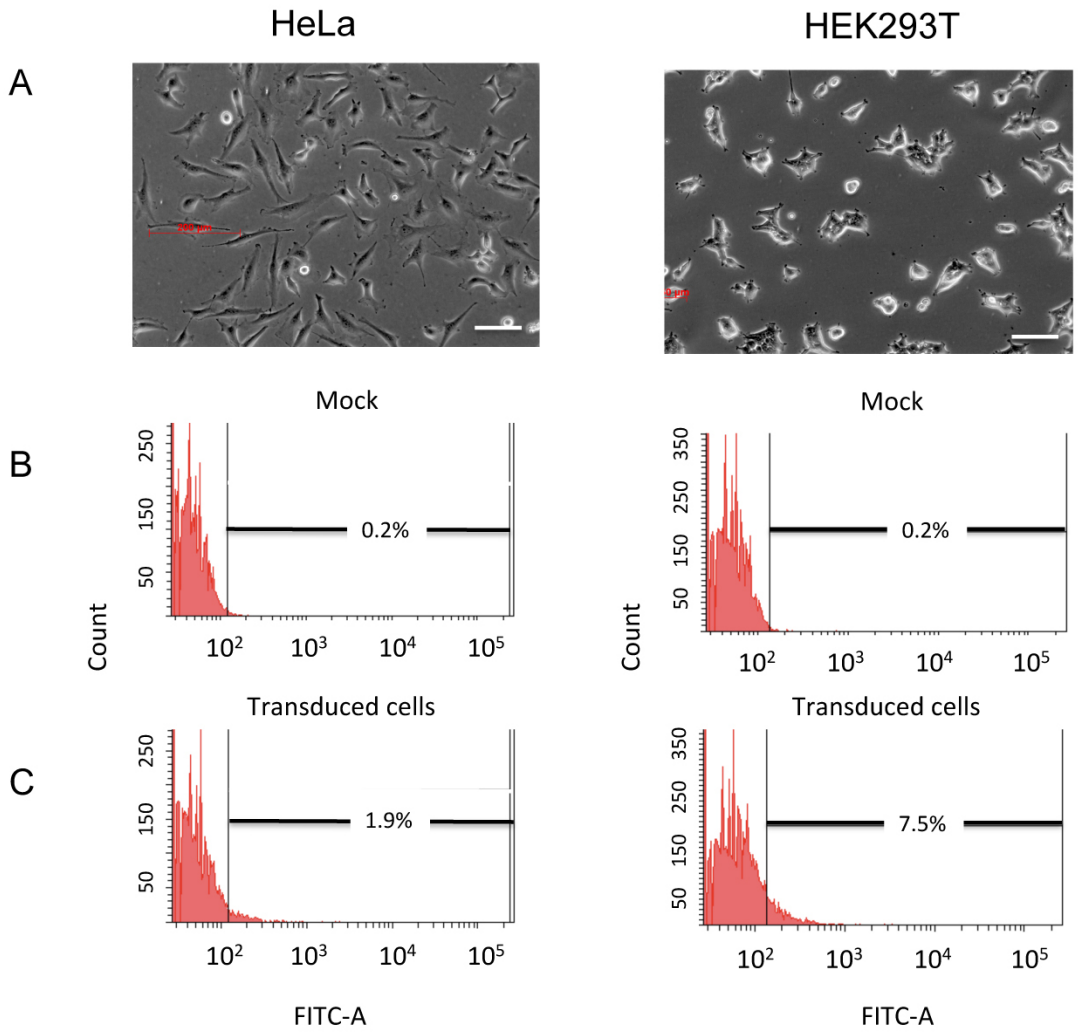

Figure 3. 9: Transduction efficiency of scAAV9Cage*GFP* in mammalian cell lines.
HeLa and HEK293T cells were transduced at qPCR MOI 10,000 and harvested 72 hours later. All transduction experiments are shown with a bright field image of the cells prior to transduction at D0 (**A**). For the flow cytometry analysis, the respective mock cells were used to identify the negative population (**B**) for the quantification of eGFP+ cells harvested at D3 **(C**). Scale bar= 100 µm.

3.2 rH1LVs

3.2.1 CHARACTERISATION OF THE TRANSFER PLASMID IDENTITY

The rH1LV transfer plasmid pCCLsc_HB9_*RFP*_W was kindly provided by Dr. Fred Gage (Salk Institute, USA). However, no plasmid map was made available with the construct and only some of features were known. **Figure 3.10** shows the map constructed for the plasmid from the GenBank sequences of the various elements. The identity of the short version of the HB9 promoter was confirmed by DNA sequencing. The identity of the plasmid was also checked through restriction analysis with the two enzymes originally used by the provider lab to clone the HB9:RFP insert into the LV backbone. The enzymatic digestion

with *Cla*I + *Xba*I produced a 7867 bp and a 4488 bp fragment from the original 12355 bp plasmid (**Figure 3.10**). Other restriction analyses were also performed. The characterisation of this plasmid was part of the 3rd year project of Lauren Hutchinson, an undergraduate under my supervision.

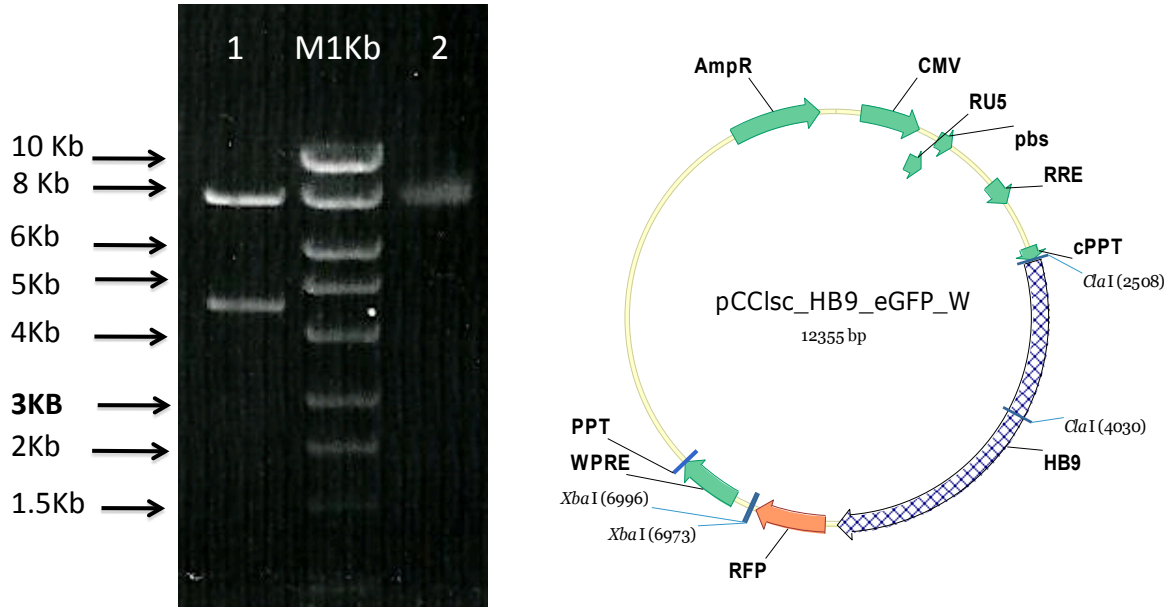

Figure 3. 10: Representative characterisation of the rH1LV transfer plasmid pCCLsc_HB9_*RFP*_W through its restriction pattern.
pCCLsc_HB9_*RFP*_W was digested with *Cla*I and *Xba*I yielding 7867 bp and 4488 bp fragments (**1**). Undigested plasmid (**2**). M: 1 Kb molecular size marker. 200 ng of DNA were loaded in all lanes except for the marker that contained 500 ng. The map of the plasmid is presented along with the restriction analysis. The main elements of the plasmid are as follows: CMV: cytomegalovirus promoter; RU5 and dLTR: recombinant sequences of the long terminal repeats; pbs: primer binding site; RRE: rev response element; PPT: polypurine track; HB9: short version of MN- specific HB9 promoter; RFP: red fluorescent protein; WPRE: Woodchuck hepatitis virus post transcriptional regulatory element; AmpR: ampicillin resistance. Relevant restriction sites are also indicated.

CHAPTER 4: RESULTS- iPSC GENERATION AND CHARACTERISATION

This chapter describes the generation and quality control of iPSCs from fibroblasts obtained from skin biopsies of the members of the discordant consanguineous family of study. In this family, both parents are carriers of a 4-bp deletion in exon 3 (c.399_402delAGAG) of the *SMN1* gene, which produces a frame-shift that predicts a stop codon 40 bp downstream (Bussaglia *et al.* 1995). Four of the offspring received the mutated allele in homozygosis, nevertheless the clinical manifestations are discrepant, ranging early-onset SMA type III (age of onset ≥18 months, bound to wheelchair since infancy) to SMA type IV/Asymptomatic (walker presenting cramps and minor electromyographic abnormalities). The pedigree of the family is shown in **Figure 4.1**, and a more detailed description summarizing the results of previous studies involving the family can be found in **Table 4.1**. For abbreviation purposes, cells from the unaffected carrier mother are coded as "RC", the SMA type IV/asymptomatic sibling as "AC", and the SMA type III siblings as "TC", "NC" and "CC" (**section 2.1.8.3)**.

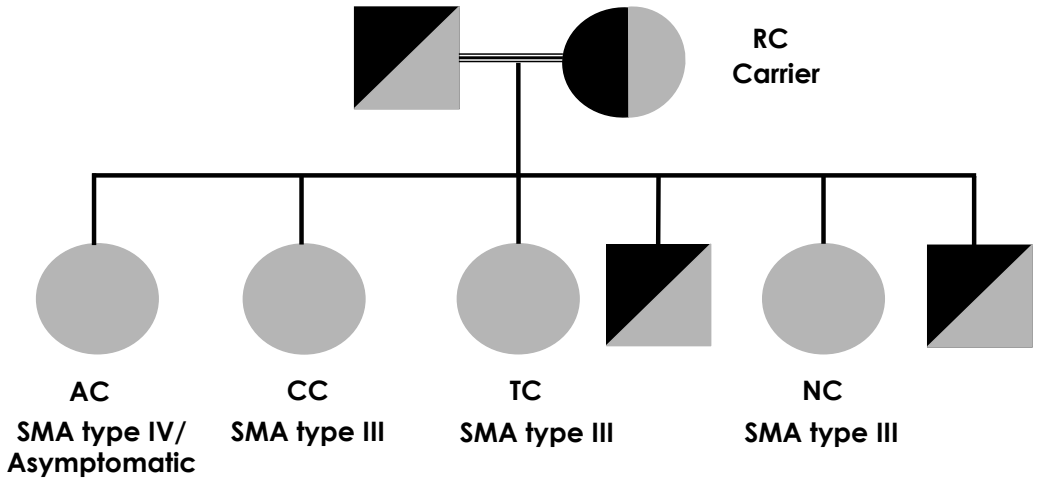

Figure 4. 1: Pedigree chart of the family under study.
The diagram shows the carrier parents and siblings (grey/black circle and squares) and the SMA type IV/unaffected and SMA type III siblings (grey circles) harbouring the *SMN1* mutation (c.399_402delAGAG, exon 3). The code for each individual within this study is shown along with the respective symbol of representation within the diagram.

Table 4. 1: Clinical and molecular data of the individuals included in this study.

Patient	RC	AC	TC	NC	CC
Ethnicity	Spanish	Spanish	Spanish	Spanish	Spanish
Sex	Female	Female	Female	Female	Female
***SMN2* copy number**	3	4	4	4	4
Presence of variant c.859 G>C in *SMN2*	NA	No	No	No	No
Presence of *NAIP*	NA	Yes	Yes	Yes	Yes
SMA locus	NA	All sibling are haploidentical for the SMA locus (*Also-Rallo et al*, unpublished data)			
***mRNA *PLS3* levels in lymphoblasts**	NA	1.92	0.008. Similar to control sample	0.59. Similar to control sample	8.76
***mRNA *PLS3* levels in fibroblasts**	NA	1.25	0.73. Similar to control sample	0.89. Similar to control sample	0.73. Similar to control sample
Age of onset of weakness	NA	NA	18 months	18 months	24 months
Wheelchar bound (age they stopped being able to walk)	NA	NA	14 years	8 years	8 years
Electromyography results	NA	Minimal changes	Denervation	Denervation	Denervation
Phenotype	Healthy carrier of mutation	Asymptomatic or SMA type IV	SMA type III	SMA type III	SMA type III
Age of indivual when biopsy for iPSC generation was taken	>60	45	38	36	30

*Values were calibrated to the one of a control individual without SMA, which expression was set to 1. The data in this table are described in (Also-Rallo *et al.* 2011; Bernal *et al.* 2011). NAIP: neuronal apoptosis inhibitory protein; NA: not applicable/not determined.

Further chapters will describe the differentiation of the clones obtained here as well as the molecular analyses of these cells and their differentiated progeny regarding key proteins known to be involved in SMA pathogenesis.

4.1 iPSC PRODUCTION

This section provides a description of the characteristics of the fibroblasts before and after retroviral transduction and the emergence of iPSC clones. A diagram of the reprogramming procedure can be found in **section 2.3.6.1**

4.1.1 FIBROBLAST REPROGRAMMING.

The morphology and doubling time (DT) of the fibroblasts were assessed before and during reprogramming in order to determine the health and mitotic potential of the primary cells (**Figure 4.2**). All fibroblasts showed a healthy morphology. They had an average 50 h DT after thawing from liquid nitrogen (passage 3-4), but they started to divide faster in subsequent passages and just before transduction (passage 5-6 for AC, RC and CC and p6-p7 for TC and NC), their average DT was 26.5 hours. NC had a comparatively longer DT

just before transduction. After transduction, all the cells except NC showed an increase in their DT, in particular TC. The decrease in the DT of NC was persistent even after further seeding on gelatin-coated plates.

Given the different growth rates of the cells, transduced fibroblast were seeded in 6-well plates (TC and CC) or in 6-well plates and 10 cm dishes (AC, RC and NC) at an average density of 7 x 10^4 cells/cm^2. The morphology of the transduced fibroblasts after seeding on gelatin-coated surfaces in shown in **Figure 4.3.**

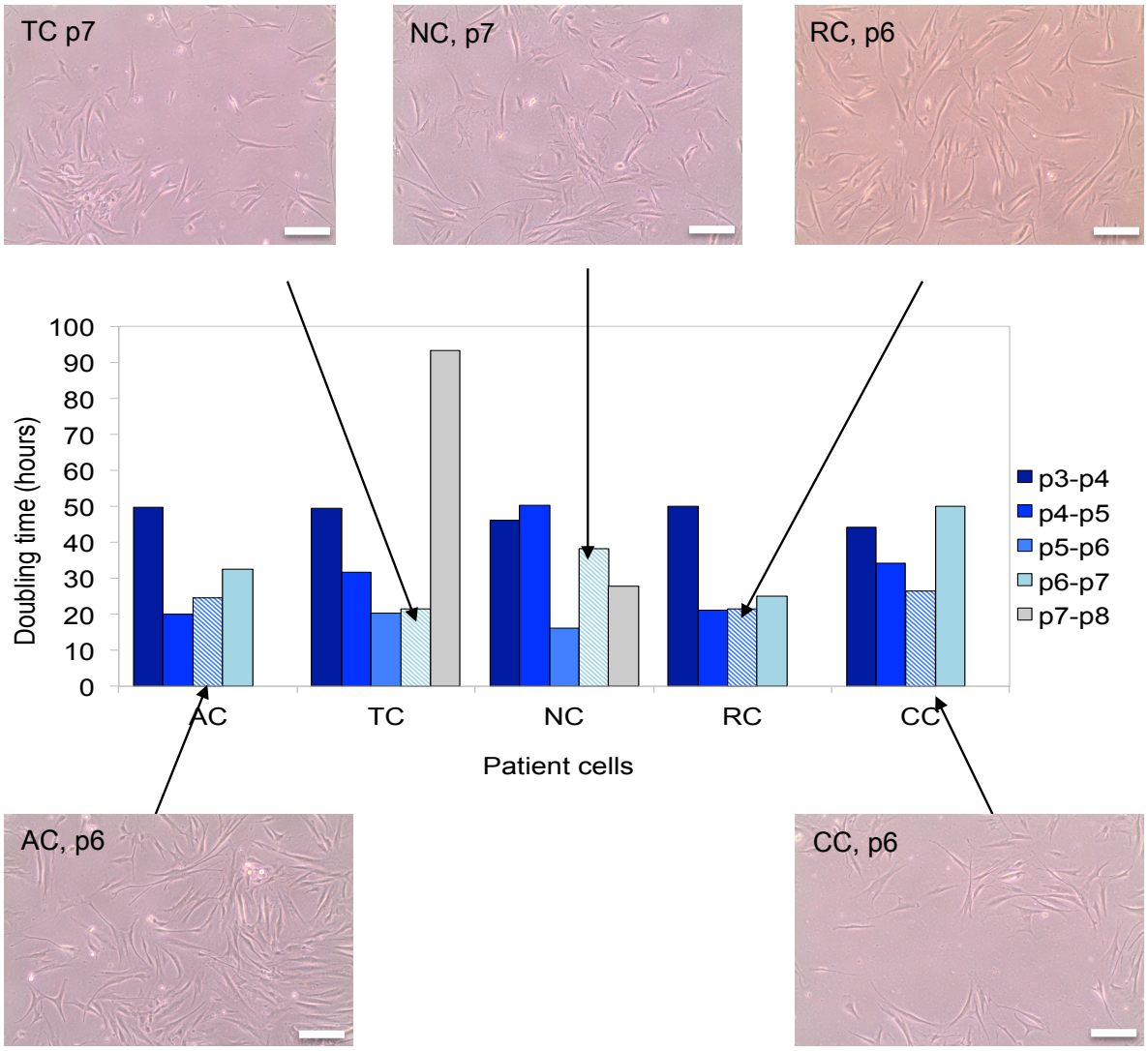

Figure 4. 2: Morphology and growth of fibroblasts before and after RV transduction.
The doubling time of the fibroblasts from the five family members from passage 3 to passage 8 is shown on the histogram. Passage 3-4 corresponds to the first passage after thawing the cells and the last passage shown (p6-p7 for AC, RC and CC and p7-p8 for TC and NC) corresponds to the count made before seeding the cells in gelatin-coated plates after retroviral transduction. Pictures of the cells from each family member a few hours before viral transduction are shown with their corresponding passage number. Scale bar= 200 µm. p: passage number.

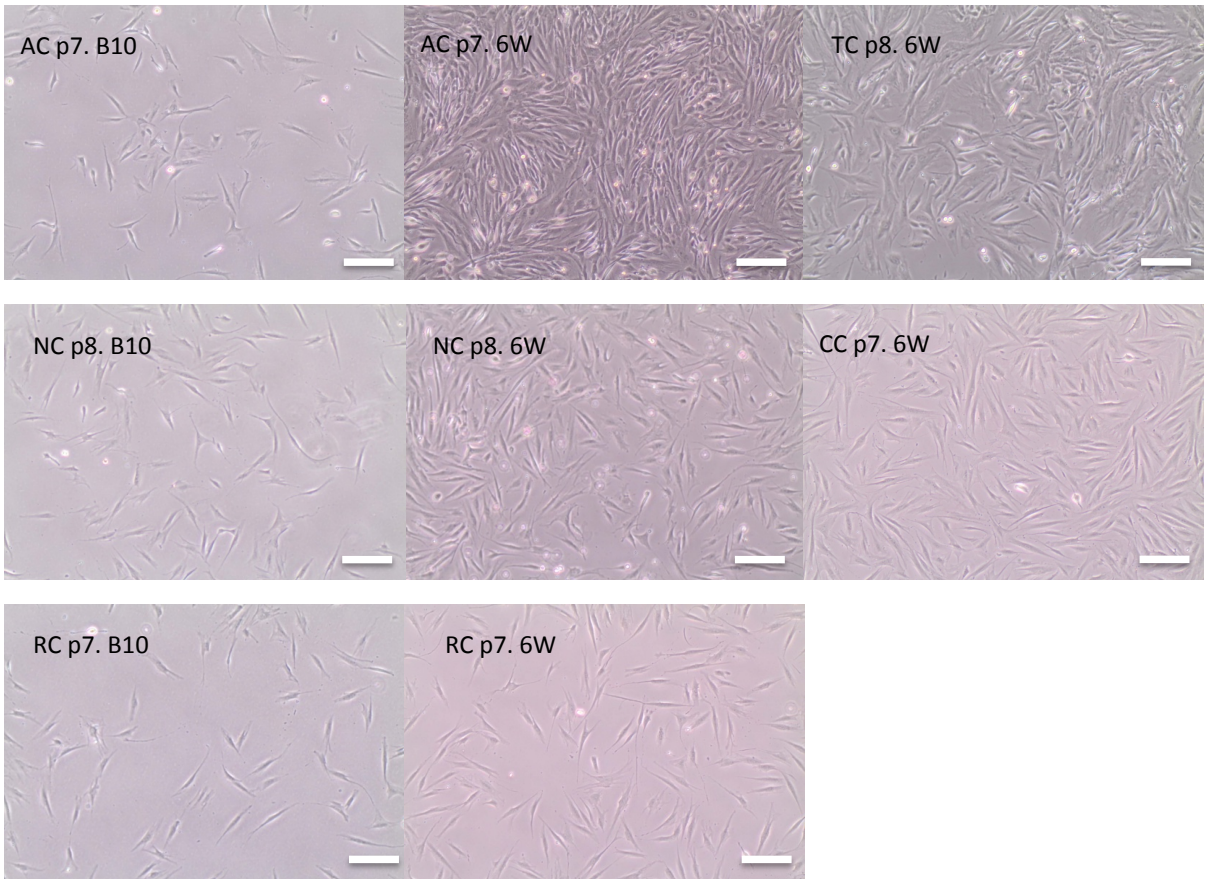

Figure 4. 3: Fibroblast morphology after rMMLV transduction.
Images shown correspond to transduced cells 24 hours after seeding them with supplemented hESC medium on gelatin-coated surfaces for maintenance in culture until the emergence of iPSC clones. Scale bar= 200 µm. B10: cells seeded in 10 cm dish, 6W: cells seeded in wells of a 6-well plate.

4.1.2 iPSC EMERGENCE

12-15 days post-transduction iPSC-like colonies began emerging from the cells of all patients except for CC (the deceased SMA type III patient). Transduced cells grew very fast, quickly forming a layer over the whole plate; nevertheless, close monitoring could still identify potential iPSC colonies. As it can be seen in **Figure 4.4** different morphologies were observed in emerging iPSC-like colonies: round brown clusters of cells, brown/bright oval-like clusters and bright round clusters. All cell clusters presenting these morphologies were selected for a first expansion over feeder cells.

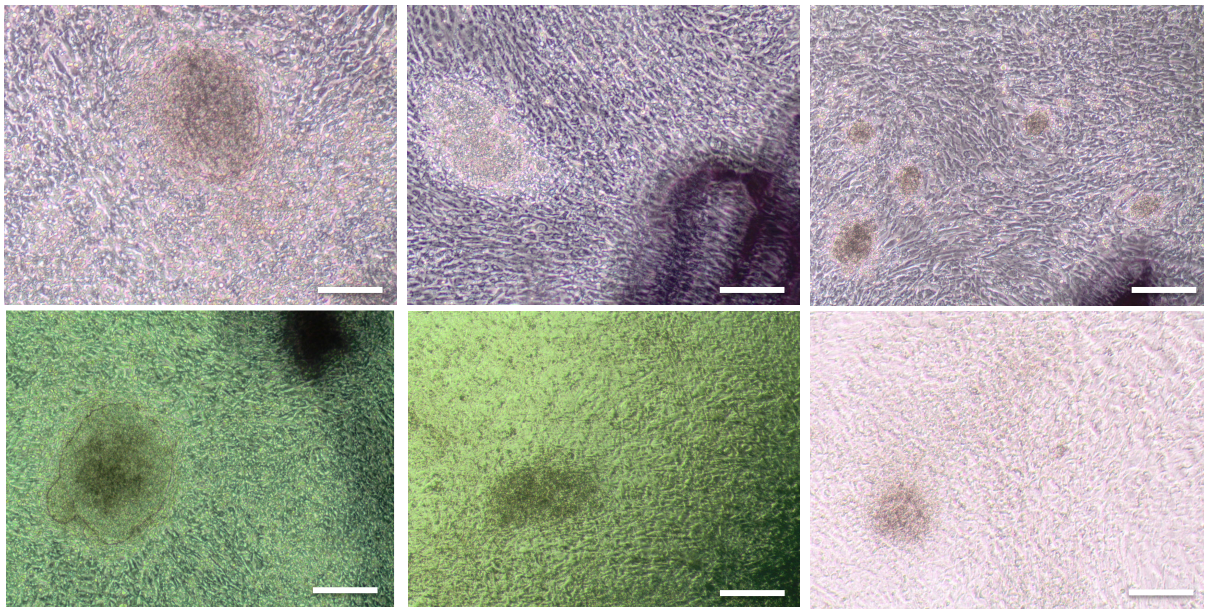

Figure 4. 4: Representative iPSC-like clones emerging from reprogrammed cells.
Different morphologies and appearances are shown in order to represent the heterogeneity of the emerging iPSC-like clones 2-3 weeks after retroviral transduction. Scale bar= 200 µm.

The behaviour of the iPSC-like clones during the first passages was also very heterogeneous. Some clones that made it to passage 2 presenting a good morphology on passage 1, spontaneously developed a differentiated morphology a few days after being passaged (**Figure 4.5, p1 and p2 respectively**). In this case, a new passage 2 was done from the cells left behind in the plate corresponding to passage 1, where after the first picking and passage some clumps detached and formed new colonies (**Figure 4.5, p1'**). This emphasized the importance of keeping the plates until the attachment and expansion of the colonies in the new passages was confirmed.

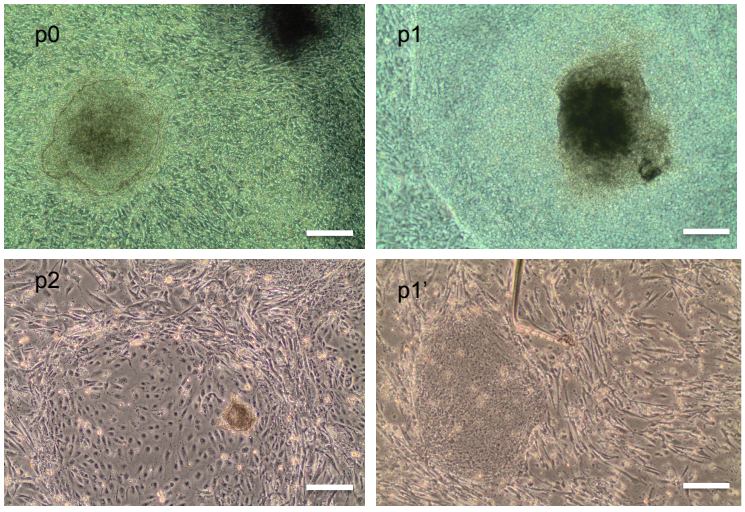

Figure 4. 5: Emergency and first passages of clone AC28.
Morphology on p0, p1 and p2 just before cutting and passaging. Cells at p2 differentiated, as judged by their morphology. In order to recover the clone, a new colony was picked and passaged from the same p1 plate some days after (p1´) and further expanded into a new plate. Scale bar= 200 µm. p: passage number.

Approximately 70 iPSC-like clones from all patients altogether were picked and cultured individually over feeders in organ cells. Most of them did not grow and after 10 days those plates were discarded. The fibroblasts that produced more iPSC-like colonies were AC (type IV/asymptomatic sister), followed by NC (SMA type III patient). iPSC-like colonies from RC (healthy mother) and TC (SMA type III patient) cells were very rare and none were observed in the case of CC cells. A table with the clones finally selected from each family member is included in **Appendix 4**. For AC and NC 5 clones were selected, but several more were generated in the original plates.

4.2 iPSC QUALITY CONTROL

This section presents the results for the quality control of selected iPSC clones. Several parameters were measured in order to assess pluripotency, differentiation potential, stability and identity of the clones. After the initial expansion of several clones from each family member, one single clone from each of them (except from CC, from whom no clone was obtained) was selected for further expansion and characterisation: clone 28 from AC, clone 21 from NC, clone 64 from TC and clone 26 from RC. Unfortunately, after the assessment of these first 4 clones, two of them (TC64 and NC21) did not pass all the requirements of the quality control and three new clones were expanded and characterised: clone 63 from TC and clones 42 and 32 from NC. The results from all seven clones are presented together.

4.2.1 PLURIPOTENCY ASSESMENT

The first parameters to assess pluripotency were the morphology and the expression of the proper surface and nuclear markers. As it is shown in **Figures 4.6 and 4.7**, all seven clones have a typical hESC morphology (round shape, large nucleoli and scant cytoplasm) and they all express AP, *OCT4, NANOG, SOX2* and *TRA-1-60*. *NANOG* and *OCT4* staining in clone RC26 is dimmer than in the rest of the clones.

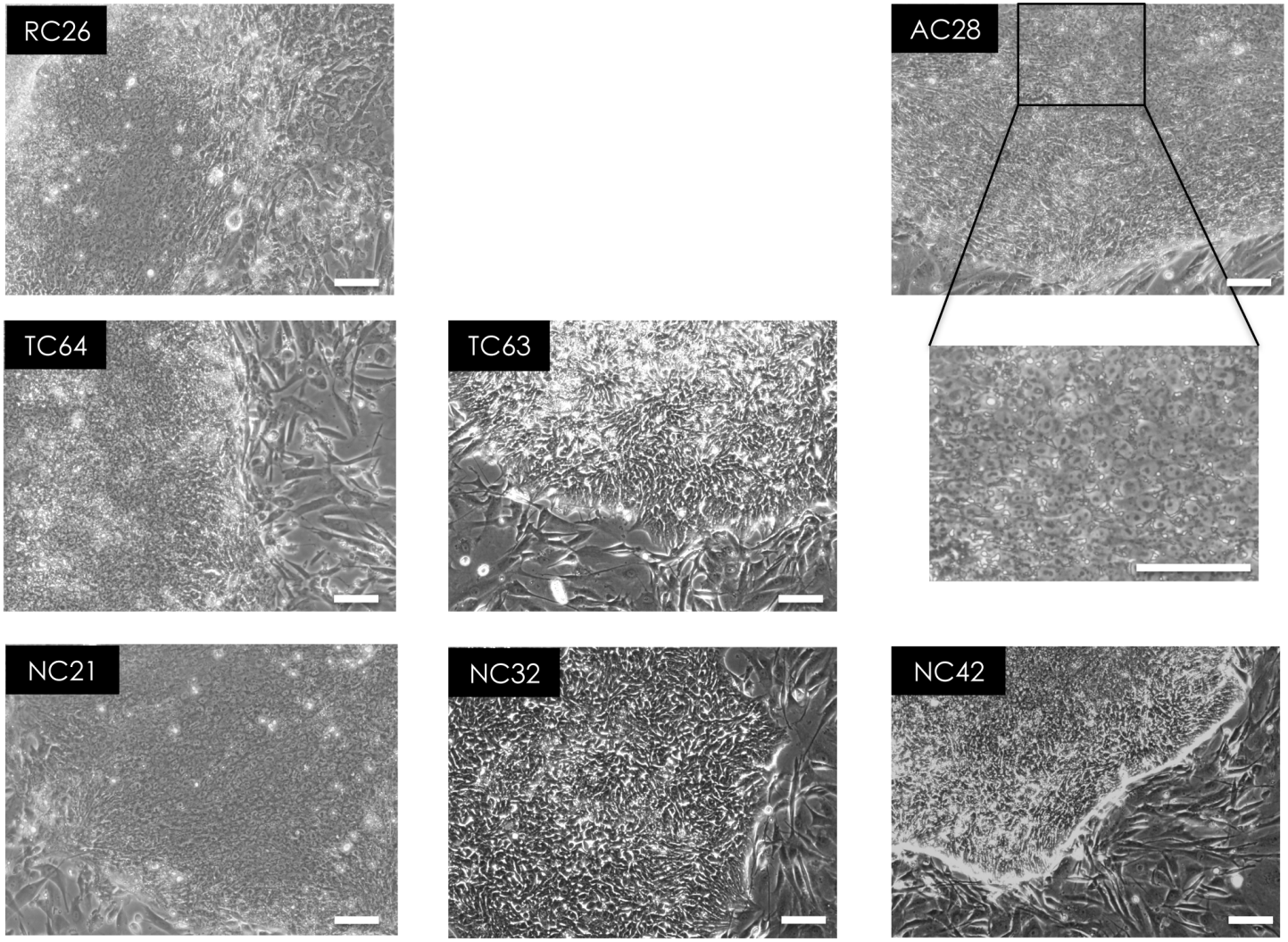

Figure 4. 6: Morphology of a representative colony in selected iPSC clones.
iPSCs were grown on of human feeders as described in M&M. Scale bar= 100 µm.

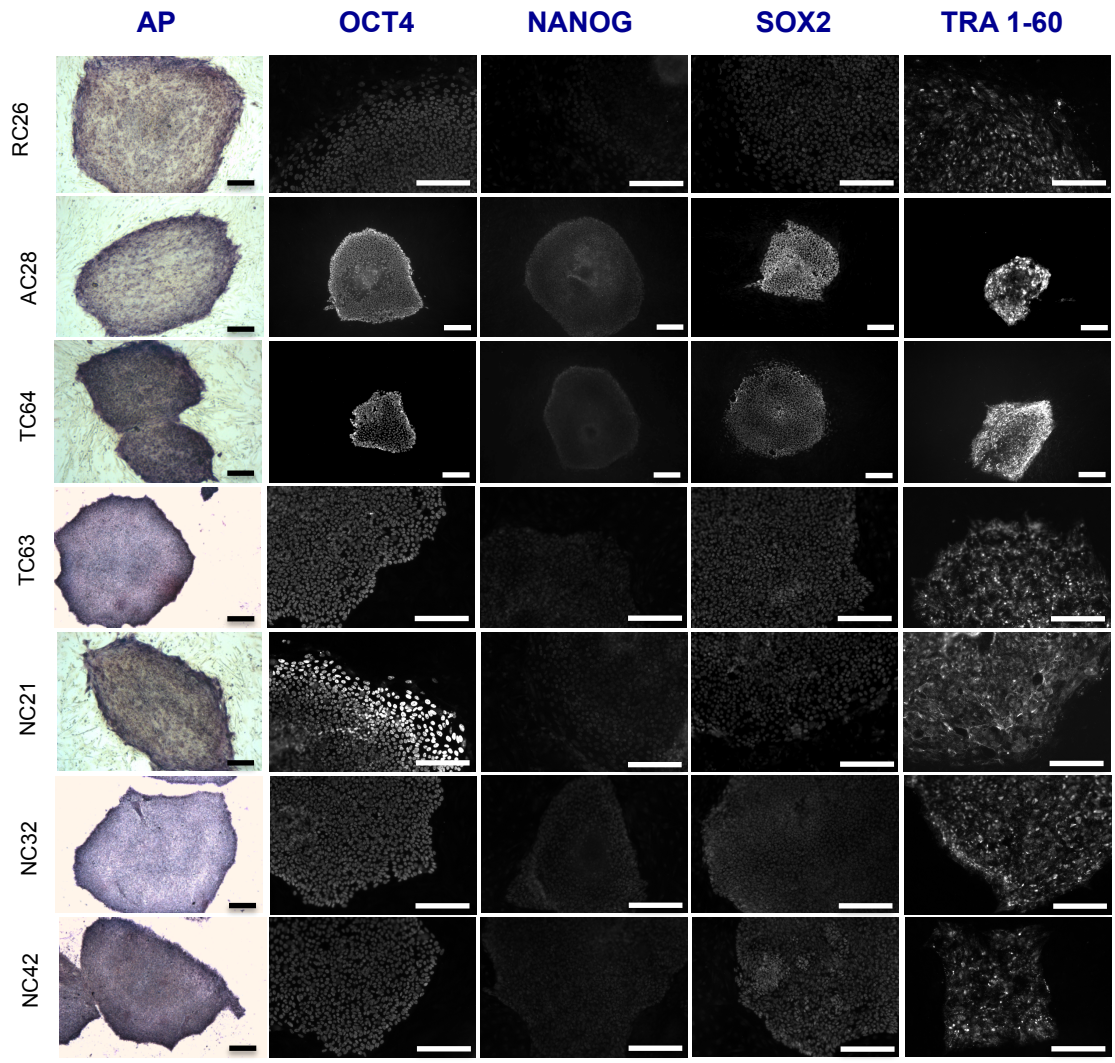

Figure 4. 7: Expression of pluripotency markers in selected iPSC clones.
AP, OCT4, NANOG, SOX2, and TRA-1-60 are all produced in representative iPSC colonies from the selected clones. Scale bar= 200 µm.

In order to assess quantitatively the proportion of cells expressing pluripotency markers, a multi-parameter flow cytometry-based analysis was performed. *SSEA3* and TRA *1-81* were chosen for the analysis, and the percentage of double-positive cells was the criteria chosen for assessing the level of pluripotency of the culture. Conversely, the difference between 100 and the percentage of double-positive cells represents the proportion of cells undergoing spontaneous differentiation. As can be seen in **Figure 4.8**, most clones are ≥85% *SSEA3*+/*TRA 1-81*+, with the exception of clones AC28 and TC64, which are 66% and 71% *SSEA3*+/*TRA 1-81*+, respectively. These results are consistent with the morphologies found in culture, were these two clones have a higher propensity for spontaneous differentiation and require a more aggressive cleaning procedure.

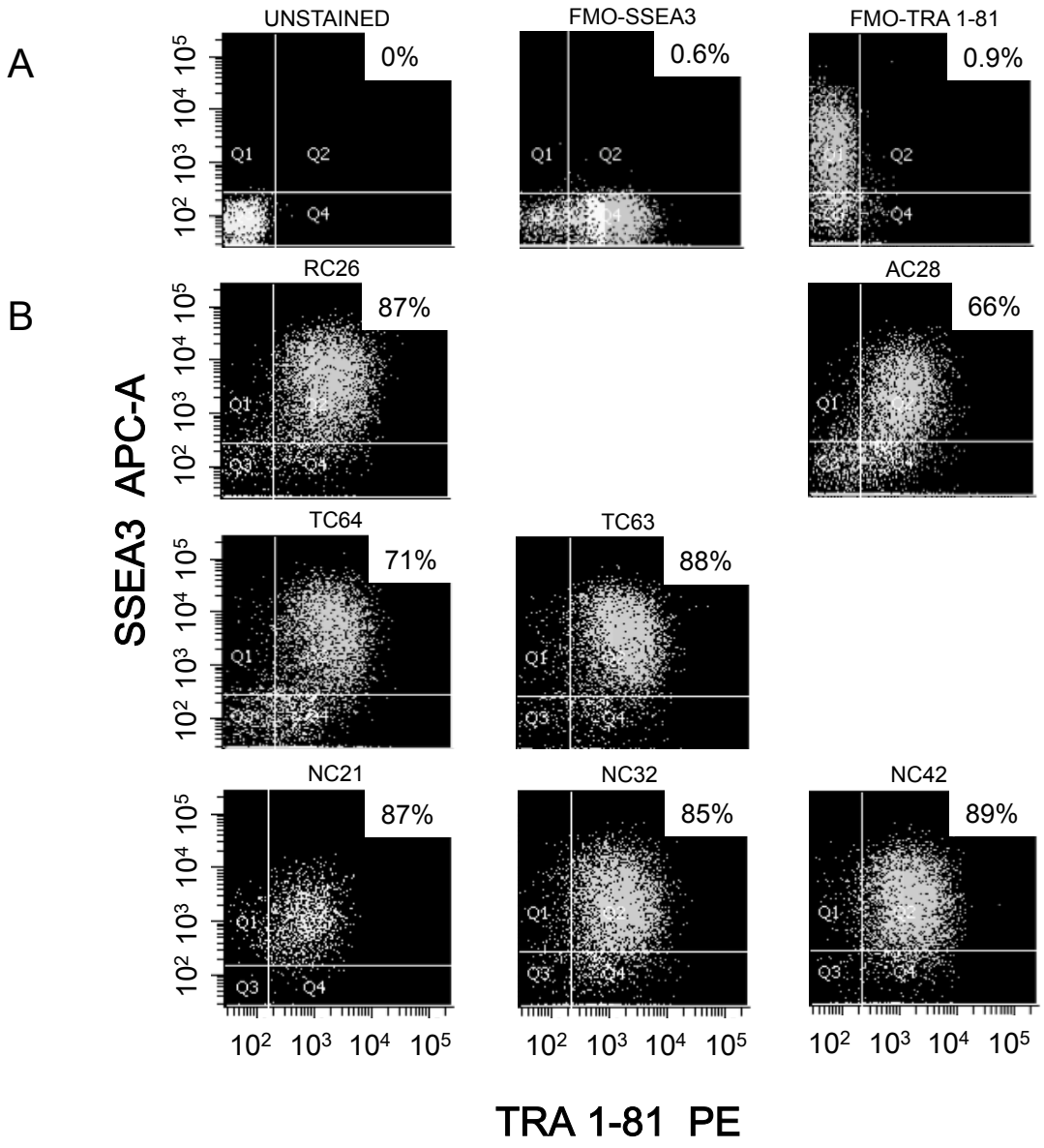

Figure 4. 8: Quantitative assessment of pluripotency markers in iPSCs through flow cytometry. Multi-parameter flow cytometry was performed on the selected iPCS clones for the determination of the proportion of cells co-expressing the surface markers SSEA3 and TRA 1-81. (**A**) The top three plots correspond to the control samples (unstained and FMOs) after calibration and setting of appropriate thresholds. (**B**) The percentage of double-positive SSEA3/TRA1-81 cells is shown on the plot corresponding to each clone. Feeder cells were excluded from the analysis using the FITC channel, given their stable expression of *GFP*. FMO: fluorescence minus one.

One key event during the establishment of true iPSC is the down-regulation of the exogenous expression of the RTFs and the up-regulation of their endogenous expression. **Figure 4.9** shows the qRT-PCR quantification of the endogenous and total expression of the four RTFs used during reprogramming (*OCT4, SOX2, KFL4* and *c-MYC*) in mRNA samples from iPSCs harvested at p37 (AC28), p40 (RC26), p40 (TC64), p12 (TC63), p15 (NC32) p16 (NC42) and p27 (NC21). Two cell lines were used as standards of pluripotency: hESC H9 and EP2102. hESC H9 is common human embryo-derived pluripotent cell line used as standard reference for pluripotency (Thomson *et al.* 1998) and EP2102 is a human embryonic carcinoma cell line with simple culture conditions that expresses most of the pluripotent markers found in hESCs (Andrews *et al.* 1982; Josephson *et al.* 2007). Given the fact that the RNA extraction and cDNA synthesis from the hESC H9 sample were not performed in the same way as it was done for the rest of the samples, EP2102 was chosen as the calibrator instead. Total expression should be comparable across all samples, because the amplification primers are located within the genes. However, endogenous expression may not be comparable with hESC H9 (where a mix of poly dT and random primers was used for cDNA synthesis, unlike the poly dT primers used on the other samples). The expression of all four transgenes was down-regulated in the seven clones, as judged by the similar values of their endogenous and total expression and by comparison with the expression profile in IMR90 fibroblast undergoing reprogramming and harvested 4 days post transduction (IMR90 D4). There was however, a high persistent *SOX2* transgene expression in all iPSC clones. *OCT4* and *SOX2* were expressed at very low levels in BJ1 cells and their expression was induced after reprograming (IMR90 D4), whereas *KFL4* and *c-MYC* were already expressed in fibroblasts at comparable levels to those in iPSCs. Total expression of *OCT4* and *SOX2* in all clones seems to be similar to those in hESC H9 (despite variation among the clones), but for *c-MYC* and *KFL4* total expression in the iPSC clones is at least one log lower than in hESC H9 (**Figure 4.9**). RT-PCR analyses with primers amplifying transgene-specific sequences (**Figure 4.10)** showed that there was residual transgene expression of one or more RTFs in some clones, particularly in clones AC28 and TC64. Transgenic expression in clone TC63 seemed to be completely silenced.

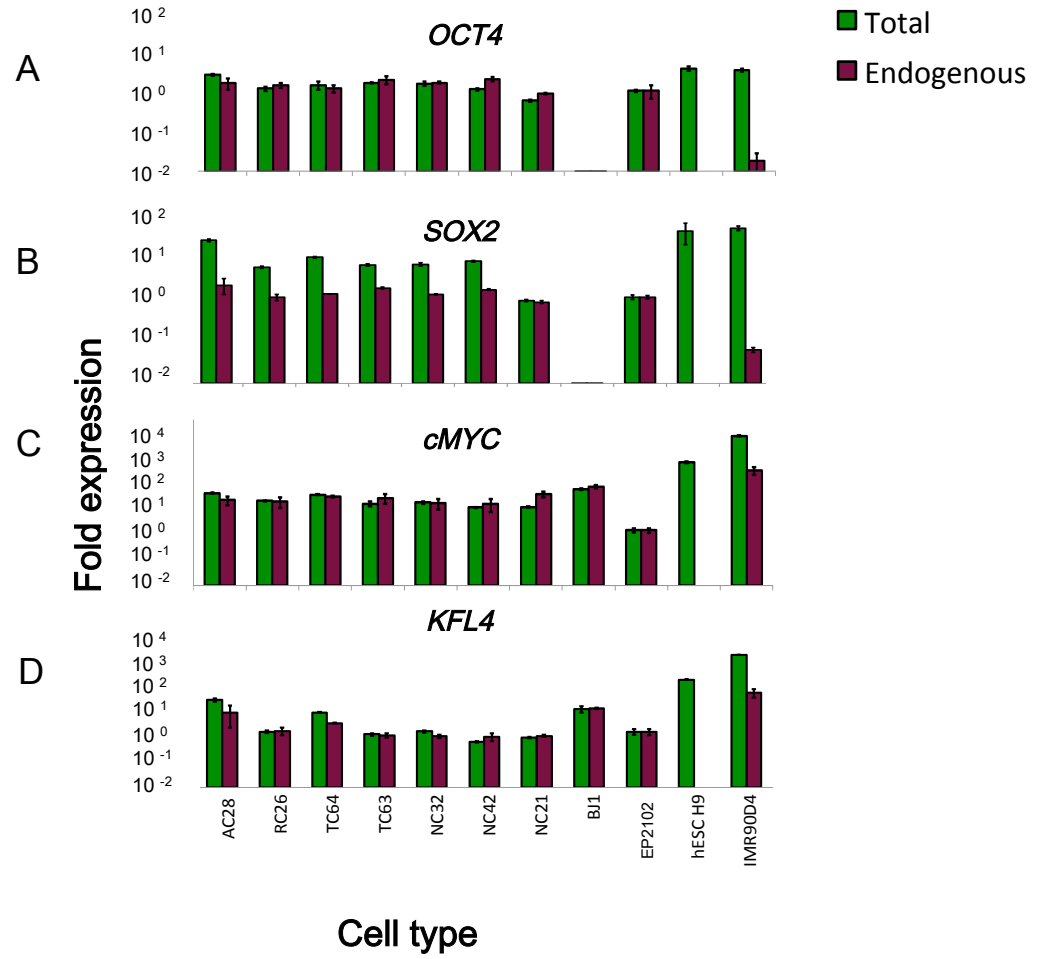

Figure 4. 9: Down-regulation of transgenes in selected iPSCs.
qRT-PCR was performed to measure the endogenous and total expression of the transgenes (**A**) *OCT4*, (**B**) *SOX2*, (**C**) *cMYC* and (**D**) *KFL4*. Gene expression was normalized to *RPL13* and *18S* and plotted ($\log_{10}$ scale) relative to the expression in EP2102, which was arbitrarily set to 1. BJ1, IMR90 D4 and hESC H9 were included in the analysis as references. Data is presented as mean ± standard deviation.

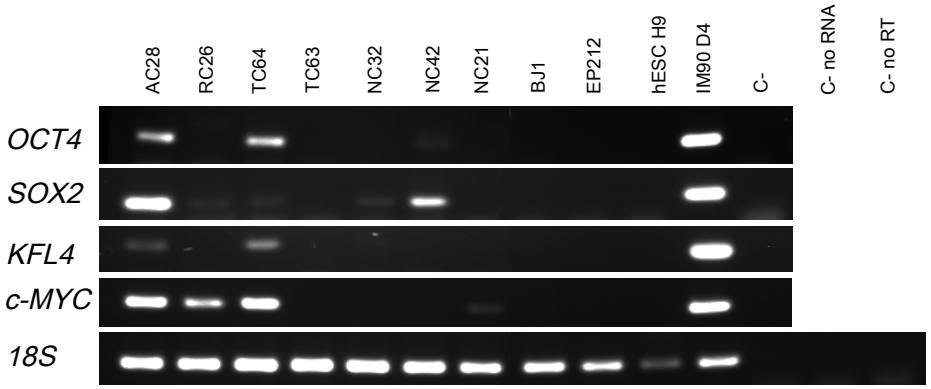

Figure 4. 10: Transgenic expression in selected iPSC clones.
The expression of each transgene was measured by RT-PCR with a primer from retroviral vector sequence and another internal to the corresponding gene. 18S is shown as a loading control. BJ1, IMR90 D4 and hESC H9 were included in the analysis as references.

4.2.2 DIFFERENTIATION POTENTIAL

True iPSCs should, as it is the case in hESCs, be able to differentiate into cells of the three germ layers. An *in vitro* assessment of differentiation potential was undertaken by producing EBs. iPSC-derived EBs are a mix of cell populations in differentiation, and when plated, multiple cell lineages start growing out the cluster, so representatives of all germ layers can be found in the same well. **Figure 4.11** shows that indeed, markers from all three layers can be found in cells from iPSC-derived EBs of the selected clones: TUJ1 as representative of the ectoderm, SMA and Desmin for mesoderm and AFP for endoderm. NC21, unlike the other clones, underwent low differentiation levels, producing iPSC colonies even after EB formation. Very few cells representative of each layer could be found for this clone, particularly for mesoderm.

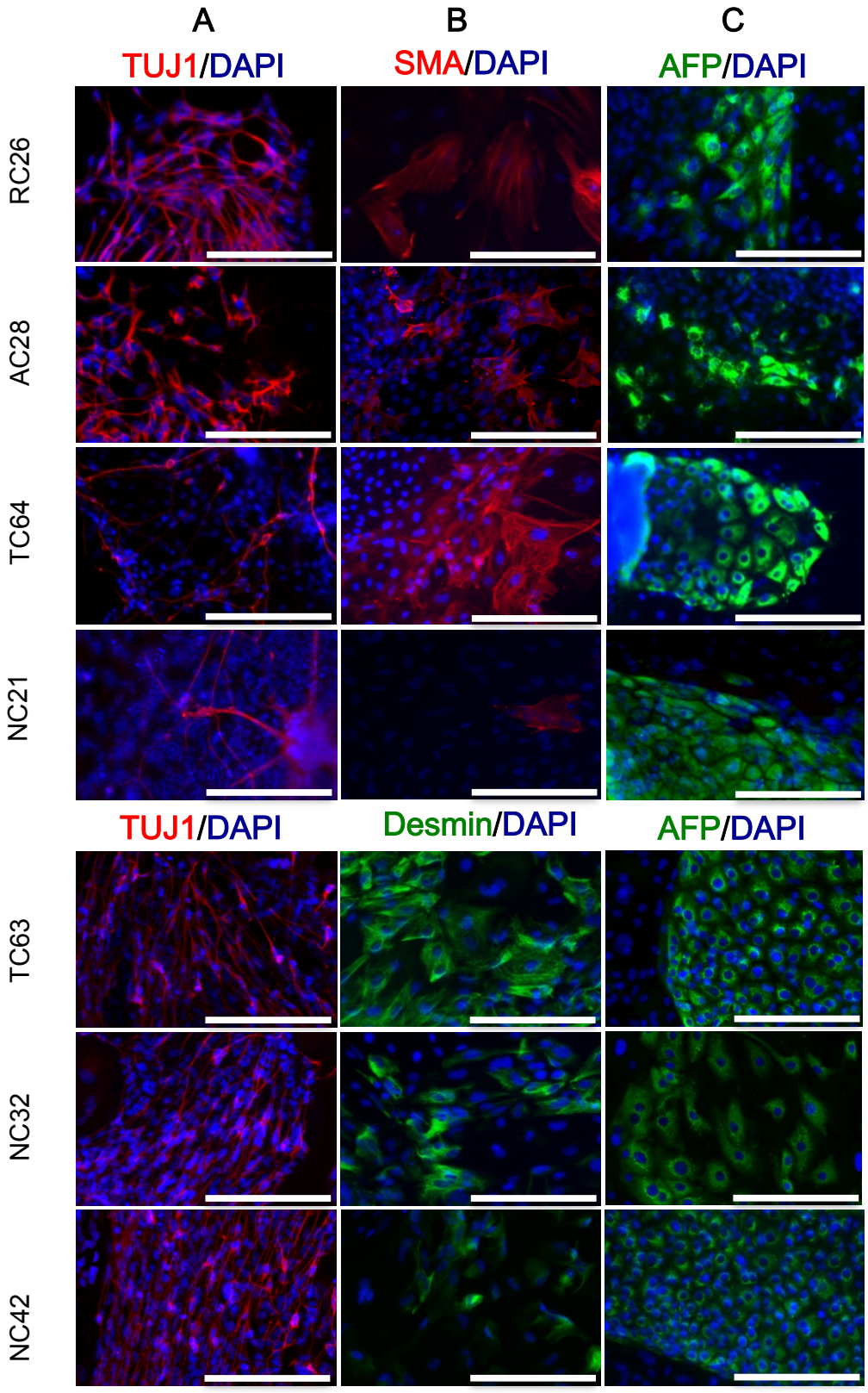

Figure 4. 11: ***In vitro*** **differentiation potential of selected clones of iPSCs.**
EBs produced from the representative clones generated cell derivatives of the three primary germ cell layers. Immunofluorescence analysis shows the expression of markers from (**A**) ectoderm (TUJ1, red), (**B**) mesoderm (SMA red/ or Desmin, green) and (**C**) endoderm (AFP, green). Cell nuclei were counterstained with DAPI (blue). Scale bar= 200 µm.

4.2.3 STABILITY AND IDENTITY ASSESMENT

Karyotype and genotype analyses of selected clones were performed in order to assess their chromosomal stability and genetic identity respectively. Two types of karyotype analyses were performed by two different laboratories: the first four clones expanded after iPSC generation (AC28, RC26, TC64 and NC21) were analyzed by mFISH in iSTEM (Evry, France), while the three clones expanded later (NC32, NC42 and TC63) were analyzed by G-banding in Santa Creu i Sant Pau Hospital (Barcelona, Spain). **Figure 4.12** shows a representative karyotype analysis for each clone, along with the passage number at the time of cell preparation. All clones show a normal karyotype, except for TC64, which presents a partial gain of chromosome X on chromosome 1 (1qter). This abnormality seems to have arisen early in the reprogramming process or have been present in the reprogrammed fibroblast, given the fact that it is present in all the metaphases analysed for this particular clone.

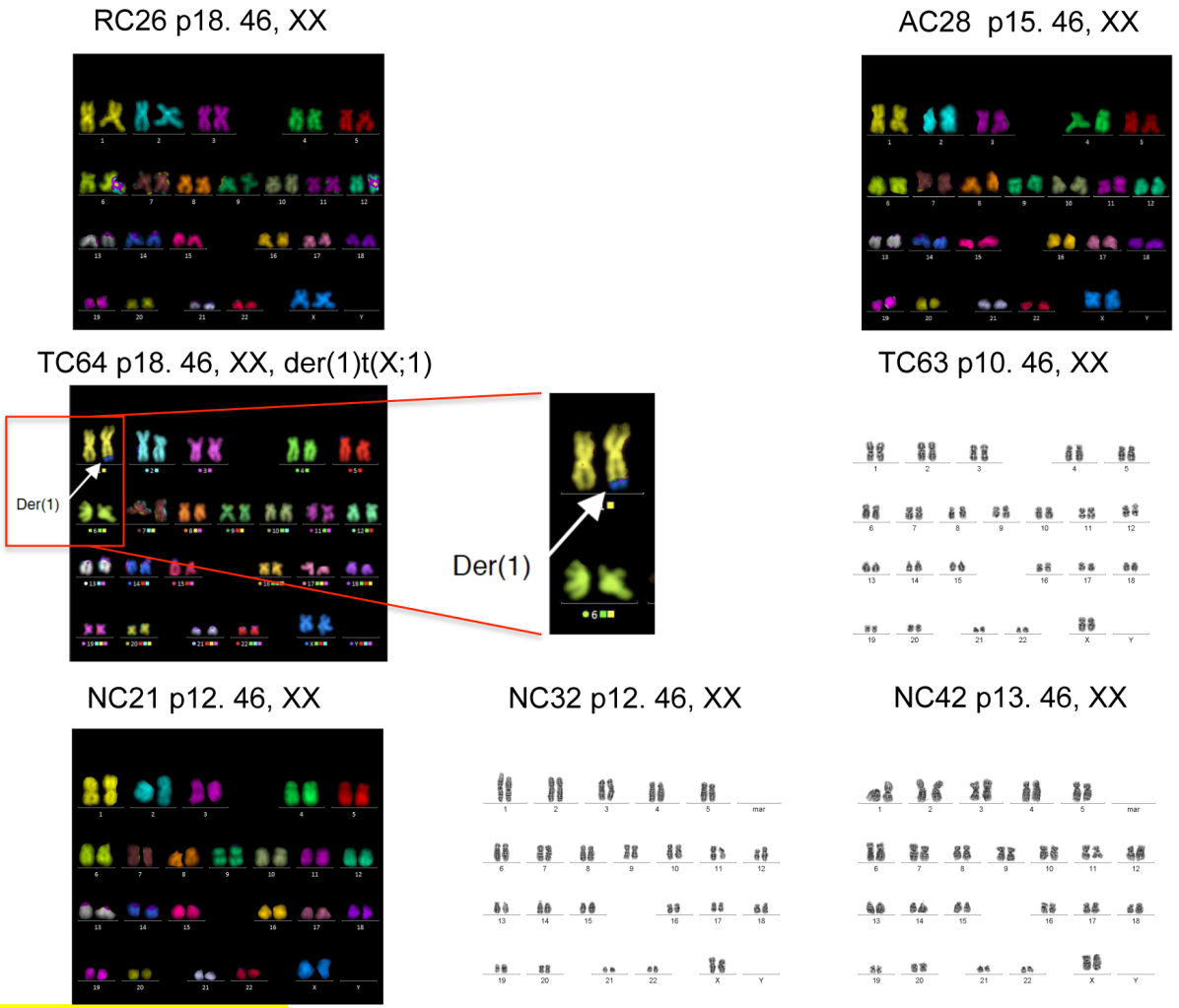

Figure 4. 12: Karyotype analysis of selected clones.
mFISH or G-banding analyses were performed in metaphase preparations from clones AC28, RC26, TC64, NC21 and clones NC32, NC42, TC63, respectively. The passage number at the time of metaphase preparation is shown along the clone name and karyotype.

The genetic identity of the clones was assessed by comparing the profile of several STRs between the selected clones and the parental fibroblasts from which they were generated as well as peripheral blood taken from the corresponding patient. **Table 4.2** shows the correspondence between the STR profiles confirming the identity of all seven clones. The STR analysis shown here was performed by Dr Sara Bernal in Santa Creu i Sant Pau Hospital (Barcelona, Spain).

Table 4. 2: STR profile of selected clones and their parental fibroblasts and peripheral blood.
Numbers correspond to the length of the amplification products, which is directly related to the number of repeats

	Chrom 1 D1S305	Chrom 2 D2S443	Chrom 2 D2S291	Chrom 19 D19S420	Chrom 19 D19S112	Chrom 19 D19S562	Chrom X INT25-2.0
RC26 iPSCs	215 / 219	223 / 231	183 / 183	109 / 109	116 /118	340 / 381	341 / 345
RC Fibroblasts	215 / 219	223 / 231	183 / 183	109 / 109	116 /118	340 / 381	341 / 345
RC Peripheral blood	215 / 219	223 / 231	183 /183	109 / 109	116 /118	340 / 381	341 / 345
AC28 iPSCs	219 / 219	231 / 231	183 / 198	109 / 109	116 /118	340 / 381	341 / 343
AC Fibroblasts	219 / 219	231 / 231	183 / 198	109 / 109	116 /118	340 / 381	341 / 343
AC Peripheral blood	219 / 219	231 / 231	183 / 198	109 / 109	116 /118	340 / 381	341 / 343
TC63 iPSCs	219 / 227	231 / 231	183 / 198	107 / 109	116 / 126	340 / 369	343 / 345
TC64 iPSCs	219 / 227	231 / 231	183 / 198	107 / 109	116 / 126	-	343 / 345
TC Fibroblasts	219 / 227	231 / 231	183 / 198	107 / 109	116 / 126	340 / 369	343 / 345
TC Peripheral blood	219 / 227	231 / 231	183 / 198	107 / 109	116 / 126	340 / 369	343 / 345
NC32 iPSCs	215 / 227	223 / 227	183 / 183	-	118 / 118	381 / 381	341 / 343
NC42 iPSCs	215 / 227	223 / 227	183 / 183	109 / 109	118 / 118	381 / 381	341 / 343
NC21 iPSCs	215 / 227	223 / 227	183 / 183	109 / 109	118 / 118	-	341 / 343
NC Fibroblasts	215 / 227	223 / 227	183 / 183	109 / 109	118 / 118	381 / 381	341 / 343
NC Peripheral blood	215 / 227	223 / 227	183 / 183	109 / 109	118 / 118	381 / 381	341 / 343

Based on all the quality control assessments, two clones were excluded from further experiments: clone TC64 was excluded because of its karyotype abnormality and clone NC21 was excluded because of its low *in vitro* differentiation potential. The four selected clones were AC28, RC26, TC63 and NC32. Clone NC42 passed all quality control assessments, but was not used for further experiments. **Table 4.3** summarizes the results from the quality control assessment.

Table 4. 3: Summary of the results from the quality control assessments of selected clones

QC test	RC26	AC28	TC64	TC63	NC21	NC32	NC42
Alkaline Phosphatase	Positive						
Pluripotency markers expressed as assesed by IF	OCT4, NANOG, SOX2, SSEA4, TRA 1-60						
Proportion of SSEA3+/TRA 1-81+ cells by FC	87%	66%	71%	88%	87%	85%	89%
Transgene downregulation	All downregulated						
in vitro differentiation	Excellent	Excellent	Excellent	Excellent	Poor	Excellent	Excellent
Karyotype	46, XX	46, XX	46, XX, der(1)t(x;1)	46, XX	46, XX	46, XX	46, XX
STR profile	iPSC clone corresponds to parental primary cells	iPSC clone corresponds to parental primary cells	iPSC clone corresponds to parental primary cells	iPSC clone corresponds to parental primary cells	iPSC clone corresponds to parental primary cells	iPSC clone corresponds to parental primary cells	iPSC clone corresponds to parental primary cells
Final QC criteria	Passed	Passed	Did not pass	Passed	Did not pass	Passed	Passed
Clones selected	x	x		x		x	

QC: quality control; IF: immunofluorescence; FC: flow cytometry.

CHAPTER 5: RESULTS- iPSC DIFFERENTIATION

This chapter describes the phenotypic characterisation of the cells derived through directed differentiation of iPSCs to MNs and hepatocytes. Six clones were differentiated into MNs: the four selected clones (AC28, RC26, TC63 and NC32) from the members of the Spanish family, whose characterisation was presented in the previous chapter (**Chapter 4**), and two additional clones (SMA1 and 4603) generated and characterised by our collaborators. Clone SMA1 was derived in the Beckman Research Institute (California, USA) from fibroblasts of a patient with Spinal Muscular Atrophy type 1 (SMA1) and clone 4603 was derived in I-STEM from fibroblasts of a healthy adult (Please refer to **section 2.1.8** for more details). Only clone RC26 was differentiated into hepatocytes, as an alternative mature lineage for comparison purposes in the next chapter (**Chapter 6**).

5.1 iPSC-DERIVED MNS

This section describes the cellular work related to the differentiation of iPSCs into MNs, including the assessment of the identity of the intermediate progenitors and the fully differentiated cells, the description of the behaviour of the cells during the period of culture, the neurite growth test and the co-culture of iPSC-derived MNs with mouse myotubes. MN transduction with rH1LVs and rAAV9s carrying reporter and/or therapeutic genes is also presented here.

5.1.1 TRACKING THE DIFFERENTIATION OF iPSCs INTO MNs

iPSC clones AC28 and RC26 were differentiated to MNs three times, iPSC clones TC63 and NC32 two times and the reference iPSC clones SMA1 and 4603 one time. The difference in the number of iPSC-MN differentiations is related to the time frame when the clones were fully characterised or available from our collaborators. The results presented here correspond to the last iPSC-MN differentiation performed, where all mentioned clones were included.

As described in detail in Materials and Methods (**2.3.7.2**), iPSC differentiation into MNs is a stepwise process that involves the generation and selection of intermediate progenitors whose fate is directed by the culture conditions, particularly by the presence of RA and purmorphamine. A diagram summarizing the complete iPSC-MN protocol is shown in **Figure 5.1**, along with representative images of the markers expressed at different stages of the procedure, which will be described in detail in the this section

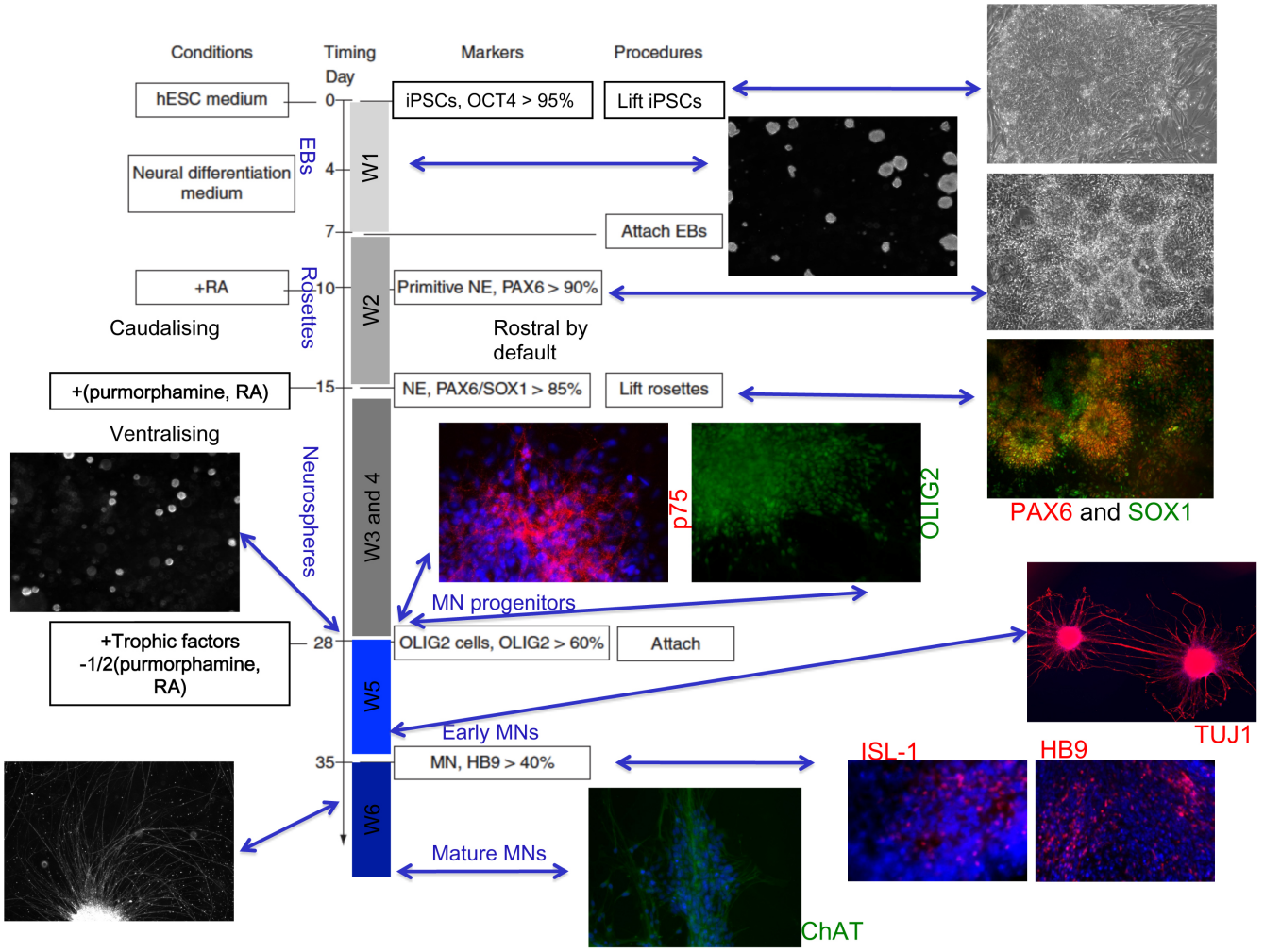

Figure 5. 1: MN differentiation from iPSCs
MN differentiation was performed following *Hu and Zhang's* protocol. Details of the procedure are provided in the text. PAX6 and SOX1 are neuroepithelial markers, OLIG2 and p75 are MN progenitor makers, TUJ1 is a neural marker and ISL-1, HB9 and ChAT are MN markers. All images depicted were taken from the differentiation of iPSC clone AC28. Diagram taken and modified from (Hu & Zhang 2009).

The fist steps of the differentiation were the formation of EBs (D0-D7) and their plating in laminin-coated 6-well plates (D7). Fourteen days after the start of the differentiation protocol several neural tube-like rosettes appeared within the clusters of plated EBs, which were distinguished by their columnar disposition (**Figure 5.2A)**. Clones AC28, TC63 and NC32 showed a similar yield of rosettes (covering ~50-60% of the cluster area in ~80% of the plated clusters), whereas clones RC26 and 4603 presented a higher neural induction with almost 100% coverage of rosettes in all clusters, which also started to appear earlier than in the rest of the clones. Clone SMA1 had the lowest neural induction, with only a few clusters (~10-20%) containing rosettes and with many cells detaching from the plate. The same behaviour described for clones AC28, RC26, NC32 and TC63 was also observed in previous MN differentiations from these clones. Neuroepithelial cell identity was confirmed in the cells forming rosettes by the co-expression of Paired box gene 6 (PAX6) and Sex determining region Y-box1 (SOX1) (**Figure 5.2B**).

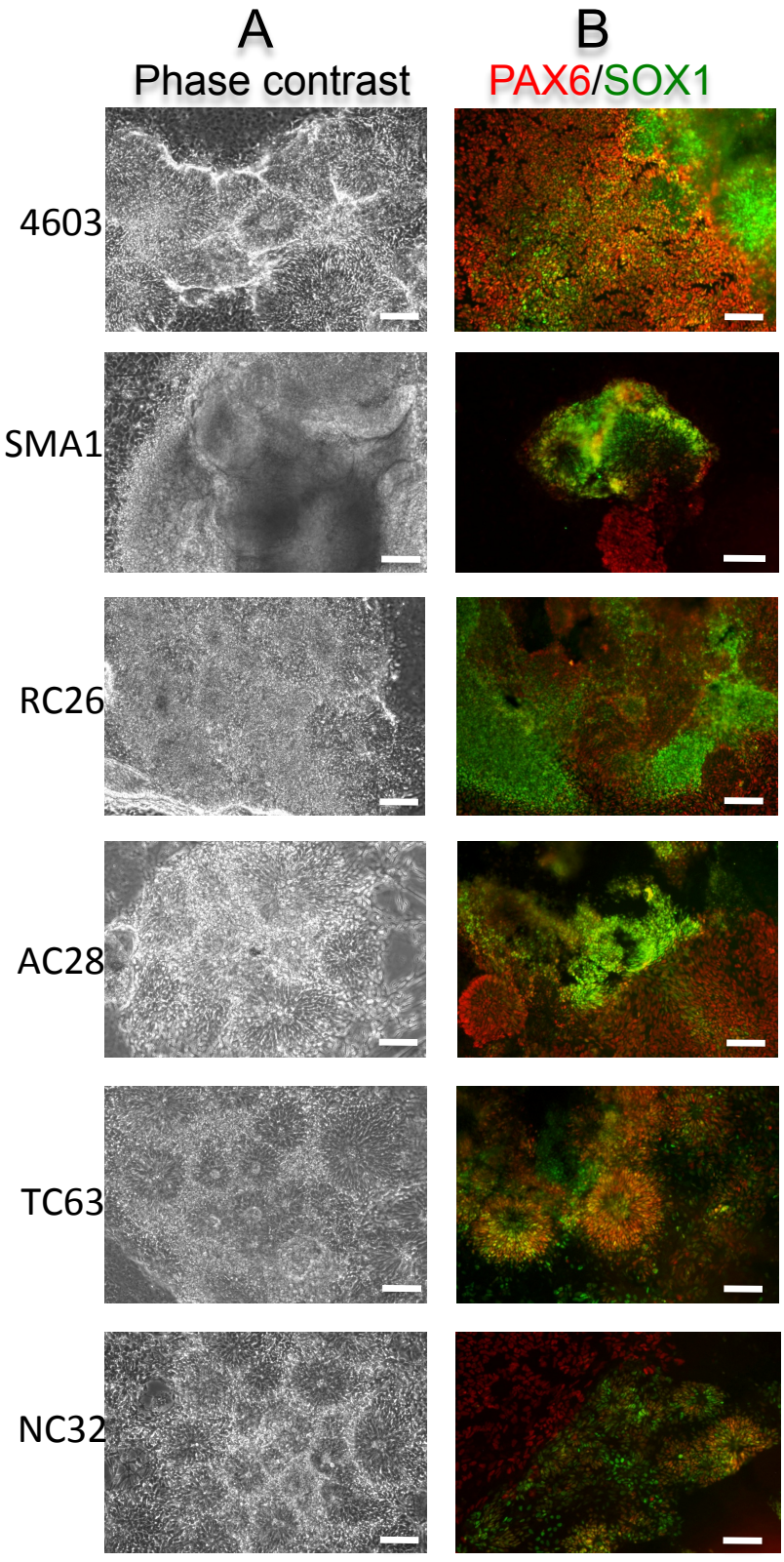

Figure 5. 2: Rosette formation and neuroepithelial identity. (**A**) Several neural–tube like rosettes are found within each cluster of the plated embryoid bodies 14-15 days after the start of the differentiation protocol. (**B**) Co-expression of PAX6 (red) and SOX1 (green) confirms neuroepithelial identity. Images A and B for each clone are taken from different fields/wells. Scale bar= 100µm.

Subsequently, the rosettes were manually separated from the EBs and grown in suspension as neurospheres, which were then plated on polyornithine-laminin (PO-Laminin) surfaces. **Figure 5.3** shows the presence of two MN progenitor markers (p75-NGFR and OLIG2) in a high percentage of the population. Almost all cells within the cultures of each of the clones were positive for OLIG2, even though the exact proportion could not be quantified due to the three dimensional disposition of the cells within the clusters (this will be discussed in the following sections). P75-NGFR expression was also found to be very high (~80-85% of the population) when dissociated cells were subjected to immunopanning with this antibody, as judged by the proportion of cells that effectively remained attached to the antibody-treated plate after the washing steps (data not shown). The results from the immunopanning experiments are not presented here, since single cells did not survive in culture.

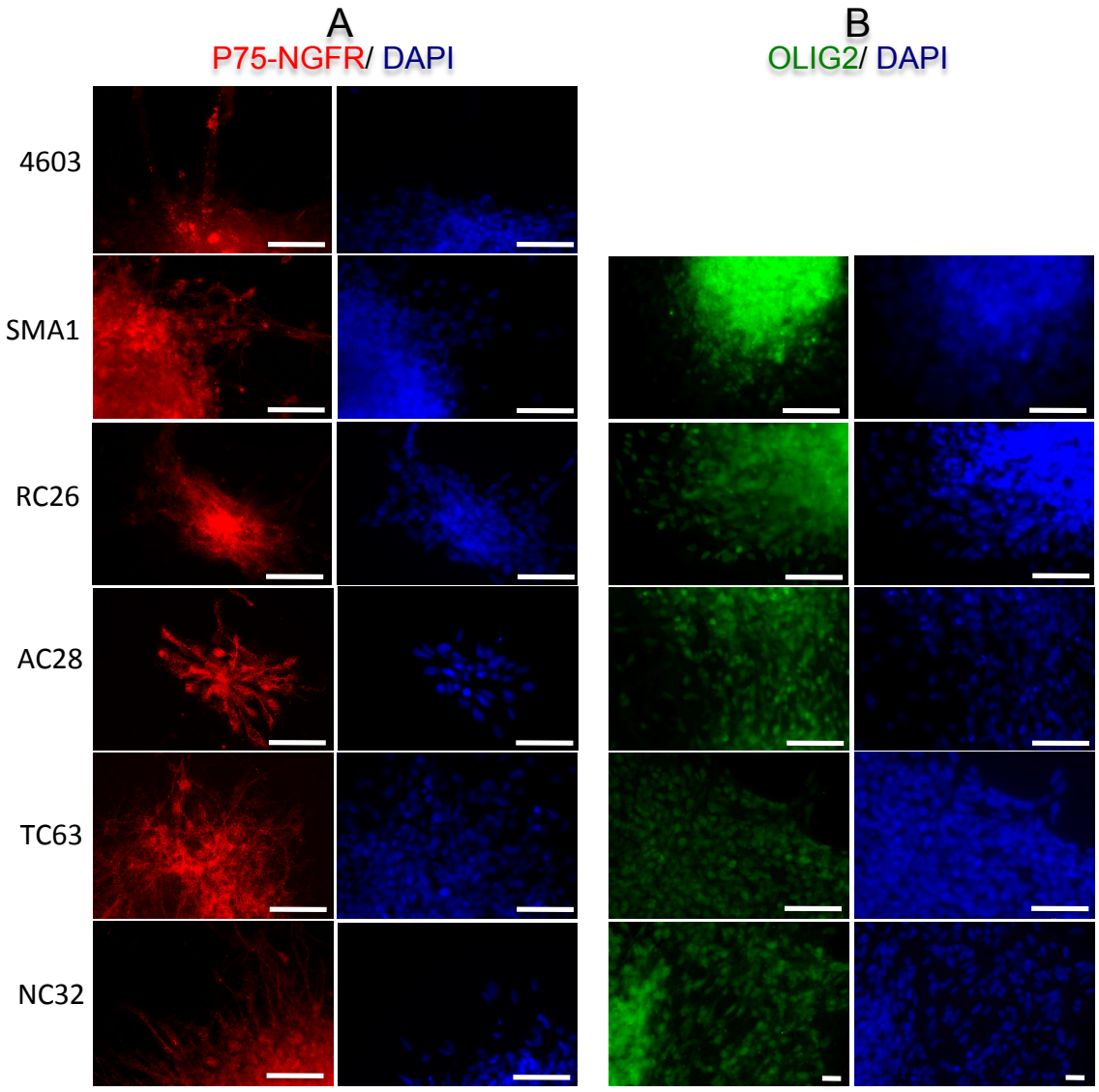

Figure 5. 3: **iPSC differentiation into MN progenitors.**
Neurospheres from all clones were plated on PO-laminin coated-coverslips and stained on D28 for the MN progenitor markers **(A)** p75-NGFR (red) and **(B)** OLIG2 (green). Cell nuclei were counterstained with DAPI (blue). Images for each clone were taken from different fields/wells. Images for OLIG2 staining of clone 4603 could not be obtained due to technical issues with cell attachment. Scale bar= 50µm

Several hours after the neurospheres were plated on PO-laminin surfaces, they started extending projections (putative neurites), which progressively grew reaching lengths of more than 3 mm after one week in some cases. **Figure 5.4** shows the typical morphology and organization of the cells in culture. In all clones, the clusters contained most of the cell bodies within a 3D structure from which long projections extended. In general, plating more neurospheres into the same well produced healthier cultures and longer neurites. On the other hand, plating big neurospheres (>300 μm in diameter) usually had a negative effect on their ability to attach, a situation that made the long-term culture and staining cumbersome. Since the outgrowth behaviour of different neurospheres of the same clone varied considerably, no conclusions can be made about possible differences in the phenotype of the cultures between the different clones. Only the cells of clone SMA1 repeatedly presented an idiosyncratic migration behaviour with many cell bodies migrating out of the clusters. As can be seen in **Figure 5.5**, most of the projections in the MN cultures extended from neuronal cells as shown by the positive staining for TUJ1, thus confirming them as neurites. Neurite growth estimates are presented in the next section of this chapter. There was also a small proportion of glial cells present in the cultures as judged by positive Glial fibrillary acidic protein (GFAP) staining (data not shown).

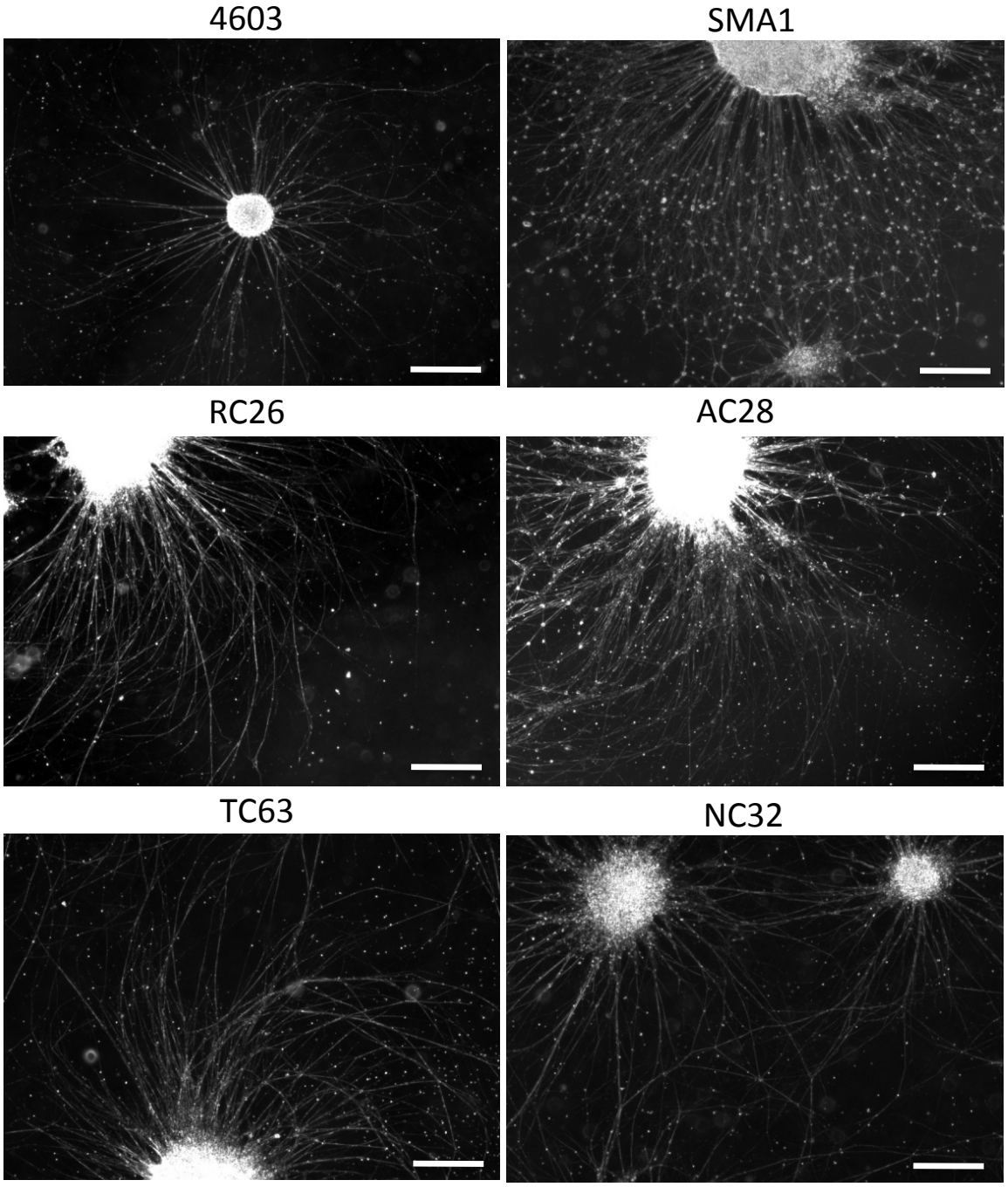

Figure 5. 4: **Cytoplasmatic projections after plating of neurospheres.**
A few hours after plating neurospheres on PO-laminin surfaces, long projections began to grow the clusters. The images shown here were taken from clusters seeded at high confluence on D28 and photographed twelve days later. Scale bar= 500 μm.

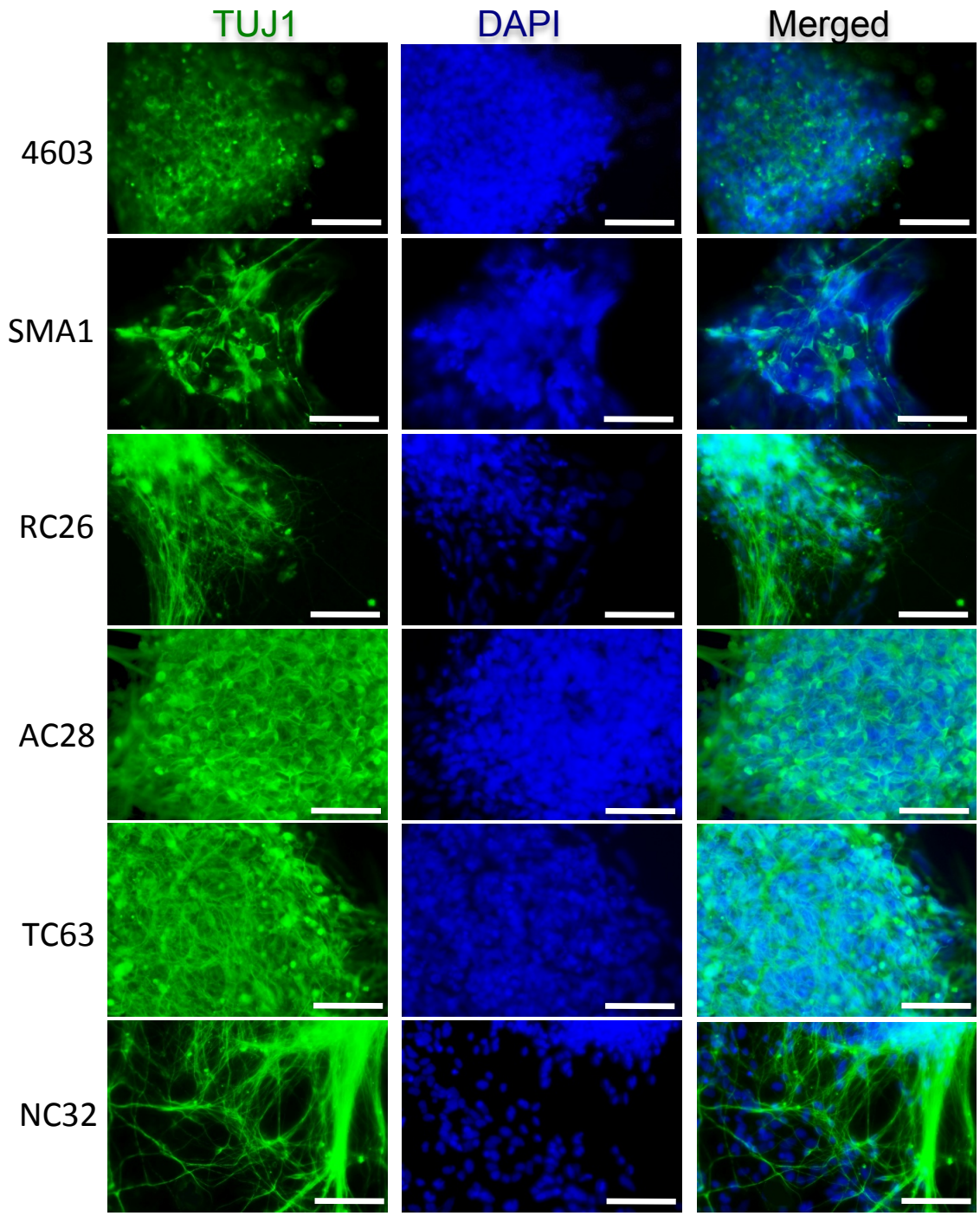

Figure 5. 5: Neuronal identity of cytoplasmatic projections.
TUJ1 expression on D35 shows that a high proportion of projections in the cultures are of neuronal origin, confirming them as neurites. Cell nuclei were counterstained with DAPI (blue). Scale bar= 100 µm.

From D28 onwards, definitive MN markers started to be expressed, with the postmitotic immature MN marker ISL-1 showing earlier that the mature MN marker Choline Acetyletransferase (ChAT). **Figure 5.6** shows positive signals for both markers, confirming the presence of MNs in the cultures derived from iPSCs of all clones. Nuclear markers such as ISL-1 and HB9 could not be quantified within the three-dimensional clusters, since the density of cells was too high and even confocal microscopy could not resolve the layers properly. Given that most of the cells bodies of the MNs were immersed within these clusters, it was not possible to determine the yield of MNs in the culture. An estimation from the pictures seems to suggest that the average MN yield was ~10-15%, again, with a high degree of variability between the clusters of the same clone. MN cultures were only maintained until the presence of ChAT was assessed (around D47).

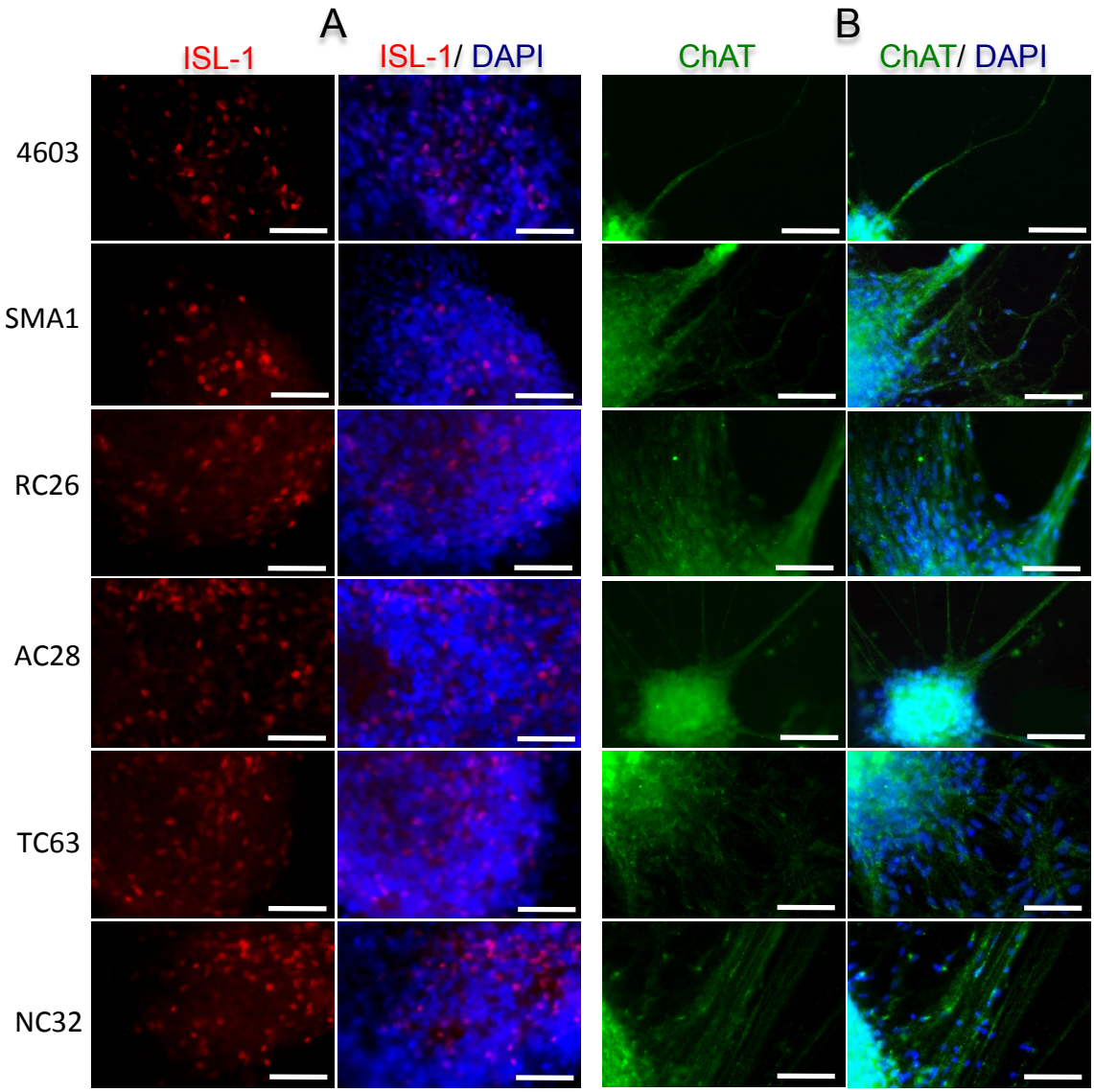

Figure 5. 6: Definitive MN identity.
Between days 28-47 of MN differentiation, the cells in the neurospheres start expressing definitive MN markers. Neurospheres from all clones were plated on D28 on PO-laminin coated coverslips and stained **(A)** on D35 for ISL-1 (red) and **(B)** on D46 for ChAT (green). Cell nuclei were counterstained with DAPI (blue). Images of panels A and B were taken from different fields/wells of the respective clone. Scale bar= 50µm.

5.1.2 NEURITE GROWTH IN iPSC-DERIVED MNS

Neurite growth was monitored during the first 8 days after the plating of neurospheres. In order to avoid the overlapping of neurites during their outgrowth, 10 neurospheres of similar size were homogeneously seeded in 30 mm dishes. At least 5 neurospheres per clone remained attached and were used for analysis and the measurements were performed on the 5 longest neurites on the day of observation (out of a total of 5-50 distinguishable neurites). All clones presented a similar neurite growth profile during the period of measurement, even though their mean absolute neurite length values were significantly different between each other (One-way ANOVA, repeated measures $P<0.001$). The absolute length of all selected neurites increased from 228-428 µm on day 1 to 1050-1744 µm on day 8 (**Figure 5.7A).** In order to avoid the influence of the innate neural differentiation propensity (Hu *et al.* 2010; Boulting *et al.* 2011) and the efficiency of attachment of neurospheres from different clones, growth rates were compared in addition to the absolute length **(Figure 5.7B)**. The comparison between the growth rates across the seven-day observation period shows no significant difference between the clones (One-way ANOVA, repeated measures $P>0.05$).

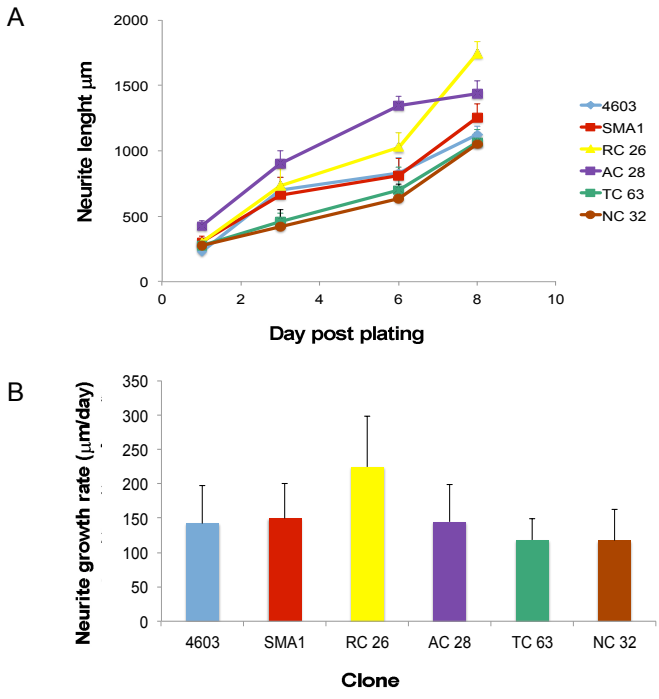

Figure 5. 7: Neurite outgrowth from neurospheres.
D26 neurospheres were plated on PO-laminin coated dishes and the lengths of the five longest neurites from each five neurospheres per clone were measured at different points for 8 days. **(A)** Absolute neurite length between day 1 and 8. **(B)** Average neurite growth rate during three consecutive time intervals (d3-d1, d6-d3, d8-d6). Data are presented as mean ± SEM.

5.1.3 iPSC-DERIVED MNS IN CO-CULTURE WITH MOUSE MYOTUBES

While most reports about SMA focus on MNs, there is evidence that actually their connection point with muscles, the NMJ, may be critically involved in disease development. The NMJ is the synapse between lower alpha MNs and muscle fibres, and the functional interaction between these two entities is primarily mediated by the transmitter ACh (Sanes & Lichtman 2001). In order to simulate this system *in vitro*, D39 neurospheres were co-cultured on differentiated mouse C2C12 myotubes for three days in 1:1 mix of C2C12 differentiation medium and complete MN differentiation medium as described in Materials and Methods (**2.3.7.2.1**). Several hours after plating, neurites started to extend out of the neurospheres, exhibiting a stable attachment in this configuration as compared to their attachment in the absence of muscle cells. Neurite growth accelerated the differentiation and further fusion of C2C12 myoblasts and promoted the clustering of ACh receptors (AChRs). **Figure 5.8** illustrates how AChRs were clustered in fibres surrounding the neurospheres. Indeed, in the co-cultures of all clones it is possible to observe the specific co-localization of TUJ1+ neurites with compact clusters of AChRs stained with α-bungarotoxin. It is not possible to confirm if functional NMJs are formed, but certainly, there is co-localization of the structures involved. Aneural cultures also showed expression of AChRs (**Figure 5.9**), but they were mostly dispersed along the fibres. A few diffused clusters were present in the aneural cultures as well. No difference in the clustering of AChRs was observed between the co-cultures of the different clones. Further electrophysiological analysis would be needed in order to assess a potential SMA disease phenotype with the use of this co-culture system. Pictures of the co-cultures were taken by Dr Tizzano's group in in Santa Creu i Sant Pau Hospital (Barcelona, Spain).

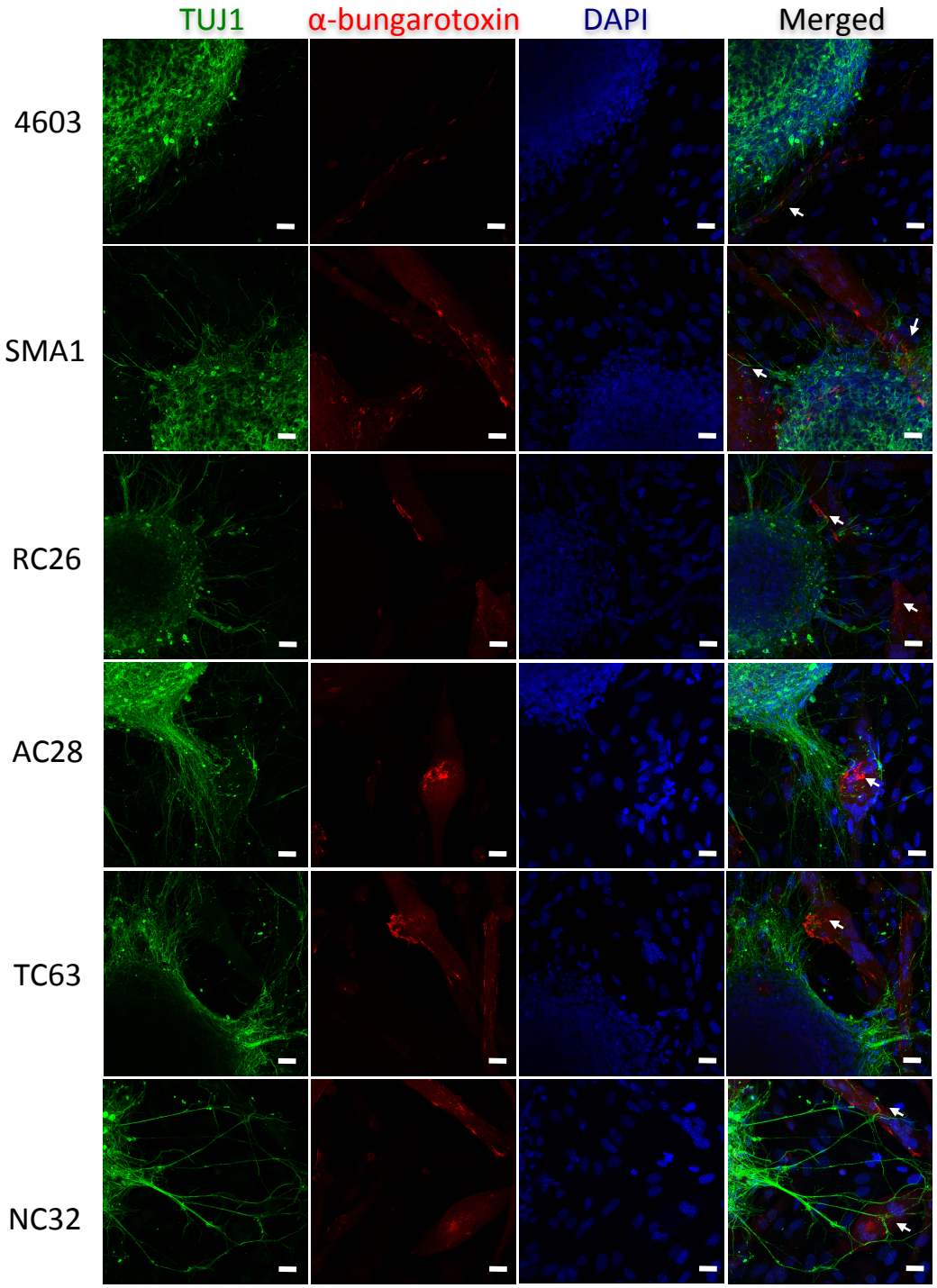

Figure 5. 8: Co-culture of iPSC-derived MNs and mouse myotubes.
D39 neurospheres were seeded on differentiated C2C12 mouse myoblasts and cultured for 3 days in a mixed MN/muscle medium. AChRs, identified by α-bungarotoxing staining (red), clustered in myofibres neighbouring the cells of the neuropheres. TUJ1+ (green) neurites emerging from the neurospheres were observed in close proximity to the AChR clusters (as indicated by arrows). The same behaviour was observed in the co-cultures of all iPSC clones. Cell nuclei were counterstained with DAPI (blue). Scale bar: 20 µm.

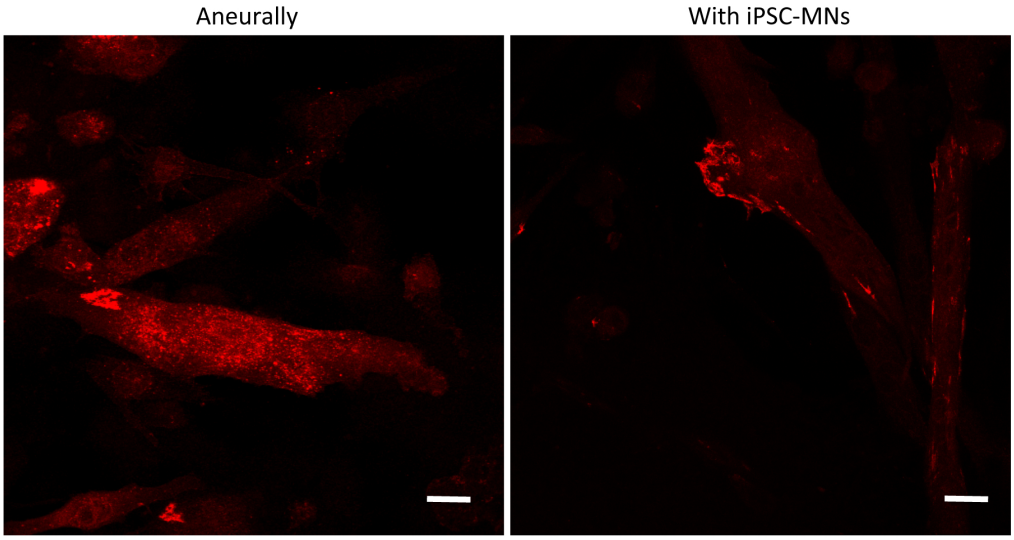

Figure 5. 9: AChR expression in C2C12 mouse myoblasts cultured aneurally or with iPSC-derived MNs The diffused pattern of AChR expression in C2C12 mouse myoblasts cultured aneurally was reorganized upon co-culture with neurospheres into localized expression within defined clusters. Aneural and neural cultures were maintain in a mixed MN/muscle medium. AChRs are identified by α-bungarotoxing staining (red). Scale bar: 20 µm.

5.1.4 MN TRANSDUCTION

The results shown in this section are primarily a qualitative assessment of transduction efficiency from rH1LVs and rAAV9s in iPSC-derived MNs, and the data presented correspond specifically to experiments performed with iPSC clone TC63.

As described in Materials and Methods (**2.3.5.2.4 and 2.3.5.3.4.2***)*, the transduction of iPSC-derived MNs was performed by incubating the viral vectors with the neurospheres prior to plating. This method was used to minimize the volume of medium during transduction in order to increase transduction efficiency. Nevertheless, the results seem to suggest that the vectors were not able to penetrate far into the neurospheres and thus, only images from cells on the edges of the neurospheres or cells which migrated out of the clusters are shown. The representative images of transduced cells presented here are taken to provide a qualitative estimation of transduction efficiencies of accessible cells.

5.1.4.1 rAAV TRANSDUCTION WITH A REPORTER GENE

Cells from D22 neurospheres transduced at MOI 50,000 with scAAV9Cage*GFP*, which carries a ubiquitous promoter driving the expression of the *eGFP* reporter, started to show a high level of eGFP approximately 72 hours after transduction (**Figure 5.10A**). For all neurospheres, preferential expression was observed on one side on the clusters, suggesting that not all cells were equally exposed or accessible to the viral vector during transduction.

An estimation from the pictures seems to suggest that approximately 25% of the cells within the whole cluster were eGFP+ five days post transduction (**Figure 5.10B**).

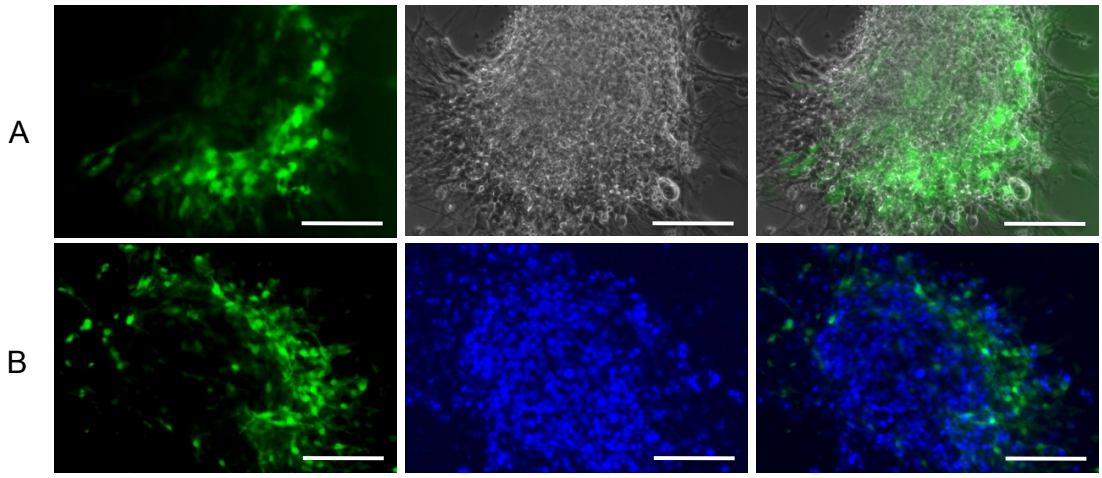

Figure 5. 10: rAAV9 transduction in iPSC-derived MNs.
D22 neurospheres obtained from the differentiation of clone TC63 were transduced with scAAV9Cage*GFP* at an MOI of 50,000 (qPCR titre). (**A**) Three days after transduction GFP+ (green) cells were preferentially observed at one edge of the cluster as seen when superimposing bright field and fluorescent images. (**B**) Five days after transduction cells were fixed and stained with DAPI (blue) for a better estimation of the transduction efficiency. Scale bar = 100µm.

5.1.4.2 rH1LV TRANSDUCTION WITH A REPORTER GENE UNDER A MN ENHANCER/PROMOTER

Cells from D22 neurospheres were transduced with HB9:RFP rH1LVs at a MOI of 100. The HB9 enhancer/promoter driving the expression of the *RFP* in this vector is a MN specific promoter, and particularly, the short version used in these recombinant vectors has been shown to be highly cell-type specific *in vitro* (Lee *et al.* 2004; Marchetto *et al.* 2008; Hester *et al.* 2011). In this particular experiment many of the cells from clone TC63 migrated out of the clusters and grew in less confluent layers as compared with the previously described experiments. It was still not possible at this stage to estimate transduction efficiency prior to DAPI staining, but the proportion of RFP+ cells increased over time, particularly from D34 **(Figure 5.11).** These results are in agreement with what was previously described in section **5.1.1**, which states that definitive MNs markers start to be expressed between days 28-47 of MN differentiation, with HB9 particularly peaking towards days 35-47 (Hu & Zhang 2009), suggesting active MN production during this period. In order to estimate the proportion of cells expressing the reporter after rH1LV transduction in cells that migrated out of the neurospheres, cultures were fixed and stained with DAPI. Quantifications made in three different fields where individual cells could be

counted using the Image J software **(Figure 5.12).** Between 12-17% of the migrated cells were RFP+ at D43, indicating active MN-specific promoter expression and providing an estimate of the efficiency of MN production at this time-point (which is in agreement with the rough estimations made by ISL-1 staining on D35)**.** In this regard, it is important to mention again, that the proportion of positive cells varied between clusters and that the transduction efficiency percentages are not representative for the whole structure of the neurosphere.

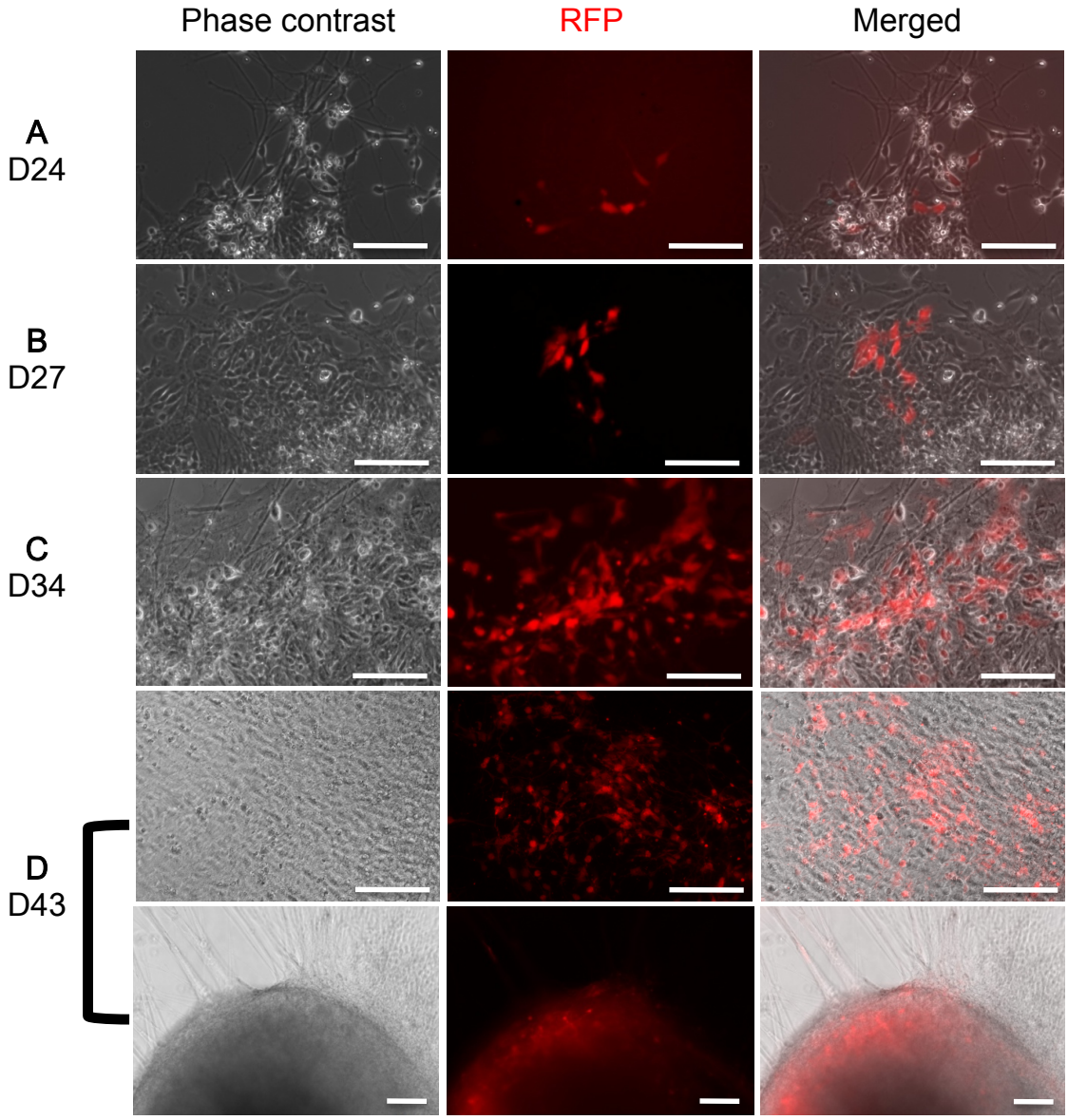

Figure 5. 11: Temporal pattern of *RFP* expression under a MN specific enhancer/promoter in iPSC-derived MNs transduced with rH1LVs.
D22 neurospheres obtained from the differentiation of clone TC63 were transduced with HB9:RFP rH1LVs at a MOI of 100 (qPCR titre). Bright field and RFP (red) fluorescence are shown individually and merged in images taken **(A)** 2, **(B)** 5, **(C)** 12 and **(D)** 21 days post-transduction (corresponding to days 24, 27, 34 and 43 of MN differentiation, respectively). Lower images in panel D show the typical aspect of RFP expression seen inside the clusters. Scale bar = 100µm.

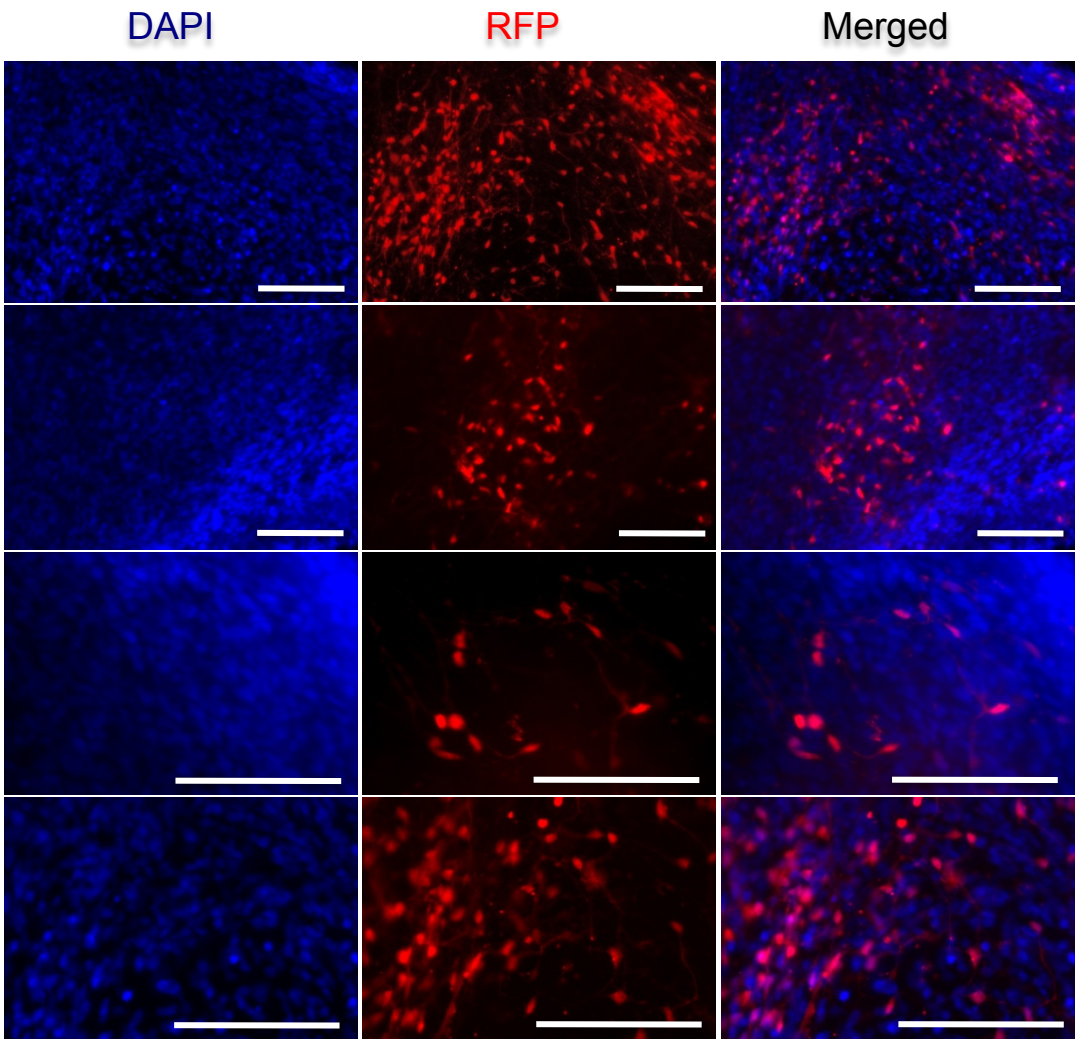

Figure 5. 12: *RFP* expression as an indicator of MN yield.
Cells described in **Figure 5.10D (**21 days post-transduction, corresponding to day 43 of MN differentiation). were fixed and stained with DAPI (blue) for a better approximation of the proportion of cells expressing RFP (red) under the MN-specific enhancer/promoter HB9. Four different fields are presented. Scale bar = 100µm.

5.2 iPSC-DERIVED HEPATOCYTES

iPSC clone RC26 was differentiated into hepatocytes in order to provide an alternative mature cell type differentiated from an iPSC clone for the molecular experiments described in the next chapter regarding SMN regulation during iPSC differentiation. In this section, the characterisation of the differentiated hepatic cells is shown.

As described in Materials and Methods (**2.3.7.3**), hepatocyte differentiation was done according to the method outlined by *(Song et al. 2009)*. Unlike in the case of MN differentiation, hepatic differentiating cells were not manually selected or passaged during the 21 days of the protocol. Linage coaxing was accomplished by the sequential addition of signalling molecules such as Activin A (for endoderm induction, D1-D3), FGF_4 and BMP_2 (for hepatic specification, D4-D7), HGF and KGF (for hepatoblast expansion, D8-D13), oncostatin M, dexamethasone, N2 and B27 (for hepatic maturation, D14-21). **Figure 5.13** shows a characterization of markers in the derived cells to assess hepatocyte identity. D21 cells showed high and broad expression of the hepatic marker α-fetoprotein (**Figure 5.13B**) as well as storage of lipids (**Figure 5.13C**) and glycogen (**Figure 5.13D**). The specificity of the glycogen storage during the Periodic Acid-Schiff (PAS) test was confirmed by treating the cells with α-amylase before the staining procedure, a treatment that abolished the positive signal of the test.

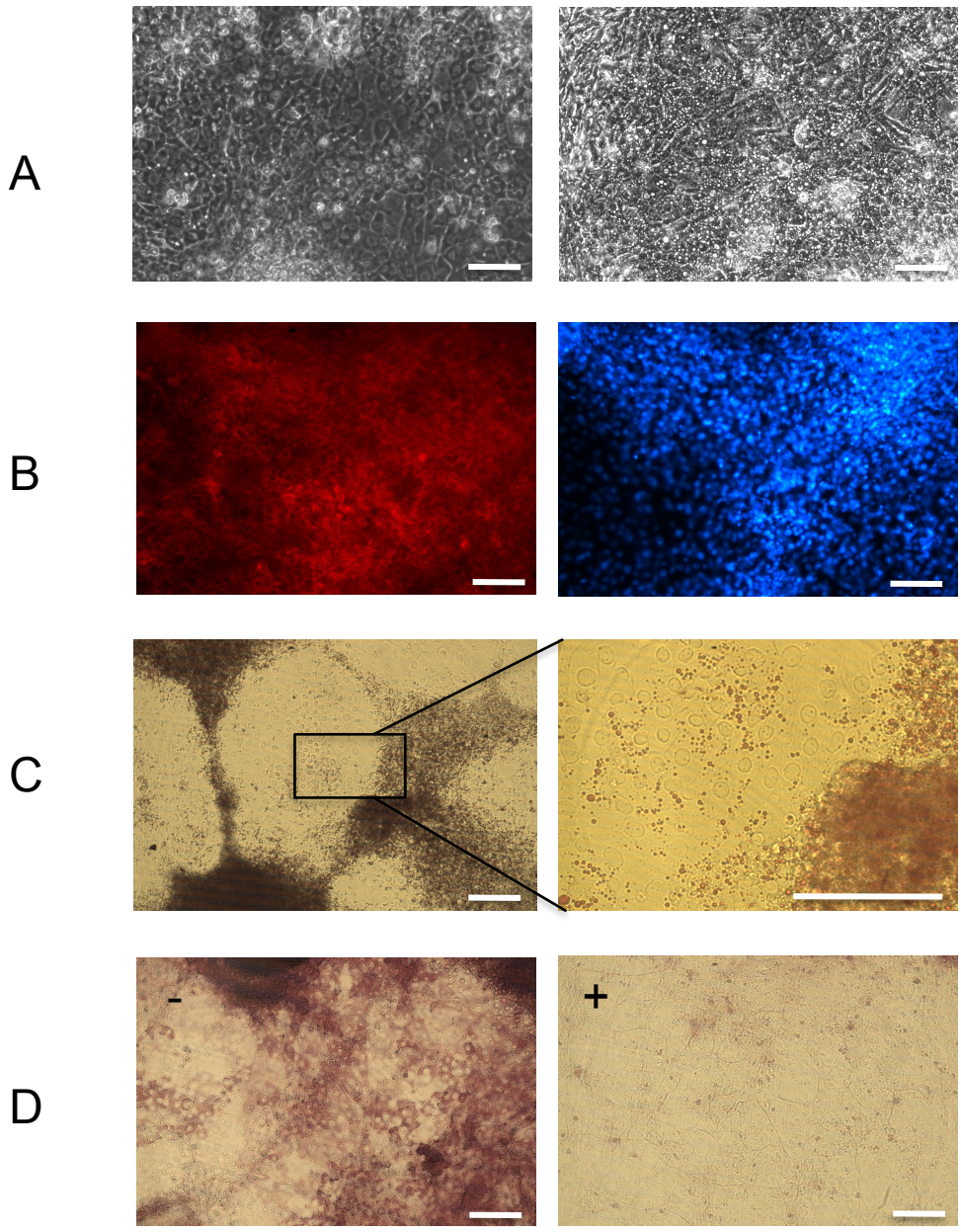

Figure 5. 13: Phenotypic and functional characterisation of D21 RC26 iPSC-derived hepatocytes.
(A) Morphology of cells in bright field. **(B)** Expression of the hepatic cell marker AFP, (red). Cell nuclei were counterstained with DAPI (blue). **(C)** Sudan staining exposing the storage of lipid vesicles. A higher magnification field of the first picture is shown on the right hand side. **(D)** PAS staining showing the storage of glycogen ("-"). Treatment with alpha amylase ("+") eliminated the positive signal in the PAS staining, confirming the intracellular accumulation of glycogen. Scale bar= 50µm.

CHAPTER 6: RESULTS- SMN AND PLS3 LEVELS DURING iPSC DIFFERENTIATION

This chapter presents all the molecular analyses performed with the populations described in the previous chapter including fibroblasts, iPSCs, EBs, rosettes, neurospheres, MNs, immature hepatocytes and mature hepatocytes. The results from all terminally differentiated clones are presented here. Within all cell populations the expression of *SMN* splicing isoforms and *PLS3* were assessed at the transcriptional (mRNA) and translational (protein) level, with the aim of comparing these critical SMA-related products between individuals and between cells types. mRNA-related experiments were performed by Dr. Tizzano's group in Santa Creu i Sant Pau Hospital (Barcelona). Clones SMA1 and 4603 were only included in this study during the last iPSC-MN differentiation, in order to provide a reference for the most severe disease state (SMA1) and an unaffected control reference with no *SMN1* mutations (4603). No differentiation replicates were performed for the last two clones. Results from three and two iPSC-MN differentiations are presented for clones AC28 and RC26 and clones NC32 and TC63, respectively.

6.1 SMN-RELATED ISOFORM LEVELS

The transcription and further processing of the *SMN1* and *SMN2* genes produces two main mRNAs: *FL-SMN* and *Δ7-SMN* (please refer to introduction for more details). *FL-SMN* produces a stable functional protein, whereas it is thought that the putative translation of *Δ7-SMN* produces a less functional protein that is rapidly degraded (Lorson *et al.* 1998; Lorson & Androphy 2000). As of today, no antibody has been produced against the *Δ7-SMN* isoform. Therefore, only the quantification of the FL-SMN protein is shown in this section. Regarding transcript quantification, three different sets of primers were used. The first set amplified a sequence at the junction between exons 1 and 2 of the *SMN* mRNA and thus measured all spliced isoforms, denominated here as total *SMN* (*tSMN*). The second set amplified a sequence at the junction between exons 6 and 7 that is only present in *FL-SMN* and the third set amplified a sequence in the junction between exons 6 and 8 that is unique to *Δ7-SMN*. Please refer to **Appendix 2** for details of the primers.

6.1.1 ORIGIN OF FL-SMN TRANSCRIPTS

As it has been stated before, *FL-SMN* can be transcribed from both *SMN1* and *SMN2* genes. Nonetheless, given that the members in the family of study possess a mutation in the *SMN1* gene that predicts an early stop codon (but does not block *SMN1* transcription), I aimed to investigate if this mutation also prevented the generation of stable *FL-SMN* mRNA. For

this, a fragment containing exons 6-8 of the *SMN* transcripts (*SMN1* and *SMN2*) were amplified by RT-PCR and further digested with *Dde*I. Given that only the *SMN2* gene possess a recognition site for this enzyme, their transcripts can be distinguish from the ones originating from the *SMN1* gene by their molecular size (**Figure 6.1A**). **Figure 6.1B** shows that all 4603 unaffected control cells (iPSCs [D0], EBs [D7], rosettes [D15], neurospheres [D28] and MNs [D42]) produced *FL-SMN* from both *SMN1* and *SMN2* genes, same as cells from the carrier mother (RC). In contrast, essentially all *FL-SMN* transcripts in cells from the siblings of study (AC, TC and NC) originated from their *SMN2* genes; this was also the case in SMA1 cells. However, we did observe very faint *FL-SMN1* bands in some samples from siblings of the family of study (see for instance the neurospheres in **Figure 6.1B**). This indicates that this transcript is produced at high enough levels to allow detection in some cases.

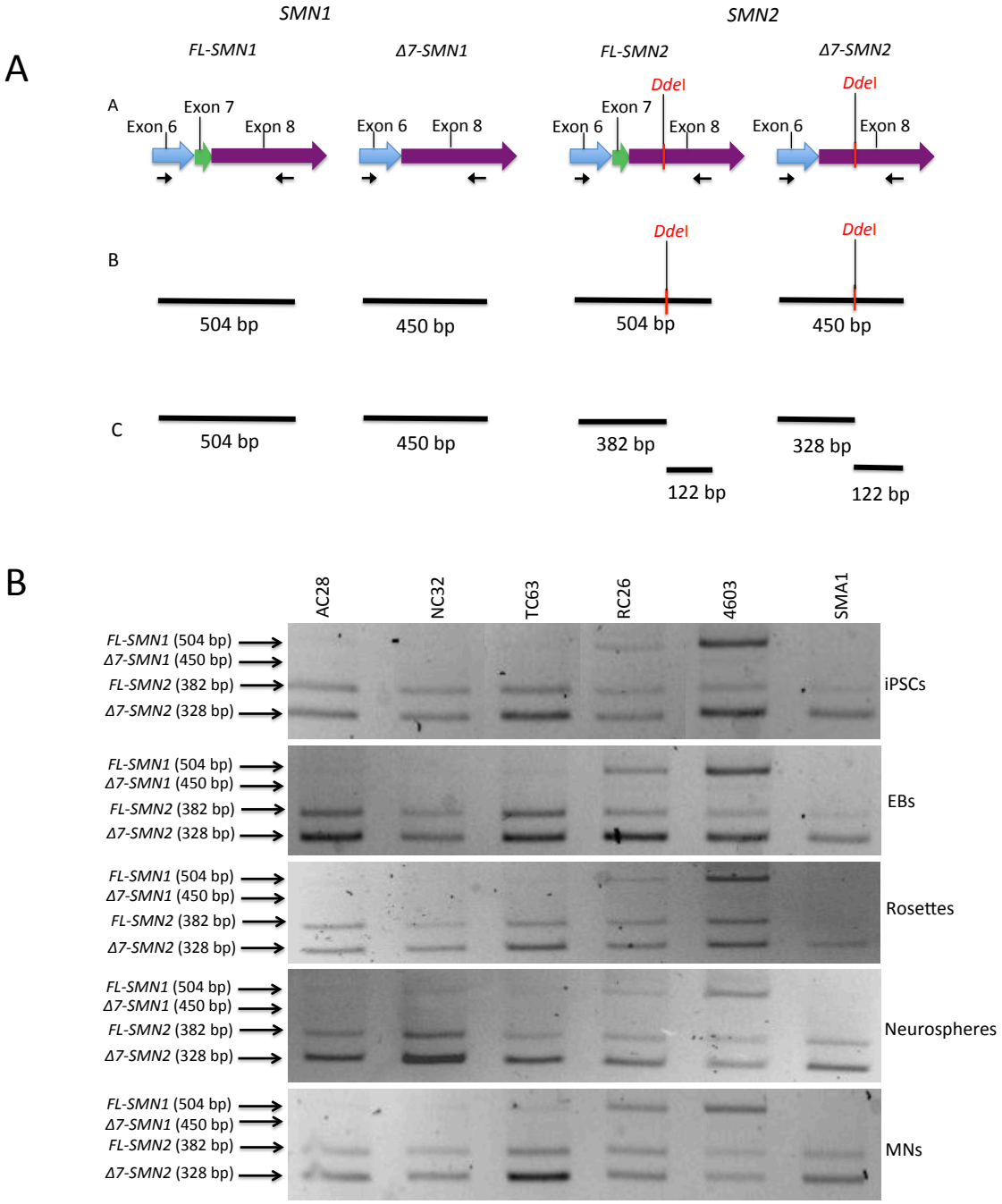

Figure 6. 1: Origin of *FL-SMN* transcripts.
(A) Diagram showing the amplification and restriction pattern analysis performed for the determination of the locus from which *FL-SMN* transcripts originated. (**A1, A2**) Exons 6-8 from the *SMN1* and *SMN2* genes were amplified by RT-PCR producing 504 bp and 450 bp fragments, corresponding to *FL-SMN* and *Δ7-SMN* transcripts respectively. (**A3**) The following *DdeI* digestion of the PCR products produced the specific cleavage of the *SMN2* transcripts generating 382 bp and 328 bp fragments, corresponding to *FL-SMN2* and *Δ7-SMN2* respectively. (**B**) Restriction analysis of iPSCs (D0), EBs (D7), rosettes (D15), neurospheres (D28) and MNs (D42) from the six clones of study. *Δ7-SMN1* transcripts are produced at very low levels.

6.1.2 GENERAL VARIATION OF SMN RNA AND PROTEIN LEVELS DURING iPSC-MN DIFFERENTIATION

In order to follow the pattern of SMN RNA and protein levels during iPSC-MN differentiation, clonal values were pooled together by cell type into two groups: unaffected individuals (RC26 and 4603) and SMA patients (SMA1, AC28, TC63, NC32) (**Figure 6.2**). AC was included in the SMA group given the patient's lack of functional *SMA1* genes (as her SMA type III symptomatic siblings) and the presence of minimal electromyography alterations. The fibroblasts used for iPSC reprogramming are included in the graphics as a reference, but they are not part of the cell types harvested during the iPSC-MN differentiation and thus are not included in the statistical analyses to avoid bias. Unaffected and SMA groups showed similar variation across cell types along the MN differentiation process for all the parameters measured ($P > 0.05$), but *FL-SMN* mRNA, SMN protein and the *FL/Δ7-SMN* mRNA ratio were all in general significantly higher in unaffected individuals ($P<0.001$, $P<0.05$, $P<0.001$ respectively). Statistically significant changes were however found between both groups during post hoc analyses in the EB *FL-SMN* mRNA ($P<0.05$) and the rosette and MN of the *FL/Δ7-SMN* mRNA ratio ($P<0.001$). Moreover, further cell type analyses combining unaffected and SMA patients show that, although mRNA levels of *FL-SMN* and *tSMN* did not significantly vary between cell types (**Figure 6.2A and E**), SMN protein levels did ($P<0.01$) (**Figure 6.2B**). Furthermore, SMN protein levels showed a gradual decay during the iPSC-MN differentiation process (linear trend $P<0.05$), with the lowest value observed specifically in MNs.

In order to see if the decay in SMN protein was specific to iPSC-MN differentiation or a general pattern of iPSC differentiation, RC26 iPSCs were differentiated into hepatocytes. As it can be seen in **Figure 6.3** during iPSC-hepatocyte differentiation the mRNA levels of *tSMN*, *FL-SMN* and *Δ7-SMN* did not change greatly, whereas SMN protein levels fluctuated considerably. SMN protein increased 4-fold between iPSCs and the D7 hepatocyte differentiation culture (corresponding to immature hepatocytes), and then decreased by D21 (corresponding to mature hepatocytes) but to a level 2-fold higher than in iPSCs. Notably, SMN protein levels in the mature D21 hepatocyte cultures were also at least 2-fold higher than in mature MN cultures (all values shown in this chapter were calibrated against the same sample [SMA type II fibroblasts] unless otherwise stated). Therefore, it seems that the progressive reduction in SMN protein levels during

differentiation was peculiar to the MN cultures. It is important to emphasize again that hepatocyte values correspond to only one iPSC differentiation round, from a single clone and that RC26 iPSCs had the lowest SMN protein levels among all clones.

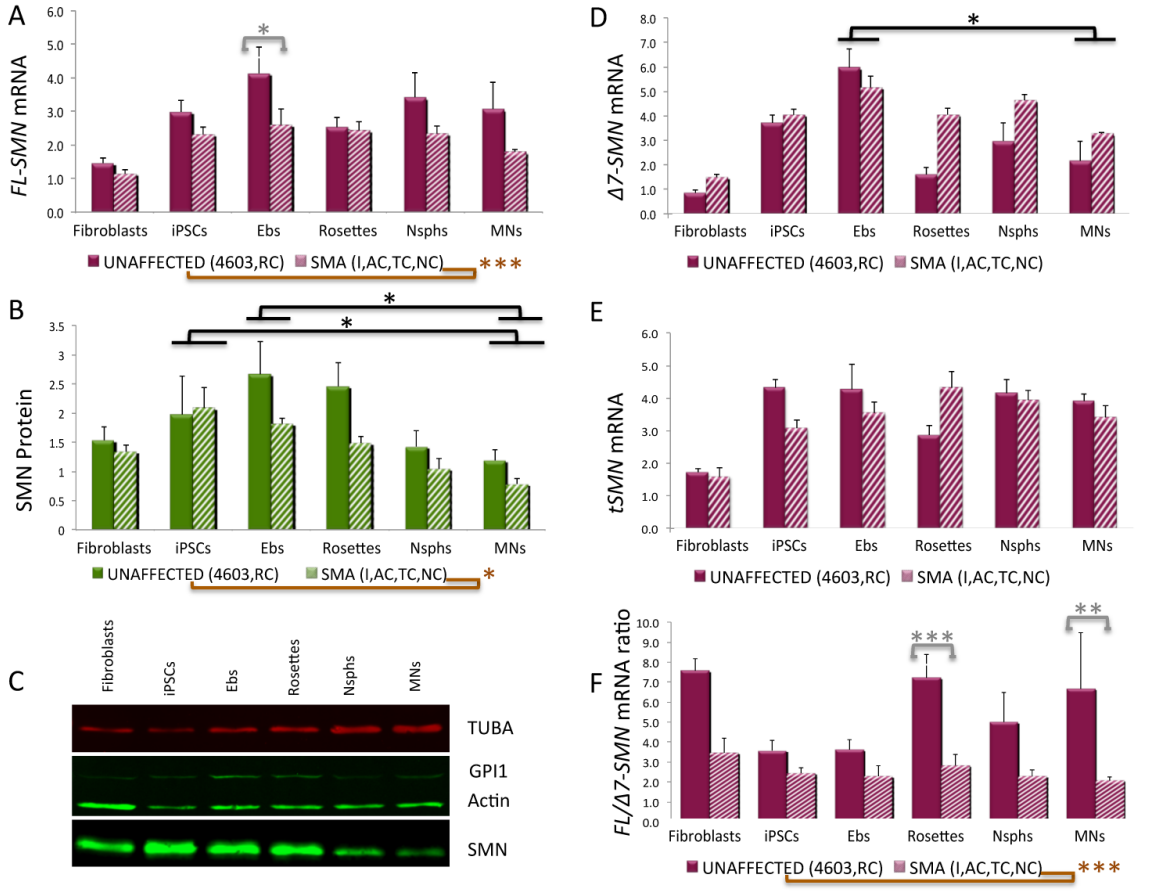

Figure 6. 2: Variation of SMN RNA and protein levels during IPSC-MN differentiation.
The expression of *FL-SMN* mRNA (**A**), SMN protein (**B**), *Δ7-SMN* mRNA (**D**), *tSMN* mRNA (**E**) and the *FL/Δ7-SMN* mRNA ratio (**F**) is shown for each cell type. Unaffected individuals (RC+4603) and SMA patients (SMA1, AC28, TC63 and NC32) are shown separately. Data are presented as mean ± SEM. Samples were calibrated to a common stock derived from SMA type II fibroblasts. For qRT-PCR, samples were normalized with the geometric mean of the values from *beta actin (ACTB), glyceraldehyde-3-phosphate dehydrogenase (GADPH)* and *peptidylprolyl isomerase A (PPIA*). For western blot, samples were normalized with the geometric mean of the values from *alpha tubulin (TUBA)*, *glucose phosphate isomerase* (*GPI1*) and *actin*. Brown, black and gray asterisks/lines in each panel compare unaffected group *vs* SMA group in general, cell types in general and unaffected group *vs* SMA group by cell type, respectively. *, P<0.05; **, P<0.01; ***, P<0.001. **(C)** Representative western blot showing decay in SMN protein during the iPSC-MN differentiation of clone TC63.

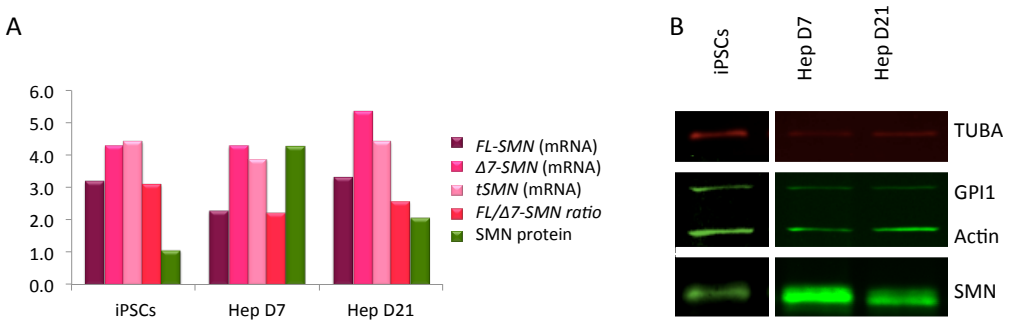

Figure 6. 3: Variation of SMN RNA and protein levels during iPSC-hepatocyte differentiation.
(**A**) Expression of *FL-SMN* mRNA, *Δ7-SMN*, *tSMN* mRNA, *FL/Δ7-SMN* mRNA ratio and SMN protein in iPSCs, intermediate hepatocyte progenitors harvested at day 7 of RC26 iPSC differentiation (Hep D7) and mature hepatocytes harvested at day 21 (Hep D21). Samples were calibrated to a common stock derived from SMA type II fibroblasts. For qRT-PCR, samples were normalized with the geometric mean of the values from *ACTB, GADPH* and *PPIA*. For western blot, samples were normalized with the geometric mean of the values from *TUBA*, *GPI1* and *actin*. (**B)** Western blot showing the fluctuation in SMN protein during iPSC-hepatocyte diferentiation.

6.1.3 PATIENT SPECIFIC VARIATION OF SMN RNA AND PROTEIN LEVELS DURING IPCS-MN DIFFERENTIATION

Variation in SMN RNA and protein levels during iPSC-MN differentiation for each individual clone was also assessed. Individual clones showed heterogeneous mRNA expression levels of *FL-SMN* and *Δ7-SMN,* but fairly constant t*SMN* and *FL/Δ7-SMN* mRNA ratios between differentiation stages, with the exception of the increasing *FL/Δ7-SMN* ratio in wt clone 4603 (**Figure 6.4A, C D and E respectively**). Most importantly, consistent with the observation made when clones were grouped by developmental stage (**Figure 6.2B**), all individual clones exhibited a gradual decrease in SMN protein during the MN differentiation process (**Figure 6.4B**). When all the cell types from each clone were pooled together, unaffected clones (particularly clone 4603) could be distinguished from the other clones by their higher *FL/Δ7-SMN* ratios. The distinction was shown to be statistically significant, but only for 4603 ($P<0.001$) (**Figure 6.5A).** These results reflect the high *FL-SMN* and low *Δ7-SMN* mRNA levels observed for the unaffected group in the previous graphics, particularly towards the most differentiated stages (**Fig 6.2A and D**). Furthermore, the pooled *tSMN* mRNA values of SMA1 cells were found to be significantly lower than those observed in the clone from the carrier mother RC26 and the siblings (AC28, NC32 and TC63) ($p<0.001$) (**Figure 6.5B**), perhaps reflecting the reduced number of *SMN* gene copies present in SMA1.

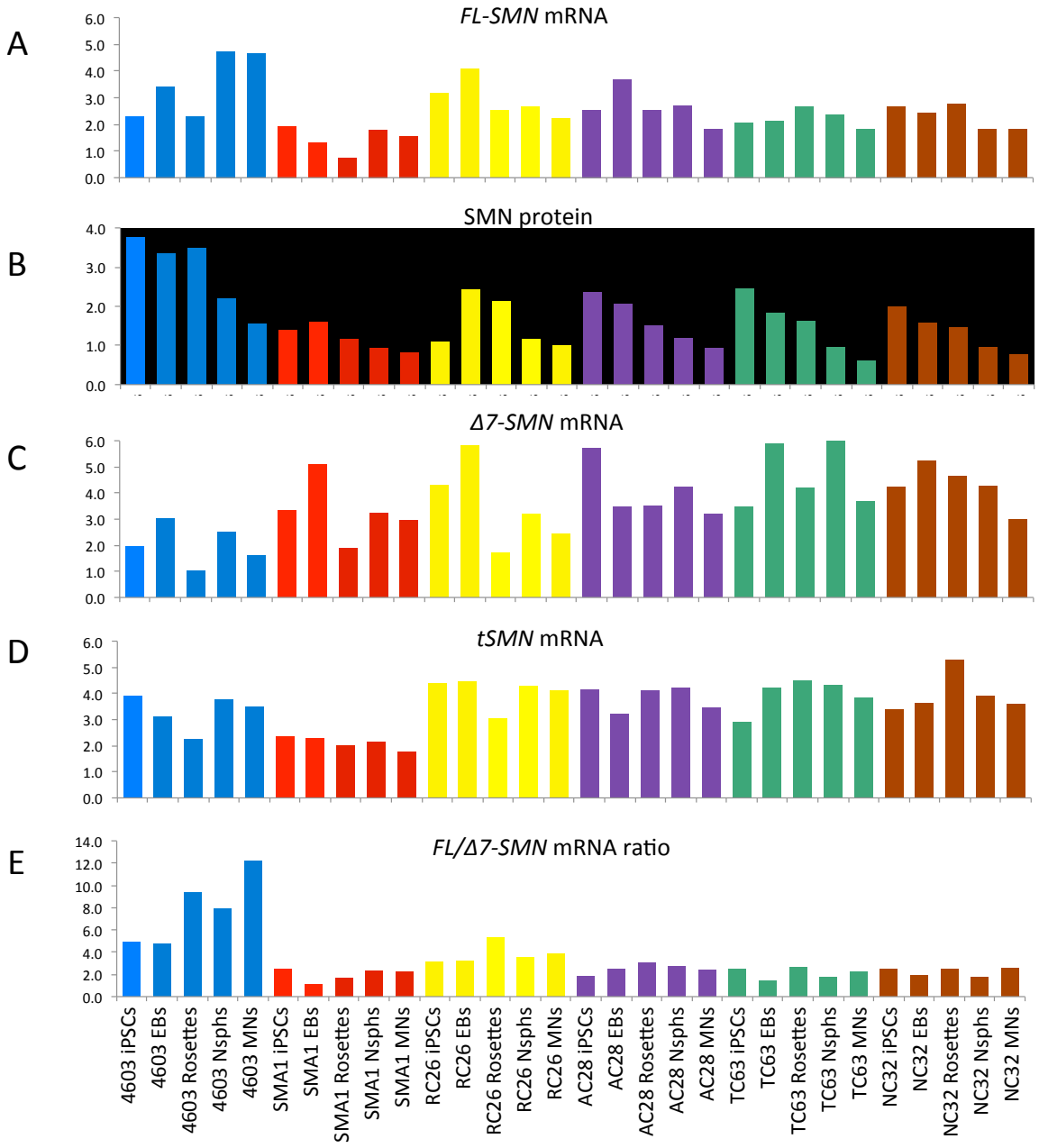

Figure 6. 4: Patient specific variation of SMN RNA and protein levels during IPSC-MN differentiation. The expression of *FL-SMN* mRNA (**A**), SMN protein (**B**), *Δ7-SMN* mRNA (**C**) *tSMN* mRNA (**D**) and *FL/Δ7-SMN* mRNA ratio (**E**) is shown for each clone/patient along all its cell types. Samples were calibrated to a common stock derived from SMA type II fibroblasts. For qRT-PCR, samples were normalized with the geometric mean of the values from *ACTB, GADPH* and *PPIA*. For western blot, samples were normalized with the geometric mean of the values from *TUBA*, *GPI1* and *actin*.

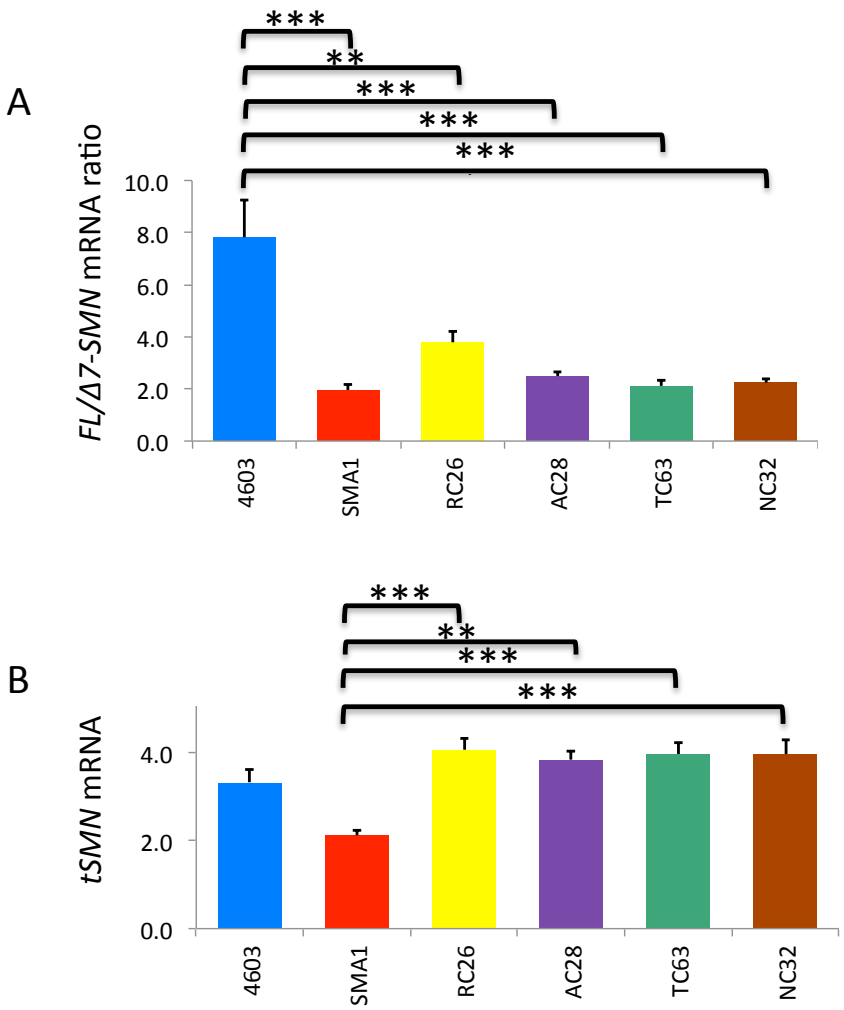

Figure 6. 5: Patient specific variation of pooled values during IPSC-MN differentiation.
FL/Δ7-SMN mRNA ratio (**A**) and *tSMN* mRNA (**B**) values from all tissues (iPSCs, EBs, Rosettes, neurospheres and MNs) were pooled together for comparison. Data are presented as mean ± SEM. Samples were calibrated to a common stock derived from SMA type II fibroblasts. For qRT-PCR, samples were normalized with the geometric mean of the values from *ACTB, GADPH* and *PPIA*. For western blot, samples were normalized with the geometric mean of the values from *TUBA*, *GPI1* and *actin*. **P<0.01, ***P<0.001.

6.1.4 PATIENT SPECIFIC SMN RNA AND PROTEIN LEVELS IN MOTOR NEURONS

Given that MNs are the main affected cell type in SMA, a separate analysis was performed to evaluate specifically the differences in SMN RNA and protein levels between individuals in this particular cell type. As can be seen in **Figure 6.6,** both *FL-SMN* mRNA and protein levels are particularly high for 4603 MNs, whereas the levels in SMA1 MNs are similar to the one seen in the siblings. The *FL/Δ7-SMN* ratio is also very high for 4603 cells.

The mRNA analysis also includes levels in SMA1 MNs transduced with scAAV9s carrying the h*SMN1* gene (scAAVCag*hSMN1*F), which could not be assessed at the protein level

given the low protein yield. The results suggest an up-regulation in *FL-SMN* mRNA levels and a down-regulation in *Δ7-SMN* mRNA, congruent with the behaviour of unaffected 4603 MNs. No statistical significance can be given since these data correspond only to 2 iPSC-MN differentiation experiments.

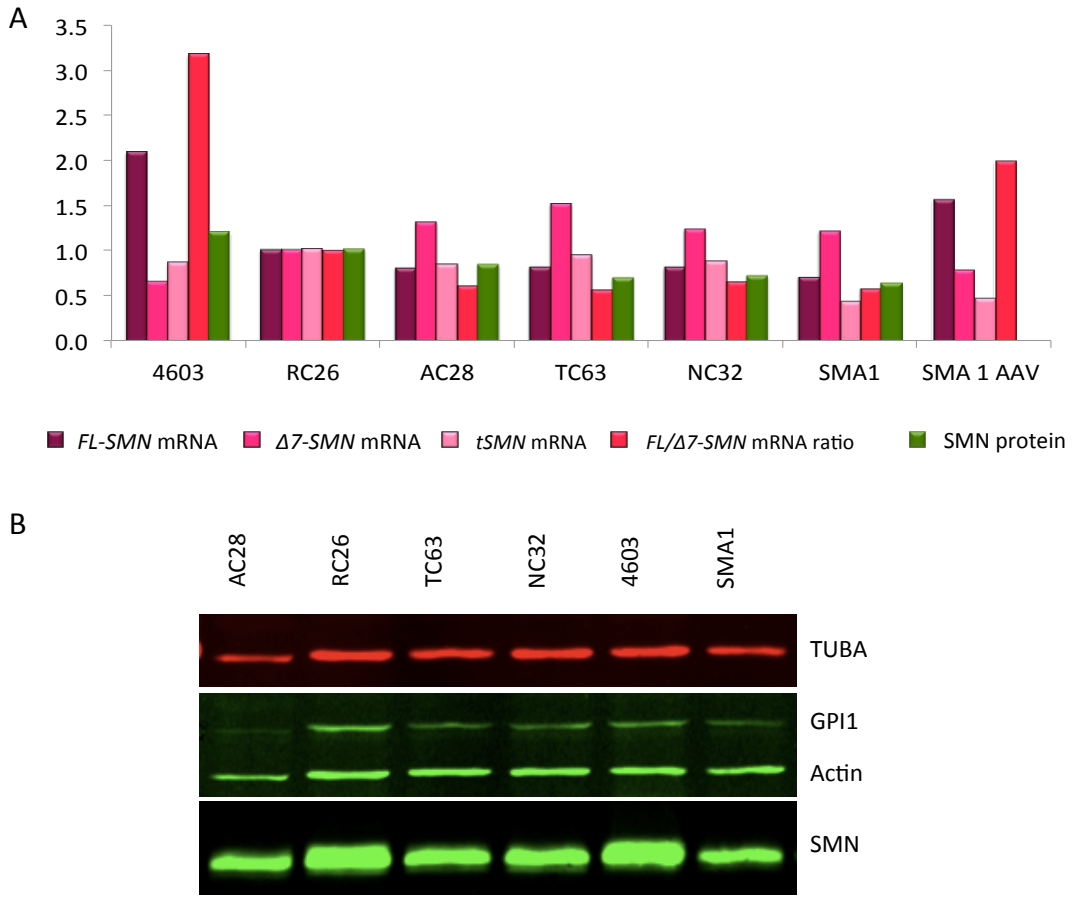

Figure 6. 6: Patient specific SMN RNA and protein levels in MNs.
(A) Expression of *FL-SMN* mRNA, *Δ7-SMN* mRNA, *tSMN* mRNA, *FL/Δ7-SMN* mRNA ratio and SMN protein for the iPSC-derived MNs of all individuals. Samples were calibrated to RC26 MNs. For qRT-PCR, samples were normalized with the geometric mean of the values from *ACTB, GADPH* and *PPIA*. For western blot, samples were normalized with the geometric mean of the values from *TUBA*, *GPI1* and *actin*. **(B)** Representative western blot of SMN proteins in MNs.

6.2 PLS3 LEVELS

PLS3 levels were followed and analysed in a similar way as in the case of SMN.

6.2.1 GENERAL VARIATION OF PLS3 RNA AND PROTEIN LEVELS DURING iPCS-MN DIFFERENTIATION

In order to follow the pattern of PLS3 levels during iPSC-MN differentiation, the values of all six clones were grouped by cell type (**Figure 6.7**). Individuals were not separated in unaffected individuals and SMA patients as in the previous analysis given that the level of PLS3 has only been reported as a modifier factor of the severity of SMA and not as the cause. The fibroblasts used for iPSC reprogramming are included in the graphics as a reference, but they are not part of the cell types harvested during the iPSC-MN differentiation and thus are not included in the statistical analyses to avoid bias. Both, *PLS3* mRNA and protein levels were found to vary between cell types ($P<0.001$) and in both cases there is a gradual decay during iPSC-MN differentiation (linear trend $P<0.0001$). As in the case of SMN, cells harvested from RC26 iPSC differentiation into hepatocytes were used to assess the specificity of the decay. As shown in **Figure 6.8**, *PLS3* mRNA and protein levels, as FL-SMN protein levels (**Figure 6.3**) increase from iPSCs to immature hepatocytes (D7), and then decreased by D21 in mature hepatocytes. PLS3 protein levels in mature hepatocytes are considerably higher (4 to 5-fold) than those found in neural cells. Hepatocyte values correspond to only one round of RC26 iPSC differentiation.

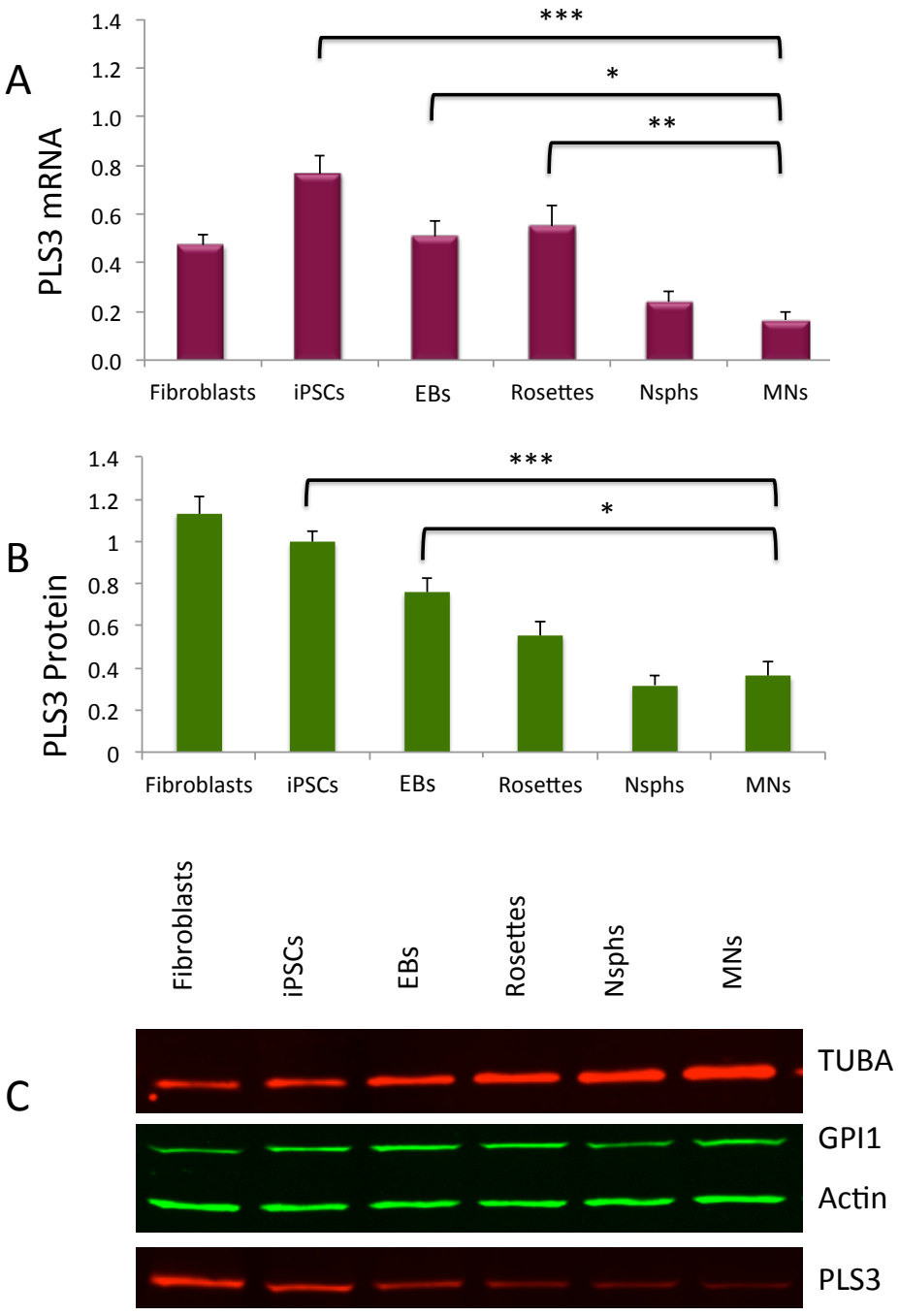

Figure 6. 7: Variation of PLS3 RNA and protein levels during iPSC-MN differentiation.
The Expression of *PLS3* mRNA (**A**) and PLS3 protein (**B**) is shown for each cell type. Data are presented as mean ± SEM. Samples were calibrated to a common stock derived from SMA type II fibroblasts. For qRT-PCR, samples were normalized with the geometric mean of the values from *ACTB, GADPH* and *PPIA*. For western blot, samples were normalized with the geometric mean of the values from *TUBA*, *GPI1* and *actin*. *P<0.05, **P<0.01, ***P<0.001. (**C**) Representative western blot showing the decay in the PLS3 protein along the iPSC-MN differentiation of clone TC63.

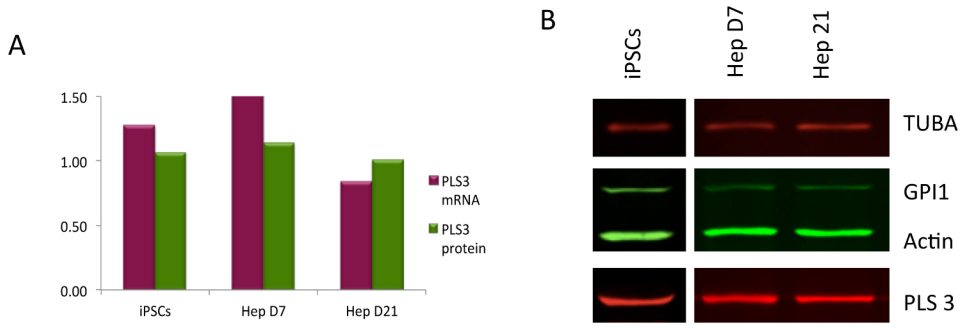

Figure 6. 8: Variation of PLS3 RNA and protein levels during iPSC-hepatocyte differentiation.
(**A)** The expression of *PLS3* mRNA and PLS3 protein is shown for intermediate hepatocyte progenitors harvested at day 7 of RC26 iPSC differentiation (Hep D7) and mature hepatocytes harvested at day 21 (Hep D21). Samples were calibrated to a common stock derived from SMA type II fibroblasts. For qRT-PCR, samples were normalized with the geometric mean of the values from *ACTB, GADPH* and *PPIA*. For western blot, samples were normalized with the geometric mean of the values from *TUBA*, *GPI1* and *actin*. **(B)** Western blot showing the levels of PLS3 protein during iPSC-hepatocyte differentiation.

6.2.2 PATIENT SPECIFIC VARIATION OF PLS3 RNA AND PROTEIN LEVELS DURING iPCS-MN DIFFERENTIATION

The clone specific variation of PLS3 levels during iPSC-MN differentiation was also evaluated. In general terms, all individuals showed the previously described gradual decay in *PLS3* mRNA and protein (**Figure 6.9**). Control 4603 cells present lower *PLS3* mRNA and protein levels compared to the rest of the clones.

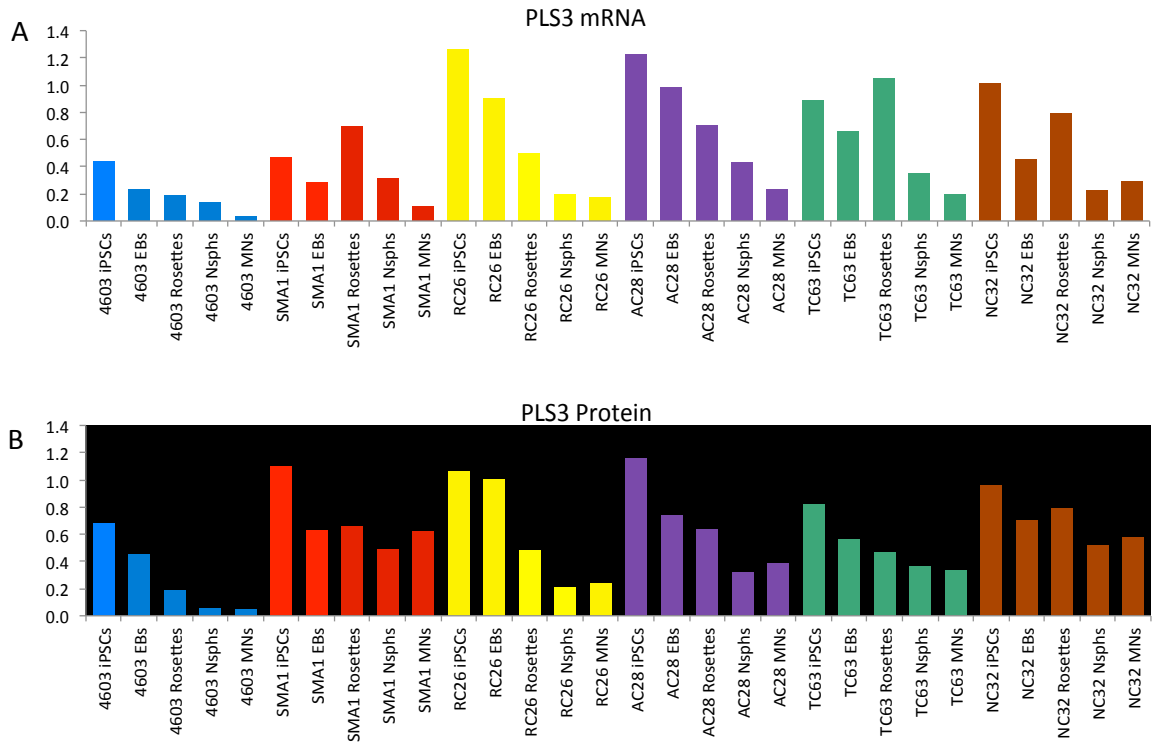

Figure 6. 9: Patient specific variation of PLS3 RNA and protein levels during iPSC-MN differentiation. The expression of *PLS3* mRNA (**A**) and PLS3 protein (**B**) is shown for each clone/patient during the differentiation process. Samples were calibrated to a common stock derived from SMA type II fibroblasts. For qRT-PCR, samples were normalized with the geometric mean of the values from *ACTB, GADPH* and *PPIA*. For western blot, samples were normalized with the geometric mean of the values from *TUBA*, *GPI1* and *actin*.

6.1.4 PATIENT SPECIFIC PLS3 RNA AND PROTEIN LEVELS IN MNs

MN-specific PLS3 level in iPSC-derived cells from members of the family of study are compared in this section. As can be seen in **Figure 6.10** the PLS3 protein level in the MNs of AC28 is 150% higher than the one observed in the carrier unaffected mother (RC26) and it is also 65% higher than the affected siblings (TC63 and NC32). The highest mRNA levels were nonetheless observed in cells from NC32. No statistical significance can be given since the data correspond to only 2 iPSC-MN differentiation experiments. It is worth mentioning that apparently different forms of PLS3 were found on the western blots of fibroblasts and MNs which differ in ~2 kDa (**Figure 6.11**).

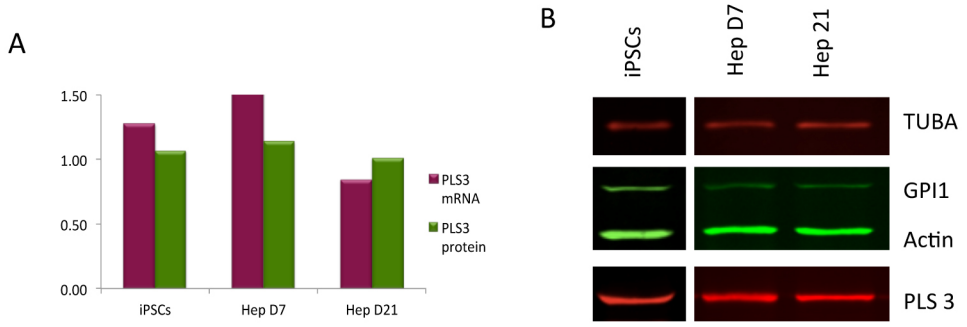

Figure 6. 10: Patient specific PLS3 RNA and protein levels in MNs.
(A) Expression of PLS3 mRNA and PLS3 protein in iPSC-derived MNs of the individuals of the family of study. Samples were calibrated to RC26 MNs. For qRT-PCR, samples were normalized with the geometric mean of the values from *ACTB, GADPH* and *PPIA*. For western blot, samples were normalized with the geometric mean of the values from *TUBA*, *GPI1* and *actin*. **(B)** Representative western blot of PLS3 protein.

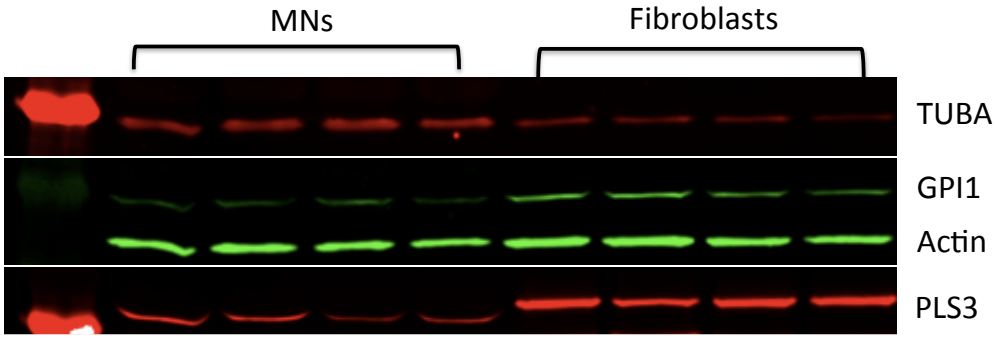

Figure 6. 11: PLS3 expression in different cell types.
Detection of PLS3 by western blot shows proteins of apparently different sizes in MNs and fibroblasts.

CHAPTER 7. DISCUSSION

Since the *SMN1* gene responsible for the SMA pathology was first identified in 1995 (Lefebvre *et al.* 1995), there have been many efforts to determine the specific function that this gene and its highly homologous *SMN2* gene accomplish in the cells. Moreover, since SMN is expressed in all cell types, the particular susceptibility of MNs continues to be a matter of controversy, which is hindered by the inaccessibility of this cell type in humans. iPSC technology has made possible the generation of MNs from accessible somatic cells which allows the study of the disease in the human relevant cell types. I have reprogrammed cells from a consanguineous discordant SMA family and further differentiated these cells into MNs. I had three main aims with the reprogramming of the cells: (1) to study potential disease phenotypes in iPSC-derived MNs, (2) to follow the expression of SMN isoforms at the transcriptional and translational level during the iPSC-MN differentiation process and (3) to determine whether PLS3 could be the modifier factor in the discordant SMA family. To accomplish these main objectives, viral vectors were produced for diverse purposes, iPSC clones were generated and characterised, iPSC to MN differentiation protocols were adapted and applied, iPSCs were differentiated to hepatocytes, and several molecular analyses were performed in various cell types harvested during the differentiation process. Given the diversity of results described, this discussion will be split in sections in order to provide a comprehensible structure.

7.1 VIRAL VECTORS

Viral vectors were used in this project for several purposes: rMMLVs were used for the generation of iPSCs and their selection and transduction efficiency will be discussed in that section. rH1LVs on the other hand were used as vehicles for the transfer of a reporter gene expressed under the control of a MN specific promoter and will discussed in the iPSC-MN differentiation section. Lastly, rAAV9s were used primarily to restore the expression of *SMN* in cells from a patient with SMA1 for molecular studies and they will be discussed here and in the last section.

rAAVs, were the viral vectors I used the most during my project, given that I cloned two versions of the h*SMN1* therapeutic gene in the rAAV backbone (**Figures 3.3**, **3.4** and **3.6**), produced the viral vectors (**Figure 3.8**) and I tested their transduction efficiency *in vitro* in continuous cells line prior to iPSC-MN transduction (**Figure 3.9**). The methods for rAAV9 production and quantification as well as the vector transduction efficiency are discussed here.

I have modified the protocol for the production of rAAV9s over time in order to increase the yield and I found that one of the key aspects was the confluence of the HEK293T cells at the time of calcium phosphate transfection (**Figure 3.7**). It seems that the less confluent the cells are, the higher is their metabolism and hence their ability to produce viruses. This parameter also influences rH1LV production, since rLV plasmids were transfected following the same calcium phosphate protocol. Alternative methods have been developed in order to standardise the efficiency of cell transfection. A polyethylenimine (PEI)-based transfection method recently showed to have similar transfection efficiency than the calcium phosphate method in mammalian cells. Protocols based on PEI transfection have now been optimized for rAAV production with the main advantage of being technically less cumbersome and more robust than the calcium phosphate method. (Lock *et al.* 2010).

A second parameter affecting viral vector yield was the recovery of the particles in the supernatant by PEG precipitation, which was found to contain >50% of the viral particles produced, as shown by the one log unit increase in the viral titre (**Figure 3.8**). Indeed it has been shown that rAAV9s unlike rAAV2s are efficiently released from the cells and thus can be harvested from the culture medium (Vandenberghe *et al.* 2010). Moreover, if particles are harvested 5 days post transfection instead of 3, most of the particles are contained in the supernatant alone (Lock *et al.* 2010).

The most suitable method to determine the titre of rAAVs is a matter of discussion. In general there are 3 possible ways: (i) detection of fully assembled and empty particles with an enzyme-linked immunosorbent assay (ELISA) using the A20 antibody (this is usually used only for rAAV2) (Grimm *et al.* 1999), (ii) detection of the genome copy number of viral particles, through DNA extraction followed by qPCR or dot blotting (Veldwijk *et al.* 2002) and (iii) detection of infectious particles by functional assays with an rAAV encoding a reporter gene (Zolotukhin *et al.* 1999).

The three approaches measure different parameters: the ELISA measures how many assembled capsids are present but not how many of them contain an rAAV genome, and it has been reported that ~80% of rAAV particles can be empty (Grimm *et al.* 1999); the qPCR and the dot blotting measure how many genome copies contained within the capsids (resistant to DNAse treatment) are present, but not how many of them are in truly infectious particles; and the functional assay (usually performed by transduction of cells with a

reporter vector encoding *eGFP* and assessed by epifluorescent microscopy/flow cytometry) measures specifically the number of infectious particles.

In the titrations for the rAAVs produced here, I used qPCR and dot blot in order to determine the genome copy number. It was intriguing that even though both techniques measure the same parameter (genome copy number), the dot blot titre was always higher. I anticipated that given that the dot blot titre consistently gave one log unit more than the qPCR titre, there might be additional difficulties associated with genomic complexities in the determination of the genome copy number in self complementary (sc) vectors. Indeed, it has been recently published that the qPCR titre in scAAVs is systematically underestimated (by 10 fold, as compared to the dot blot titre) because of the presence of a hairpin at one end on the genome (Please refer to **Figure 1.13** in the introduction) (Fagone *et al.* 2012). It seems that the hairpin enhances the re-annealing of the strands at the expense of primer binding. Given that the primers used for qPCR titration recognized the same segment in all my rAAV9s (in the Poly [A] tail next to the to the hairpin), the hairpin inhibition should have been consistent in all amplifications, a hypothesis that is supported by the constant difference with the dot blot titre.

The functional titration assay for rAAV on the other hand is more cumbersome, particularly for AAV9, which is a serotype with very low transduction efficiency *in vitro*, as compared with AAV2 (Gao *et al.* 2004). Given this handicap, the usual functional assay involves the co-transduction of rAAVs with adenoviruses serotype 5 (Zolotukhin *et al.* 1999; Warrington *et al.* 2004). The use of these wild-type viruses requires containment level 2 and is not standard in our laboratory hence it was not employed. It is important to mention that even when the co-transduction with adenoviruses is used, the quantification of functional transducing rAAV particles is influenced by the cell type used, the promoter driving the transgene or the transgene itself and the helper virus used (Grimm *et al.* 1999).
Assessing the viral titre is extremely important in preclinical and clinical studies and for standardising results among laboratories (Grimm *et al.* 1999). Nevertheless, titres are only approximate due to semi-quantitative titration methods, and in some cases (like in the case of iPSCs generation) no accurate MOIs are used. The determination of the titre of RVs is performed in a similar way, but genome copy numbers are determined after viral transduction and retro-transcription in suitable cells (Sastry *et al.* 2002).

In order to test the *in vitro* transduction efficiency of the rAAV9s (without the use of adenovirus type 5) two cell lines were used: HeLas and HEK293Ts (**Figure 3.9**). As expected, the transduction efficiency (assessed by the number of eGFP positive cells by flow cytometry) was very low, even with a MOI of 10,000 (qPCR titre). HEK293T cells showed a better transduction efficiency than HeLas (7.5% vs 1.9%). It is possible that the endogenous expression of some adenoviral genes in HEK293Ts could enhance AAV transduction given that this cell line was originally derived by transformation of human embryonic kidney cells with sheared adenovirus 5 DNA(Graham *et al.* 1977).

Each viral vector has its own advantages and disadvantages, whereas rAAV9 shows a low transduction *in vitro*, it presents a high one *in vivo*. For RVs such as rMMLVs, the transduction efficiency *in vitro* is high, but it is restricted to particular proliferating cell types. Moreover, in recombinant technologies the RV tropism is given by a process of pseudotyping, which can confer ecotropic (narrow host range, mouse and rats), amphotropic (wide host range of mammalian cell types), or pantropic (no host range restriction) properties. Fibroblasts, such as the ones harvested from the family of study for further iPSC reprogramming are one of the cell types efficiently transduced by rMMLVs and these were indeed selected for this purpose.

7.2 iPSC REPROGRAMMING

iPSCs have been generated from several types of cells, using different combinations of RTFs and different methods for nucleic acid/protein delivery. Each protocol has been adjusted in order to reprogram cells with the highest efficiency (increasing the percentage of reprogrammed cells), easily distinguishing true reprogrammed clones from intermediate states, using the least number of RTFs and avoiding the use of integrative vectors such as classical rRVs and integration proficient rLVs. For the reprogramming of fibroblasts in this study, the complete Yamanaka's RTF cocktail was used (Takahashi *et al.* 2007), with transgene delivery by four independent ecotropic rMMLVs (Park *et al.* 2008), through a "gesicle" mediated transduction strategy (Mangeot *et al.* 2011) and transduced cells were cultured following Meltons' VPA protocol (Huangfu *et al.* 2008b). The advantages and disadvantages of the elements involved in reprogramming method will be discussed in this section.

The reprogramming efficiency of the cells from the five family members was very heterogeneous even though all fibroblasts propagated very well before transduction and they all had healthy morphology and good viability as judged by trypan blue exclusion and general observations under microscope (**Figure 4.2**). No correlation was found between the doubling time and the reprogramming efficiency, even though this is known to be an important parameter for effective retroviral transduction (Miller *et al.* 1990). Because the transduced fibroblasts in this study showed very rapid growth, a layer of detached floating cells formed on the surface making the identification of iPSC colonies particularly difficult. Other fibroblasts that were reprogrammed at the same time with the same protocol (from patients with other diseases) did not show this behaviour and it is probable that other factors intrinsic to the cells (maybe even the SMA pathology) could have played a role in this regard. Indeed, it has been shown that the disease mechanism of some pathologies can significantly hinder iPSC reprogramming (Raya *et al.* 2009; Muller *et al.* 2012), and previous studies involving reprogramming of SMA cells have shown very low efficiency *(Ebert et al. 2009)*. Even though the parameters for measuring reprogramming efficiency are not well defined (Gonzalez *et al.* 2011), the general idea is to assess the percentage of plated somatic cells that were transfected/transduced/treated with RTFs and actually became iPSCs or iPSC-like colonies (i.e. 100,000 cells plated and 100 iPSC colonies obtained= 0.1%). Given the fact that most of the iPSC-like colonies picked did not actually survive and propagate, the estimations given are very likely to be inaccurate as a measure for true iPSC reprogramming. The cells that produced more iPSC-like colonies (~80) were from AC, followed by NC, and five clones were propagated from each of them (the term "clone" is applied here to iPSC colonies that managed to propagate for at least 5 passages). Their reprogramming efficiency as measured by their ESC-like morphology was ~ 0.1%. Sixteen iPSC-like clones were picked from TC cells, but only two of them propagated. For RC, seven clones were picked and only one propagated. The reprogramming efficiency of the two latter clones was less that 0.01% (Please refer to **Appendix 4** for a final list of the clones). Although heterogeneous, the range of reprogramming efficiency corresponds to those reported by other groups using rRV-base delivery for iPSC reprogramming, with clones TC and RC located in the lower limit of that range *(Gonzalez et al. 2011)*. CC on the other hand did not produce any iPSC colonies.

Several factors can influence the reprogramming efficiency independently of the intrinsic characteristics of the donor's cells, including: (i) RTFs used for reprogramming (ii) method and stoichiometry of RTF delivery, (iii) use of small molecules and (iv) type of somatic cell to be reprogrammed.

Some of the first questions to be addressed prior to reprogramming are: what RTFs to use, Yamanaka's cocktail or Thomson's cocktail? the standard sets of four RTFs, more factors or fewer factors? *(Takahashi et al. 2007; Yu et al. 2007)*. Most iPSCs-related publications have used (at least for the positive control derivation) Yamanaka's cocktail instead of Thomson cocktail. Indeed, in I-STEM (the institute where I reprogrammed the fibroblasts), Yamanaka's cocktail was chosen particularly because at that time in their hands, Thomson's cocktail (delivered through rLVs) was not producing iPSCs.

Within the last four years, several factors have been excluded from the reprogramming cocktail and *OCT4* has been found to be the only indispensable RTF required for reprogramming (Kim *et al.* 2009b; Kim *et al.* 2009c), excluding the iPSC derivation through microRNAs (Miyoshi *et al.* 2011). Indeed, using a similar protocol to the one followed for the generation of the iPSCs in my study, it was shown that the reprogramming of human fibroblasts was also achieved using only *SOX2*, *OCT4* and VPA, but the reprogramming efficiency dropped by 1000 fold (Huangfu *et al.* 2008b). Since retroviral *c-MYC* reactivation has been associated with tumour formation in iPSC-derived chimeric mice (Okita *et al.* 2007), there has been an increasing pressure to dismiss this RTF from the reprogramming cocktail in cell therapy studies. Given that my project was designed as a disease modelling study and not for a therapeutic approach, we agreed to use all the factors in Yamanaka's cocktail, including the oncogenes *c-MYC* and *KFL4* in order to increase the probability of getting clones from the cells of all family members.

As it is described in the introduction, several integrating, non-integrating and excisable methods have been developed for the delivery of RTFs, nonetheless the classical methods, which provide the highest reprogramming efficiencies, rely in the use of MMLV-based rRVs and rLVs (Takahashi & Yamanaka 2006; Blelloch *et al.* 2007; Wernig *et al.* 2007; Yu *et al.* 2007; Aasen *et al.* 2008; Park *et al.* 2008; Kim *et al.* 2009b). rMMLVs, unlike rLVs are known to be down-regulated during reprogramming (a hallmark of complete reprogramming), while rLVs are poorly attenuated in the pluripotent state (Okita *et al.* 2007; Yu *et al.* 2007; Hotta *et al.* 2009). On the other hand, LVs transduce dividing and

non-dividing cells while MMLVs can only infect dividing cells, limiting the types of cells that can be reprogrammed (Naldini *et al.* 1996; Kafri *et al.* 1997; Miyoshi *et al.* 1997; Wanisch & Yanez-Munoz 2009). In the protocol followed in this study I used four of the six MMLV-based plasmids that were produced by Daley's group (Park *et al.* 2008), but viral vectors were generated in Plat-E, in order to produce ecotropic viruses that could be used in a French level II containment laboratory. In order to allow the entry of the ecotropic viral vectors into the human cells, the latter were incubated with "gesicles" carrying the mCAT-1 receptor prior to transduction. Even though this protocol differs from the archetypical amphotropic rMMLV reprogramming, the transduction efficiencies of both methods have been shown to be similar (~85%) (Mangeot *et al.* 2011). The batch of gesicles used for the reprogramming of my cells was also tested in I-STEM by the transduction of wild type fibroblasts with an ecotropic rMMLV carrying a reporter protein, and it was found to have similar efficiency.

Apart from the delivery method of the RTFs, their relative levels also seem to have an impact of the reprogramming efficiency, and it has been suggested that the optimal stoichiometry consists of equal amounts (protein levels) of all the factors except for a 3-fold excess of *OCT4* (Papapetrou *et al.* 2009). Retroviral titres were not determined prior to the reprogramming transduction of fibroblasts in this project, and instead a pragmatic approach was employed. Based on a previous titration of ecotropic rRV production in Plat-E (performed by I-STEM's group), the MOI was expected to be ~250. Additionally, since the rMMLVs used were not naturally able to infect human cells, any MOI estimates should be taken with caution. In our favour, since RVs integrate efficiently in the genome, only one round of transduction was necessary.

The culture of the transduced cells until iPSC emergence was performed following and I-STEM-adapted version of the protocol published by Melton's group (Harvard University, USA) (Huangfu *et al.* 2008b). The two main features shared by Melton's and I-STEM protocols are: (i) seeding of the transduced fibroblasts on gelatine-coated plates until iPSC colony formation, instead of seeding immediately on feeder cells, and (ii) use of 0.5 mM VPA during the first two weeks post-transduction. On the one hand, seeding the infected cells on gelatine coated plates provided a source for the attachment of the cells that allowed at the same time an easier identification of the iPSC colonies in formation. This procedure circumvented the common difficulty associated with the distinction under the

microscope/stereoscope of the feeder cells from the infected cells growing on top of them. On the other hand, it has been shown that VPA increases the efficiency of reprogramming in human fibroblasts (up to 1%), up-regulating pluripotency genes and down-regulating linage specific genes, although the exact mechanism is not known. It seems however, that VPA enables an easier epigenetic remodelling through its histone desacetylase inhibitor function (Huangfu *et al.* 2008a; Huangfu *et al.* 2008b). This high reprogramming efficiency was unfortunately not observed in any of my cells, suggesting that either VPA did not enhance their reprogramming efficiencies or that they would have been lower in the absence of VPA.

In this respect, some cell populations are more likely to be reprogrammed than others. The experiments from Scholer's group (Max Planck Institute, Germany) show that the epigenetic pattern of the donor cells has a big influence in the efficiency and kinetics of the reprogramming process due to the pluripotency-associated genes already expressed in them. Indeed, neural stem cells endogenously express *SOX2, KFL4 and c-MYC*, as well as *AP* and *SSEA-1*, and their reprogramming can be achieved by ectopic *OCT4* expression alone in both mice and humans (Kim *et al.* 2009b; Kim *et al.* 2009c). On the other hand, Hochedlinger's group (Harvard University, USA) has shown that using the whole set of Yamanaka's cocktail in mouse cells, hematopoietic stem and progenitor cells give rise to iPSCs up to 300 times more efficiently than terminally differentiated B and T cells do (Eminli *et al.* 2009). Another theory about cells that are more easily reprogrammed, comes from the observation that keratinocytes undergo faster reprogramming than fibroblasts, and this suggests that the culture of some cell types might contain more progenitors than others (Aasen *et al.* 2008). In this study, we chose to reprogram fibroblasts mainly because they can be easily obtained from the patients, cultured and transported, and because they are a well-established system for reprogramming. It is important to mention that the techniques used to obtain the tissue biopsy and to culture the cells until the time of reprogramming could have an important influence on reprogramming efficiency. In this regard, comparisons cannot be made between the cells of the individuals of my study and the cells from other patients also reprogrammed in I-STEM, since they were harvested and maintained in different conditions. The fibroblasts from the Spanish family were harvested in Spain from punch biopsies from the forearm, which were cultured over plasma-gelatine coated dishes in medium containing FBS, glutamine, insulin, FGF_2 and EGF. The medium

was changed every three days and cells were tryptinised twice before shipping them to France (Please refer to **Section 2.3.6.1**). One potential important difference between fibroblasts from CC and those from AC, TC, RC and NC is that the former were from an old frozen biopsy (the patient died before this study commenced), whereas the latters were from fresh biopsies, purpose-obtained for reprogramming. It is possible that no clones were obtained from CC because the cells had a metabolic disadvantage (consequence of their prolonged or inadequate storage), even though they were at the same passage as the others

The exact mechanism of reprogramming is unknown and the field of iPSCs although very promising is also very young. As a result it is not yet understood why reprogramming protocols work for some cells and do not work for others. Moreover, in cells from patients with diseases, as in my case with SMA cells, there might be different intracellular pathways altering the reprogramming process. The quality control of the reprogrammed cells is therefore critical, because the chances of an incomplete reprogramming could potentially be increased.

7.3 iPSCs QUALITY CONTROL

There is no strict or precise consensus on the specific characteristics that an iPSC clone has to show in order to be considered truly and stably pluripotent (especially in the case of human cells), and most criteria are based on the presence of certain ESC markers, as described in the Introduction. In general terms, true human iPSCs are characterized by silencing/down-regulation of viral transgenes (in the cases where integrating strategies are used), activation of pluripotency genes, activation of telomerase, reactivation of the inactive X chromosome in female cells, a normal, stable karyotype, and capacity for *in vitro*/*in vivo* differentiation into cells/tissues of the three embryonic layers (Hochedlinger & Plath 2009). Nonetheless, some of these features have not been assessed in clones that have been used in many publications during the last six years. Some other characteristics such as chromosomal, epigenetic and genomic stability are starting to become fundamental in the assessment process (Laurent *et al.* 2010; Mayshar *et al.* 2010; Gore *et al.* 2011; Hussein *et al.* 2011; Lister *et al.* 2011; Pasi *et al.* 2011), but again, not many studies address these issues. Furthermore, even though germline transmission followed by chimaeric mice generation is the gold standard for pluripotency demonstrating the ability to make all cell types (including germ cells), these assays cannot be performed in humans. The most

stringent assay in human cells is generation of teratomas after injection in immunodeficient mice (Cox & Rizzino 2010; Muller *et al.* 2010).

The markers selected to assess whether the reprogramming process has been completed are crucial to iPSC clone selection. In this protocol, iPSCs were obtained 4-5 weeks after transduction and morphological criteria (clusters of round shape, large nucleoli and scant cytoplasm cells) were initially used to pick the clones most likely to be fully reprogrammed (**Figure 4.6**). Given that the expansion and characterization of multiple clones is very demanding, we were aiming to pick five clones from each of the five patients, for a total of 25 clones; unfortunately, this was only achievable for NC and AC cells. After expansion until passage 5 (with exception of the unique clone from RC, which was particularly difficult to expand), all clones were frozen and quality control was performed initially in one selected clone from each family member. Again, the selection of the four clones was made based on the morphology of the colonies and their ability to expand within the first passages, which in general correlates very well with the expression of pluripotency markers. After the initial quality control however, (which included assessment of pluripotent markers, down-regulation of transgenes, *in vitro* differentiation potential, karyotype and STR analyses), two clones (TC64 and NC21) failed to fulfil the full criteria and new clones (TC63, NC42 and NC32) were expanded and characterized.

For the assessment of the expression of pluripotent markers, we used qualitative and a quantitative methods. The seven selected clones expressed *AP*, *OCT4, NANOG, SOX2,* and *TRA-1-60* as well as *SSEA3* and *TRA1-81* (**Figure 4.7 and 4.8**). Quantitative assessment of the co-expression of the two later markers suggests that there is only a small proportion of cells going through spontaneous differentiation in the cultures (<15%) (**Figure 4.8**). Clones AC28 and TC64 nonetheless, showed a higher tendency to differentiation, which correlated with their behaviour in culture. I tested two different culture media in order to reduce the proportion of differentiation, as it is known that this has a direct effect in the maintenance of pluripotency (Akopian *et al.* 2010; Roobrouck *et al.* 2011). The second medium (a defined xeno-free medium from Stemgent, Stemedia™ NutrI-STEM™ XF/FF Culture Medium) dramatically reduced the differentiation of the cells in culture as compared to the first medium from Gibco, and the addition of a Rho-associated kinase inhibitor further increased the survival of cells (Xu *et al.* 2010). The use of natural or synthetic matrixes could potentially improve even more the pluripotency state of the cells (Miyazaki *et al.* 2012), although this was not tested in this project. Passaging methods also vary and could

influence the level of pluripotency (Stover & Schwartz 2011) (complete or partial enzymatic dissociation, manual cutting, cutting with special devices), but in my hands they did not show any particular difference.

Transgene down-regulation was also assessed in our selected clones. Exogenous RTF expression is spontaneously down-regulated (in integrating reprogramming strategies) at the time when genuine iPSCs become apparent (Okita *et al.* 2007; Maherali & Hochedlinger 2008; Chan *et al.* 2009; Papapetrou *et al.* 2009; Lister *et al.* 2011; Pasi *et al.* 2011). There seems to be again a lack consensus in this regard, since some studies state that transgenes should be silenced while others state that it is enough to prove that they are down-regulated. The methods to detect this phenomenon are also different, some studies perform RT-PCR on sequences specific to the transgene and base their results in the presence or absence of a band (Okita *et al.* 2007; Park *et al.* 2008) and some studies perform a quantitative approach by qRT-PCR. Within the qRT-PCR studies, some compare endogenous and total (endogenous + exogenous) expression (Yu *et al.* 2007; Chan *et al.* 2009), while others directly quantify transgenic expression *(Takahashi et al. 2007)*. Finally the scale bars used to compare the expression values are also variable (linear or logarithmic), creating further differences for global comparison across laboratories.

To test the expression profile in my clones I used a comprehensive variety of methods. First I compared by qRT-PCR the endogenous and total expression of each gene against the expression pattern in IMR90 fibroblast undergoing reprogramming and harvested 4 days post-transduction (IMR90 D4) (**Figure 4.9)**. Down-regulation is effectively seen in all clones and for all transgenes, even though there seems to be some residual transgene expression of one or more RTFs in some clones. The RT-PCR amplification approach confirmed these residual expressions (**Figure 4.10**). Some studies suggest that the absence of proviral silencing makes iPSCs more prone to genomic instability, especially in the case of *c-MYC* (Ramos-Mejia *et al.* 2010; Pasi *et al.* 2011). This hypothesis is based on anticipated oncogene-induced DNA replication stress, but formal proof has not been provided; however, retroviral *c-MYC* reactivation can occur and it can induce tumours *in vivo* (Okita *et al.* 2007). Even though the cells reprogrammed in this study are not meant to be used for a therapeutically approach, genomic integrity is also deemed important in order to study the disease mechanism. While *c-MYC* is not silenced in four of the seven clones, it is certainly down-regulated and its total levels in all clones are even lower than in hESCs.

It has also been suggested that removal of the reprogramming vector significantly increase iPSCs capacity to undergo directed differentiation *in vitro* (Sommer *et al.* 2010), but other studies systematically show that there is no difference in the differentiation capacity of iPSCs generated with integrating or non-integrating vectors (Hu *et al.* 2010; Boulting *et al.* 2011). The total expression levels of some RTFs have also been shown to be important in this regard, since increments in the expression of some pluripotency RTFs such as *SOX2* and *OCT4* promote the spontaneous differentiation of hESCs in culture (Niwa *et al.* 2000; Kopp *et al.* 2008). Even though the range of RTF expression in pluripotent cells is not known, the total levels of *SOX2* and *OCT4* in all my clones seemed to be fairly similar to those found in hESCs.

Even in the presence of some degree of transgenic RTF expression, all clones were able to differentiate *in vitro* into representative cells of the three embryonic layers, as shown by the embryoid body assay (**Figure 4.11**). It is important to emphasize in this regard that clone NC21 was particularly resistant to differentiation; a behaviour that was further confirmed when the cells were subjected specifically to MN differentiation. It is possible that this particular clone has genetic/epigenetic anomalies that prevent it to differentiate. For this reason it was considered that clone NC21 failed the quality control criteria. *In vivo* differentiation potential through teratoma formation is currently being carried out by Applied Stem Cell, and was not performed within the time frame of the current thesis for financial limitations. In the teratoma assay, iPSCs/ESCs (approximately 1 million) are injected into immunocompromised mice, in our case under kidney capsule and testis, until a tumour is formed. The tumour is then harvested, fixed, sectioned and stained with haematoxylin and eosin in order to identify tissues representative of the three embryonic layers (Tran *et al.* 2012). The teratoma assay is currently considered the gold standard of pluripotency for human pluripotent cells since it demonstrates that mature histologically distinct tissue types from all embryonic layers can be differentiated *in vivo* from these cells. Nonetheless the teratoma assay does not show if germline transmission is possible (Muller *et al.* 2010). Moreover, it has been shown that even though many clones fulfil most of the criteria regarding pluripotency phenotype, an important proportion of them are not able to form all the embryonic layers during the teratoma assay, and that similarly, clones that do form tissues from all embryonic layers *in vivo*, do not display a complete pluripotent phenotype (Boulting *et al.* 2011; Vitale *et al.* 2012). A lack of standardization in the methodology used to generate and analyse teratomas has been previously highlighted,

questioning the real value of this assay as a standard of pluripotency (Muller *et al.* 2010). It is worth to mention as well that less than half of the novel hESC and hiPSCs reported in the scientific literature do not shown proof of teratoma formation (Muller *et al.* 2010). An alternative to the teratomas assay based on the comparison of global gene expression data (determined by microarray analysis) against a data-base of validated pluripotent lines has been recently proposed (Goldmann *et al.* 2012).

Genomic, epigenetic and karyotype stability are characteristics whose importance has been progressively acknowledged in the quality control of iPSCs. It is known that the reprogramming process places a heavy burden on cellular integrity, and there seem to be major genomic and epigenetic abnormalities during the reprogramming process (Mayshar *et al.* 2010; Gore *et al.* 2011; Hussein *et al.* 2011; Lister *et al.* 2011). All my clones showed a normal karyotype except for TC64, which presented a partial gain of chromosome X on chromosome 1 (1qter), probably present in the reprogrammed fibroblast or acquired early during the reprogramming process (**Figure 4.12**). As the consequences of this chromosomal abnormality are not known, I cannot foresee their potential effect on my study, which could very well be of relevance to pathways involved in SMA pathology. Therefore, I decided to discontinue the propagation of this clone and seek an alternative clone from this patient. It should be noted that this was a conservative approach, because iPSCs have been reported to contain hundreds and maybe thousands of genomic and epigenetic abnormalities such as protein-coding point mutations (Gore *et al.* 2011), copy number variations (Hussein *et al.* 2011) and somatic memory and aberrant reprogramming of DNA methylation (Lister *et al.* 2011).

Lastly, the identity of all selected clones was confirmed by comparing STR profiles with parental fibroblasts and individual lymphocytes, with positive identification in all cases (**Table 4.2**).

All in all, five clones passed the full set of quality control criteria (excluding the results from the on-going teratoma assay): AC28, RC36, TC63, NC32 and NC42 and the first four were used for further study, mainly through their differentiation into MNs (**Table 4.3**). Both clone NC32 and NC42, showed similar pluripotency properties and the selection of the former for further experiments was arbitrary.

7.4 iPSC DIFFERENTIATION INTO MNs

The first reported comprehensive protocol to differentiate MN from stem cells (in this case mouse ESC) was published by Jesell's group (Columbia University, USA) (Wichterle *et al.* 2002). This group implemented steps that are known to promote MN differentiation (as observed *in vivo*) into *in vitro* conditions, obtaining functional MNs that could repopulate the spinal cord *in vivo*, extend axons into the periphery and form synapses with muscles.

After this pioneering study, several protocols for the generation of MNs from human stem cells have been reported. The first protocol employing human iPSCs (hiPSCs) was reported in 2008 (Dimos *et al.* 2008). Even though only very few publications have so far used hiPSCs for differentiation into MN (as compared to hESCs), it has been shown that these cells are also able to generate electrically active MNs *(Karumbayaram et al. 2009)*. Differentiation protocols mostly vary in (i) the density and culture type of the stem cells at the starting point (feeder dependant or feeder free, media containing serum or defined media), (ii) the use of exogenous signalling molecules such as FGF_2 and/or BMP antagonists, (iii) the way to achieve neuroephitelial identity (with or without EB formation), (iv) the concentration of RA and SHH or purmorphamine (used for caudalization and ventralization respectively) and (v) the specific components of the neural media *(Nizzardo et al. 2010)*. The protocol used in my study was designed by Zhang's group (University of Wisconsin, USA) for the differentiation of hESC to MNs and it was selected for the differentiation of the iPSCs in this study because it offered several advantages over other protocols (Hu & Zhang 2009). First, the seeding of EBs prior to rosette formation facilitated the identification of neuroephitelial cells and enhanced purity of the manually selected rosettes (**Figure 5.2**). In this configuration, cells were also more homogeneously exposed to the key signalling molecules. The second important aspect in this protocol was the timing of RA exposure, which has been found to dramatically affect the caudal patterning of cells, and which was done here at an earlier time point compared to other protocols. Indeed, it has been shown that primitive neuroephitelial cells are more responsive than definitive neuroepithelial cells to RA (Pankratz *et al.* 2007). This protocol also replaces SHH with purmorphamine, a small molecule that activates the SHH signalling (Wu *et al.* 2004; Sinha & Chen 2006), shows the same efficiency for MN differentiation and is also less expensive and more chemically stable in culture *(Li et al. 2008)*. The most important advantage of this protocol is the high yield of MNs obtained (50% MN for hESC). However, the same protocol has been reported to yield much lower numbers (which

vary between 7% and 30%) with iPSCs (Karumbayaram *et al.* 2009; Hu *et al.* 2010; Chang *et al.* 2011). Although the proportion of MNs could not be quantified in my study, given the three dimensional disposition of the cells (which will be discussed in the next section), an estimation of the number of ISL-1+ cells suggests that the MN yield in my cultures was also within the latter range (10-15%) (**Figure 5.6)**. It is important to highlight that almost all the cells in our culture were positive for the MN precursor markers OLIG2 and p75-NGFR (**Figure 5.3**). The latter is in agreement with the results from Zhang's group and it suggests that most of our cells were committed to a spinal ventral fate (Du *et al.* 2006; Hu & Zhang 2009). High *OLIG2* expression has already been reported to be a recurrent characteristic in iPSC-derived MNs, along with low expression of *HB9*, which is a marker for post-mitotic MNs *(Hu et al. 2010).* This behaviour is in contrast to the one found in MNs derived from hESCs. Sustained *OLIG2* expression, which is dependant on SHH signalling, prevents the exit from the cell cycle (Du *et al.* 2009). Reducing the levels of SHH nonetheless does not accelerate the cell cycle exit in iPSC-derived MN cultures (Hu *et al.* 2010).

Yields of MNs not only vary when comparing the differentiation from hESC and hiPSCs, but also between laboratories. This might at least partly be explained by differences in the markers used to determine the identity of MNs, as well as variations in the timing of the expression assessment. HB9 is considered to be the most specific post mitotic MN marker, but it is not expressed at the same levels all the time (Arber *et al.* 1999; Hester *et al.* 2011). ISL-1 is an earlier MN marker, but it is also expressed in some interneurons and in some cells from the dorsal root ganglia (Ericson *et al.* 1992; Arber *et al.* 1999; Wichterle *et al.* 2002). In spite of these considerations, both markers are indistinguishably used for assessing MN yield. Some studies relevant to my project (Ebert *et al.* 2009; Sareen *et al.* 2012) also use SMI-32 immunoreactivity for MN identification. SMI-32 antibodies recognise a non-phosphorylated epitope of neurofilaments, which is expressed in mature MNs (Carriedo *et al.* 1996), but also in several other neurons in the CNS (Ouda *et al.* 2012). The timing is also a critical factor for assessing MN yield, since some MN progenitors continue to proliferate in the culture at the same time as others commit to the MN fate. Indeed, previous studies from Zhang's group, whose protocol was followed in this study, have shown that *OLIG2* expression peaks at the 4th week of differentiation and then goes down, whereas *HB9* expression starts appearing at the 4th week, peaks at the 5th week and then decreases (Li *et al.* 2008). In order to follow the generation of post-mitotic

MNs over time, cells were transduced with an LV construct (HB9:RFP H1LVs) expressing RFP under the control of an HB9 enhancer/promoter (**Figure 5.11**). This particular construct, along with its GFP version, has previously been shown to be highly specific for MN identification in iPSC-derived MN cultures and also in spinal cord MNs *in vivo* (Lee *et al.* 2004; Marchetto *et al.* 2008; Hester *et al.* 2011). The enhancer/promoter used in this construct is in fact a shorter version of the 9 kb regulatory sequence located in the 5' upstream region of the *HB9* gene, which has been found to be sufficient to promote the expression of target reporters in MNs (Arber *et al.* 1999; Lee *et al.* 2004). The observations made from the temporal transduction pattern of TC63 iPSC-derived MNs with HB9:RFP H1LVs, agrees with Zhang's group observations regarding the variation in the proportion of cells expressing *HB9*, since the proportion of RFP+ cells dramatically increased in the cultures during and after the 5th week (days 35-41 of the MN differentiation protocol) in comparison with the 4th week (days 28-34 of the MN differentiation protocol).

Even though much effort has been put into the generation of functional MNs from human stem cells over the years, two main outstanding issues remain: overall low efficiency of MN differentiation and presence of mixed populations. Regarding the first issue, a recent study has shown that forced expression of three key MN transcription factors (*NGN2, ISL-1, and LIM/homeobox protein 3 [LHX3]*) into NE cells significantly increased the rate of MN differentiation and the overall yield of these cells *(Hester et al. 2011)*. Indeed, electrophysiologically mature MNs were observed 27 days earlier than with conventional protocols and MN yield accounted for 50-70% of the cultured cells. The main disadvantage of this approach, however, is that cells are subjected to additional genetic manipulations, which could possibly interfere with the expression of the disease phenotypes or affect drug targets. Furthermore, these cells would not be applicable to any cell therapeutic approaches for which efforts currently on-going to develop methods for iPSCs production without genome integration or genetic manipulation would be more relevant (Kim *et al.* 2009a; Warren *et al.* 2010; Okita *et al.* 2011). Regarding the second issue (mixed populations), there are several approaches that have been reported specifically for the purification of hESC-derived MNs: immunopanning for the transiently expressed p75-NGFR (Silani *et al.* 1998; Silani *et al.* 2001), fluorescence-activated cell sorting (FACS) after the introduction of an *HB9*-driven *GFP* cassette in the NE cells prior to MN differentiation (Singh Roy *et al.* 2005), and discontinuous Biocoll gradient centrifugation (Wada *et al.* 2009). There are, however, some disadvantages associated with any of these methods. First, p75-NGFR

immunopanning is not based on a surface marker which is specific for human MNs. Although p75-NGFR has proven to be useful for isolating MNs *ex vivo* from spinal cord of various organisms such as rat, mouse and human (Silani *et al.* 1998), (Camu & Henderson 1992; Wiese *et al.* 2010), this maker is also expressed in a wide range of cells within the CNS during development, all of which are likely to be present in the rather heterogeneous cultures derived from differentiating stem cells (Nizzardo *et al.* 2010; Ibanez & Simi 2012). Indeed, I attempted p75-NGFR immunopanning in my cultures by adapting the protocols used for mice (Wiese *et al.* 2010) and for differentiating MNs from mESCs (Bibel *et al.* 2007), which I learnt during a visit to Prof Michael Sendtner's group at the University of Wuerzburg, Germany. Unfortunately, the cells from my iPSC-derived neurospheres did not survive after complete dissociation. A positive outcome of this attempt was that the proportion of cells attached to the immunopanning plate could be estimated, suggesting that almost all cells in my iPSC-derived MN cultures produced p75-NGFR (data not shown), which was confirmed by the results obtained through immunofluorescent staining (**Figure 5.3A**). The broad expression of p75-NGFR in the cultures makes this purification technique redundant in the iPSC differentiation context.

On the other hand, the purification method involving the FACS of HB9-driven *GFP*-expressing cells has been shown to yield significantly fewer MNs (~1% of the cells in culture) and the survival of the cells was severely affected (reduced to only a few days or 2 weeks if co-cultured on skeletal muscle cells). Furthermore, this method also introduced an additional genetic manipulation with the previously mentioned disadvantages (Singh Roy *et al.* 2005). The most cost and time-effective technique reported so far seems to be the Biocoll gradient centrifugation, which also preserves the naïve condition of the cells (Wada *et al.* 2009). This protocol may still require some improvement in order to increase the MN purity above 80%. Also, the viability of the purified cells over long-term in cultures needs to be assessed since this method requires full dissociation jeopardizing cell viability, as previously mentioned

7.5 MODELLING SMA THROUGH iPSC-DERIVED MNS

One of the main advantages of being able to differentiate iPSC into MN-like cells, irrespectively of the limitations previously discussed, is the provision of a human cell type which could not be obtained directly from patients. For SMA particularly, where the genetic cause is known, but the pathological mechanism is still unclear and no clinical

therapy has yet been developed, human iPSC-derived MNs offer an invaluable resource for disease modelling and drug screening. The aim of this study was focused on this premise: the recreation of the MN developmental process under the genetic background of SMA affected and unaffected individuals, a genetic background that predisposed them or protected them respectively from the pathology.

In my study, iPSC clones from two SMA type III siblings (NC, TC), their SMA type IV/asymptomatic haploidentical sister (AC) and their unaffected mother (RC, carrier of the *SMN1* mutation) were differentiated and studied, along with an unrelated unaffected clone (4603) and an unrelated clone from a type I SMA patient (SMA1). Given that the affected siblings of the Spanish family present a mild form of SMA and the onset of the pathology is thought to develop late in these patients (Martinez-Hernandez *et al.* 2012), more subtle (if any) abnormalities were expected to be found in their MNs as compared to SMA1.

So far, three groups have reported the generation of iPSCs from SMA patients, in all cases from SMA type I fibroblasts. Two of these groups have attempted to model the disease in differentiated MNs (Ebert *et al.* 2009; Chang *et al.* 2011; Sareen *et al.* 2012), while the third one has only produced iPSCs (Luo *et al.* 2012). Five parameters have been assessed in these studies to characterise and distinguish the phenotype of unaffected and diseased iPSC-derived MNs: proportion/number of MNs after differentiation (Ebert *et al.* 2009; Chang *et al.* 2011; Sareen *et al.* 2012), neurite outgrowth (Chang *et al.* 2011), number of MN neurites (Sareen *et al.* 2012), total MN cell body area (Ebert *et al.* 2009; Sareen *et al.* 2012), and MN pre-synaptic defects *(Ebert et al. 2009)*. The latter phenotype will be discussed in the next section about functional SMA studies in NMJ models (**section 7.6**).

In my study, counting the absolute number of MNs after differentiation was not possible, as it turned out to be problematic to identify and count single cells within the three-dimensional cluster of differentiating MNs (**Figures 5.6 and 5.12**). Svendsen's group (University of Wisconsin-Madison, USA) was the first one to find SMA-related differences in the proportion of iPSC-derived MNs (Ebert *et al.* 2009). This group's main finding at the time was that MNs generated from an SMA type I iPSC clone showed selective decline (proportionally) in long-term cultures when compared to the MNs derived from a iPSC clone of the unaffected carrier mother (4% *vs* 24% remaining respectively after 2 weeks of the beginning of ChAT expression), even though the MN yield was similar at early time points (~11%). Nevertheless, certain aspects in this study are not clear, in particular the method used for assessing cell number in a three-dimensional cluster. The same is true for

the study carried out by Yee's group (Chang *et al.* 2011). The second more recent publication from Svendsen's group (Sareen *et al.* 2012) reported dissociation of the cells before plating and counting, while not providing a detailed description of the procedure. The attempt at this approach in my study however, impaired the viability of the MNs as observed in the p75-NGFR immunopanning trial (data not shown), and could not be used to produce a quantitative analysis. An estimation of MN numbers, as assessed by ISL-1 positive staining, suggests that about 10-15% of the cells within the cultures are MNs between days 35-43 (weeks 5 and 6) (**Figure 5.6**). No obvious differences were observed between the clones. A similar proportion of MNs was found when the neurospheres were transduced with a LV conferring MN-specific expression of RFP (HB9:RFP H1LVs, **Figure 5.12**). Full cell dissociation prior to plating would be necessary to reliably quantify these numbers for each clone.

The second disease phenotype assessed was the outgrowth of neurites. In order to systematically follow the length or area of neurons, they should be plated as single cells and at low density, but both requisites affect MN survival significantly (Hu & Zhang 2009). Yee's group measured the length of neurites emerging from neurospheres two and five days post-plating and reported retarded neurite outgrowth in SMA type I iPSC-derived cultures as compared to matched, rescued control lines *(Chang et al. 2011)*. Unlike Yee's group (i) I measured the average length of the five longest neurites per neurosphere instead of the average neurite length, (ii) I compared the average growth rate instead of absolute lengths and (iii) I measured one, three, six and eight days post-plating instead of only two and five. The reason for measuring only the five longest neurites is derived from the difficulty in correctly identifying the smaller neurites without staining, although it is acknowledged that with this decision a possible bias is introduced. On the other hand growth rates were preferred over absolute lengths in order to avoid the masking effect given by inter clonal variation (Hu *et al.* 2010; Boulting *et al.* 2011) which will be further addressed within this section. Following my adapted protocol, however, I did not find any difference between the clones analysed, which included an SMA type I (**Figure 5.7**). Even though neurite growth was heterogeneous between clones, growth rates were not statistically different. It is important to mention that the neurites measured by this method may belong to different types of cells and not only MNs. For MN-specific measurements, cells would have to be fixed and stained for MN markers in order to identify them, but this would not allow time course studies on the same sample over several days.

Svendsen's group focused on the number of neurites in SMI-32+ cells over longer time intervals instead of general neurite length growth over short intervals. Their study shows that the number of neurites in MNs derived from two SMA type I iPSC clones decreases over time (ratio at 7-10 weeks over 3-4 weeks), unlike in unaffected iPSC cultures where it increases. Similarly, they reported a reduction in total cell body area over time for the SMA MNs *(Sareen et al. 2012)*. Here, cells were from independent differentiations, as they had been fixed and stained to identify the MNs for the analysis. The lack of a continuous assessment introduces bias regarding the intra-clonal variability in the differentiation efficiency (which is reflected in the large error bars of their results) and thus, this may not necessarily be the ideal method. However, as discussed before, the lack of staining can also create bias in these types of measurements. Live expression of MN-specific fluorescent reporters such as our HB9:RFP H1LVs (**Figure 5.11)** will be a more suitable method.

Three important variables are potentially accounting for much of the differences found between Svendsen's, Yee's and my own study: the timing of the analysis, the inter variability between clones and the technical procedure for MN generation,

The timing of appearance on the SMA phenotypes in culture reveals a significant discrepancy between the results of Yee's group and Svendsen's group. Svendsen's group has shown that iPSCs-derived MNs from unaffected individuals and SMA type I patients present similar phenotypes (such as MN yield, cell body area and number of processes) during the first weeks of culture when the cells are acquiring all the mature MNs markers (weeks 4-6) and that phenotypic differences are observed only in long-term cultures (8-10 weeks) (Ebert *et al.* 2009; Sareen *et al.* 2012). These same results regarding the MN yield have been obtained by Henderson's group (Columbia University, USA) in a similar study (Henderson Unpublished data). Yee's group did not provide data about long-term cultures of MNs, and the phenotypes reported (lower MN yield and retarded neurite growth) correspond only to the 4^{th}-6^{th} week of Svendsen's MN differentiation protocol. Interestingly, the SMA type I iPSCs from Yee's group are reprogrammed from the same patient's fibroblast used in the second study from Svendsen's group. Similarly our cultures were only kept until D47, when ChAT expression was evident, which also corresponds approximately to the 5^{th} week of differentiation in Svendsen's protocol (in Svendsen's protocol, D0 correspond to the rosettes stage, whereas in mine's and Yee's D0 corresponds to the formation of EBs). Therefore, this time-point may be too early to observe differences in my MN cultures even if the number of MNs could be analysed systematically.

A second confounding factor already mentioned before when comparing results is the variability between different clones regarding their propensity to terminal differentiation. Indeed, it has been shown that each clone has an inherent propensity towards neural and terminal differentiation and that this propensity might mask or mislead the true phenotype of a given disease (Hu *et al.* 2010; Boulting *et al.* 2011). This situation represents a particular disadvantage for the first publication of Svendsen's group where only one affected and one unaffected clone were studied (Ebert *et al.* 2009). Nonetheless, the recent second publication from this group (Sareen *et al.* 2012) employed two different clones (from 2 controls and two SMA type I patients). Yee's group on the other hand, produced 5 clones of iPSCs from one SMA type I patient, and used two of them to study the phenotype of the derived MNs *(Chang et al. 2011).* In my study I differentiated one clone from each patient, which allowed me to study unaffected individuals (RC+4603) *versus* SMA patients (AC, TC, NC, SMA1) taking into account more than one clone. The direct comparison between the siblings was nonetheless one clone from each.

Furthermore, variability is added when the system to generate neurospheres does not produce homogeneous clusters of cells, a factor that can dramatically affect the attachment of cells and their growth. This issue can be solved by performing a "temporal and longitudinal study" were normalized values are compared instead of absolute values. This is the case of the measurement of neurite growth in my study, were growth rates were compared instead of absolute neurite length values. In this regard, Svendsen's group reported ratios generated from average measures recorded on last days of data collection (weeks 7-10) and the ones recorded on earlier days (weeks 3-4), taking into account four different experiments (Sareen *et al.* 2012).

The published studies have also attempted to rescue phenotype or restore SMN levels either pharmacologically (Ebert *et al.* 2009; Sareen *et al.* 2012) or using gene therapeutic LVs (Chang *et al.* 2011). Pharmacological approaches included histone deacetylases (VPA), aminoglycosides (tobramycin) and apoptosis inhibitors (a neutralising antibody for Fas-receptor or a caspase-3 inhibitor). While at least partially successful, the applicability of results from these attempts is however limited, as treatments were applied on iPSCs or from early differentiation stages and not to mature MNs. Please refer to section 1.1.4 on the Introduction for more information about current pharmacological treatment for SMA. Among the mentioned treatments it is worth briefly describing the apoptosis inhibition approach where Svendsen's group showed improved MN numbers (SMI-32 positive cells)

at 8 weeks of differentiation by applying continuous apoptosis-inhibiting treatments from early time points of the differentiation process (week 2) (Sareen *et al.* 2012). I attempted to restore SMN levels in SMA1 iPSC-derived MNs using scAAV9s, but the outcome was only evaluated at the molecular level. These results, as well as Yee's gene therapeutic LV approach will be discussed in section 7.7.

The failure to observe an SMA-related phenotype in my study of MNs was probably due to a combination of factors, including the three-dimensional nature of the cultures, the timing chosen for the assessment (short-term cultures) and possibly the sensitivity of the analytical methods employed. Increased sensitivity may be achieved through more sophisticated instrumentation and methods, which may be particularly important when comparing less severe forms of SMA. Nonetheless, although the differentiated SMA MNs in my cultures did not show a distinct phenotype as described in literature, there was an abnormality observed with the SMA1 clone during MN differentiation: Whereas the other five iPSC clones efficiently formed rosettes between D10-D15, the differentiating SMA1 iPSC clone exhibited a conspicuous reduced capacity to form rosettes and showed features consistent with reduced viability, including morphological changes and cell detachment (**Figure 5.2**). Interestingly, this reduced frequency of rosettes has already been pointed out in Yee's study (Supplementary Discussion) of clones SMA-23 and SMA-25 (our SMA1 clone is their SMA-19 clone). Furthermore, restoration of SMN expression in clones SMA-23 and SMA-25 did not improve the rosette-forming efficiency and thus, the behaviour was attributed to a different developmental program between iPSCs and hESCs (which were the control cells used by this group) (Chang *et al.* 2011). My study of five iPSC clones with high rosette formation efficiency, all of them generated following a similar retroviral infection protocol to the one employed by Yee's group (including VPA treatment), argues against this conclusion. Instead, it is tempting to speculate that the reduced rosette formation phenotype is specific of severe SMA (with the caveat that all three clones showing phenotype have been generated from the same fibroblasts). Unfortunately, the MN differentiation protocol of Svendsen's group did not involved the generation of rosettes and hence is not informative in this respect.

7.6 FUNCTIONAL SMA STUDIES IN NMJ MODELS

No functional SMA phenotype has yet been reported in cultured human MNs. One observation of relevance has been made: SMI32+ SMA type I iPSC-derived MNs showed

diffused synapsin staining after 8 weeks of differentiation, as opposed to the punctuated staining in control iPSC-derived MNs, suggesting defective pre-synaptic maturation (Ebert *et al.* 2009). Studies of SMA MNs in a co-culture system, functional or otherwise, have not been reported.

Deficits in the NMJ have consistently been found in several models of SMA (Murray *et al.* 2008; usaKariya *et al.* 2008; Kong *et al.* 2009; Ling *et al.* 2010; Ruiz *et al.* 2010; Lee *et al.* 2011) and in post-mortem human tissue (Martinez-Hernandez *et al.* 2012). From these studies, it is now generally accepted that synaptic dysfunction in the NMJ precedes MN cell death. Zhangs's group (University of Wisconsin-Madison, USA) have already shown that hESC-derived MNs can establish functional neuro-muscular transmission in co-culture systems (Li *et al.* 2005). In order to simulate this system in the SMA context, I plated D39 neurospheres onto differentiated mouse myotubes and cultured them for three days. The results suggest that the plating of neurospheres induced the clustering of AChRs and that neural terminals were observed in close proximity to these clusters (**Figure 5.8**). The clustering of AChRs in C2C12 myotubes has previously been reported to occur in the absence of neurons (aneural cultures) (Kummer *et al.* 2004). Furthermore, it is thought that during human development there are pre-patterned AChRs similar to the ones consistently observed in developing mice, rats, chicks and frogs (see (Sanes & Lichtman 2001) for a review on neural induction of AChR aggregates). In agreement with this, we observed some AChR clusters in myotubes cultured aneurally (within the predominantly disperse distribution), but they were less abundant and less defined when compared to the pattern seen after seeding the neurospheres. Indeed, the disperse AChR expression in myotubes of aneural cultures was reorganized upon co-culture with neurospheres into localized expression within defined clusters observed in close proximity to the neurites (**Figure 5.9**). No difference was observed between clones, but the system is suitable for electrophysiological recordings, which may detect SMA-related differences as part of future studies. Recent results from Tizzano's group (Martinez-Hernandez *et al.* 2012) suggest that defects such as poor clustering of AChRs, axonal swellings and vesicle accumulation in the nerve terminal are already present in human SMA type I foetuses. We were aiming to observe SV2 (a marker for synaptic vesicles) accumulation in nerve terminals of SMA1 iPSC-derived MNs, but it seems that SV2 requires more time in co-culture to be expressed in the differentiating MNs (Ebert *et al.* 2009).

The study of MNs in co-culture systems would be more relevant with human myoblasts instead of mouse cells. The ideal system would include iPSC-derived MNs growing on human myotubes, using all possible combinations of control and affected cells to test whether the lack of SMN in MN and/or muscle affects the NMJ. A recent study using conditional SMA mice with tissue-specific increases in SMN expression seems to suggest that NMJ defects are derived specifically from the lack of SMN in the MN (Martinez *et al.* 2012). Nonetheless, other studies suggest otherwise *(Hayhurst et al. 2012).* Short and long term co-cultures should both be studied, since it has also been suggested that clustering of AChRs in SMA foetuses does occurs early in development (12 weeks), but it is lost afterwards (14 weeks) (Martinez-Hernandez *et al.* 2012).

7.7 ORIGIN OF *FL-SMN* TRANSCRIPTS IN THE CELLS OF STUDY

Parallel to phenotypic studies, several molecular analyses were also performed. As described in the Introduction, the main source of *FL-SMN* mRNA is the *SMN1* gene, but a smaller percentage is also produced from the *SMN2* gene (Lefebvre *et al.* 1995). In SMA patients, no functional SMN protein from the *SMN1* gene is produced, but not all *SMN1* mutations are deletions or completely inhibit the transcriptional activity of the defective genes (Alias *et al.* 2009). Our collaborators in Spain have previously described the lack of *FL-SMN* transcripts from the mutated *SMN1* gene in fibroblasts from the siblings of study (Also-Rallo *et al.* 2011). I further assessed this event in the seven selected iPSC clones of study (SMA1, 4603, RC26, AC28, TC63 and NC32) and their derived cells during the iPSC-MN differentiation process (**Figure 6.1**). As expected, *FL-SMN* in all SMA1 cell cultures originated specifically from *SMN2*, whereas *FL-SMN* expressed from *SMN1* was detected in all 4603 cell cultures (which carry two functional *SMN1* alleles) and in all RC26 cell cultures from the carrier mother (which possess one functional *SMN1* allele). In the cell cultures derived from the siblings of study (AC, TC and NC), essentially all *FL-SMN* was found to originate from their *SMN2* genes. However, in some cases very minor bands of *FL-SMN* mRNA apparently originating from their mutant *SMN1* genes could be detected (**Figure 6.1**). These observations suggest that mutant *SMN1* transcripts have very low stability and are perhaps degraded by the non-sense decay mechanism. The non-sense decay is a surveillance mechanism for mRNAs with premature stop codons, such as the ones generated by the *SMN1* mutation present in the siblings of our study (Silva & Romao

2009). The remaining transcripts however, are not expected to be translated into functional protein.

7.8 SMN AND PLS3 DURING iPSC-MN DIFFERENTIATION

In addition to the temporal appearance of phenotypic defects in SMA, another important question yet to be answered concerns the developmental expression pattern of SMN and related proteins. Addressing this issue, the second main focus of my study was to assess the variation in the levels of SMN and PLS3 mRNA and protein during the iPSC-MN differentiation process in the clones derived from the family of study and my two reference clones (SMA1 and 4603).

7.8.1 SMN

It has been proposed that even though the lack of SMN preferentially affects MNs, it also impacts many other tissues, but with different thresholds of sensitivity (Sleigh *et al.* 2011). According to this view, there is a vulnerability-resistance spectrum and MNs are at the sensitive end. Since the regulation of SMN levels in MNs seems to be more critical than in other tissues, I anticipated that there should be important variations during the MN differentiation process.

Several lines of study have suggested that SMA pathology begins during the prenatal period, at least in the most severe cases (SMA type 1). In less severe cases the results are not clear, but a similar process with more subtle manifestations is thought to take place. Through the study of severe mouse models of SMA, Sendtner's group (University of Wuerzburg, Germany) have found that *in vitro* cultures of embryonic MNs have shorter axons, smaller growth cones with decreased expression of beta actin and defects in spontaneous excitability (Rossoll *et al.* 2003; Jablonka *et al.* 2007). On the other hand, *in vitro* cultures of neurospheres from SMA mouse models showed compromised neuronal differentiation and neuritogenesis (Shafey *et al.* 2008). Defects in axon outgrowth and path finding have been found in *Smn*-depleted zefrafish and Xenopus models (McWhorter *et al.* 2003; Ymlahi-Ouazzani *et al.* 2010). Even though most mouse *in vivo* studies do not suggest a developmental defect, there is certainly controversy regarding the appearance and development of the disease (Sleigh *et al.* 2011). Studies on human foetuses have provided significant evidence for a developmental defect with prenatal onset. Indeed, it has been found that predicted SMA type I foetuses show enhanced neuronal cell death at 12 weeks post-conception (Soler-Botija *et al.* 2002), decreased/delayed expression of antiapoptotic

proteins in MNs at 15 weeks post-conception (Soler-Botija *et al.* 2003) and presynaptic retention of vesicles, loss of AChR clustering and aberrant ultrastructure on nerve terminals of the NMJ at 14 weeks post-conception (Martinez-Hernandez *et al.* 2012).

Very few studies describe human SMN protein levels, but it is known that SMN is high in the prenatal period and levels suffer a marked decay in the postnatal period, particularly in skeletal muscle, heart and brain tissues (Burlet *et al.* 1998). In adult tissues, SMN is present at particularly high levels in brain, kidney and liver (Coovert *et al.* 1997). Since iPSC differentiation attempts to recapitulate *in vivo* development, the iPSC-MN differentiation system provides a unique model to assess the variation in mRNA and protein levels of SMN during human MN development.

I decided to follow transcript levels of the two more abundant isoforms, *FL-SMN* and *Δ7-SMN*. Total *SMN* transcript levels (*tSMN*) were also measured as a reference of transcriptional activity. All protein measurements assessed are thought to correspond to FL-SMN, since a Δ7-SMN isoform has not been reported or detected at the protein level in the absence of induced genetic modifications or overexpression, probably due to its low stability (Lorson & Androphy 2000).

The most significant findings from the SMN analyses were: (i) there is a gradual decay in SMN protein during iPSC-MN differentiation; (ii) there is a mismatch between FL-SMN RNA and protein levels during iPSC-MN differentiation; (iii) unaffected individuals show higher *FL/Δ7-SMN* mRNA ratios than SMA patients; (iv) the severity of SMA phenotypes can be distinguished by comparing *tSMN* mRNA levels. All these findings will be discussed in depth in this section.

In order to try to identify SMA-related cell type-specific differences, clones were grouped into two categories: unaffected individuals (4603+RC26) and SMA patients (SMA1, AC28, TC63, NC32). AC was included in the SMA group given the patient's lack of functional *SMA1* genes (as her SMA type III symptomatic siblings) and the presence of minimal electromyography alterations. Statistically significant differences were only found in the *FL/Δ7-SMN* ratio at the rosette and MN stages and in the *FL-SMN* mRNA at the EB stage (**Figure 6.2)**, probably due to the small sample size of the control group.

From the diversity of results obtained, I formulated a hypothesis describing the molecular basis for the onset of SMA. It is plausible to think that the requirement for SMN is more crucial in some differentiation stages than in others, for example prior to or during the neural specialisation of the cells (EBs/rosette stage) where the main differences in the *FL-*

SMN mRNA and protein between control individuals and SMA patients were observed (**Figure 6.2 A and B**). In agreement with this, Yee's group (Chang *et al.* 2011) and I have observed specific deficits in rosette formation in three iPSC clones derived from the same SMA type I patient. If this is true, low levels of SMN like those seen in our SMA cases (SMA1, TC63, NC32 and AC28), may predispose the cells to a pathological state without necessarily compromising their terminal differentiation potential, as it is the case. A continuous relative decreased expression in SMN during the subsequent phases would however prompt the appearance of the pathology, whose severity will be subjected to narrow variations of SMN. Indeed as it can be seen in the analysis at the MN stage (**Figure 6.6**), the cells from the siblings with SMA type III (TC and NC) have very similar values to the one seen in SMA1 cells (except in the case of *tSMN* mRNA), but very different from the unaffected 4603 cells. The analysis of more clones from patients with SMA type I and II would be needed to confer statistical power to this last statement, but similar narrow SMN protein differences have been previously found in SMA type I and type III spinal cord samples from human foetuses (showing a 23% and 39% reduction of the normal SMN levels, respectively) (Lefebvre *et al.* 1997). Moreover, the difference in the protein levels between the unaffected clone with two functional *SMN1* alleles (4603) and the SMA1 clone (≥2 fold for both, RNA and protein levels) is in agreement with the significant reduction found the in spinal cords from human tissues (Coovert *et al.* 1997; Soler-Botija *et al.* 2005). Given that all clones, irrespectively of their phenotype suffer a statistically significant decline in the SMN protein levels during their MN differentiation, regardless of the maintenance or increase in the *FL-SMN* mRNA expression (**Figure 6.4**), it seems logical to think that there is either (i) a general post-transcriptional mechanism inhibiting the translation of the protein; (ii) a general post-translational mechanism producing a faster turnover of the protein; or (ii) a combination of the previous two mechanisms. Supporting the role of a post-translational regulation, a very recent report has shown that ubiquitin-specific protease 9x deubiquitinates *FL-SMN* (but not *Δ7-SMN*) preventing its degradation by the proteasome (Han *et al.* 2012). Moreover the described mechanism/s might not be specific to MN differentiation, since it is also observed in the hepatocyte differentiation (**Figure 6.3**). In this regard, whereas it is true that iPSCs show lower SMN protein values than immature and mature hepatocytes, this behaviour can be attributed to an iPSC clone-specific low SMN expression, given that specifically RC26 iPSCs also show lower values than its differentiated EBs, rosettes, neurospheres and MNs (**Figure 6.4B**). The lack of

correlation between transcript and protein levels of *FL-SMN* has been reported before in the study of blood samples (Crawford *et al.* 2012). Following the adapted threshold theory (Sleigh *et al.* 2011), if cells are able to cope with the protein decay, they will remain healthy, but if they level fall beyond a certain point or "threshold", the cells will be affected. The way unaffected MNs (4603 mainly) and mature hepatocytes seem to deal with this problem is by up-regulating their *FL-SMN* mRNA expression, which could be compensating for the post-transcriptional/post-translational inhibition (**Figures 6.3 and 6.4**). Since SMA cells do not possess functional *SMN1* alleles, they can only cope by up-regulating the transcription from the *SMN2* alleles, whose main product is Δ*7-SMN* (Lefebvre *et al.* 1995). Indeed, Δ*7-SMN* is maintained at high levels (but not up-regulated) in SMA cells during the whole iPSC-MN differentiation process (**Figure 6.2 D**), as opposed to the control unaffected 4603 clone. The expression profile of the clone from the carrier (RC26) mother is more similar to the one observed in SMA clones than to the one seen in the unaffected control clone. The transcription of other isoforms, particularly of the isoform lacking exon 5 and 7 (which is indistinguishable in our assay from the isoform lacking only exon 7), are probably also occurring (Gennarelli *et al.* 1995). It is important to mention as well that although the putative Δ7-SMN protein is thought to be less functional (with defective self-association and decrease ability to stimulate *in vitro* splicing) and less stable (Lorson *et al.* 1998; Pellizzoni *et al.* 1998; Lorson & Androphy 2000), its overexpression does ameliorates significantly the SMA phenotype in the severe SMA mouse model. It seems that Δ7-SMN is able to oligomerise with the low levels of FL-SMN thus becoming stable and functional (Le *et al.* 2005).

7.8.2 SMN BIOMARKERS

Due to the expression profile present in SMA cells by the lack of functional *SMA1* alleles, the *FL/Δ7-SMN* mRNA ratio is a very convenient biomarker to distinguish between unaffected and affected individuals. Indeed, the *FL/Δ7-SMN* mRNA ratio is significantly higher in cells from 4603 than in cells from all SMA patients (**Figure 6.5A**). This difference is particularly evident in more susceptible cells types such as MNs, where there is an average 3.5 fold difference (**Fig 6.6**). As mentioned earlier, the carrier mother seems to display an SMA-like expression profile. The *FL/Δ7-SMN* mRNA ratio has been suggested before as a biomarker, and indeed the higher difference between SMA and control individuals have been found in spinal cord tissues (Soler-Botija *et al.* 2005). Unfortunately, the ratio does not allow to distinguish between SMA types, probably

because the level of *Δ7-SMN* expression is correlated to the number of *SMN2* copies present in the cell (Crawford *et al.* 2012), and these values are variable between clones: AC28, TC63 and NC32 have 4 copies, RC26 has 3 copies, SMA1 has 2 copies and the copy number in 4603 was not determined. Interestingly the *tSMN* mRNA levels in the SMA1 clone are consistently lower than in the rest of the clones, suggesting that this parameter could be use to distinguish the type of SMA (**Figure 6.5B**). The same correlation has been found in blood samples from SMA patients in the recent bforSMA study *(Crawford et al. 2012).*

7.8.3 GENE THERAPY

It has been suggested that augmenting the MN SMN levels by means of gene therapy could rescue the SMA phenotype, and results derived from studies in SMA mouse models are indeed promising (Azzouz *et al.* 2004; Foust *et al.* 2010; Passini *et al.* 2010; Valori *et al.* 2010; Dominguez *et al.* 2011). In order to study the expression of *SMN* mRNA and protein isoforms after the restoration of *SMN1* in MNs, I transduced SMA1 iPSC-derived MNs with a scAAV9 carrying the therapeutic gene (scAAVCag*hSMN1*F). The transduction efficiency in the neurosphere configuration was predicted to be ~25% after 5 days, according to a transduction test performed with a reporter sAAV9 (scAAVCag*eGFP*). (**Figure 5.10**). As anticipated, *FL-SMN* mRNA levels were increased as compared to non-transduced SMA1 MNs; surprisingly however, *Δ7-SMN* mRNA levels were decreased (**Figure 6.6**). The expression profile adopted after SMN augmentation is similar to the one observed in unaffected control cells (clone 4603) and indeed the *FL/Δ7- SMN* mRNA ratio increases significantly. Although SMN levels could not be assessed at the protein level, they are not necessarily expected to be increased into a great extend giving the putative post-transcriptional/post translational mechanism previously described. Yee's group have demonstrated that if SMN is restored in SMA type I iPSCs prior to MN differentiation, the pathological phenotype is rescued (Chang *et al.* 2011), but this does not necessarily mean that the same is true if SMA is restored after MN generation.

7.8.4 PLS3

The fact that AC28 behaves similarly to the rest of the SMA clones shows that the influence of modifier factors in the disease severity cannot be anticipated or discriminated by any of the previously described measurements. Asymptomatic or less severely affected siblings in discordant SMA families have been an important subject of study since they can provide insights into modifying factors that bypass or compensate the molecular

pathological mechanism caused by the lack of SMN. Moreover, they could provide new targets for treating the disease. High PLS3 levels in lymphoblast have been associated with a positive modification of the SMA phenotype in females (Oprea *et al.* 2008; Stratigopoulos *et al.* 2010) (Please refer to **section 1.1.3** in the introduction). Plastins are a family of actin binding proteins, which in humans have three isoforms: PLS1 or fimbrin, lymphocyte cytosolic protein 1 or PLS-L/PLS2, and PLS3 or PLS-T. PLS3 is found in all normal cells with a replicative potential, while PLS-L is expressed in hematopoietic cells and PLS1 is expressed specifically at high levels in the small intestine (*Entrez Gene ID: 5358*). Wirth's group (University of Cologne) found that PLS3 was expressed in the lymphoblasts of some patients, contrary to what was previously thought (Lin *et al.* 1993; Oprea *et al.* 2008). The level of PLS3 (mRNA) has already been analysed in the lymphoblasts of the siblings of study, and it was not found to be a SMA modifier factor in the family. Even though the SMA type IV/asymptomatic sister (AC) had higher levels than two of her SMA type III siblings (TC and NC), the third SMA type III sibling (CC, from whom we could not obtain iPSC clones) showed even higher levels (Bernal *et al.* 2011) (**Please refer to Table 4.1)**. It is intriguing that high levels of PLS3 in lymphoblasts can act as a modifier in a MN disease, since they do not necessarily translate into a higher relative level at the MN per se. Moreover, no correlation was found in a previous study between the PLS3 expression in lympholasts, whole blood and fibroblasts (Bernal *et al.* 2011). In order to determine the PLS3 level at the MN per se, as well as in the preceding cells types, I followed its expression through the iPSC-MN differentiation process. Similar to the case of SMN, all clones showed a statiscally significant decay in the levels of PLS3 protein along the iPSC-MN differentiation process, which in this case was congruent with their mRNA levels (**Figure 6.7**). A correlation between SMN protein decay and PLS3 protein decay has also been recently reported in zebrafish models (Hao le *et al.* 2012). I found that the PLS3 mRNA and the protein levels in MNs were significantly lower than in most of the other cells types, showing a direct conflict with the opposite behaviour found by Wirth's group during the neural differentiation of PC12 cells (Oprea *et al.* 2008). All clones showed a similar gradual decay (**Figure 6.9**). Although the unaffected clone 4603 showed lower mRNA and protein levels during the whole process of differentiation, the difference between unaffected individuals (RC26+4603) and SMA patients (AC28+TC63+NC32+SMA1) was in general not statistically significant (data not shown). At the MN level, AC28 showed higher protein levels (but not mRNA levels) of PLS3 than

her SMA type III siblings (**Figure 6.10),** partially supporting the results found in lymphoblasts (Bernal *et al.* 2011). Unfortunately, no iPSC clone could be generated from the cells of the 4th sibling, CC (who presented the highest PLS3 levels in lymphoblasts) and therefore, I cannot determined whether the relative higher PLS3 protein levels in the MNs of AC28 could be significant or not. In Wirth's study, *PLS3* mRNA levels were empirically categorized as high and low based on the differential expression between the symptomatic siblings and the asymptomatic sibling in discordant families; unfortunately we cannot identify that threshold without the samples from CC.

Interestingly, I found what appear to be different forms of PLS3 in fibroblast and in MNs (**Figure 6.11**). At least 3 alternative spliced mRNAs have been reported for the *PLS3* gene, generating two different protein isoforms (NCBI, Gene ID: 5358). The antibody I used recognizes aminoacids 235-456 of PLS3, which is present in both isoforms. Nevertheless, the PLS3 size difference observed between MNs and fibroblasts is smaller than the difference between the isoforms (21 aminoacids). A post-translational modification such as phosphorylation could explain the difference, but this was not studied in this work (UnipProtKB P13797).

Taken together, the SMN and PLS3 molecular analyses performed in cell cultures derived from the iPSC-MN model confirm the findings made from surrogate human cells and foetal samples. Furthermore, it expands the array of cell types available to study the SMA pathology to include cells from MN progenitor pools and functionally mature MNs, among others. The same is true for the study of phenotypic differences; nevertheless, several parameters should be improved during future studies: (i) neurospheres should be dissociated into single cells, such that markers can be systematically quantified without any bias, (ii) MNs should be purified, plated at the same confluence, synchronized in their cell cycle and studied over long-term periods, (iii) more than one clone should be studied from each patient and each clone must be differentiated several times in order to give consistency and statistical significance to the results. Finally, since SMA affects the MN within the NMJ context, co-culture systems like the one presented in this work, will provide more reliable insights that the ones obtained by study of the MN alone.

CHAPTER 8. CONCLUSIONS

- ✓ Fibroblasts from four of the five members of the family of study (AC, TC, NC and RC, but not CC) were efficiently reprogrammed into iPSCs. One clone from each individual was fully characterized passing all quality control standards.
- ✓ SMA type I iPSCs (reference clone SMA1) showed an impaired ability to form rosettes, which may be specific to the severe form of the disease.
- ✓ The four selected iPSC clones and the two reference clones (SMA1 and 4603) were able to efficiently differentiate into ISL-1+/ChAT+ MNs. The MN yield could not be determined accurately because of the three-dimensional structure of the cell culture, but it was estimated to be between 10-15% for all clones.
- ✓ rH1LVs and scAAV9 transduced iPSC-derived MN cultures, but their transduction efficiencies could not be determined accurately in the three-dimensional structures of the cell culture. Increasingly efficient transduction of the developing cultures was obtained with a rH1LV where a fluorescent reporter was driven by the MN-specific HB9 promoter, confirming the progressive generation of MNs from iPSCs.
- ✓ The reported SMA iPSC-derived MN phenotypes (proportion of MNs and neurite outgrowth) were not observed in my short time cultures (phenotypes evaluated <10 days after plating of neurospheres). An assay of neurite growth yielded similar results in all clones within the first 8 days after the plating of neurospheres.
- ✓ iPSC-derived MNs promoted clustering of mouse myotube AChRs in co-cultures. Close proximity of AChR clusters and TUJ1+ neurites was observed by confocal microscopy.
- ✓ One iPSC clone from the carrier mother (RC26) was efficiently differentiated into mature AFP+ hepatocytes able to store lipids and glycogen.
- ✓ SMN protein and PLS3 mRNA and protein levels showed a progressive decay during the iPSC-MN differentiation process in both SMA patients and unaffected individuals. The progressive decay was peculiar to the iPSC-MN differentiation and, the levels found in terminal differentiated cells was lower than in the iPSC-hepatocyte differentiation.
- ✓ There seems to be a post-transcriptional/post-translational regulation of *FL-SMN* transcripts.
- ✓ SMA patients could be distinguished from the unaffected individual carrying two functional *SMN1* alleles (4603), but not from the unaffected carrier (RC26), by their

significantly lower *FL/Δ7-SMN* mRNA ratios, particularly in the late stages of MN differentiation.

- ✓ The *FL-SMN* mRNA and protein levels at the MN stage were similar between SMA type I (SMA1), III (TC63, NC32) and IV (AC28) patients. Clone SMA1 could only be distinguished from the siblings of the Spanish family of study by its constant lower *tSMN* mRNA levels.
- ✓ scAAV9-mediated *SMN1* restoration in SMA1 iPSC-derived MNs switched the expression pattern of *SMN* transcripts to a profile similar to that observed in the unaffected control individual (4603).
- ✓ The iPSC-derived MNs from the SMA type IV/asymptomatic sibling (AC28) showed higher PLS3 protein levels (but not mRNA levels) than the ones from her SMA type III siblings (TC63 and NC32), partially confirming the previous findings in lymphoblasts. However, it was not possible to determine if PLS3 was a modifier factor of the SMA severity in the family of study because of the lack of an iPSC clone from CC.
- ✓ PLS3 protein apparently shows a small difference in PAGE mobility between MNs and fibroblasts, which may reflect different isoforms or a post-translational modification.

REFERENCES

Aasen T, Raya A, Barrero MJ, Garreta E, Consiglio A, Gonzalez F, Vassena R, Bilic J, Pekarik V, Tiscornia G, Edel M, Boue S , Izpisua Belmonte JC (2008). Efficient and rapid generation of induced pluripotent stem cells from human keratinocytes. *Nature biotechnology*. **26**, 1276-1284.

Abe A, Miyanohara A , Friedmann T (1998). Enhanced gene transfer with fusogenic liposomes containing vesicular stomatitis virus G glycoprotein. *J Virol*. **72**, 6159-6163.

Agarwal S, Loh YH, McLoughlin EM, Huang J, Park IH, Miller JD, Huo H, Okuka M, Dos Reis RM, Loewer S, Ng HH, Keefe DL, Goldman FD, Klingelhutz AJ, Liu L , Daley GQ (2010). Telomere elongation in induced pluripotent stem cells from dyskeratosis congenita patients. *Nature*. **464**, 292-296.

Akache B, Grimm D, Pandey K, Yant SR, Xu H , Kay MA (2006). The 37/67-kilodalton laminin receptor is a receptor for adeno-associated virus serotypes 8, 2, 3, and 9. *Journal of virology*. **80**, 9831-9836.

Akkina RK, Walton RM, Chen ML, Li QX, Planelles V , Chen IS (1996). High-efficiency gene transfer into CD34+ cells with a human immunodeficiency virus type 1-based retroviral vector pseudotyped with vesicular stomatitis virus envelope glycoprotein G. *J Virol*. **70**, 2581-2585.

Akopian V, Andrews PW, Beil S, Benvenisty N, Brehm J, Christie M, Ford A, Fox V, Gokhale PJ, Healy L, Holm F, Hovatta O, Knowles BB, Ludwig TE, McKay RD, Miyazaki T, Nakatsuji N, Oh SK, Pera MF, Rossant J, Stacey GN , Suemori H (2010). Comparison of defined culture systems for feeder cell free propagation of human embryonic stem cells. *In Vitro Cell Dev Biol Anim*. **46**, 247-258.

Alias L, Bernal S, Fuentes-Prior P, Barcelo MJ, Also E, Martinez-Hernandez R, Rodriguez-Alvarez FJ, Martin Y, Aller E, Grau E, Pecina A, Antinolo G, Galan E, Rosa AL, Fernandez-Burriel M, Borrego S, Millan JM, Hernandez-Chico C, Baiget M , Tizzano EF (2009). Mutation update of spinal muscular atrophy in Spain: molecular characterization of 745 unrelated patients and identification of four novel mutations in the SMN1 gene. *Hum Genet*. **125**, 29-39.

Allocca M, Mussolino C, Garcia-Hoyos M, Sanges D, Iodice C, Petrillo M, Vandenberghe LH, Wilson JM, Marigo V, Surace EM , Auricchio A (2007). Novel adeno-associated virus serotypes efficiently transduce murine photoreceptors. *Journal of virology*. **81**, 11372-11380.

Also-Rallo E, Alias L, Martinez-Hernandez R, Caselles L, Barcelo MJ, Baiget M, Bernal S , Tizzano EF (2011). Treatment of spinal muscular atrophy cells with drugs that upregulate SMN expression reveals inter- and intra-patient variability. *Eur J Hum Genet*. **19**, 1059-1065.

Amabile G , Meissner A (2009). Induced pluripotent stem cells : current progress and potential for regenerative medicine. *Trends in molecular medicine*. **15**, 59-86.

Andreassi C, Angelozzi C, Tiziano FD, Vitali T, De Vincenzi E, Boninsegna A, Villanova M, Bertini E, Pini A, Neri G , Brahe C (2004). Phenylbutyrate increases SMN expression in vitro: relevance for treatment of spinal muscular atrophy. *Eur J Hum Genet*. **12**, 59-65.

Andrews PW, Goodfellow PN, Shevinsky LH, Bronson DL , Knowles BB (1982). Cell-surface antigens of a clonal human embryonal carcinoma cell line: morphological and antigenic differentiation in culture. *Int J Cancer*. **29**, 523-531.

Anokye-Danso F, Trivedi CM, Juhr D, Gupta M, Cui Z, Tian Y, Zhang Y, Yang W, Gruber PJ, Epstein JA , Morrisey EE (2011). Highly efficient miRNA-mediated reprogramming of mouse and human somatic cells to pluripotency. *Cell stem cell*. **8**, 376-388.

Arber S, Han B, Mendelsohn M, Smith M, Jessell TM , Sockanathan S (1999). Requirement for the homeobox gene Hb9 in the consolidation of motor neuron identity. *Neuron*. **23**, 659-674.

Avila AM, Burnett BG, Taye AA, Gabanella F, Knight MA, Hartenstein P, Cizman Z, Di Prospero NA, Pellizzoni L, Fischbeck KH , Sumner CJ (2007). Trichostatin A increases SMN expression and survival in a mouse model of spinal muscular atrophy. *J Clin Invest*. **117**, 659-671.

Azzouz M, Le T, Ralph GS, Walmsley L, Monani UR, Lee DC, Wilkes F, Mitrophanous KA, Kingsman SM, Burghes AH , Mazarakis ND (2004). Lentivector-mediated SMN replacement in a mouse model of spinal muscular atrophy. *J Clin Invest*. **114**, 1726-1731.

Barkats M (Unpublished data). AAV9 Gene Therapy Startegies For Spinal Muscular Atrophy. In *16th Annual International Spinal Muscular Atrophy Research Group Meeting*ed^eds). USA.

Bear M, B C , M P (2007). Spinal Control of Movement. In *Neurocience. Exploring the Brain*. (E Lupash, E Connnolly , B Dilernia, eds). Philadelphia: Lippincott Williams & Wilkins.

Bernal S, Also-Rallo E, Martinez-Hernandez R, Alias L, Rodriguez-Alvarez FJ, Millan JM, Hernandez-Chico C, Baiget M , Tizzano EF (2011). Plastin 3 expression in discordant spinal muscular atrophy (SMA) siblings. *Neuromuscul Disord*. **21**, 413-419.

Berns K (2007). "Adeno-Associated Viruses (AAV)", in Palese, P. (ed.), Viruses and Viral Diseases: Emerging threats to humans and animalsed^eds): The Biomedical & Life Sciences Collection, Henry Stewart Talks Ltd, London.

Bibel M, Richter J, Lacroix E , Barde YA (2007). Generation of a defined and uniform population of CNS progenitors and neurons from mouse embryonic stem cells. *Nat Protoc*. **2**, 1034-1043.

Blelloch R, Venere M, Yen J , Ramalho-Santos M (2007). Generation of induced pluripotent stem cells in the absence of drug selection. *Cell stem cell*. **1**, 245-247.

Boland MJ, Hazen JL, Nazor KL, Rodriguez AR, Gifford W, Martin G, Kupriyanov S , Baldwin KK (2009). Adult mice generated from induced pluripotent stem cells. *Nature*. **461**, 91-94.

Boulting GL, Kiskinis E, Croft GF, Amoroso MW, Oakley DH, Wainger BJ, Williams DJ, Kahler DJ, Yamaki M, Davidow L, Rodolfa CT, Dimos JT, Mikkilineni S, MacDermott AB, Woolf CJ, Henderson CE, Wichterle H , Eggan K (2011). A functionally characterized test set of human induced pluripotent stem cells. *Nat Biotechnol*. **29**, 279-286.

Boyer LA, Lee TI, Cole MF, Johnstone SE, Levine SS, Zucker JP, Guenther MG, Kumar RM, Murray HL, Jenner RG, Gifford DK, Melton DA, Jaenisch R , Young RA (2005). Core transcriptional regulatory circuitry in human embryonic stem cells. *Cell*. **122**, 947-956.

Brambrink T, Foreman R, Welstead GG, Lengner CJ, Wernig M, Suh H , Jaenisch R (2008). Sequential expression of pluripotency markers during direct reprogramming of mouse somatic cells. *Cell stem cell*. **2**, 151-159.

Brennand KJ, Simone A, Jou J, Gelboin-Burkhart C, Tran N, Sangar S, Li Y, Mu Y, Chen G, Yu D, McCarthy S, Sebat J , Gage FH (2011). Modelling schizophrenia using human induced pluripotent stem cells. *Nature*. **473**, 221-225.

Brichta L, Hofmann Y, Hahnen E, Siebzehnrubl FA, Raschke H, Blumcke I, Eyupoglu IY , Wirth B (2003). Valproic acid increases the SMN2 protein level: a well-known drug as a potential therapy for spinal muscular atrophy. *Hum Mol Genet*. **12**, 2481-2489.

Briscoe J, Pierani A, Jessell TM , Ericson J (2000). A homeodomain protein code specifies progenitor cell identity and neuronal fate in the ventral neural tube. *Cell*. **101**, 435-445.

Broccolini A, Engel WK , Askanas V (1999). Localization of survival motor neuron protein in human apoptotic-like and regenerating muscle fibers, and neuromuscular junctions. *Neuroreport*. **10**, 1637-1641.

Brow DA (2002). Allosteric cascade of spliceosome activation. *Annu Rev Genet*. **36**, 333-360.

Brzustowicz LM, Lehner T, Castilla LH, Penchaszadeh GK, Wilhelmsen KC, Daniels R, Davies KE, Leppert M, Ziter F, Wood D , et al. (1990). Genetic mapping of chronic childhood-onset spinal muscular atrophy to chromosome 5q11.2-13.3. *Nature*. **344**, 540-541.

Buchthal F , Olsen PZ (1970). Electromyography and muscle biopsy in infantile spinal muscular atrophy. *Brain*. **93**, 15-30.

Burlet P, Huber C, Bertrandy S, Ludosky MA, Zwaenepoel I, Clermont O, Roume J, Delezoide AL, Cartaud J, Munnich A , Lefebvre S (1998). The distribution of SMN protein complex in human fetal tissues and its alteration in spinal muscular atrophy. *Hum Mol Genet*. **7**, 1927-1933.

Bussaglia E, Clermont O, Tizzano E, Lefebvre S, Burglen L, Cruaud C, Urtizberea JA, Colomer J, Munnich A, Baiget M , et al. (1995). A frame-shift deletion in the survival motor neuron gene in Spanish spinal muscular atrophy patients. *Nat Genet*. **11**, 335-337.

Bussaglia E, Tizzano EF, Illa I, Cervera C , Baiget M (1997). Cramps and minimal EMG abnormalities as preclinical manifestations of spinal muscular atrophy patients with homozygous deletions of the SMN gene. *Neurology*. **48**, 1443-1445.

Byrne JA, Pedersen DA, Clepper LL, Nelson M, Sanger WG, Gokhale S, Wolf DP , Mitalipov SM (2007). Producing primate embryonic stem cells by somatic cell nuclear transfer. *Nature*. **450**, 497-502.

Caiazzo M, Dell'Anno MT, Dvoretskova E, Lazarevic D, Taverna S, Leo D, Sotnikova TD, Menegon A, Roncaglia P, Colciago G, Russo G, Carninci P, Pezzoli G, Gainetdinov RR, Gustincich S, Dityatev A , Broccoli V (2011). Direct generation of functional dopaminergic neurons from mouse and human fibroblasts. *Nature*. **476**, 224-227.

Camu W , Henderson CE (1992). Purification of embryonic rat motoneurons by panning on a monoclonal antibody to the low-affinity NGF receptor. *J Neurosci Methods*. **44**, 59-70.

Capon F, Levato C, Merlini L, Angelini C, Mostacciuolo ML, Politano L, Novelli G , Dallapiccola B (1996). Discordant clinical outcome in type III spinal muscular atrophy sibships showing the same deletion pattern. *Neuromuscul Disord*. **6**, 261-264.

Carissimi C, Saieva L, Baccon J, Chiarella P, Maiolica A, Sawyer A, Rappsilber J , Pellizzoni L (2006a). Gemin8 is a novel component of the survival motor neuron complex and functions in small nuclear ribonucleoprotein assembly. *J Biol Chem*. **281**, 8126-8134.

Carissimi C, Saieva L, Gabanella F , Pellizzoni L (2006b). Gemin8 is required for the architecture and function of the survival motor neuron complex. *J Biol Chem*. **281**, 37009-37016.

Carr AJ, Vugler AA, Hikita ST, Lawrence JM, Gias C, Chen LL, Buchholz DE, Ahmado A, Semo M, Smart MJ, Hasan S, da Cruz L, Johnson LV, Clegg DO , Coffey PJ (2009). Protective effects of human iPS-derived retinal pigment epithelium cell transplantation in the retinal dystrophic rat. *PloS one*. **4**, e8152.

Carriedo SG, Yin HZ , Weiss JH (1996). Motor neurons are selectively vulnerable to AMPA/kainate receptor-mediated injury in vitro. *J Neurosci*. **16**, 4069-4079.

Cartegni L , Krainer AR (2002). Disruption of an SF2/ASF-dependent exonic splicing enhancer in SMN2 causes spinal muscular atrophy in the absence of SMN1. *Nat Genet*. **30**, 377-384.

Carvajal-Vergara X, Sevilla A, D'Souza SL, Ang YS, Schaniel C, Lee DF, Yang L, Kaplan AD, Adler ED, Rozov R, Ge Y, Cohen N, Edelmann LJ, Chang B, Waghray A, Su J, Pardo S, Lichtenbelt KD, Tartaglia M, Gelb BD , Lemischka IR (2010). Patient-specific induced pluripotent stem-cell-derived models of LEOPARD syndrome. *Nature*. **465**, 808-812.

Cell Biolabs (2008). Platinum Retrovirus Expression System. (C Biolabs, ed^eds).

Cepko C , Pear W (2001). Overview of the retrovirus transduction system. *Curr Protoc Mol Biol*. **Chapter 9**, Unit9 9.

Chan EM, Ratanasirintrawoot S, Park IH, Manos PD, Loh YH, Huo H, Miller JD, Hartung O, Rho J, Ince TA, Daley GQ , Schlaeger TM (2009). Live cell imaging distinguishes bona fide human iPS cells from partially reprogrammed cells. *Nature biotechnology*. **27**, 1033-1037.

Chang JG, Hsieh-Li HM, Jong YJ, Wang NM, Tsai CH , Li H (2001). Treatment of spinal muscular atrophy by sodium butyrate. *Proc Natl Acad Sci U S A*. **98**, 9808-9813.

Chang T, Zheng W, Tsark W, Bates S, Huang H, Lin RJ , Yee JK (2011). Brief report: phenotypic rescue of induced pluripotent stem cell-derived motoneurons of a spinal muscular atrophy patient. *Stem Cells*. **29**, 2090-2093.

Chari A, Paknia E , Fischer U (2009). The role of RNP biogenesis in spinal muscular atrophy. *Curr Opin Cell Biol*. **21**, 387-393.

Cheung AY, Horvath LM, Grafodatskaya D, Pasceri P, Weksberg R, Hotta A, Carrel L , Ellis J (2011). Isolation of MECP2-null Rett Syndrome patient hiPS cells and isogenic controls through X-chromosome inactivation. *Hum Mol Genet*. **20**, 2103-2115.

Chikhovskaya JV, Jonker MJ, Meissner A, Breit TM, Repping S , van Pelt AM (2012). Human testis-derived embryonic stem cell-like cells are not pluripotent, but possess potential of mesenchymal progenitors. *Hum Reprod*. **27**, 210-221.

Cifuentes-Diaz C, Frugier T , Melki J (2002). Spinal muscular atrophy. *Semin Pediatr Neurol*. **9**, 145-150.

Cobben JM, van der Steege G, Grootscholten P, de Visser M, Scheffer H , Buys CH (1995). Deletions of the survival motor neuron gene in unaffected siblings of patients with spinal muscular atrophy. *Am J Hum Genet*. **57**, 805-808.

Coil DA , Miller AD (2004). Phosphatidylserine is not the cell surface receptor for vesicular stomatitis virus. *J Virol*. **78**, 10920-10926.

Conrad S, Renninger M, Hennenlotter J, Wiesner T, Just L, Bonin M, Aicher W, Buhring HJ, Mattheus U, Mack A, Wagner HJ, Minger S, Matzkies M, Reppel M, Hescheler J, Sievert KD, Stenzl A , Skutella T (2008). Generation of pluripotent stem cells from adult human testis. *Nature*. **456**, 344-349.

Cooper O, Hargus G, Deleidi M, Blak A, Osborn T, Marlow E, Lee K, Levy A, Perez-Torres E, Yow A , Isacson O (2010). Differentiation of human ES and Parkinson's disease iPS cells into ventral midbrain dopaminergic neurons requires a high activity form of SHH, FGF8a and specific regionalization by retinoic acid. *Molecular and cellular neurosciences*.

Coovert DD, Le TT, McAndrew PE, Strasswimmer J, Crawford TO, Mendell JR, Coulson SE, Androphy EJ, Prior TW , Burghes AH (1997). The survival motor neuron protein in spinal muscular atrophy. *Hum Mol Genet*. **6**, 1205-1214.

Coppola G, Choi SH, Santos MM, Miranda CJ, Tentler D, Wexler EM, Pandolfo M , Geschwind DH (2006). Gene expression profiling in frataxin deficient mice: microarray evidence for significant expression changes without detectable neurodegeneration. *Neurobiol Dis*. **22**, 302-311.

Corti S, Nizzardo M, Nardini M, Donadoni C, Salani S, Ronchi D, Saladino F, Bordoni A, Fortunato F, Del Bo R, Papadimitriou D, Locatelli F, Menozzi G, Strazzer S, Bresolin N , Comi GP (2008). Neural stem cell transplantation can ameliorate the phenotype of a mouse model of spinal muscular atrophy. *J Clin Invest*. **118**, 3316-3330.

Corti S, Nizzardo M, Nardini M, Donadoni C, Salani S, Ronchi D, Simone C, Falcone M, Papadimitriou D, Locatelli F, Mezzina N, Gianni F, Bresolin N , Comi GP (2010). Embryonic stem cell-derived neural stem cells improve spinal muscular atrophy phenotype in mice. *Brain*. **133**, 465-481.

Cowan CA, Atienza J, Melton DA , Eggan K (2005). Nuclear reprogramming of somatic cells after fusion with human embryonic stem cells. *Science (New York, N.Y.)*. **309**, 1369-1373.

Cox JL , Rizzino A (2010). Induced pluripotent stem cells: what lies beyond the paradigm shift. *Experimental biology and medicine (Maywood, N.J.)*. **235**, 148-158.

Crawford TO, Paushkin SV, Kobayashi DT, Forrest SJ, Joyce CL, Finkel RS, Kaufmann P, Swoboda KJ, Tiziano D, Lomastro R, Li RH, Trachtenberg FL, Plasterer T , Chen KS (2012). Evaluation of SMN protein, transcript, and copy number in the biomarkers for spinal muscular atrophy (BforSMA) clinical study. *PloS one*. **7**, e33572.

Cronin J, Zhang XY , Reiser J (2005). Altering the tropism of lentiviral vectors through pseudotyping. *Curr Gene Ther*. **5**, 387-398.

Cusco I, Barcelo MJ, Rojas-Garcia R, Illa I, Gamez J, Cervera C, Pou A, Izquierdo G, Baiget M , Tizzano EF (2006). SMN2 copy number predicts acute or chronic spinal muscular atrophy but does not account for intrafamilial variability in siblings. *J Neurol*. **253**, 21-25.

Cusco I, Lopez E, Soler-Botija C, Jesus Barcelo M, Baiget M , Tizzano EF (2003). A genetic and phenotypic analysis in Spanish spinal muscular atrophy patients with c.399_402del AGAG, the most frequently found subtle mutation in the SMN1 gene. *Hum Mutat*. **22**, 136-143.

Dambrot C, Passier R, Atsma D , Mummery CL (2011). Cardiomyocyte differentiation of pluripotent stem cells and their use as cardiac disease models. *Biochem J*. **434**, 25-35.

Darr H , Benvenisty N (2009). Genetic analysis of the role of the reprogramming gene LIN-28 in human embryonic stem cells. *Stem cells (Dayton, Ohio)*. **27**, 352-362.

Davis RL, Weintraub H , Lassar AB (1987). Expression of a single transfected cDNA converts fibroblasts to myoblasts. *Cell*. **51**, 987-1000.

De Souza N (2010). Primer: induced pluripotency. *Nature Methods*. **7**, 20-21.

Deakin CT, Alexander IE , Kerridge I (2009). Accepting risk in clinical research: is the gene therapy field becoming too risk-averse? *Mol Ther*. **17**, 1842-1848.

Dent EW , Gertler FB (2003). Cytoskeletal dynamics and transport in growth cone motility and axon guidance. *Neuron*. **40**, 209-227.

Devine MJ, Ryten M, Vodicka P, Thomson AJ, Burdon T, Houlden H, Cavaleri F, Nagano M, Drummond NJ, Taanman JW, Schapira AH, Gwinn K, Hardy J, Lewis PA , Kunath T (2011). Parkinson's disease induced pluripotent stem cells with triplication of the alpha-synuclein locus. *Nat Commun*. **2**, 440.

Dimos JT, Rodolfa KT, Niakan KK, Weisenthal LM, Mitsumoto H, Chung W, Croft GF, Saphier G, Leibel R, Goland R, Wichterle H, Henderson CE , Eggan K (2008). Induced pluripotent stem cells generated from patients with ALS can be differentiated into motor neurons. *Science*. **321**, 1218-1221.

Ding W, Zhang L, Yan Z , Engelhardt JF (2005). Intracellular trafficking of adeno-associated viral vectors. *Gene therapy*. **12**, 873-880.

Dominguez E, Marais T, Chatauret N, Benkhelifa-Ziyyat S, Duque S, Ravassard P, Carcenac R, Astord S, Pereira de Moura A, Voit T , Barkats M (2011). Intravenous scAAV9 delivery of a codon-optimized SMN1 sequence rescues SMA mice. *Hum Mol Genet*. **20**, 681-693.

Dong JY, Fan PD , Frizzell RA (1996). Quantitative analysis of the packaging capacity of recombinant adeno-associated virus. *Hum Gene Ther*. **7**, 2101-2112.

Dornburg R (2003). The history and principles of retroviral vectors. *Front Biosci*. **8**, d818-835.

Du ZW, Hu BY, Ayala M, Sauer B , Zhang SC (2009). Cre recombination-mediated cassette exchange for building versatile transgenic human embryonic stem cells lines. *Stem Cells*. **27**, 1032-1041.

Du ZW, Li XJ, Nguyen GD , Zhang SC (2006). Induced expression of Olig2 is sufficient for oligodendrocyte specification but not for motoneuron specification and astrocyte repression. *Mol Cell Neurosci*. **33**, 371-380.

Dull T, Zufferey R, Kelly M, Mandel RJ, Nguyen M, Trono D , Naldini L (1998). A third-generation lentivirus vector with a conditional packaging system. *J Virol*. **72**, 8463-8471.

Duque S (Unpublished data). Delivery And Correction of SMA Using AAV Vectors In A Large Animal Model. In *16th Annual International Spinal Muscular Atrophy Research Group Meeting*ed^eds). USA.

Durston AJ, van der Wees J, Pijnappel WW , Godsave SF (1998). Retinoids and related signals in early development of the vertebrate central nervous system. *Curr Top Dev Biol*. **40**, 111-175.

Eberling JL, Jagust WJ, Christine CW, Starr P, Larson P, Bankiewicz KS , Aminoff MJ (2008). Results from a phase I safety trial of hAADC gene therapy for Parkinson disease. *Neurology*. **70**, 1980-1983.

Ebert AD, Yu J, Rose FF, Jr., Mattis VB, Lorson CL, Thomson JA , Svendsen CN (2009). Induced pluripotent stem cells from a spinal muscular atrophy patient. *Nature*. **457**, 277-280.

Emery AE, Hausmanowa-Petrusewicz I, Davie AM, Holloway S, Skinner R , Borkowska J (1976). International collaborative study of the spinal muscular atrophies. Part 1. Analysis of clinical and laboratory data. *J Neurol Sci*. **29**, 83-94.

Eminli S, Foudi A, Stadtfeld M, Maherali N, Ahfeldt T, Mostoslavsky G, Hock H , Hochedlinger K (2009). Differentiation stage determines potential of hematopoietic

cells for reprogramming into induced pluripotent stem cells. *Nat Genet*. **41**, 968-976.

Ericson J, Rashbass P, Schedl A, Brenner-Morton S, Kawakami A, van Heyningen V, Jessell TM , Briscoe J (1997). Pax6 controls progenitor cell identity and neuronal fate in response to graded Shh signaling. *Cell*. **90**, 169-180.

Ericson J, Thor S, Edlund T, Jessell TM , Yamada T (1992). Early stages of motor neuron differentiation revealed by expression of homeobox gene Islet-1. *Science*. **256**, 1555-1560.

Fagone P, Wright JF, Nathwani AC, Nienhuis AW, Davidoff AM , Gray JT (2012). Systemic errors in quantitative polymerase chain reaction titration of self-complementary adeno-associated viral vectors and improved alternative methods. *Hum Gene Ther Methods*. **23**, 1-7.

Fallini C, Bassell GJ , Rossoll W (2010). High-efficiency transfection of cultured primary motor neurons to study protein localization, trafficking, and function. *Mol Neurodegener*. **5**, 17.

Fallini C, Zhang H, Su Y, Silani V, Singer RH, Rossoll W , Bassell GJ (2011). The Survival of Motor Neuron (SMN) Protein Interacts with the mRNA-Binding Protein HuD and Regulates Localization of Poly(A) mRNA in Primary Motor Neuron Axons. *J Neurosci*. **31**, 3914-3925.

Fan L , Simard LR (2002). Survival motor neuron (SMN) protein: role in neurite outgrowth and neuromuscular maturation during neuronal differentiation and development. *Hum Mol Genet*. **11**, 1605-1614.

Feigin A, Kaplitt MG, Tang C, Lin T, Mattis P, Dhawan V, During MJ , Eidelberg D (2007). Modulation of metabolic brain networks after subthalamic gene therapy for Parkinson's disease. *Proceedings of the National Academy of Sciences of the United States of America*. **104**, 19559-19564.

Feldkotter M, Schwarzer V, Wirth R, Wienker TF , Wirth B (2002). Quantitative analyses of SMN1 and SMN2 based on real-time lightCycler PCR: fast and highly reliable carrier testing and prediction of severity of spinal muscular atrophy. *Am J Hum Genet*. **70**, 358-368.

Foust KD, Nurre E, Montgomery CL, Hernandez A, Chan CM , Kaspar BK (2009). Intravascular AAV9 preferentially targets neonatal neurons and adult astrocytes. *Nature biotechnology*. **27**, 59-65.

Foust KD, Wang X, McGovern VL, Braun L, Bevan AK, Haidet AM, Le TT, Morales PR, Rich MM, Burghes AH , Kaspar BK (2010). Rescue of the spinal muscular atrophy phenotype in a mouse model by early postnatal delivery of SMN. *Nature biotechnology*. **28**, 271-274.

Friedmann T , Roblin R (1972). Gene therapy for human genetic disease? *Science (New York, N.Y.)*. **175**, 949-955.

Gabanella F, Butchbach ME, Saieva L, Carissimi C, Burghes AH , Pellizzoni L (2007). Ribonucleoprotein assembly defects correlate with spinal muscular atrophy severity and preferentially affect a subset of spliceosomal snRNPs. *PLoS One*. **2**, e921.

Gao G, Vandenberghe LH, Alvira MR, Lu Y, Calcedo R, Zhou X , J.M. W (2004). Clades of Adeno-associated viruses are widely disseminated in human tissues. *Jounal of Virology*. **78**, 6381-6388.

Gardner RL , Lyon MF (1971). X chromosome inactivation studied by injection of a single cell into the mouse blastocyst. *Nature*. **231**, 385-386.

Gennarelli M, Lucarelli M, Capon F, Pizzuti A, Merlini L, Angelini C, Novelli G , Dallapiccola B (1995). Survival motor neuron gene transcript analysis in muscles

from spinal muscular atrophy patients. *Biochem Biophys Res Commun*. **213**, 342-348.

Glascock JJ, Shababi M, Wetz MJ, Krogman MM , Lorson CL (2012). Direct central nervous system delivery provides enhanced protection following vector mediated gene replacement in a severe model of spinal muscular atrophy. *Biochem Biophys Res Commun*. **417**, 376-381.

Goff S (2006). Retroviruses and their replication. In *Fields Virology*. (D Knipe, P Howley, D Griffin, R Lamb, M Martin, B Roizman , S Straus, eds): Lippincott Williams & Wilkins, pp. 3177.

Goldmann JE, Schuldt BM, Lenz M , Muller FJ (2012). Chapter 18- PluriTest Molecular Diagnostic Assay for Pluripotency in Human Stem Cells. In *Human Stem Cell Manual*): Elsevier Inc.

Goncalves MA (2005). Adeno-associated virus: from defective virus to effective vector. *Virol J*. **2**, 43.

Gonzalez F, Boue S , Izpisua Belmonte JC (2011). Methods for making induced pluripotent stem cells: reprogramming a la carte. *Nat Rev Genet*. **12**, 231-242.

Gore A, Li Z, Fung HL, Young JE, Agarwal S, Antosiewicz-Bourget J, Canto I, Giorgetti A, Israel MA, Kiskinis E, Lee JH, Loh YH, Manos PD, Montserrat N, Panopoulos AD, Ruiz S, Wilbert ML, Yu J, Kirkness EF, Izpisua Belmonte JC, Rossi DJ, Thomson JA, Eggan K, Daley GQ, Goldstein LS , Zhang K (2011). Somatic coding mutations in human induced pluripotent stem cells. *Nature*. **471**, 63-67.

Graf T , Enver T (2009). Forcing cells to change lineages. *Nature*. **462**, 587-594.

Graham FL, Smiley J, Russell WC , Nairn R (1977). Characteristics of a human cell line transformed by DNA from human adenovirus type 5. *J Gen Virol*. **36**, 59-74.

Gray SJ, Matagne V, Bachaboina L, Yadav S, Ojeda SR , Samulski RJ (2011). Preclinical differences of intravascular AAV9 delivery to neurons and glia: a comparative study of adult mice and nonhuman primates. *Mol Ther*. **19**, 1058-1069.

Grimm D, Kern A, Pawlita M, Ferrari F, Samulski R , Kleinschmidt J (1999). Titration of AAV-2 particles via a novel capsid ELISA: packaging of genomes can limit production of recombinant AAV-2. *Gene therapy*. **6**, 1322-1330.

Guenechea G, Gan OI, Inamitsu T, Dorrell C, Pereira DS, Kelly M, Naldini L , Dick JE (2000). Transduction of human CD34+ CD38- bone marrow and cord blood-derived SCID-repopulating cells with third-generation lentiviral vectors. *Mol Ther*. **1**, 566-573.

Hacein-Bey-Abina S, Garrigue A, Wang GP, Soulier J, Lim A, Morillon E, Clappier E, Caccavelli L, Delabesse E, Beldjord K, Asnafi V, MacIntyre E, Dal Cortivo L, Radford I, Brousse N, Sigaux F, Moshous D, Hauer J, Borkhardt A, Belohradsky BH, Wintergerst U, Velez MC, Leiva L, Sorensen R, Wulffraat N, Blanche S, Bushman FD, Fischer A , Cavazzana-Calvo M (2008). Insertional oncogenesis in 4 patients after retrovirus-mediated gene therapy of SCID-X1. *The Journal of clinical investigation*. **118**, 3132-3142.

Hacein-Bey-Abina S, Von Kalle C, Schmidt M, McCormack MP, Wulffraat N, Leboulch P, Lim A, Osborne CS, Pawliuk R, Morillon E, Sorensen R, Forster A, Fraser P, Cohen JI, de Saint Basile G, Alexander I, Wintergerst U, Frebourg T, Aurias A, Stoppa-Lyonnet D, Romana S, Radford-Weiss I, Gross F, Valensi F, Delabesse E, Macintyre E, Sigaux F, Soulier J, Leiva LE, Wissler M, Prinz C, Rabbitts TH, Le Deist F, Fischer A , Cavazzana-Calvo M (2003). LMO2-associated clonal T cell proliferation in two patients after gene therapy for SCID-X1. *Science*. **302**, 415-419.

Hahnen E, Eyupoglu IY, Brichta L, Haastert K, Trankle C, Siebzehnrubl FA, Riessland M, Holker I, Claus P, Romstock J, Buslei R, Wirth B , Blumcke I (2006). In vitro and ex vivo evaluation of second-generation histone deacetylase inhibitors for the treatment of spinal muscular atrophy. *J Neurochem*. **98**, 193-202.

Hahnen E, Forkert R, Marke C, Rudnik-Schoneborn S, Schonling J, Zerres K , Wirth B (1995). Molecular analysis of candidate genes on chromosome 5q13 in autosomal recessive spinal muscular atrophy: evidence of homozygous deletions of the SMN gene in unaffected individuals. *Hum Mol Genet*. **4**, 1927-1933.

Han KJ, Foster DG, Zhang NY, Kanisha K, Dzieciatkowska M, Sclafani RA, Hansen KC, Peng J , Liu CW (2012). Ubiquitin-specific Protease 9x Deubiquitinates and Stabilizes the Spinal Muscular Atrophy Protein - Survival Motor Neuron. *J Biol Chem*.

Hao le T, Wolman M, Granato M , Beattie CE (2012). Survival motor neuron affects plastin 3 protein levels leading to motor defects. *J Neurosci*. **32**, 5074-5084.

Hauke J, Riessland M, Lunke S, Eyupoglu IY, Blumcke I, El-Osta A, Wirth B , Hahnen E (2009). Survival motor neuron gene 2 silencing by DNA methylation correlates with spinal muscular atrophy disease severity and can be bypassed by histone deacetylase inhibition. *Hum Mol Genet*. **18**, 304-317.

Hayhurst M, Wagner AK, Cerletti M, Wagers AJ , Rubin LL (2012). A cell-autonomous defect in skeletal muscle satellite cells expressing low levels of survival of motor neuron protein. *Dev Biol*. **368**, 323-334.

Henderson CE (Unpublished data). Human Embryonic Stem Cells As A Model To Study Spinal Muscular Atrophy. In *16th Annual International Spinal Muscular Atrophy Research Group Meeting*ed^eds). USA.

Hermonat PL , Muzyczka N (1984). Use of adeno-associated virus as a mammalian DNA cloning vector: transduction of neomycin resistance into mammalian tissue culture cells. *Proc Natl Acad Sci U S A*. **81**, 6466-6470.

Herweijer H , Wolff JA (2003). Progress and prospects: naked DNA gene transfer and therapy. *Gene Ther*. **10**, 453-458.

Herzog CD, Brown L, Gammon D, Kruegel B, Lin R, Wilson A, Bolton A, Printz M, Gasmi M, Bishop KM, Kordower JH , Bartus RT (2009). Expression, bioactivity, and safety 1 year after adeno-associated viral vector type 2-mediated delivery of neurturin to the monkey nigrostriatal system support cere-120 for Parkinson's disease. *Neurosurgery*. **64**, 602-612; discussion 612-603.

Hester ME, Murtha MJ, Song S, Rao M, Miranda CJ, Meyer K, Tian J, Boulting G, Schaffer DV, Zhu MX, Pfaff SL, Gage FH , Kaspar BK (2011). Rapid and efficient generation of functional motor neurons from human pluripotent stem cells using gene delivered transcription factor codes. *Mol Ther*. **19**, 1905-1912.

Hochedlinger K , Plath K (2009). Epigenetic reprogramming and induced pluripotency. *Development (Cambridge, England)*. **136**, 509-523.

Hotta A, Cheung AY, Farra N, Vijayaragavan K, Seguin CA, Draper JS, Pasceri P, Maksakova IA, Mager DL, Rossant J, Bhatia M , Ellis J (2009). Isolation of human iPS cells using EOS lentiviral vectors to select for pluripotency. *Nature methods*. **6**, 370-376.

Howarth JL, Lee YB , Uney JB (2009). Using viral vectors as gene transfer tools (Cell Biology and Toxicology Special Issue: ETCS-UK 1 day meeting on genetic manipulation of cells). *Cell biology and toxicology*.

Howlett SK , Reik W (1991). Methylation levels of maternal and paternal genomes during preimplantation development. *Development (Cambridge, England)*. **113**, 119-127.

Hu BY, Weick JP, Yu J, Ma LX, Zhang XQ, Thomson JA , Zhang SC (2010). Neural differentiation of human induced pluripotent stem cells follows developmental principles but with variable potency. *Proc Natl Acad Sci U S A*. **107**, 4335-4340.

Hu BY , Zhang SC (2009). Differentiation of spinal motor neurons from pluripotent human stem cells. *Nat Protoc*. **4**, 1295-1304.

Huangfu D, Maehr R, Guo W, Eijkelenboom A, Snitow M, Chen AE , Melton DA (2008a). Induction of pluripotent stem cells by defined factors is greatly improved by small-molecule compounds. *Nature biotechnology*. **26**, 795-797.

Huangfu D, Osafune K, Maehr R, Guo W, Eijkelenboom A, Chen S, Muhlestein W , Melton DA (2008b). Induction of pluripotent stem cells from primary human fibroblasts with only Oct4 and Sox2. *Nat Biotechnol*. **26**, 1269-1275.

Hussein SM, Batada NN, Vuoristo S, Ching RW, Autio R, Narva E, Ng S, Sourour M, Hamalainen R, Olsson C, Lundin K, Mikkola M, Trokovic R, Peitz M, Brustle O, Bazett-Jones DP, Alitalo K, Lahesmaa R, Nagy A , Otonkoski T (2011). Copy number variation and selection during reprogramming to pluripotency. *Nature*. **471**, 58-62.

Ibanez CF , Simi A (2012). p75 neurotrophin receptor signaling in nervous system injury and degeneration: paradox and opportunity. *Trends Neurosci*. **35**, 431-440.

Ieda M, Fu JD, Delgado-Olguin P, Vedantham V, Hayashi Y, Bruneau BG , Srivastava D (2010). Direct reprogramming of fibroblasts into functional cardiomyocytes by defined factors. *Cell*. **142**, 375-386.

Inagaki K, Fuess S, Storm TA, Gibson GA, McTiernan CF, Kay MA , Nakai H (2006). Robust systemic transduction with AAV9 vectors in mice: efficient global cardiac gene transfer superior to that of AAV8. *Molecular therapy : the journal of the American Society of Gene Therapy*. **14**, 45-53.

Israel MA, Yuan SH, Bardy C, Reyna SM, Mu Y, Herrera C, Hefferan MP, Van Gorp S, Nazor KL, Boscolo FS, Carson CT, Laurent LC, Marsala M, Gage FH, Remes AM, Koo EH , Goldstein LS (2012). Probing sporadic and familial Alzheimer's disease using induced pluripotent stem cells. *Nature*. **482**, 216-220.

Itzhaki I, Maizels L, Huber I, Zwi-Dantsis L, Caspi O, Winterstern A, Feldman O, Gepstein A, Arbel G, Hammerman H, Boulos M , Gepstein L (2011). Modelling the long QT syndrome with induced pluripotent stem cells. *Nature*. **471**, 225-229.

Iwasaki H , Akashi K (2007). Myeloid lineage commitment from the hematopoietic stem cell. *Immunity*. **26**, 726-740.

Jablonka S, Beck M, Lechner BD, Mayer C , Sendtner M (2007). Defective Ca2+ channel clustering in axon terminals disturbs excitability in motoneurons in spinal muscular atrophy. *J Cell Biol*. **179**, 139-149.

Jacobson SG, Cideciyan AV, Ratnakaram R, Heon E, Schwartz SB, Roman AJ, Peden MC, Aleman TS, Boye SL, Sumaroka A, Conlon TJ, Calcedo R, Pang JJ, Erger KE, Olivares MB, Mullins CL, Swider M, Kaushal S, Feuer WJ, Iannaccone A, Fishman GA, Stone EM, Byrne BJ , Hauswirth WW (2012). Gene therapy for leber congenital amaurosis caused by RPE65 mutations: safety and efficacy in 15 children and adults followed up to 3 years. *Arch Ophthalmol*. **130**, 9-24.

Jakovcevski I , Zecevic N (2005). Olig transcription factors are expressed in oligodendrocyte and neuronal cells in human fetal CNS. *J Neurosci*. **25**, 10064-10073.

Jedrzejowska M, Borkowska J, Zimowski J, Kostera-Pruszczyk A, Milewski M, Jurek M, Sielska D, Kostyk E, Nyka W, Zaremba J , Hausmanowa-Petrusewicz I (2008).

Unaffected patients with a homozygous absence of the SMN1 gene. *Eur J Hum Genet*. **16**, 930-934.

Jessell TM (2000). Neuronal specification in the spinal cord: inductive signals and transcriptional codes. *Nat Rev Genet*. **1**, 20-29.

Josephson R, Ording CJ, Liu Y, Shin S, Lakshmipathy U, Toumadje A, Love B, Chesnut JD, Andrews PW, Rao MS , Auerbach JM (2007). Qualification of embryonal carcinoma 2102Ep as a reference for human embryonic stem cell research. *Stem Cells*. **25**, 437-446.

Kafri T, Blomer U, Peterson DA, Gage FH , Verma IM (1997). Sustained expression of genes delivered directly into liver and muscle by lentiviral vectors. *Nature genetics*. **17**, 314-317.

Kaji K, Norrby K, Paca A, Mileikovsky M, Mohseni P , Woltjen K (2009). Virus-free induction of pluripotency and subsequent excision of reprogramming factors. *Nature*. **458**, 771-775.

Kang L, Wang J, Zhang Y, Kou Z , Gao S (2009). iPS cells can support full-term development of tetraploid blastocyst-complemented embryos. *Cell stem cell*. **5**, 135-138.

Kaplitt MG, Feigin A, Tang C, Fitzsimons HL, Mattis P, Lawlor PA, Bland RJ, Young D, Strybing K, Eidelberg D , During MJ (2007). Safety and tolerability of gene therapy with an adeno-associated virus (AAV) borne GAD gene for Parkinson's disease: an open label, phase I trial. *Lancet*. **369**, 2097-2105.

Karumbayaram S, Novitch BG, Patterson M, Umbach JA, Richter L, Lindgren A, Conway AE, Clark AT, Goldman SA, Plath K, Wiedau-Pazos M, Kornblum HI , Lowry WE (2009). Directed differentiation of human-induced pluripotent stem cells generates active motor neurons. *Stem Cells*. **27**, 806-811.

Kay MA, Glorioso JC , Naldini L (2001). Viral vectors for gene therapy: the art of turning infectious agents into vehicles of therapeutics. *Nat Med*. **7**, 33-40.

Kim D, Kim CH, Moon JI, Chung YG, Chang MY, Han BS, Ko S, Yang E, Cha KY, Lanza R , Kim KS (2009a). Generation of human induced pluripotent stem cells by direct delivery of reprogramming proteins. *Cell stem cell*. **4**, 472-476.

Kim JB, Greber B, Arauzo-Bravo MJ, Meyer J, Park KI, Zaehres H , Scholer HR (2009b). Direct reprogramming of human neural stem cells by OCT4. *Nature*. **461**, 649-643.

Kim JB, Sebastiano V, Wu G, Arauzo-Bravo MJ, Sasse P, Gentile L, Ko K, Ruau D, Ehrich M, van den Boom D, Meyer J, Hubner K, Bernemann C, Ortmeier C, Zenke M, Fleischmann BK, Zaehres H , Scholer HR (2009c). Oct4-induced pluripotency in adult neural stem cells. *Cell*. **136**, 411-419.

Kissel JT, Scott CB, Reyna SP, Crawford TO, Simard LR, Krosschell KJ, Acsadi G, Elsheik B, Schroth MK, D'Anjou G, LaSalle B, Prior TW, Sorenson S, Maczulski JA, Bromberg MB, Chan GM , Swoboda KJ (2011). SMA CARNIVAL TRIAL PART II: a prospective, single-armed trial of L-carnitine and valproic acid in ambulatory children with spinal muscular atrophy. *PloS one*. **6**, e21296.

Kong L, Wang X, Choe DW, Polley M, Burnett BG, Bosch-Marce M, Griffin JW, Rich MM , Sumner CJ (2009). Impaired synaptic vesicle release and immaturity of neuromuscular junctions in spinal muscular atrophy mice. *J Neurosci*. **29**, 842-851.

Kopp JL, Ormsbee BD, Desler M , Rizzino A (2008). Small increases in the level of Sox2 trigger the differentiation of mouse embryonic stem cells. *Stem Cells*. **26**, 903-911.

Krencik R , Zhang SC (2011). Directed differentiation of functional astroglial subtypes from human pluripotent stem cells. *Nat Protoc*. **6**, 1710-1717.

Kummer TT, Misgeld T, Lichtman JW , Sanes JR (2004). Nerve-independent formation of a topologically complex postsynaptic apparatus. *J Cell Biol*. **164**, 1077-1087.

Laurent L, Wong E, Li G, Huynh T, Tsirigos A, Ong CT, Low HM, Kin Sung KW, Rigoutsos I, Loring J , Wei CL (2010). Dynamic changes in the human methylome during differentiation. *Genome Res*. **20**, 320-331.

Le TT, Pham LT, Butchbach ME, Zhang HL, Monani UR, Coovert DD, Gavrilina TO, Xing L, Bassell GJ , Burghes AH (2005). SMNDelta7, the major product of the centromeric survival motor neuron (SMN2) gene, extends survival in mice with spinal muscular atrophy and associates with full-length SMN. *Hum Mol Genet*. **14**, 845-857.

Lee G, Papapetrou EP, Kim H, Chambers SM, Tomishima MJ, Fasano CA, Ganat YM, Menon J, Shimizu F, Viale A, Tabar V, Sadelain M , Studer L (2009). Modelling pathogenesis and treatment of familial dysautonomia using patient-specific iPSCs. *Nature*. **461**, 402-406.

Lee SK, Jurata LW, Funahashi J, Ruiz EC , Pfaff SL (2004). Analysis of embryonic motoneuron gene regulation: derepression of general activators function in concert with enhancer factors. *Development*. **131**, 3295-3306.

Lee SK , Pfaff SL (2001). Transcriptional networks regulating neuronal identity in the developing spinal cord. *Nat Neurosci*. **4 Suppl**, 1183-1191.

Lee TH, Song SH, Kim KL, Yi JY, Shin GH, Kim JY, Kim J, Han YM, Lee SH, Shim SH , Suh W (2010). Functional recapitulation of smooth muscle cells via induced pluripotent stem cells from human aortic smooth muscle cells. *Circ Res*. **106**, 120-128.

Lee YI, Mikesh M, Smith I, Rimer M , Thompson W (2011). Muscles in a mouse model of spinal muscular atrophy show profound defects in neuromuscular development even in the absence of failure in neuromuscular transmission or loss of motor neurons. *Dev Biol*. **356**, 432-444.

Lefebvre S, Burglen L, Reboullet S, Clermont O, Burlet P, Viollet L, Benichou B, Cruaud C, Millasseau P, Zeviani M , et al. (1995). Identification and characterization of a spinal muscular atrophy-determining gene. *Cell*. **80**, 155-165.

Lefebvre S, Burlet P, Liu Q, Bertrandy S, Clermont O, Munnich A, Dreyfuss G , Melki J (1997). Correlation between severity and SMN protein level in spinal muscular atrophy. *Nat Genet*. **16**, 265-269.

Li XJ, Du ZW, Zarnowska ED, Pankratz M, Hansen LO, Pearce RA , Zhang SC (2005). Specification of motoneurons from human embryonic stem cells. *Nat Biotechnol*. **23**, 215-221.

Li XJ, Hu BY, Jones SA, Zhang YS, Lavaute T, Du ZW , Zhang SC (2008). Directed differentiation of ventral spinal progenitors and motor neurons from human embryonic stem cells by small molecules. *Stem Cells*. **26**, 886-893.

Lin CS, Park T, Chen ZP , Leavitt J (1993). Human plastin genes. Comparative gene structure, chromosome location, and differential expression in normal and neoplastic cells. *J Biol Chem*. **268**, 2781-2792.

Ling KK, Lin MY, Zingg B, Feng Z , Ko CP (2010). Synaptic defects in the spinal and neuromuscular circuitry in a mouse model of spinal muscular atrophy. *PloS one*. **5**, e15457.

Lister R, Pelizzola M, Kida YS, Hawkins RD, Nery JR, Hon G, Antosiewicz-Bourget J, O'Malley R, Castanon R, Klugman S, Downes M, Yu R, Stewart R, Ren B, Thomson JA, Evans RM , Ecker JR (2011). Hotspots of aberrant epigenomic reprogramming in human induced pluripotent stem cells. *Nature*. **471**, 68-73.

Liu GH, Barkho BZ, Ruiz S, Diep D, Qu J, Yang SL, Panopoulos AD, Suzuki K, Kurian L, Walsh C, Thompson J, Boue S, Fung HL, Sancho-Martinez I, Zhang K, Iii JY , Belmonte JC (2011). Recapitulation of premature ageing with iPSCs from Hutchinson-Gilford progeria syndrome. *Nature*.

Liu J, Verma PJ, Evans-Galea MV, Delatycki MB, Michalska A, Leung J, Crombie D, Sarsero JP, Williamson R, Dottori M , Pebay A (2010). Generation of Induced Pluripotent Stem Cell Lines from Friedreich Ataxia Patients. *Stem Cell Rev*.

Liu Q , Dreyfuss G (1996). A novel nuclear structure containing the survival of motor neurons protein. *EMBO J*. **15**, 3555-3565.

Lock M, Alvira M, Vandenberghe LH, Samanta A, Toelen J, Debyser Z , Wilson JM (2010). Rapid, simple, and versatile manufacturing of recombinant adeno-associated viral vectors at scale. *Hum Gene Ther*. **21**, 1259-1271.

Lorson CL , Androphy EJ (2000). An exonic enhancer is required for inclusion of an essential exon in the SMA-determining gene SMN. *Hum Mol Genet*. **9**, 259-265.

Lorson CL, Strasswimmer J, Yao JM, Baleja JD, Hahnen E, Wirth B, Le T, Burghes AH , Androphy EJ (1998). SMN oligomerization defect correlates with spinal muscular atrophy severity. *Nat Genet*. **19**, 63-66.

Lunn MR , Wang CH (2008). Spinal muscular atrophy. *Lancet*. **371**, 2120-2133.

Luo Y, Fan Y, Chen X, Yu B, Yue L, Wang D, Li Q, Chen Y , Sun X (2012). Generation of induced pluripotent stem cells from asian patients with chronic neurodegenerative diseases. *J Reprod Dev*. **58**, 515-521.

Maehr R, Chen S, Snitow M, Ludwig T, Yagasaki L, Goland R, Leibel RL , Melton DA (2009). Generation of pluripotent stem cells from patients with type 1 diabetes. *Proc Natl Acad Sci U S A*. **106**, 15768-15773.

Maherali N , Hochedlinger K (2008). Guidelines and techniques for the generation of induced pluripotent stem cells. *Cell stem cell*. **3**, 595-605.

Maherali N, Sridharan R, Xie W, Utikal J, Eminli S, Arnold K, Stadtfeld M, Yachechko R, Tchieu J, Jaenisch R, Plath K , Hochedlinger K (2007). Directly reprogrammed fibroblasts show global epigenetic remodeling and widespread tissue contribution. *Cell stem cell*. **1**, 55-70.

Mangeot PE, Dollet S, Girard M, Ciancia C, Joly S, Peschanski M , Lotteau V (2011). Protein transfer into human cells by VSV-G-induced nanovesicles. *Mol Ther*. **19**, 1656-1666.

Marchetto MC, Carromeu C, Acab A, Yu D, Yeo GW, Mu Y, Chen G, Gage FH , Muotri AR (2010). A model for neural development and treatment of Rett syndrome using human induced pluripotent stem cells. *Cell*. **143**, 527-539.

Marchetto MC, Muotri AR, Mu Y, Smith AM, Cezar GG , Gage FH (2008). Non-cell-autonomous effect of human SOD1 G37R astrocytes on motor neurons derived from human embryonic stem cells. *Cell Stem Cell*. **3**, 649-657.

Marks WJ, Jr., Bartus RT, Siffert J, Davis CS, Lozano A, Boulis N, Vitek J, Stacy M, Turner D, Verhagen L, Bakay R, Watts R, Guthrie B, Jankovic J, Simpson R, Tagliati M, Alterman R, Stern M, Baltuch G, Starr PA, Larson PS, Ostrem JL, Nutt J, Kieburtz K, Kordower JH , Olanow CW (2010). Gene delivery of AAV2-neurturin for Parkinson's disease: a double-blind, randomised, controlled trial. *Lancet Neurol*. **9**, 1164-1172.

Marks WJ, Jr., Ostrem JL, Verhagen L, Starr PA, Larson PS, Bakay RA, Taylor R, Cahn-Weiner DA, Stoessl AJ, Olanow CW , Bartus RT (2008). Safety and tolerability of intraputaminal delivery of CERE-120 (adeno-associated virus serotype 2-neurturin)

to patients with idiopathic Parkinson's disease: an open-label, phase I trial. *Lancet neurology*. **7**, 400-408.

Martinez TL, Kong L, Wang X, Osborne MA, Crowder ME, Van Meerbeke JP, Xu X, Davis C, Wooley J, Goldhamer DJ, Lutz CM, Rich MM , Sumner CJ (2012). Survival motor neuron protein in motor neurons determines synaptic integrity in spinal muscular atrophy. *J Neurosci*. **32**, 8703-8715.

Martinez-Hernandez R, Bernal S, Also-Rallo E, Alias L, Barcelo M, Hereu M, Esquerda JE , Tizzano EF (2012). Synaptic defects in type i spinal muscular atrophy in human development. *J Pathol*.

Matsa E, Rajamohan D, Dick E, Young L, Mellor I, Staniforth A , Denning C (2011). Drug evaluation in cardiomyocytes derived from human induced pluripotent stem cells carrying a long QT syndrome type 2 mutation. *Eur Heart J*.

Mattis VB, Ebert AD, Fosso MY, Chang CW , Lorson CL (2009). Delivery of a read-through inducing compound, TC007, lessens the severity of a spinal muscular atrophy animal model. *Hum Mol Genet*. **18**, 3906-3913.

May C, Rivella S, Callegari J, Heller G, Gaensler KM, Luzzatto L , Sadelain M (2000). Therapeutic haemoglobin synthesis in beta-thalassaemic mice expressing lentivirus-encoded human beta-globin. *Nature*. **406**, 82-86.

Mayshar Y, Ben-David U, Lavon N, Biancotti JC, Yakir B, Clark AT, Plath K, Lowry WE , Benvenisty N (2010). Identification and classification of chromosomal aberrations in human induced pluripotent stem cells. *Cell stem cell*. **7**, 521-531.

McCarty DM (2008). Self-complementary AAV vectors; advances and applications. *Molecular therapy : the journal of the American Society of Gene Therapy*. **16**, 1648-1656.

McWhorter ML, Monani UR, Burghes AH , Beattie CE (2003). Knockdown of the survival motor neuron (Smn) protein in zebrafish causes defects in motor axon outgrowth and pathfinding. *J Cell Biol*. **162**, 919-931.

Meister G, Eggert C , Fischer U (2002). SMN-mediated assembly of RNPs: a complex story. *Trends Cell Biol*. **12**, 472-478.

Mercuri E, Bertini E, Messina S, Pelliccioni M, D'Amico A, Colitto F, Mirabella M, Tiziano FD, Vitali T, Angelozzi C, Kinali M, Main M , Brahe C (2004). Pilot trial of phenylbutyrate in spinal muscular atrophy. *Neuromuscul Disord*. **14**, 130-135.

Miller DG, Adam MA , Miller AD (1990). Gene transfer by retrovirus vectors occurs only in cells that are actively replicating at the time of infection. *Mol Cell Biol*. **10**, 4239-4242.

Miranda CJ, Santos MM, Ohshima K, Tessaro M, Sequeiros J , Pandolfo M (2004). Frataxin overexpressing mice. *FEBS Lett*. **572**, 281-288.

Miyazaki T, Futaki S, Suemori H, Taniguchi Y, Yamada M, Kawasaki M, Hayashi M, Kumagai H, Nakatsuji N, Sekiguchi K , Kawase E (2012). Laminin E8 fragments support efficient adhesion and expansion of dissociated human pluripotent stem cells. *Nat Commun*. **3**, 1236.

Miyoshi H, Takahashi M, Gage FH , Verma IM (1997). Stable and efficient gene transfer into the retina using an HIV-based lentiviral vector. *Proceedings of the National Academy of Sciences of the United States of America*. **94**, 10319-10323.

Miyoshi N, Ishii H, Nagano H, Haraguchi N, Dewi DL, Kano Y, Nishikawa S, Tanemura M, Mimori K, Tanaka F, Saito T, Nishimura J, Takemasa I, Mizushima T, Ikeda M, Yamamoto H, Sekimoto M, Doki Y , Mori M (2011). Reprogramming of mouse and human cells to pluripotency using mature microRNAs. *Cell stem cell*. **8**, 633-638.

Mizuguchi R, Sugimori M, Takebayashi H, Kosako H, Nagao M, Yoshida S, Nabeshima Y, Shimamura K , Nakafuku M (2001). Combinatorial roles of olig2 and neurogenin2 in the coordinated induction of pan-neuronal and subtype-specific properties of motoneurons. *Neuron*. **31**, 757-771.

Moretti A, Bellin M, Welling A, Jung CB, Lam JT, Bott-Flugel L, Dorn T, Goedel A, Hohnke C, Hofmann F, Seyfarth M, Sinnecker D, Schomig A , Laugwitz KL (2010). Patient-specific induced pluripotent stem-cell models for long-QT syndrome. *N Engl J Med*. **363**, 1397-1409.

Muhr J, Andersson E, Persson M, Jessell TM , Ericson J (2001). Groucho-mediated transcriptional repression establishes progenitor cell pattern and neuronal fate in the ventral neural tube. *Cell*. **104**, 861-873.

Muller FJ, Goldmann J, Loser P , Loring JF (2010). A call to standardize teratoma assays used to define human pluripotent cell lines. *Cell stem cell*. **6**, 412-414.

Muller LU, Milsom MD, Harris CE, Vyas R, Brumme KM, Parmar K, Moreau LA, Schambach A, Park IH, London WB, Strait K, Schlaeger T, Devine AL, Grassman E, D'Andrea A, Daley GQ , Williams DA (2012). Overcoming reprogramming resistance of Fanconi anemia cells. *Blood*. **119**, 5449-5457.

Munsat TL (1992). International SMA collaboration. (26-28 June 1992, Bonn, Germany). *Neuromuscul Disord*. **2**, 423-428.

Murray LM, Comley LH, Thomson D, Parkinson N, Talbot K , Gillingwater TH (2008). Selective vulnerability of motor neurons and dissociation of pre- and post-synaptic pathology at the neuromuscular junction in mouse models of spinal muscular atrophy. *Hum Mol Genet*. **17**, 949-962.

Naldini L, Blomer U, Gallay P, Ory D, Mulligan R, Gage FH, Verma IM , Trono D (1996). In vivo gene delivery and stable transduction of nondividing cells by a lentiviral vector. *Science (New York, N.Y.)*. **272**, 263-267.

Nanou A , Azzouz M (2009). Gene therapy for neurodegenerative diseases based on lentiviral vectors. *Progress in brain research*. **175**, 187-200.

Nelson DL , Gibbs RA (2004). Genetics. The critical region in trisomy 21. *Science*. **306**, 619-621.

Nguyen HN, Byers B, Cord B, Shcheglovitov A, Byrne J, Gujar P, Kee K, Schule B, Dolmetsch RE, Langston W, Palmer TD , Pera RR (2011). LRRK2 mutant iPSC-derived DA neurons demonstrate increased susceptibility to oxidative stress. *Cell stem cell*. **8**, 267-280.

NIH (Last accessed September 2012). ClinicalTrials.goved^eds): NIH.

Niwa H, Miyazaki J , Smith AG (2000). Quantitative expression of Oct-3/4 defines differentiation, dedifferentiation or self-renewal of ES cells. *Nat Genet*. **24**, 372-376.

Nizzardo M, Simone C, Falcone M, Locatelli F, Riboldi G, Comi GP , Corti S (2010). Human motor neuron generation from embryonic stem cells and induced pluripotent stem cells. *Cell Mol Life Sci*. **67**, 3837-3847.

Nonnenmacher M , Weber T (2012). Intracellular transport of recombinant adeno-associated virus vectors. *Gene Ther*. **19**, 649-658.

Novitch BG, Chen AI , Jessell TM (2001). Coordinate regulation of motor neuron subtype identity and pan-neuronal properties by the bHLH repressor Olig2. *Neuron*. **31**, 773-789.

Okita K, Ichisaka T , Yamanaka S (2007). Generation of germline-competent induced pluripotent stem cells. *Nature*. **448**, 313-317.

Okita K, Matsumura Y, Sato Y, Okada A, Morizane A, Okamoto S, Hong H, Nakagawa M, Tanabe K, Tezuka K, Shibata T, Kunisada T, Takahashi M, Takahashi J, Saji H , Yamanaka S (2011). A more efficient method to generate integration-free human iPS cells. *Nat Methods*. **8**, 409-412.

Okita K, Nakagawa M, Hyenjong H, Ichisaka T , Yamanaka S (2008). Generation of mouse induced pluripotent stem cells without viral vectors. *Science (New York, N.Y.)*. **322**, 949-953.

Olson LE, Richtsmeier JT, Leszl J , Reeves RH (2004). A chromosome 21 critical region does not cause specific Down syndrome phenotypes. *Science*. **306**, 687-690.

Oprea GE, Krober S, McWhorter ML, Rossoll W, Muller S, Krawczak M, Bassell GJ, Beattie CE , Wirth B (2008). Plastin 3 is a protective modifier of autosomal recessive spinal muscular atrophy. *Science*. **320**, 524-527.

Orive G, Hernandez RM, Gascon AR, Calafiore R, Chang TM, De Vos P, Hortelano G, Hunkeler D, Lacik I, Shapiro AM , Pedraz JL (2003). Cell encapsulation: promise and progress. *Nat Med*. **9**, 104-107.

Otter S, Grimmler M, Neuenkirchen N, Chari A, Sickmann A , Fischer U (2007). A comprehensive interaction map of the human survival of motor neuron (SMN) complex. *J Biol Chem*. **282**, 5825-5833.

Ouda L, Druga R , Syka J (2012). Distribution of SMI-32-immunoreactive neurons in the central auditory system of the rat. *Brain Struct Funct*. **217**, 19-36.

Pang ZP, Yang N, Vierbuchen T, Ostermeier A, Fuentes DR, Yang TQ, Citri A, Sebastiano V, Marro S, Sudhof TC , Wernig M (2011). Induction of human neuronal cells by defined transcription factors. *Nature*. **476**, 220-223.

Pankratz MT, Li XJ, Lavaute TM, Lyons EA, Chen X , Zhang SC (2007). Directed neural differentiation of human embryonic stem cells via an obligated primitive anterior stage. *Stem Cells*. **25**, 1511-1520.

Papapetrou EP, Tomishima MJ, Chambers SM, Mica Y, Reed E, Menon J, Tabar V, Mo Q, Studer L , Sadelain M (2009). Stoichiometric and temporal requirements of Oct4, Sox2, Klf4, and c-Myc expression for efficient human iPSC induction and differentiation. *Proceedings of the National Academy of Sciences of the United States of America*. **106**, 12759-12764.

Park IH, Zhao R, West JA, Yabuuchi A, Huo H, Ince TA, Lerou PH, Lensch MW , Daley GQ (2008). Reprogramming of human somatic cells to pluripotency with defined factors. *Nature*. **451**, 141-146.

Pasi CE, Dereli-Oz A, Negrini S, Friedli M, Fragola G, Lombardo A, Van Houwe G, Naldini L, Casola S, Testa G, Trono D, Pelicci PG , Halazonetis TD (2011). Genomic instability in induced stem cells. *Cell Death Differ*.

Passini MA, Bu J, Richards AM, Kinnecom C, Sardi SP, Stanek LM, Hua Y, Rigo F, Matson J, Hung G, Kaye EM, Shihabuddin LS, Krainer AR, Bennett CF , Cheng SH (2011). Antisense oligonucleotides delivered to the mouse CNS ameliorate symptoms of severe spinal muscular atrophy. *Sci Transl Med*. **3**, 72ra18.

Passini MA, Bu J, Roskelley EM, Richards AM, Sardi SP, O'Riordan CR, Klinger KW, Shihabuddin LS , Cheng SH (2010). CNS-targeted gene therapy improves survival and motor function in a mouse model of spinal muscular atrophy. *The Journal of clinical investigation*. **120**, 1253-1264.

Pearn J (1980). Classification of spinal muscular atrophies. *Lancet*. **1**, 919-922.

Pellizzoni L (2007). Chaperoning ribonucleoprotein biogenesis in health and disease. *EMBO Rep*. **8**, 340-345.

Pellizzoni L, Kataoka N, Charroux B , Dreyfuss G (1998). A novel function for SMN, the spinal muscular atrophy disease gene product, in pre-mRNA splicing. *Cell*. **95**, 615-624.

Pfaff SL, Mendelsohn M, Stewart CL, Edlund T , Jessell TM (1996). Requirement for LIM homeobox gene Isl1 in motor neuron generation reveals a motor neuron-dependent step in interneuron differentiation. *Cell*. **84**, 309-320.

Pfisterer U, Kirkeby A, Torper O, Wood J, Nelander J, Dufour A, Bjorklund A, Lindvall O, Jakobsson J , Parmar M (2011). Direct conversion of human fibroblasts to dopaminergic neurons. *Proc Natl Acad Sci U S A*. **108**, 10343-10348.

Philippe S, Sarkis C, Barkats M, Mammeri H, Ladroue C, Petit C, Mallet J , Serguera C (2006). Lentiviral vectors with a defective integrase allow efficient and sustained transgene expression in vitro and in vivo. *Proc Natl Acad Sci U S A*. **103**, 17684-17689.

Prior TW, Krainer AR, Hua Y, Swoboda KJ, Snyder PC, Bridgeman SJ, Burghes AH , Kissel JT (2009). A positive modifier of spinal muscular atrophy in the SMN2 gene. *Am J Hum Genet*. **85**, 408-413.

Rabinowitz JE, Xiao W , Samulski RJ (1999). Insertional mutagenesis of AAV2 capsid and the production of recombinant virus. *Virology*. **265**, 274-285.

Ramos-Mejia V, Munoz-Lopez M, Garcia-Perez JL , Menendez P (2010). iPSC lines that do not silence the expression of the ectopic reprogramming factors may display enhanced propensity to genomic instability. *Cell Res*. **20**, 1092-1095.

Raya A, Rodriguez-Piza I, Guenechea G, Vassena R, Navarro S, Barrero MJ, Consiglio A, Castella M, Rio P, Sleep E, Gonzalez F, Tiscornia G, Garreta E, Aasen T, Veiga A, Verma IM, Surralles J, Bueren J , Izpisua Belmonte JC (2009). Disease-corrected haematopoietic progenitors from Fanconi anaemia induced pluripotent stem cells. *Nature*. **460**, 53-59.

Reiser J, Harmison G, Kluepfel-Stahl S, Brady RO, Karlsson S , Schubert M (1996). Transduction of nondividing cells using pseudotyped defective high-titer HIV type 1 particles. *Proc Natl Acad Sci U S A*. **93**, 15266-15271.

Rochette CF, Gilbert N , Simard LR (2001). SMN gene duplication and the emergence of the SMN2 gene occurred in distinct hominids: SMN2 is unique to Homo sapiens. *Hum Genet*. **108**, 255-266.

Roep BO (2007). Are insights gained from NOD mice sufficient to guide clinical translation? Another inconvenient truth. *Ann N Y Acad Sci*. **1103**, 1-10.

Roobrouck VD, Vanuytsel K , Verfaillie CM (2011). Concise review: culture mediated changes in fate and/or potency of stem cells. *Stem Cells*. **29**, 583-589.

Rossoll W, Jablonka S, Andreassi C, Kroning AK, Karle K, Monani UR , Sendtner M (2003). Smn, the spinal muscular atrophy-determining gene product, modulates axon growth and localization of beta-actin mRNA in growth cones of motoneurons. *J Cell Biol*. **163**, 801-812.

Ruiz R, Casanas JJ, Torres-Benito L, Cano R , Tabares L (2010). Altered intracellular Ca2+ homeostasis in nerve terminals of severe spinal muscular atrophy mice. *J Neurosci*. **30**, 849-857.

Russman BS (2007). Spinal muscular atrophy: clinical classification and disease heterogeneity. *J Child Neurol*. **22**, 946-951.

Sanes JR , Lichtman JW (2001). Induction, assembly, maturation and maintenance of a postsynaptic apparatus. *Nat Rev Neurosci*. **2**, 791-805.

Santos F, Hendrich B, Reik W , Dean W (2002). Dynamic reprogramming of DNA methylation in the early mouse embryo. *Developmental biology*. **241**, 172-182.

Sareen D, Ebert AD, Heins BM, McGivern JV, Ornelas L , Svendsen CN (2012). Inhibition of apoptosis blocks human motor neuron cell death in a stem cell model of spinal muscular atrophy. *PLoS One*. **7**, e39113.

Sastry L, Johnson T, Hobson MJ, Smucker B , Cornetta K (2002). Titering lentiviral vectors: comparison of DNA, RNA and marker expression methods. *Gene Ther*. **9**, 1155-1162.

Schultz BR , Chamberlain JS (2008). Recombinant adeno-associated virus transduction and integration. *Molecular therapy : the journal of the American Society of Gene Therapy*. **16**, 1189-1199.

Seibler P, Graziotto J, Jeong H, Simunovic F, Klein C , Krainc D (2011). Mitochondrial Parkin recruitment is impaired in neurons derived from mutant PINK1 induced pluripotent stem cells. *J Neurosci*. **31**, 5970-5976.

Seki T, Yuasa S, Oda M, Egashira T, Yae K, Kusumoto D, Nakata H, Tohyama S, Hashimoto H, Kodaira M, Okada Y, Seimiya H, Fusaki N, Hasegawa M , Fukuda K (2010). Generation of induced pluripotent stem cells from human terminally differentiated circulating T cells. *Cell stem cell*. **7**, 11-14.

Sendtner M (2010). Therapy development in spinal muscular atrophy. *Nat Neurosci*. **13**, 795-799.

Shafey D, MacKenzie AE , Kothary R (2008). Neurodevelopmental abnormalities in neurosphere-derived neural stem cells from SMN-depleted mice. *J Neurosci Res*. **86**, 2839-2847.

Shen S, Bryant KD, Brown SM, Randell SH , Asokan A (2011). Terminal N-linked galactose is the primary receptor for adeno-associated virus 9. *J Biol Chem*. **286**, 13532-13540.

Silani V, Braga M, Botturi A, Cardin V, Bez A, Pizzuti A , Scarlato G (2001). Human developing motor neurons as a tool to study ALS. *Amyotroph Lateral Scler Other Motor Neuron Disord*. **2 Suppl 1**, S69-76.

Silani V, Brioschi A, Braga M, Ciammola A, Zhou FC, Bonifati C, Ratti A, Pizzuti A, Buscaglia M , Scarlato G (1998). Immunomagnetic isolation of human developing motor neurons. *Neuroreport*. **9**, 1143-1147.

Silva AL , Romao L (2009). The mammalian nonsense-mediated mRNA decay pathway: to decay or not to decay! Which players make the decision? *FEBS Lett*. **583**, 499-505.

Singh Roy N, Nakano T, Xuing L, Kang J, Nedergaard M , Goldman SA (2005). Enhancer-specified GFP-based FACS purification of human spinal motor neurons from embryonic stem cells. *Exp Neurol*. **196**, 224-234.

Sinha S , Chen JK (2006). Purmorphamine activates the Hedgehog pathway by targeting Smoothened. *Nat Chem Biol*. **2**, 29-30.

Slack JM (2002). Conrad Hal Waddington: the last Renaissance biologist? *Nature reviews.Genetics*. **3**, 889-895.

Sleigh JN, Gillingwater TH , Talbot K (2011). The contribution of mouse models to understanding the pathogenesis of spinal muscular atrophy. *Dis Model Mech*. **4**, 457-467.

Soldner F, Hockemeyer D, Beard C, Gao Q, Bell GW, Cook EG, Hargus G, Blak A, Cooper O, Mitalipova M, Isacson O , Jaenisch R (2009). Parkinson's disease patient-derived induced pluripotent stem cells free of viral reprogramming factors. *Cell*. **136**, 964-977.

Soler-Botija C, Cusco I, Caselles L, Lopez E, Baiget M , Tizzano EF (2005). Implication of fetal SMN2 expression in type I SMA pathogenesis: protection or pathological gain of function? *J Neuropathol Exp Neurol*. **64**, 215-223.

Soler-Botija C, Ferrer I, Alvarez JL, Baiget M , Tizzano EF (2003). Downregulation of Bcl-2 proteins in type I spinal muscular atrophy motor neurons during fetal development. *J Neuropathol Exp Neurol*. **62**, 420-426.

Soler-Botija C, Ferrer I, Gich I, Baiget M , Tizzano EF (2002). Neuronal death is enhanced and begins during foetal development in type I spinal muscular atrophy spinal cord. *Brain*. **125**, 1624-1634.

Somers A, Jean JC, Sommer CA, Omari A, Ford CC, Mills JA, Ying L, Sommer AG, Jean JM, Smith BW, Lafyatis R, Demierre MF, Weiss DJ, French DL, Gadue P, Murphy GJ, Mostoslavsky G , Kotton DN (2010). Generation of transgene-free lung disease-specific human induced pluripotent stem cells using a single excisable lentiviral stem cell cassette. *Stem Cells*. **28**, 1728-1740.

Sommer CA, Sommer AG, Longmire TA, Christodoulou C, Thomas DD, Gostissa M, Alt FW, Murphy GJ, Kotton DN , Mostoslavsky G (2010). Excision of reprogramming transgenes improves the differentiation potential of iPS cells generated with a single excisable vector. *Stem Cells*. **28**, 64-74.

Song B, Sun G, Herszfeld D, Sylvain A, Campanale NV, Hirst CE, Caine S, Parkington HC, Tonta MA, Coleman HA, Short M, Ricardo SD, Reubinoff B , Bernard CC (2012). Neural differentiation of patient specific iPS cells as a novel approach to study the pathophysiology of multiple sclerosis. *Stem Cell Res*. **8**, 259-273.

Song Z, Cai J, Liu Y, Zhao D, Yong J, Duo S, Song X, Guo Y, Zhao Y, Qin H, Yin X, Wu C, Che J, Lu S, Ding M , Deng H (2009). Efficient generation of hepatocyte-like cells from human induced pluripotent stem cells. *Cell Res*. **19**, 1233-1242.

Stadtfeld M, Nagaya M, Utikal J, Weir G , Hochedlinger K (2008). Induced pluripotent stem cells generated without viral integration. *Science (New York, N.Y.)*. **322**, 945-949.

Stover AE , Schwartz PH (2011). Adaptation of human pluripotent stem cells to feeder-free conditions in chemically defined medium with enzymatic single-cell passaging. *Methods Mol Biol*. **767**, 137-146.

Stratigopoulos G, Lanzano P, Deng L, Guo J, Kaufmann P, Darras B, Finkel R, Tawil R, McDermott MP, Martens W, Devivo DC , Chung WK (2010). Association of plastin 3 expression with disease severity in spinal muscular atrophy only in postpubertal females. *Arch Neurol*. **67**, 1252-1256.

Sumner CJ, Huynh TN, Markowitz JA, Perhac JS, Hill B, Coovert DD, Schussler K, Chen X, Jarecki J, Burghes AH, Taylor JP , Fischbeck KH (2003). Valproic acid increases SMN levels in spinal muscular atrophy patient cells. *Ann Neurol*. **54**, 647-654.

Swoboda KJ, Scott CB, Crawford TO, Simard LR, Reyna SP, Krosschell KJ, Acsadi G, Elsheik B, Schroth MK, D'Anjou G, LaSalle B, Prior TW, Sorenson SL, Maczulski JA, Bromberg MB, Chan GM , Kissel JT (2010). SMA CARNI-VAL trial part I: double-blind, randomized, placebo-controlled trial of L-carnitine and valproic acid in spinal muscular atrophy. *PloS one*. **5**, e12140.

Tada M, Takahama Y, Abe K, Nakatsuji N , Tada T (2001). Nuclear reprogramming of somatic cells by in vitro hybridization with ES cells. *Current biology : CB*. **11**, 1553-1558.

Takahashi K, Tanabe K, Ohnuki M, Narita M, Ichisaka T, Tomoda K , Yamanaka S (2007). Induction of pluripotent stem cells from adult human fibroblasts by defined factors. *Cell*. **131**, 861-872.

Takahashi K , Yamanaka S (2006). Induction of pluripotent stem cells from mouse embryonic and adult fibroblast cultures by defined factors. *Cell*. **126**, 663-676.

Thomson JA, Itskovitz-Eldor J, Shapiro SS, Waknitz MA, Swiergiel JJ, Marshall VS , Jones JM (1998). Embryonic stem cell lines derived from human blastocysts. *Science*. **282**, 1145-1147.

Tiruchinapalli DM, Ehlers MD , Keene JD (2008). Activity-dependent expression of RNA binding protein HuD and its association with mRNAs in neurons. *RNA Biol*. **5**, 157-168.

Tiscornia G, Vivas EL , Izpisua Belmonte JC (2011). Diseases in a dish: modeling human genetic disorders using induced pluripotent cells. *Nat Med*. **17**, 1570-1576.

Tran H, Leonardo T , Peterzon S (2012). Chapter 21 – Generation of Human Pluripotent Stem Cell-Derived Teratomas. In *Human Stem Cell Manual*): Elsevier Inc, pp. 337-343.

Turnpenny L, Brickwood S, Spalluto CM, Piper K, Cameron IT, Wilson DI , Hanley NA (2003). Derivation of human embryonic germ cells: an alternative source of pluripotent stem cells. *Stem Cells*. **21**, 598-609.

usaKariya S, Park GH, Maeno-Hikichi Y, Leykekhman O, Lutz C, Arkovitz MS, Landmesser LT , Monani UR (2008). Reduced SMN protein impairs maturation of the neuromuscular junctions in mouse models of spinal muscular atrophy. *Hum Mol Genet*. **17**, 2552-2569.

Valori CF, Ning K, Wyles M, Mead RJ, Grierson AJ, Shaw PJ , Azzouz M (2010). Systemic delivery of scAAV9 expressing SMN prolongs survival in a model of spinal muscular atrophy. *Science translational medicine*. **2**, 35ra42.

Van Meerbeke JP , Sumner CJ (2011). Progress and promise: the current status of spinal muscular atrophy therapeutics. *Discov Med*. **12**, 291-305.

Vandenberghe LH, Xiao R, Lock M, Lin J, Korn M , Wilson JM (2010). Efficient serotype-dependent release of functional vector into the culture medium during adeno-associated virus manufacturing. *Hum Gene Ther*. **21**, 1251-1257.

Vandendriessche T, Thorrez L, Acosta-Sanchez A, Petrus I, Wang L, Ma L, De Waele L, Iwasaki Y, Gillijns V, Wilson JM, Collen D , Chuah MK (2007). Efficacy and safety of adeno-associated viral vectors based on serotype 8 and 9 vs. lentiviral vectors for hemophilia B gene therapy. *Journal of thrombosis and haemostasis : JTH*. **5**, 16-24.

Veldwijk MR, Topaly J, Laufs S, Hengge UR, Wenz F, Zeller WJ , Fruehauf S (2002). Development and optimization of a real-time quantitative PCR-based method for the titration of AAV-2 vector stocks. *Molecular therapy : the journal of the American Society of Gene Therapy*. **6**, 272-278.

Virag T, Cecchini S , Kotin RM (2009). Producing recombinant adeno-associated virus in foster cells: overcoming production limitations using a baculovirus-insect cell expression strategy. *Human Gene Therapy*. **20**, 807-817.

Vitale AM, Matigian NA, Ravishankar S, Bellette B, Wood SA, Wolvetang EJ , Mackay-Sim A (2012). Variability in the generation of induced pluripotent stem cells: importance for disease modeling. *Stem Cells Transl Med*. **1**, 641-650.

Vogt P (1997). Retroviral Virions and Genomes. In *Retroviruses*. (J Coffin, S Hughes , H Varmus, ed^eds): Cold Spring Harbor (NY).

Wada T, Honda M, Minami I, Tooi N, Amagai Y, Nakatsuji N , Aiba K (2009). Highly efficient differentiation and enrichment of spinal motor neurons derived from human and monkey embryonic stem cells. *PloS one*. **4**, e6722.

Waddington CH (1957). *The Strategy of the Genes*. London: George Allen & Unwin.

Wang CH, Xu J, Carter TA, Ross BM, Dominski MK, Bellcross CA, Penchaszadeh GK, Munsat TL , Gilliam TC (1996). Characterization of survival motor neuron (SMNT) gene deletions in asymptomatic carriers of spinal muscular atrophy. *Hum Mol Genet*. **5**, 359-365.

Wanisch K , Yanez-Munoz RJ (2009). Integration-deficient lentiviral vectors: a slow coming of age. *Molecular therapy : the journal of the American Society of Gene Therapy*. **17**, 1316-1332.

Warren L, Manos PD, Ahfeldt T, Loh YH, Li H, Lau F, Ebina W, Mandal PK, Smith ZD, Meissner A, Daley GQ, Brack AS, Collins JJ, Cowan C, Schlaeger TM , Rossi DJ (2010). Highly efficient reprogramming to pluripotency and directed differentiation of human cells with synthetic modified mRNA. *Cell stem cell*. **7**, 618-630.

Warrington KH, Jr., Gorbatyuk OS, Harrison JK, Opie SR, Zolotukhin S , Muzyczka N (2004). Adeno-associated virus type 2 VP2 capsid protein is nonessential and can tolerate large peptide insertions at its N terminus. *Journal of virology*. **78**, 6595-6609.

Wernig M, Meissner A, Foreman R, Brambrink T, Ku M, Hochedlinger K, Bernstein BE , Jaenisch R (2007). In vitro reprogramming of fibroblasts into a pluripotent ES-cell-like state. *Nature*. **448**, 318-324.

White K Advances in Viral-Based Gene Delivery Vector Systems. Stratagene, Technical supported^eds).

Wichterle H, Lieberam I, Porter JA , Jessell TM (2002). Directed differentiation of embryonic stem cells into motor neurons. *Cell*. **110**, 385-397.

Wiese S, Herrmann T, Drepper C, Jablonka S, Funk N, Klausmeyer A, Rogers ML, Rush R , Sendtner M (2010). Isolation and enrichment of embryonic mouse motoneurons from the lumbar spinal cord of individual mouse embryos. *Nat Protoc*. **5**, 31-38.

Wiley (Last updated June 2012). Gene Therapy Cinical Trials Worldwideed^eds): The Journal of Gene Medicine.

Wilmut I, Schnieke AE, McWhir J, Kind AJ , Campbell KH (1997). Viable offspring derived from fetal and adult mammalian cells. *Nature*. **385**, 810-813.

Wirth B, Brichta L, Schrank B, Lochmuller H, Blick S, Baasner A , Heller R (2006). Mildly affected patients with spinal muscular atrophy are partially protected by an increased SMN2 copy number. *Hum Genet*. **119**, 422-428.

Wistuba A, Kern A, Weger S, Grimm D , Kleinschmidt JA (1997). Subcellular compartmentalization of adeno-associated virus type 2 assembly. *Journal of virology*. **71**, 1341-1352.

Woltjen K, Michael IP, Mohseni P, Desai R, Mileikovsky M, Hamalainen R, Cowling R, Wang W, Liu P, Gertsenstein M, Kaji K, Sung HK , Nagy A (2009). piggyBac transposition reprograms fibroblasts to induced pluripotent stem cells. *Nature*. **458**, 766-770.

Wu X, Walker J, Zhang J, Ding S , Schultz PG (2004). Purmorphamine induces osteogenesis by activation of the hedgehog signaling pathway. *Chem Biol*. **11**, 1229-1238.

Wu Z, Asokan A , Samulski RJ (2006). Adeno-associated virus serotypes: vector toolkit for human gene therapy. *Molecular therapy : the journal of the American Society of Gene Therapy*. **14**, 316-327.

Xiao X, Li J , Samulski RJ (1998). Production of high-titer recombinant adeno-associated virus vectors in the absence of helper adenovirus. *J Virol*. **72**, 2224-2232.

Xie H, Ye M, Feng R , Graf T (2004). Stepwise reprogramming of B cells into macrophages. *Cell*. **117**, 663-676.

Xu Y, Zhu X, Hahm HS, Wei W, Hao E, Hayek A , Ding S (2010). Revealing a core signaling regulatory mechanism for pluripotent stem cell survival and self-renewal by small molecules. *Proc Natl Acad Sci U S A*. **107**, 8129-8134.

Yahata N, Asai M, Kitaoka S, Takahashi K, Asaka I, Hioki H, Kaneko T, Maruyama K, Saido TC, Nakahata T, Asada T, Yamanaka S, Iwata N , Inoue H (2011). Anti-Abeta drug screening platform using human iPS cell-derived neurons for the treatment of Alzheimer's disease. *PloS one*. **6**, e25788.

Yanez-Munoz RJ, Balaggan KS, MacNeil A, Howe SJ, Schmidt M, Smith AJ, Buch P, MacLaren RE, Anderson PN, Barker SE, Duran Y, Bartholomae C, von Kalle C, Heckenlively JR, Kinnon C, Ali RR , Thrasher AJ (2006). Effective gene therapy with nonintegrating lentiviral vectors. *Nat Med*. **12**, 348-353.

Yazawa M, Hsueh B, Jia X, Pasca AM, Bernstein JA, Hallmayer J , Dolmetsch RE (2011). Using induced pluripotent stem cells to investigate cardiac phenotypes in Timothy syndrome. *Nature*. **471**, 230-234.

Ymlahi-Ouazzani Q, O JB, Paillard E, Ballagny C, Chesneau A, Jadaud A, Mazabraud A , Pollet N (2010). Reduced levels of survival motor neuron protein leads to aberrant motoneuron growth in a Xenopus model of muscular atrophy. *Neurogenetics*. **11**, 27-40.

Yoshida Y , Yamanaka S (2010). Recent stem cell advances: induced pluripotent stem cells for disease modeling and stem cell-based regeneration. *Circulation*. **122**, 80-87.

Yu DL, Linnerth-Petrik NM, Halbert CL, Walsh SR, Miller AD , Wootton SK (2011). Jaagsiekte sheep retrovirus and enzootic nasal tumor virus promoters drive gene expression in all airway epithelial cells of mice but only induce tumors in the alveolar region of the lungs. *J Virol*. **85**, 7535-7545.

Yu J, Hu K, Smuga-Otto K, Tian S, Stewart R, Slukvin II , Thomson JA (2009). Human induced pluripotent stem cells free of vector and transgene sequences. *Science (New York, N.Y.)*. **324**, 797-801.

Yu J, Vodyanik MA, Smuga-Otto K, Antosiewicz-Bourget J, Frane JL, Tian S, Nie J, Jonsdottir GA, Ruotti V, Stewart R, Slukvin II , Thomson JA (2007). Induced pluripotent stem cell lines derived from human somatic cells. *Science (New York, N.Y.)*. **318**, 1917-1920.

Yue Y , Dongsheng D (2002). Development of multiple cloning site cis-vectors for recombinant adeno-associated virus production. *Biotechniques*. **33**, 672, 674, 676-678.

Zhang D, Jiang W, Liu M, Sui X, Yin X, Chen S, Shi Y , Deng H (2009a). Highly efficient differentiation of human ES cells and iPS cells into mature pancreatic insulin-producing cells. *Cell research*. **19**, 429-438.

Zhang J, Lian Q, Zhu G, Zhou F, Sui L, Tan C, Mutalif RA, Navasankari R, Zhang Y, Tse HF, Stewart CL , Colman A (2011). A human iPSC model of Hutchinson Gilford Progeria reveals vascular smooth muscle and mesenchymal stem cell defects. *Cell Stem Cell*. **8**, 31-45.

Zhang J, Wilson GF, Soerens AG, Koonce CH, Yu J, Palecek SP, Thomson JA , Kamp TJ (2009b). Functional cardiomyocytes derived from human induced pluripotent stem cells. *Circ Res*. **104**, e30-41.

Zhao XY, Li W, Lv Z, Liu L, Tong M, Hai T, Hao J, Guo CL, Ma QW, Wang L, Zeng F , Zhou Q (2009). iPS cells produce viable mice through tetraploid complementation. *Nature*. **461**, 86-90.

Zhou H, Wu S, Joo JY, Zhu S, Han DW, Lin T, Trauger S, Bien G, Yao S, Zhu Y, Siuzdak G, Scholer HR, Duan L , Ding S (2009). Generation of induced pluripotent stem cells using recombinant proteins. *Cell stem cell*. **4**, 381-384.

Zolotukhin S, Byrne BJ, Mason E, Zolotukhin I, Potter M, Chesnut K, Summerford C, Samulski RJ , Muzyczka N (1999). Recombinant adeno-associated virus purification using novel methods improves infectious titer and yield. *Gene therapy*. **6**, 973-985.

Zufferey R, Dull T, Mandel RJ, Bukovsky A, Quiroz D, Naldini L , Trono D (1998). Self-inactivating lentivirus vector for safe and efficient in vivo gene delivery. *J Virol*. **72**, 9873-9880.

APPENDIX

APPENDIX 1: List of reagents and molecules

GENERAL REAGENTS

- ✓ 3-[N-morpholino]propanesulfonic acid (MOPS) (Sigma-Aldrich)
- ✓ 30% Acrylamide/Bis-acrylamide (Merk)
- ✓ 4',6-diamino-2'-phenylindole dihydroclhoride (DAPI) (Sigma-Aldrich)
- ✓ Acetone (Sigma-Aldrich)
- ✓ Agarose (Sigma-Aldrich)
- ✓ Alpha amylase from porcine pancreas (Sigma-Aldrich)
- ✓ Ammonium persulfate (Sigma-Aldrich)
- ✓ Ampicilin (Sigma-Aldrich)
- ✓ Bacteriological agar (Sigma-Aldrich)
- ✓ Bovine serum albumin (BSA) (Sigma-Aldrich)
- ✓ Bromophenol blue (Sigma-Aldrich)
- ✓ $CaCl_2$ (Sigma-Aldrich)
- ✓ Dimethyl sulfoxide (DMSO) (Sigma-Aldrich)
- ✓ Dithiothreitol (DTT) (Sigma-Aldrich)
- ✓ Ethanol (Sigma-Aldrich)
- ✓ Ethidium bromide (Sigma-Aldrich)
- ✓ Ethylene Glycol (Sigma-Aldrich)
- ✓ Ethylenediaminetetraacetic acid (EDTA) (Sigma-Aldrich)
- ✓ Formaldehyde (Sigma-Aldrich)
- ✓ Gelatine (Sigma-Aldrich)
- ✓ Glycerol (Sigma-Aldrich)
- ✓ Glycine (Sigma-Aldrich)
- ✓ HBSS without Ca & Mg with Phenol Red (PAA, Cat. No. H15-010)
- ✓ HCl (Sigma-Aldrich)
- ✓ HEPES (Sigma-Aldrich)
- ✓ HEPES Buffer Solution (Life Technologies)
- ✓ Isopropanol (Sigma-Aldrich)
- ✓ KOAc (Sigma-Aldrich)
- ✓ Luria Broth (Sigma-Aldrich)
- ✓ Methanol (Sigma-Aldrich)
- ✓ $MgCl_2$ (Sigma-Aldrich)
- ✓ $MnC1_2$ (Sigma-Aldrich)
- ✓ Na_2HPO_4 (Sigma-Aldrich)
- ✓ NaCl (Sigma-Aldrich)
- ✓ NaOH (Sigma-Aldrich)
- ✓ PBS (PAA)
- ✓ PEG8000 (Sigma-Aldrich)
- ✓ PFA (Sigma-Aldrich)
- ✓ Phenol Red solution (Sigma-Aldrich)
- ✓ $RbC1_2$ (Sigma-Aldrich)
- ✓ Sodium acetate (Sigma-Aldrich)
- ✓ Sodium Dodecyl Sulfate (SDS) (Sigma-Aldrich)
- ✓ Sudan III (Sigma-Aldrich)
- ✓ Sudan IV (Sigma-Aldrich)

- ✓ TEMED (Sigma-Aldrich)
- ✓ Tissue culture grade water (PAA)
- ✓ Trehalosa (Sigma-Aldrich)
- ✓ Tris (Sigma-Aldrich)
- ✓ Triton X-100 (Sigma-Aldrich)
- ✓ Trypan blue (Sigma-Aldrich)
- ✓ Tween-20 (Sigma-Aldrich)

SPECIAL REAGENTS AND MEDIA COMPONENTS

- ✓ β- mercaptoetanol (Gibco, Cat. No. 31350010)
- ✓ 25:24:1 phenol/chloroform/isoamyl alcohol (Invitrogen, Cat No. 15593-031)
- ✓ Amersham Hybond™ ECL™ membrane 0.45 μM (GE Healthcare, Cat. No. RPN303D)
- ✓ Aqua-Poly/Mount (Polysciences, Cat. No 18606-20)
- ✓ b-Mercaptoethanol (Gibco, cat. no. 31350010)
- ✓ B27 supplement without vitamin A 50X (Gibco, Cat. No. 12587-010)
- ✓ Benzonase (Sigma-Aldrich, Cat. No. E8263)
- ✓ Colchicine (Sigma-Aldrich, Cat No. C 3915)
- ✓ cOmplete ULTRA Tablets, Mini, EDTA-free (Roche, Cat No. 05892791001)
- ✓ CryoStem freezing medium (Stemgent, Cat. No. 130-095-847)
- ✓ CryoStem™ Freezing Medium (Stemgent Cat. No. 01-0013)
- ✓ Cyclic AMP (Sigma-Aldrich, cat. no. D-0260)
- ✓ Dexamethasone (Sigma-Aldrich, Cat. No. D4902)
- ✓ Dispase (Gibco-BRL, cat. no. 17105-041)
- ✓ DMEM high glucose with stable glutamine (PAA, Cat. No. E15-883)
- ✓ DMEM Nutrient mix F12 (DMEM/F12) (Gibco, Cat. No 11330032)
- ✓ DMEM, high glucose with glutamax (Gibco Cat. No. 31965023)
- ✓ DNAse I (Promega, Cat. No. M6101)
- ✓ FACs Flow solution (BD Biosciences, Cat. No. 342003)
- ✓ FACs Rinse solution (BD Biosciences, Cat. No. 3403346)
- ✓ FACS shutdown solution (BD Biosciences, Cat. No. 334224)
- ✓ Fetal Bovine serum (FBS) (Gibco, Cat. No. 10099-141)
- ✓ Fetal Bovine serum (FBS) (PAA, Cat. No. H15-101)
- ✓ Fugene HG Transfection Reagent (Roche, Cat. No. 04709705001)
- ✓ Gentamicine (Gibco, Cat. No. 15710-049)
- ✓ Glutamax (Gibco, Cat. No. 35050038)
- ✓ Glycogen (Invitrogen, Cat No. 10814-010)
- ✓ HCM bullet kit (Lonza, Cat. No. cc3198)
- ✓ Heparin (Sigma-Aldrich, cat. no. H3149)
- ✓ Horse serum (Gibco, Cat. No. 16050-130)
- ✓ Hybond N+ hybridisation membrane (GE healthcare, Cat. No RPN203B)
- ✓ Insulin-Transferrin-Selenium-X (Gibco, Cat. No 51500-056)
- ✓ Knockout D-MEM (Gibco, Cat. No 10829018)
- ✓ Knockout Serum Replacement (Gibco-BRL, cat. no. 10828)
- ✓ Knockout serum replacement (Gibco, Cat. No. 10828010)
- ✓ L-Ascorbic acid (Sigma-Aldrich cat. no. A4403)
- ✓ L-Ascorbic acid 2-phosphate sesquimagnesium salt hydrate (Sigma-Aldrich cat. no. A8960)

- ✓ L-Glutamine solution (Gibco-BRL, cat. no. 25030)
- ✓ Medium 199 with Earle's BSS, with L-glutamine, HEPES and 2.2 g/L NaHCO3 (Lonza, Cat. No. 12117F)
- ✓ MEM Alpha Modification Liquid with Ribonucleosides L-glutamine (PAA, Cat. No. E15-862)
- ✓ MEM non-essential amino acids (Gibco-BRL, cat. no. 11140035)
- ✓ Mitomycin C (Sigma-Aldrich, Cat. No. M4287)
- ✓ Mouse Laminin (Sigma-Aldrich cat. no. L2020)
- ✓ N2 supplement 100X (Gibco, Cat. No. 17502-048)
- ✓ Non essential amino acids 100X (Gibco, Cat. No. 11140035)
- ✓ Oncostatin-M (R&D Systems, Cat. No. 295-OM-010)
- ✓ Optiprep Density Gradient Medium (60% (w/v) solution of iodixanol in water (Sigma-Aldrich, Cat. No. D1556).
- ✓ Penicillin and streptomycin (Pen&Strep) (PAA, Cat. No. P11-010)
- ✓ Poly-L-Ornithine solution (Sigma-Aldrich cat. no. P4957)
- ✓ Polybrene (Sigma-Aldrich, Cat No H-9268)
- ✓ Proteinase K (Ambion, Cat No. AM2546)
- ✓ Purmorphamine (CALBIOCHEM, cat. no. 540220)
- ✓ Recombinant BDNF (PeproTech, cat. no. 450-02)
- ✓ Recombinant BMP_2 (PeproTech, Cat. No 120-02)
- ✓ Recombinant EGF (Miltenyi, Cat. No. 130-093-825)
- ✓ Recombinant FGF_2 (Miltenyi, Cat. No. 130-093-837)
- ✓ Recombinant FGF_4 (PeproTech, Cat. No 100-31)
- ✓ Recombinant GDNF (PeproTech, cat. no. 450-10)
- ✓ Recombinant HGF (PeproTech, Cat. No 100-39)
- ✓ Recombinant Human Activin A (PeproTech, Cat. No 120-14E)
- ✓ Recombinant IGF-1 (PeproTech, cat. no. 100-11)
- ✓ Recombinant KGF (PeproTech, Cat. No 100-19)
- ✓ Retinoic Acid (Sigma-Aldrich, cat. no. R2625)
- ✓ Rock Inhibitor (Calbiochem, Cat. No. 688000)
- ✓ RPMI 1640 medium (Gibco, Cat. No. A10491-01)
- ✓ SensiMixPlus SYBR 1X (Quantance, Cat. No. QT605-02)
- ✓ SIGMAFAST™ BCIP®/NBT (5-bromo-4-chloro-3-indolylphosphate/nitro blue tetrazolium. Sigma-Aldrich. Cat No. B5655).
- ✓ Sodium pyruvate MEM (Gibco, Cat. No. 11360-039)
- ✓ Stemedia NutriStem XF/FF Culture Medium (Stemgent, Cat. No. 130-095-543)
- ✓ Stempro accutase (Gibco, Cat. No. A1110501)
- ✓ TaqMan® Universal PCR Master Mix (Applied Byosystems, Cat. No. 4324018)
- ✓ Thiazovivin (Stemgent, Cat. No. 130-095-568)
- ✓ Tris-EDTA endotoxin-free. Taken from Qiagen Endotoxin-free kits (12381, 12362, 12391)
- ✓ TRIZOL® Reagent (Invitrogen, Cat. No. 15596-018)
- ✓ TrypLE Express (1X), Phenol Red (Gibco, Cat. No. 12605028)
- ✓ Trypsin/EDTA (PAA , Cat. No. L11-004)
- ✓ Valproic acid (Sigma-Aldrich, Cat. No., P4543)
- ✓ Vitro PBS (VitroLife, Cat. No. 10506)
- ✓ X-tremeGENE 9 DNA Transfection Reagent (Roche, Cat No. 06365779001).
- ✓ α-Amylase (Sigma-Aldrich Cat. No. A 3176)

APPENDIX 2: Primers. Description, characteristics and sequences

Name	Use	Target	Product size (bp)	Sequence designation	Sequence (5' to 3')
Flag hSMN1	Cloning	Human *Survival Motor Neuron 1* cDNA (Designed by me)	937	Forward	GCACGTACCGGTATGGATTACAAGGATGACGACGATAAGATGGCGATGAGCAGCGG
hSMN1	Cloning		910	Forward	GCACGTACCGGTATGGCGATGAGCAGCGG
F/NoF hSMN1	Cloning			Reverse	GCTTGCCTGCAGGTTAATTTAAGGAATGTGAGCACCTTCC
Cag promoter	Sequencing	Cytomegalovirus enhancer/ chicken beta actin promoter in scAAV9Cagh*SMN1*NoF and scAAV9Cagh*SMN1*F (Designed by me)	NA	Forward	CCTATAAAAAGCGAAGCGCG
Poly A	Sequencing	Poly A in scAAV9Cagh*SMN1*NoF and scAAV9Cagh*SMN1*F (Designed by me)	NA	Reverse	CCCCCTGAACCTGAAACATAAAATG
Poly A qPCR	qPCR. AAV titter	Poly A sequence in scAAV (Designed by me)	103	Forward	CCAAGCTGACCTGACTCGATGC
				Reverse	CCCCCTGAACCTGAAACATAAAATG
CMV probe	Dot blot. AAV titter	Cytomegalovirus enhancer in scAAV (Designed by me)	333	Forward	GCGTTGACATTGATTATTGACTA
				Reverse	CATAAGGTCATGTACTGGGC
LRT	qPCR. lentiviral titter	Lonf terminal repeat sequence in lentiviral backbone *(Butlet et al., 2001*)	140	Forward	TGTGTGCCCGTCTGTTGTGT
				Reverse	GAGTCCTGCGTCGAGAGAGC
ß-actin lenti	qPCR. lentiviral titter	mRNA of human *ß-actin* (Designed by Dr Klaus Wanish)	294	Forward	TCACCCACACTGTGCCCATCTACGA
				Reverse	CAGCGGAACCGCTCATTGCCAATGG
c-MYC endo	q-RT-PCR. Quality control of iPSCs	Endogenous expression of *c-MYC (Park et al., 2008)*	192	Forward	TGCCTCAAATTGGACTTTGG
				Reverse	GATTGAAATTCTGTGTAACTGC
c-MYC total		Total expression o*f c-MYC (Park et al., 2008)*	159	Forward	ACTCTGAGGAGGAACAAGAA
				Reverse	TGGAGACGTGGCACCTCTT
OCT4 endo		Endogenous expression of *OCT4 (Park et al., 2008)*	154	Forward	CCTCACTTCACTGCACTGTA
				Reverse	CAGGTTTTCTTTCCCTAGCT
OCT4 total		Total expression of *OCT4 (Park et al., 2008)*	142	Forward	AGCGAACCAGTATCGAGAAC
				Reverse	TTACAGAACCACACTCGGAC
Kfl4 endo		Endogenous expression of *KFL4 (Park et al., 2008)*	145	Forward	GATGAACTGACCAGGCACTA
				Reverse	GTGGGTCATATCCACTGTCT
KFL4 total		Total expression of *KFL4 (Park et al., 2008)*	105	Forward	TCTCAAGGCACACCTGCGAA
				Reverse	TAGTGCCTGGTCAGTTCATC
SOX2 endo		Endogenous expression of *SOX2 (Park et al., 2008)*	151	Forward	CCCAGCAGACTTCACATGT
				Reverse	CCTCCCATTTCCCTCGTTTT
SOX2 total		Total expression of *SOX2 (Park et al., 2008)*	126	Forward	AGCTACAGCATGATGCAGGA
				Reverse	GGTCATGGAGTTGTACTGCA
RPL13A		cDNA of *ribosomal protein L13a* (Designed by me)	86	Forward	CTACGACAAGAAAAAGCGGA
				Reverse	GCCCCAGATAGGCAAAC
18S		cDNA of *18S ribosomal RNA* (Designed in iSTEM)	166	Forward	GAGGATGAGGTGGAACGTGT
				Reverse	TCTTCAGTCGCTCCAGGTCT

Name	Use	Target	Product size (bp)	Sequence designation	Sequence (5' to 3')
Transgene OCT4	RT-PCR. Quality control of iPSCs	Transgene expression of *OCT4* (*Park et al., 2008*)	~100	Forward	CCTCACTTCACTGCACTGTA
				Reverse	CCTTGAGGTACCAGAGATCT
Trangene SOX2		Transgene expression of *SOX2* (*Park et al., 2008*)	~120	Forward	CCCAGCAGACTTCACATGT
				Reverse	CCTTGAGGTACCAGAGATCT
Trangene c-MYC		Transgene expression of *c-MYC* (*Park et al., 2008*)	~180	Forward	TGCCTCAAATTGGACTTTGG
				Reverse	CGCTCGAGGTTAACGAATT
Transgene KFL4		Transgene expression of *KFL4* (*Park et al., 2008*)	~150	Forward	GATGAACTGACCAGGCACTA
				Reverse	CCTTGAGGTACCAGAGATCT
FL-SMN	q RT-PCR in cells during MN differentiation	cDNA of full length human *survival motor neuron* (*Also-Rallo et al., 2011*)		Forward	GCT GAT GCT TTG GGA AGT ATG TTA
				Reverse	CAC CTT CCT TCT TTT TGA TTT TGT C
				Taqman probe	5'FAM-TTT CAT GGT ACA TGA GTG GCT ATC ATA CTG GCT ATT AT-MGBNFQ
D7-SMN		cDNA of delta 7 human *survival motor neuron* (*Also-Rallo et al., 2011*)		Forward	TGG ACC ACC AAT AAT TCC CC
				Reverse	ATG CCA GCA TTT CCA TAT AAT AGC C
				Taqman probe	FAM-ACC ACC TCC CAT ATG TCC AGA TTC TCT TGA TG-MGBNFQ
SMN total		cDNA of human *survival of motor neuron 1, telomeric and survival of motor neuron 2, centromeric* (SMN). (Applied Biosystems Cat No. Hs00165806_m1)	126	NA	Exon junction 1-2
PLS3		cDNA of *plastin 3*. (Applied Biosystems Cat No. Hs00192406_m1)	85	NA	Exon junction 8-9
GAPDH		cDNA of *glyceraldehyde-3-phosphate dehydrogenase.* (Applied Biosystems Cat No Hs02758991_g1)	93	NA	Exon junction 7-8
PPIA		cDNA of *peptidylprolyl isomerase A (cyclophilin A)* (Applied Biosystems Hs99999904_m1)	98	NA	Exon 4
ß-actin qPCR		cDNA of beta actin (Applied Biosystems Cat Hs99999903_m1)	171	NA	Exon 1
SMN Exon 6-8	SMN Qualitative RT-PCR and spliced isoform dection	cDNA of full length and delta 7 human *survival motorn neuron* (*Soler-Botija et al., 2005*)	1000	Forward	CTCCCATATGTCCAGATTCTCTTG
				Reverse	CTACAACACCCTTCTCACAG

APPENDIX 3: Quality control of the primers used for qRT-PCR/qPCR experiments.

Target	QC performed	Melting curve	Minimum linear dilution	Efficiency	R2	Slope	Gel	Signal in gel
RPL13A	RHUL (me)	good	tested: 1:1000	1.01	0.997	"-3.307"	1 product	intermediate
18S		good	tested: 1:1000	1.01	0.998	"-3.294"	1 product	strong
SOX2 endo		good	tested: 1 in 1000	0.98	0.999	"-3.373"	1 product	strong
SOX2 total		good	tested: 1 in 1000	0.98	0.993	"-3.376"	1 product	strong
OCT4 endo		good	tested: 1 in 1000	1.03	0.990	"-3.247"	1 product with faint primer dimers	strong
OCT4 total		good	tested: 1 in 1000	1.03	0.990	"-3.250"	1 product	strong
KFL4 endo		good	1 in 100	0.98	0.970	"-3.366"	1 product	intermediate
KFL4 total		good	1 in 10	1.02	0.990	"3.323"	1 product	dim
c-MYC endo		good	1 in 10	1.07	1.0	"-3,162"	1 product	very dim
c-MYC total		good	1 in 10	1.15	0.960	"-3.241"	1 product	very strong
Poly A qPCR		good	100 copies	1.07	0.998	"-3.169"	1 product	very strong
FL-SMN	Spain (Dr Sara Bernal)		1 in 1000		0.9926			
D7-SMN			1 in 100		0.976			
SMN total			1 in 10,000		0.9997			
PLS3			1 in 10,000		0.9991			
ACTB			1 in 10,000		0.9995			
GADPH			1 in 10,000		0.9988			
PPIA			1 in 10,000		0.9988			

*Not all the data of the primers that were validated in another laboratory are available. QC: quality control.

APPENDIX 4: iPSC clones selected from each family member

Fibroblasts AC

Cryovials frozen	Clones	Passage number at the time of freezing
4	25	p5
7	28	p6
4	29	p6
4	30	p6
3	59	p5

Fibroblasts CC

Cryovials frozen	Clones	Passage number at the time of freezing
NONE		

Fibroblasts NC

Cryovials frozen	Clones	Passage number at the time of freezing
7	21	p6
4	32	p5
4	42	p5
3	43	p6
2	61	p5

Fibroblasts RC

Cryovials frozen	Clones	Passage number at the time of freezing
4 + 7	26	p12

Fibroblasts TC

Cryovials frozen	Clones	Passage number at the time of freezing
4	63	p6
4 + 4	64	p6

First clone selected for quality control
Second selection for quality control

APPENDIX 5: List of plastic ware and culture surfaces

- ✓ BD Falcon™ round-bottom tubes for flow cytometry (BD Biosciences)
- ✓ Cell strainers (BD Biosciences)
- ✓ Centre well organ culture dish 60 x 15 mm (BD Biosciences)
- ✓ Centrifugal filters Amicon Ultra -15 PL100 (Millipore)
- ✓ Conical polystyrene tubes 15 and 50ml (Corning)
- ✓ Cryovials 1.5, and 2 ml (Nalgene)
- ✓ Eppendorfs tubes 2, 1.5 and 0.5 ml (Eppendorf)
- ✓ Freezing container (Nalgene)
- ✓ Glass coverslips 10 mm No 1.5 (Marienfeld GmbH)
- ✓ Hidrocell 6 multidish (Thermo Fisher)
- ✓ Inoculation loop (Greiner bio-one)
- ✓ Multidish 4 well Nuclon Delta (Nunc)
- ✓ Needles 23 G X 1' 0.6x25 mm (Terumo)
- ✓ Pipettes polystyrene 5, 10 and 25 ml (Corning)
- ✓ qPCR tubes 0.1ml (Qiagen)
- ✓ Stericup & Steritop filtration system 250 and 500 ml (Millipore)
- ✓ Sterile Syringes (BD Biosciences)
- ✓ Syringe SFCA Filters 0.2 um and 0.45 um (Nalgene)
- ✓ Syringes 1, 5, 20 and 50 ml (BD biosciences)
- ✓ TC chamber slide 4 well gamma radiation sterilised Permanox 1.8cm2/well 0.33mm x 0.28mm x 0.2mm Lab Tek (Thermo Scientific Nunc)
- ✓ Tips and filter tips (StartLab)
- ✓ Tissue culture dish 35 mm with 4 inner rings (Cellstart, Greiner bio-one)
- ✓ Tissue culture flat tubes 10 cm_2 with screw cap (TPP)
- ✓ Tissue culture treated polystyrene Flasks 25, 75 and 175 cm_2 (Corning)
- ✓ Tissue culture treated polystyrene petri dishes 30, 60, 100 and 150 mm (Corning)
- ✓ Tissue culture treated polystyrene plates 6, 12, 24 and 96 wells (Corning)
- ✓ Tube, QuickSeal®, Polyallomer, 39 mL, 25 x 89 mm (Beckman Coulter)
- ✓ Tube, Thinwall, Polyallomer, 17 mL, 16 x 102 mm (Beckman Coulter)

APPENDIX 6: LIST OF INSTRUMENTS AND SOFTWARE

INSTRUMENTS

- ✓ Balance EK-610i (A&D Company Limited)
- ✓ BD FACSCanto™ II (BD Biosciences)
- ✓ Biophotometer 613101139 (Eppendorf)
- ✓ Biosafety cabinet Class II (Esco)
- ✓ Centrifuge tube sealer, 50 Hz (Beckman Coulter)
- ✓ Digital Block Heater D110 (Jencons-PLS)
- ✓ Electrophoresis Power Pac Basic (BIORAD) power source
- ✓ Flowgen Bioscience chamber (Model No MH1070B)
- ✓ GLOMAX 96 microplate Luminometer (Promega)
- ✓ Gyro Rocket SSL3 (Stuart)
- ✓ Heraeus Multifuge 3S Plus Series Benchtop Centrifuges. Rotor 75006441 (Thermo Scientific)
- ✓ Hot plate and stirrer PC-620D (Corning)
- ✓ Humidified tissue culture incubator CB150 (E3) (Binder. 37 ◦C, 5% CO_2)
- ✓ Hybridisation Incubator (Techne, Cat No., HB-1D) with Hybridisation Tubes (Techne, Cat No. FHB12)
- ✓ Incubator INCOmed (Memmert) (*for bacteria)
- ✓ Incubator Shaker Excella E25 (New Brunswick Scientific) (*for bacteria)
- ✓ InGenius gel documentation and analysis system (Syngene)
- ✓ Inverted microscope Axio observer.A1 (Zeiss). Filter sets: 43 HE [Red. Excitation BP 550/25 (HE), emission BP 605/70 (HE)], 38 [Green. Excitation BP 470/40, emission BP 525/50], 49 [blue. Excitation G 365, emission BP 445/50] (Zeiss).
- ✓ Lynx Stereo Dynascopic microscope (Vision Engineering)
- ✓ Microcentrifuge (Thermo Scientific Heraeus Fresco 17)
- ✓ Microcope Leica DM IRB, (Leica Microsystems)
- ✓ Microscope Olympus LX81, confocal Fluoview FV1000 (Olympus). Lasers: 440 (cyan channel), argon (green channel), helium/neon (red channel), 633 (far red channel).
- ✓ Mini Trans-Blot Cell (Biorad)
- ✓ Mini-PROTEAN Tetra Electrophoresis System (Biorad)
- ✓ Minifold (96 well dot blotter) SRC-96/1 (Schleicher & Schuell). Vacuum source – Capex L2C (Charles Austen Pumps).
- ✓ NanoDrop™ 1000 Spectrophotometer (Thermo Fisher Scientific)
- ✓ Odyssey Infrared Imaging System (Li-cor Bioscience)
- ✓ Orbital Shaker SSL1 (Stuart)
- ✓ PCR gradient Thermal cycler TC-512 (TECHME)
- ✓ Pipette Controller Bibbyjet Pro, PC2000 (Stuart)
- ✓ Pipettes LM10, LM100, LM1000 (Labmate)
- ✓ PowerWave HT microplate spectrophotometer (BioTek)
- ✓ Refrigerated Superspeed Centrifuge Sorvall RC 5B. Rotors GSA, GS-3, SS34 (Sorvall)
- ✓ Rotor-Gene ™ 6000 real-time rotary analyzer (Corbett Life Science).
- ✓ Ultracentrifuge Beckman Optima L7. Rotor SW32.1Ti (Beckman Coulter)
- ✓ Ultracentrifuge optima L-100XP. Rotor Type 70Ti (Beckman Coulter)
- ✓ UV transiluminator Gel doc 2000 (Biorad)

- ✓ Vortex mixer classic (Velp Scientific)
- ✓ Waterbath SUBAQUA12 (Grant)

SOFTWARES

- ✓ Adobe Photoshop CS4
- ✓ Axio Vision 4.8.1 (Carl Zeiss Image solution)
- ✓ BD FACSDiva™ Software (BD Biosciences)
- ✓ Gen5 Data Analysis Software (BioTek)
- ✓ GeneFlash syngene Bio Imaging software (Syngene)
- ✓ geNorm VBA applet for Microsoft Excel
- ✓ GraphPah Prism (GraphPah)
- ✓ GloMax® 96 software (Promega)
- ✓ Image J 1.45 S (NIH)
- ✓ Leica application Suite (Leica)
- ✓ Statistical Package for the Social Sciences (SPSS) (IBM)
- ✓ Odyssey Infrared Imaging System application software V1 (Li-cor Bioscience)
- ✓ Olympus FV10 –ASW Vs 3 (Olympus)
- ✓ Rotor Gene Software 1.7 (Corbett Life Science).
- ✓ Vector NTI (Invitrogen)